Project Report
STK-253

Proceedings of the 1998 Space Control Conference

L.B. Spence
Editor

14–16 April 1998

Lincoln Laboratory

MASSACHUSETTS INSTITUTE OF TECHNOLOGY

LEXINGTON, MASSACHUSETTS

DTIC QUALITY INSPECTED 1

19990323 123

The ESC Public Affairs Office has reviewed this report, and it is releasable to the National Technical Information Service, where it will be available to the general public, including foreign nationals.

This technical report has been reviewed and is approved for publication.

FOR THE COMMANDER

Gary Tutungian
Administrative Contracting Officer
Contracted Support Management

MASSACHUSETTS INSTITUTE OF TECHNOLOGY
LINCOLN LABORATORY

PROCEEDINGS OF THE 1998
SPACE CONTROL CONFERENCE

PROJECT REPORT STK-253

14–16 APRIL 1998

LEXINGTON   MASSACHUSETTS

LEXINGTON
MASSACHUSETTS

PREFACE

The Sixteenth Annual Space Control Conference sponsored by ESC and co-hosted by MIT Lincoln Laboratory and the AF Research Laboratory was held on 14, 15 and 16 April 1998. The purpose of this series of conferences is to provide a forum for the presentation and discussion of space control issues.

This *Proceedings* documents those presentations from this conference that were received in time for pre-conference publication. The papers contained were reproduced directly from copies supplied by their authors (with minor mechanical changes where necessary). It is hoped that this publication will enhance the utility of the conference.

Dr. Lee B. Spence
Editor

TABLE OF CONTENTS

Space Observation Network Study (SONS)

T. E. Payne, D. M. Payne, C. E. Tuttle (Schafer Corp.); D. E. Briscoe, G. B. Masten (Logicon RDA); J. A. Beaird, M. Enoch (Space Applications Corp.), D. Mosley (Air Force Research Laboratory)

Introduction
This study provided analyses for an augmentation of GEODSS by a ground-based small telescope network and for a space-based space surveillance system and was separated into these two tasks. The analyses conducted in this study built upon the work that was done previously by the Optical Network Mission Study (ONMS). [1]

This study supported evaluations of potential, alternative concepts for meeting Air Force Space Command (AFSPC) Space Surveillance metrics and SOI needs in high earth orbit (HEO) in the case of the ground-based small telescope augmentation task, and for meeting metrics needs in both HEO and low earth orbit (LEO) in the case of the space-based optical sensor task. Both tasks used the following as a baseline; the current Space Surveillance Requirements Document (SSRD) dated 10 July 1997, the 1996 AFSPC Space Control Mission Area Plan (MAP), and the draft USSPACECOM Space Control Mission Needs Statement (MNS). These tasks also used the battlespace projection document prepared by the ONMS which describes the space population of objects which must be detected, tracked, catalogued, and characterized by the space surveillance force structure.

Both tasks, the Ground-based Small Telescope Augmentation Study and the Space-based Study, were separated into four principle elements: 1) Identify the current requirements, operational tasks, measures of effectiveness (MOEs)/measures of performance(MOPs), and the battlespace objects and their characteristics that must be tracked for space surveillance; 2) Develop generic sensor concepts consisting of optical telescopes, detectors, associated hardware and software, and operations concepts; 3) Analyze the performance of the resulting multiple sensor network in the context of the requirements and battlespace projections; 4) Provide costing in accordance with an approved work breakdown structure (WBS) for each task, a ground-based network and a space-based network.

The HEO population was projected into the future using linear analysis. This analysis was performed as part of the ONMS. Figure 1 illustrates the population growth.
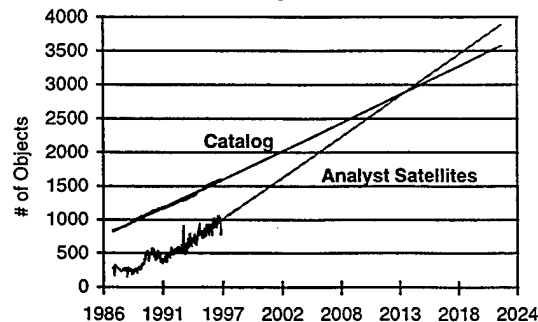
Figure 1. HEO Population Growth

Ground-based Small Telescope Augmentation Study

Battlespace Characterization
The objective of this task was to determine the number, placement, and cost of small telescopes (STs) needed to augment GEODSS in order to meet the Deep Space (HEO) surveillance requirements (metrics and SOI) for the next 25 years. The number and placement of the STs is dependent, not only on the number and growth of the total objects to surveil, but in the case of geosynchronous earth orbit (GEO) objects, the number and growth of the objects located above the various longitudes. The current longitudinal distribution of operational spacecraft was used for today's distribution. Information supplied to the International Frequency Registration Board by the International Telecommunications Union contained

longitude slots that have been filed for future use. This was used as the future distribution. Figure 2 shows both distributions.
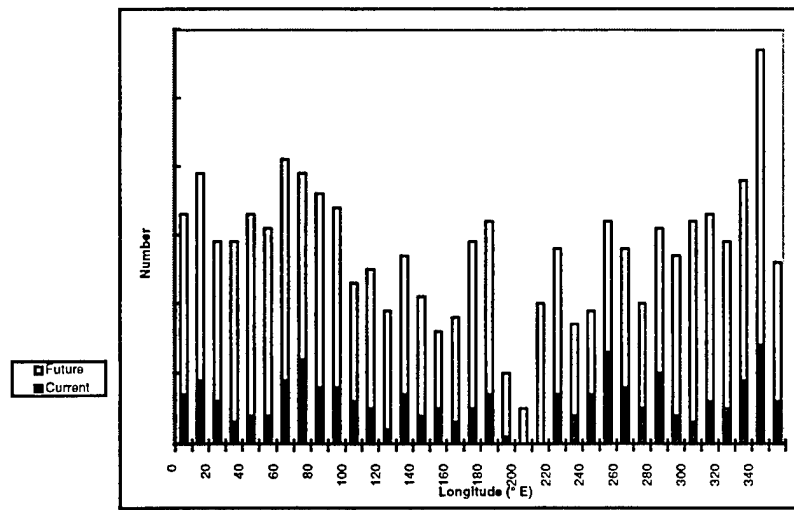
Figure 2. GEO Longitude Distribution - current and future

Another aspect to characterization is how bright the objects are. The ST network must be able to detect these objects with short integration times. The Deep Space Optical Catalog that was developed by John V. Lambert (Boeing North American - Space Operations Center) was used as a baseline for the brightnesses of the HEO objects.[2] The mean brightness of this catalog is 14 apparent visual magnitudes. The brightness distribution was assumed constant over the next 25 years.
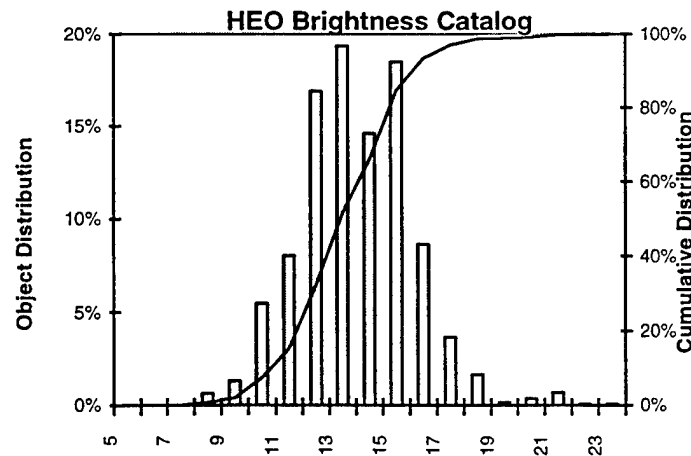
Figure 3. HEO Brightness Catalog

GEODSS Operations
Today, GEODSS provides metrics and SOI data on the HEO population (Deep Space). Two alternative operation modes were analyzed for GEODSS in this study. First, GEODSS would provide metrics and SOI. GEODSS's primary function would be to provide the SOI data (since GEODSS telescopes have larger aperture sizes and thus more sensitivity), with the remaining capabilities available for metrics tasking. Then, the STs would complete the remaining metrics tasking. Second, GEODSS would provide SOI data only. In this case, the small telescopes would provide all the metrics data.

Surveillance Strategies
Two different surveillance strategies were examined in this study. The first is a "task-track" strategy similar to today's. Each site is tasked by the Space Control Center (SCC) for data on specific objects. In this case, the number of tracks performed by the ST network is dependent on the tasking. GEODSS could operate in either mode described above.

2

The second strategy examined was "step-stare". This strategy entails a network of STs to stare at a certain section of sky by "stepping" through it during the night. In this case, each staring telescope provides data on all the objects that pass through the telescope's surveillance area. Therefore, the number of tracks performed by a network of staring telescopes is independent of tasking, similar to fence radar. In this case, the stare network would provide data on all of the objects that were available to it. Therefore, a stare network is not conducive to augmenting GEODSS metrics tasking. However, a tasked network of telescopes, either GEODSS or task-track STs, could augment a stare network.

Force Structure Assumptions
General force structure assumptions were 1) the small telescopes would be co-located with GEODSS sites. This assumption made the cost section of this study simpler and cheaper; and 2) the unavailability of each ST due to equipment failure, etc. would be 10%. This is lower than for existing telescopes in the network today because the STs would be constructed using newer and presumably more reliable technology.

The 25 year time span was examined at two points: 2007 and 2023. At each time period, the following upgrades and modifications were assumed to take place. These were based on planned and programmed improvements to the Space Surveillance Network (SSN). Where information was uncertain or unavailable, improvements and modifications were suggested based on an analysis of the SSN. Tables 1 and 2 list the assumptions made at the 2007 timeframe and the 2023 timeframe.

Table 1. 2007 Force Structure Assumptions.

2007
85% Ops availability due to O&M upgrades.
82% Weather availability due to installation of Exclusion Zone Sensors (EZS).
GMP in place.
HEO capability at Ascension and HAVE STARE.
CCDs on all telescopes.
Spain site operational.
All other current SSN capabilities are retained.

Table 2. 2023 Force Structure Assumptions.

2023
GEODSS auxs converted to mains.
Western Australia GEODSS site operational.
All previous SSN capabilities are retained.

Small Telescope Design
Four generic STs were designed to meet the objective of measuring a population of objects with the characteristics that were delineated in the Battlespace Characterization section above and with the restrictions of a ground-based system (mainly, atmospheric distortion). Design trades were made on aperture size and field of view. The detector characteristics were designed to match the field of view and spot size. The aperture size was designed to obtain a SNR of 10 at visual magnitude of 17 in a 1 second integration. The details of the four designs are in Figure 4. Point design B was recommended for a task-track telescope because point design A could not meet the tracking speed requirements. For step-stare, point design D was recommended since it had the larger field of view.

	Design Point A	Design Point B	Design Point C	Design Point D
Telescope	COTS	COTS	Custom 1	Custom 2
Gimbal	COTS	Custom	Custom	Custom
Detector	COTS	COTS	COTS	Custom
Computer	COTS	COTS	COTS	Custom

COTS = Commercial, Off-The-Shelf

3

	COTS	Custom 1	Custom 2
Telescope	• ½° FOV • 40-cm aperture • $< \lambda / 10$ at 0.6 µm	• 2° FOV • 40-cm aperture • edge of field corrected to 70% of center	• 4° FOV • 40-cm aperture • edge of field corrected to 70% of center

	COTS	Custom
Gimbal	• 10 µrad jitter (1 – 1000 Hz) • 50 µrad/min Sidereal rate error (Sidereal rate only -- unsuited for object tracking) • 200 µrad Stationary pointing accuracy	• 5 µrad jitter (1 – 1000 Hz) • 5 µrad/min Sidereal rate error • 10 µrad/sec tracking rate error • 10 µrad Stationary pointing accuracy
Detector	• 2048 × 2048, single-point correction • 12 – 16 bit • 4 fps readout with < 20-e⁻ read noise	• 4096 × 4096, two-point correction, multi-port • 12 – 16 bit • 4 fps readout with < 20-e⁻ read noise
Computer	• Star cal., sidereal, data reduction • PCI/VME Multi-processor • IRIG/GPS timing	• Star cal., sidereal/track, data reduction • PCI/VME Multi-processor • IRIG/GPS timing • More ports to handle multi-port FPA

Figure 4. Small Telescope Generic Designs.

Task-Track Surveillance Network

In order to meet the HEO metrics requirements with a network of small telescopes, 1) an estimation of the number of tracks per day[1] per ST, and 2) determination of the number of STs at each GEODSS site, needed to be made. The tracks per day for a single ST was estimated to be 398. This was calculated assuming the average available observing period was 8 hours over the course of a year and the time to track is the following:

$$t_{track} = 5\left(t_{integration} + t_{slew} + t_{acquire} + t_{process}\right) \text{ where}$$

$$t_{integration} = 1.7 \sec,$$

$$t_{slew} = 5 \sec,$$

$$t_{acquire} = t_{process} = 2 \sec.$$

The resulting total number of STs are shown in the following figures for the two operational modes. The distribution of STs by longitude was accomplished by using the total number of tracks per day required in each longitude region and dividing it by the number of tracks per day per ST yielding the number of STs needed to meet the requirements in that longitude region for that timeframe. For each longitude region, the number of STs deployed at a GEODSS site was calculated by weighting each GEODSS site's coverage of that longitude region. Figure 5 shows the force structure for both operational modes. Table 3 lists the total number of STs needed.

---

[1] A track is defined as 5 individual observations.

4

Small Telescope Force Structure
(GEODSS - metrics & SOI)

Small Telescope Force Structure
(GEODSS - SOI Only)

Figure 5. Small Telescopes Needed to Meet HEO (Metrics and SOI) Requirements. (Task-Track)

Table 3. Total Number of Small Telescopes for a Task-Track Network.

Year	Total Number of Small Telescopes Needed to Meet Requirements	
	GEODSS - Metrics and SOI	GEODSS - SOI Only
2007	16	20
2023	24	33

Step-Stare Surveillance Network

The objective of a stare network is to surveil Deep Space rather than track known objects. Over time this subtle difference from task-track would lead to an improved knowledge of the number of objects that are in Deep Space. By virtue of the fact that the position of more than one object can be measured with only one observation, the step-stare surveillance strategy is expected to be less sensitive to increases in the object population. Therefore, increases in the number of STs due to object population increases would not be expected.

Since a step-stare surveillance strategy is not an operational concept, the first task was to determine the strategy itself. Surveillance of the entire sky at each GEODSS site with a 20° elevation restriction would yield 13,570 square degrees to cover several times each night in order to get the 5 observations per object that define a track. This kind of strategy would raise several technical challenges that were beyond the scope of this study. The approach was therefore taken to 1) determine if high density regions of the sky over a GEODSS site existed where most of the HEO objects would be observable, and 2) then concentrate on developing a step-stare strategy in these regions to ensure that objects which entered these regions did not leave them without being observed at least once.

An analysis of the HEO objects[2] resulted in 2 well-defined regions: 1) the equatorial belt which contained the GEOs, and 2) a northerly (+60°) belt which contained the elliptical earth orbit (EEO) objects. The EEOs have periods ranging from .9 to 2.1 revs/day and eccentricities greater than .2. Other HEO objects, medium earth orbit (MEO) objects (revs/day less than 2.1 and eccentricities less than .2) and beyond GEO objects (periods less than .9 revs/day) were found to be uniformly distributed across the sky, therefore not lending themselves to a step-stare surveillance strategy. To ensure coverage of all HEO objects cost-effectively, it was proposed that a tracking ST be deployed at each site to track these objects in the low density areas. Another alternative is to utilize GEODSS's remaining capacity to track these objects.

The proposed step-stare strategy was based on the idea of dedicating each ST to a specific surveillance area. The strategy entails conducting a parametric analysis to determine an optimal telescope surveillance area (TSA) size that guarantees an observation of all objects that pass through that TSA. The constraints on defining a TSA were that the TSAs be contiguous and rectangular.

---

[2] An in-house code (Orbital Propagation Analysis Software - OPAS) was developed in order to perform this analysis and the analyses performed for the Space-based Study.

The ST stare network was determined from the OPAS simulations using the current catalog.[3] Improvements could be made in the optimization algorithm that creates the TSAs and these improvements would decrease the number of STs needed. Although at some sites, remaining capacity exists after meeting the SOI requirements, this is not the case at other sites, nor is it projected to be true in the future at all sites. Therefore, the conservative approach of adding a tracking ST at all sites was taken. Figure 6 shows the ST network force structure. Table 4 lists the total number of STs and the type needed in each timeframe.
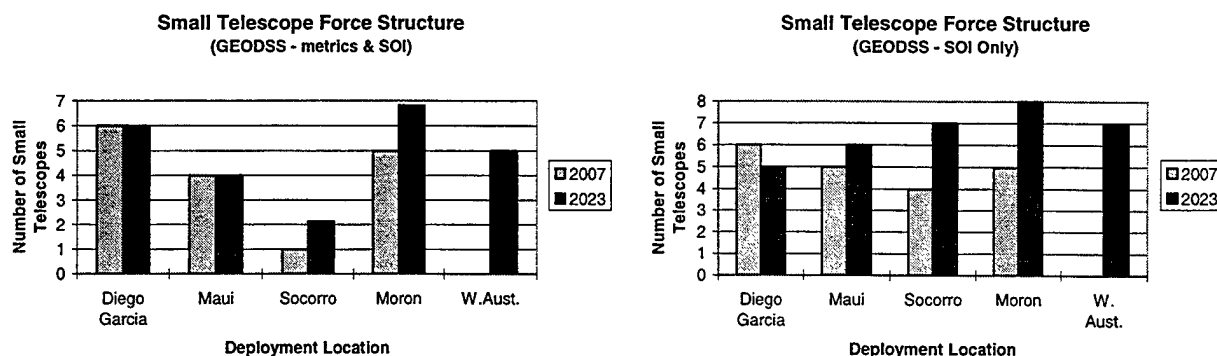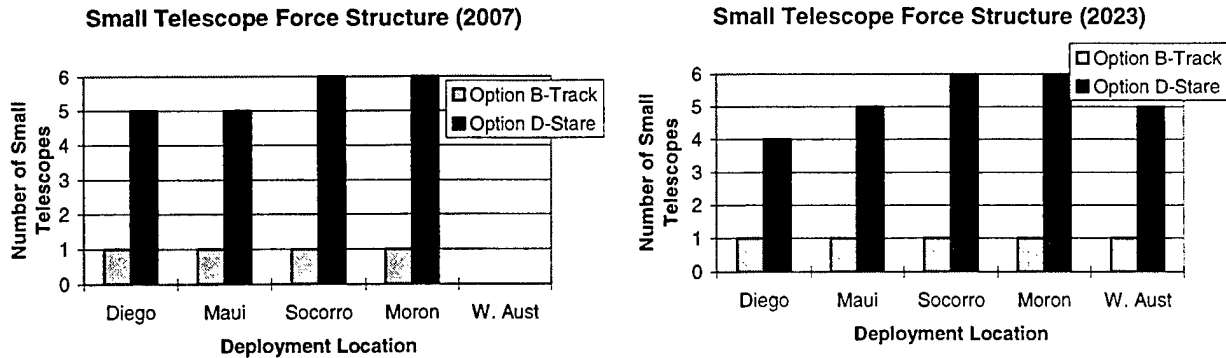

Figure 6. Small Telescopes Needed to Meet HEO (Metrics and SOI) Requirements. (Step-Stare)

Table 4. Total Number of Small Telescopes for a Step-Stare Network.

Year	Total Number of Small Telescopes Needed to Meet Requirements	
	Track STs	Stare STs
2007	4	22
2023	5	26

Conclusions
An augmentation of GEODSS by a network of small telescopes could enable the SSN to meet the HEO requirements for metrics and SOI as currently stated in the requirements documents. In order to meet these requirements, a significant number of STs would be needed. However, the step-stare strategy of meeting the HEO metrics requirements shows promise to reduce the number of telescopes needed. More analysis would have to be done on the TSA concept in order to better optimize the staring telescopes. Note that if force structure decisions are made that decrease the overall HEO capability of the SSN, more STs would be needed than are suggested in this study. Finally, it is the recommendation of this study that step-stare is a better concept of operations than task-track for the future because 1) step-stare is better suited to address the task of tracking "all man-made objects in space", and 2) a constant number of STs can perform the mission on a growing battlespace population.

Space-based Study

Battlespace Characterization
The objective of this task was to determine the number, orbit, and cost of space-based telescopes needed to meet the Near Earth (LEO) and Deep Space (HEO) surveillance requirements (metrics) for the next 25 years. The analysis performed with OPAS utilized the orbital distribution of the current catalog. It was assumed, as in the ground-based study, that the distribution would not change significantly, but increase in numbers proportionately as in Figure 1. An important characteristic of the battlespace for a space-based system is the distribution of altitudes of the objects. This attribute aided in the sensor orbit altitude determination. Figure 6 shows the altitude distribution of the current catalog.

---

[3] Since the number of stare STs needed is not dependent on the number of objects nor the projected number of objects for the next 25 years, using the current catalog does not limit the analysis.

Distribution of Satellite Altitudes

Number of Satellites (RSOs)

1200
1000
800
600
400
200
0

LEOs

HEOs

MEOs

0 2300 4600 6900 9200 11500 13800 16100 18400 20700 23000 25300 27600 29900 32200 34500 36800 39100 41400 43700 46000 48300

Altitude at Apogee (km)
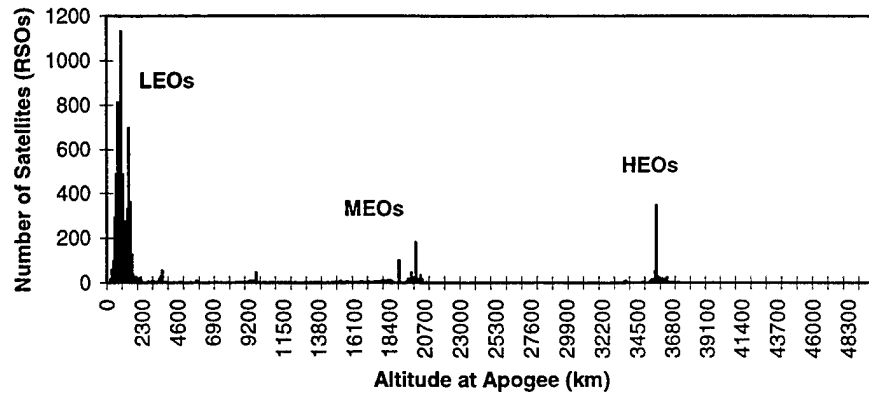
Figure 6. Distribution of Altitudes for the Current Catalog.

Figure 7 shows the orbital inclination distribution of the current catalog. Orbital inclination was a key consideration when determining the orbital inclination of the space-based surveillance sensor network.

HISTOGRAM OF HEOs

NUMBER OF SATELLITES

450
400
350
300
250
200
150
100
50
0

0 20 40 60 80 100 120 140 160 180

INCLINATION (DEGREES)

HISTOGRAM OF LEOs

NUMBER OF SATELLITES

2000
1800
1600
1400
1200
1000
800
600
400
200
0

0 20 40 60 80 100 120 140 160 180

INCLINATION (DEGREES)
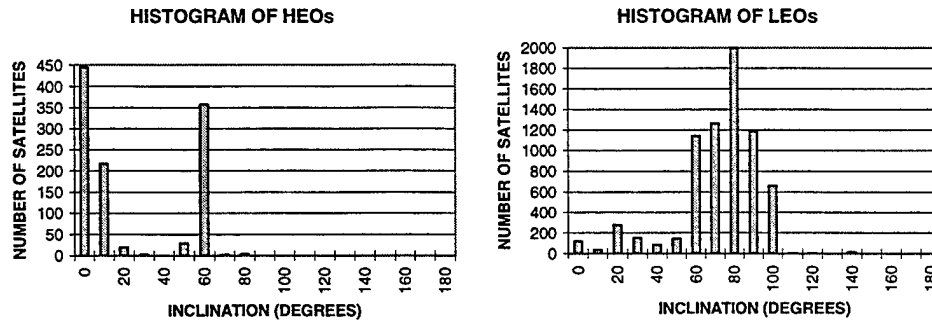
Figure 7. Orbital Inclination Distributions of the Current Catalog.

As in the ground-based study, the object brightnesses (in this case, both LEOs and HEOs) were a driver in the sensor design. The Deep Space Optical Catalog (DSOC) used in the previous study was adjusted to be applicable for the space-based sensors[4]. However, no such catalog exists for Near Earth objects. Therefore, an estimation of the brightness distribution was developed using the radar cross-section to visual magnitude conversion developed for the DSOC and this distribution was scaled based on visual magnitude measurements of LEO objects made from Maui.[3] Figure 8 shows the resulting brightness distribution estimate for LEOs. The mean average visual magnitude is 12. The uncertainty in the bias of this distribution is about 2 magnitudes over the detector response due to 1) errors in scaling the bias from the small optical data sample, 2) brightness variations of satellites with wavelength, and 3) possible earth penumbral effects on optical data. This distribution was also adjusted to take into account the range from a space-based sensor to the object.

---

[4] DSOC is a distribution of apparent magnitudes which contains the range information. Since the telescopes are no longer on the ground, the magnitudes were adjusted for range in the usual way.

LEO Brightness Catalog
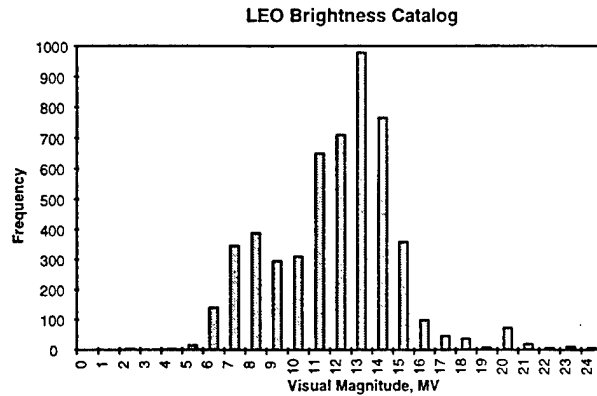
Figure 8. LEO Brightness Catalog

Concept of Operations

The Satellite Control Network (SCN) was proposed for up and down links between the ground-based Space Operations Center (SOC) at Edwards AFB and the space-based network. The use of the SCN puts constraints on the amount of data that can be downloaded in a timely fashion, so on-board processing is a necessity. The demands on the space-based processors were analyzed and it was found that the requirements were within the capabilities of space-hardened hardware that is already in use. The SOC would be the intermediary between the space-based network and the Space Control Center (SCC), both tasking the network (with direction from the SCC) and processing the data (with the processed data going to the SCC).

Design and Analysis Approach

In the case of space-based systems, the telescope volume and mass drive the spacecraft design and the launch vehicle choice. OPAS was used to determine the impact of a reduced aperture size since this drives the mass. Another factor that drives the launch vehicle is the orbit. Orbit determination was based on an analysis using OPAS of the catalog population and trial orbits. The design and analysis phase was, therefore, an iterative process which determined 1) the most favorable orbit, 2) an optimal aperture size, and 3) the size of the space-based constellation. The performance of the resulting network was then compared with the required tracks per day for LEO and HEO metrics using OPAS.

Space-based Sensor Design

The process of developing the point design was driven heavily by the resident space object (RSO) attributes: brightness, range, and the relative velocity between the space-based sensor network and the RSOs. The sensor design process used these parameters to determine aperture, optical design, and processing algorithms. The resulting point design was a balanced choice between performance and launch cost. Table 5 contains the details of the space-based sensor point design.

Table 5. Space-based Optical Payload Point Design

Diameter	25 cm
FOV	$3° \times 6°$
IFOV	~25 μrad
Detector (2)	2k x 2k
Design	Three Mirror Anastigmat
Mass	57 kg
Volume	0.65 m³
Earth Exclusion Angle	< 5°
Sun Exclusion	TBD
Not Diffraction Limited	

Space-based Space Surveillance Network

Analysis was performed using OPAS to determine three space-based network characteristics: 1) the most favorable orbit, 2) an optimal aperture size, and 3) the size of the space-based constellation. Initially, an analytical approach was used to narrow the range of possible orbits. Then, a 48 sensor constellation was chosen which contained 6 differently inclined orbital planes with 4 sensors in each plane at 2 different altitudes for the OPAS simulation. The distributions of angular rates and SNR for the entire constellation were analyzed to provide feedback to the design process. From an analysis of these results, the orbital parameters listed in Table 6 were recommended.

Table 6. Recommended Space-based Network Orbit.

Altitude	1000 km
Inclination	~ 90°
Sun Synchronicity	Yes

Second, the optimal aperture size was determined from an analysis of these same results. The range of the aperture size for a network with this type of orbit was between 15 and 40 cm. A 25 cm aperture was chosen because 1) it has more sensitivity than a 15 cm aperture, and 2) it has less mass than a 40 cm. The reduction in aperture size from 40 cm to 25 cm meant a substantial reduction in launch costs.

Third, the resulting analysis determined the number of spacecraft in the space-based network. Performance degradation could be exchanged for fewer spacecraft, but 4 spacecraft was recommended as the network size. A constellation of these 4 space-based sensors performed the mission at 91% of a 48 sensor constellation.

Finally, the number of possible tracks per day of the space-based network was estimated from the total number of observation opportunities of the network in a 24 hour period. This parameter was output by OPAS using the field of regard of each sensor in the constellation. One track was equated to 5 observation opportunities. The resulting number of possible tracks per day was over 100,000 with a 4 sensor constellation. This exceeds the projected required tracks per day for LEO and HEO metrics over the next 25 years. However, these are only possible tracks per day. A concept of operations for tasking and data processing would have to be included for a more complete analysis which would yield a more realistic number of tracks per day. Thus, it becomes apparent that the limiting factors in the performance of a space-based system are 1) the frequency of tasking, 2) the on-board data storage capacity and data reduction ability, and 3) the sensor field of view.

The final recommended spacecraft description is shown in Figure 7.

Subsystem	Mass (kg)	Power (W)	Comment
Structure	100	0	
Power	250	100	12 m² Solar Panel Area and (50 kg)Batteries
Propulsion	30	20	Propellant TBD
Communications	20	40	AFSCN/SGLS Compatible 1 Mbps Downlink
Command and Data Handling	10	25	
Guidance, Navigation and Control	115	225	3-Axis Stabilized: 4 Reaction Wheels, 3 Magnetic Torquers, 6 Sun Sensors, GPS & Payload (Star Tracker)
Thermal	30	25	
Optical Sensor Payload	180 (TMA)	225	
Total Dry Weight	705 (TMA)	710	Spacecraft without propellant
Loaded Weight	895 (TMA)	710	Spacecraft with propellant
Boosted Weight	930 (TMA)	710	Spacecraft with propellant and launch vehicle interface
Launch Vehicle			Taurus XLS

Figure 7. Space-based Space Surveillance Spacecraft Parameters.

Conclusions
A space-based network of optical telescopes could meet the LEO and HEO metrics requirements as currently stated in the requirements documents. In order to deploy a space-based network, a significant monetary investment would be needed. It was recommended that a constellation of 4 spacecraft with a sensor payload consisting of a 25 cm three mirror anastigmat constitute the space-based network. This network choice minimized cost, yet minimized the negative impact on performance that was accrued from a 25 cm aperture and a constellation size of 4. More development and analysis would have to be done on a tasking/data processing/tracking concept in order to better characterize the performance capabilities of the space-based network.

References

1 Benedict, R. (Schafer Corp.), Optical Network Mission Study 1996 - 1997. Jointly sponsored by Air Force Space Command and Air Force Research Laboratory. Final report in progress.

2 Lambert, J. V. (Boeing NA-SOC), Deep Space Optical Catalog, September 6, 1996.

3 Lambert, J. V., *et. al*, Specialized Data Report: Multispectral Signatures of Near-Earth Satellites, June 15, 1994.

Tasking and Maintenance of Deep-Space Satellites

J. G. Miller (The MITRE Corporation)

The Space Surveillance Network (SSN) has excess capacity to maintain orbital element sets on near-earth satellites because of the large capacity of several phased-array radars and the Naval Space Command (NAVSPACECOM) fence. These near-earth sensors are also large contributors in tracking deep-space satellites (period greater than 225 minutes) in highly eccentric orbits. Those satellites are within range of these sensors near perigee. Deep-space satellites with perigee too high to be tracked by the near-earth sensors must be tasked to the deep-space sensors in the SSN. Deep-space sensors include mechanical radars Millstone and ALTAIR; the Eglin phased-array radar; three Ground-based Electro-Optical Deep Space Surveillance (GEODSS) optical sites, Socorro, Maui, and Diego Garcia; the Maui Space Surveillance System (MSSS) optical site; and two RF passive sensors, Feltwell and Misawa. These sensors must be utilized efficiently to maintain orbital element sets on deep-space satellites and to meet operational requirements.

The Space Surveillance Performance Analysis Tool (SSPAT) was used to analyze the tasking and catalog maintenance of deep-space satellites. Figure 1 shows the number of untasked deep-space satellites each day in 1997 by the Space Defense Operations Center (SPADOC) due to a lack of deep-space sensor resources. Except for the occasional spikes, the daily number of untasked deep-space satellites is between approximately 250 and 400. On 1 December 1997, there were 2574 deep-space satellites in the SPADOC active satellite file, including 1666 cataloged satellites and 908 analyst satellites. Cataloged satellites which have decayed are moved to the inactive satellite file, and analyst satellites which have decayed or become lost are deleted. Lost cataloged satellites remain in the active satellite file. The SPADOC tasking function automatically sets the lost flag for those satellites whose epoch age exceeds the lost threshold in its tasking group. By design, lost satellites are not tasked by SPADOC to the SSN and are not included in Figure 1. The satellites in Figure 1 would have been tasked by SPADOC to the SSN if it had sufficient deep-space capacity.
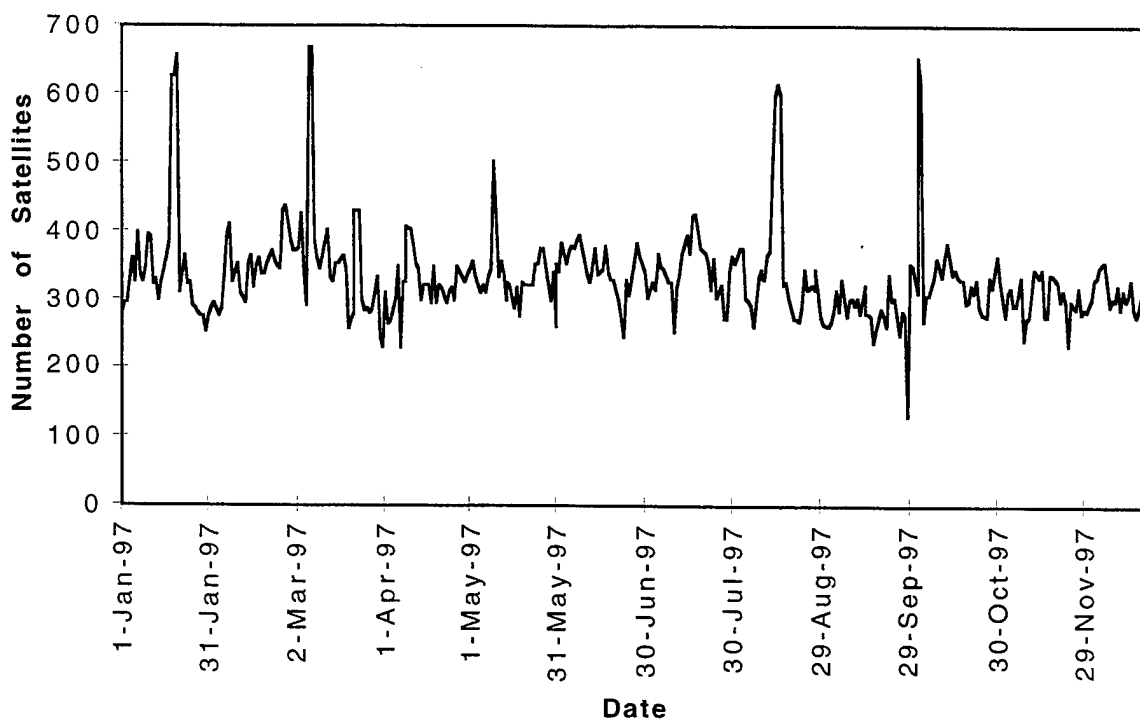
Figure 1. Untasked Deep-Space Satellites

11

Each sensor's daily track capacity is specified in its sensor tasking record in SPADOC, and the automatic tasking function tasks satellites to a sensor up to its track capacity. The SSN does not have sufficient capacity to track every deep-space satellite each day. This is particularly true for the geosynchronous belt because of the sensor sites' lack of global coverage. Fortunately, deep-space satellites with perigee above the atmosphere do not experience atmospheric drag, and hence do not need to be tracked every day to maintain good element sets. Dead payloads and rocket bodies in these types of orbits can be easily maintained if they are tracked only once a week. Active payloads that can maneuver must be tracked more frequently or they may become lost after a maneuver. The SPADOC tasking function attempts to automatically manage the sensor resources to meet the routine catalog maintenance needs of low interest deep-space satellites and to satisfy mission requirements for active deep-space payloads. The satellites in Figure 1 are low interest satellites that do not need to be tracked every day for routine catalog maintenance. SPADOC automatically decides which of these satellites needs tasking based on the epoch age of the satellite and the epoch adjustment threshold in the satellite's tasking group. A tasking group is a set of control parameters, which the user defines, to control the automatic tasking of a group of related satellites.

The number of lost deep-space cataloged satellites each day in 1997 is shown in Figure 2. There are two definitions of lost satellite, one defined by the SPADOC sensor tasking function and one defined by historical precedence. The sensor tasking function uses the lost threshold in the tasking groups, and this number varies by tasking group. SPADOC will not continue to task a lost satellite based on this definition of lost. Before SPADOC existed, the lost threshold was 30 days for all satellites. This historical definition of a lost satellite continues to be used in reporting performance metrics, even for SPADOC. To be consistent with these performance metrics, the definition of lost used in Figure 2 is the 30-day threshold. A newly lost satellite (defined arbitrarily for this paper) has an epoch age greater than or equal to 30 days and less than 90 days. A long term lost satellite has an epoch age greater than or equal to 90 days.
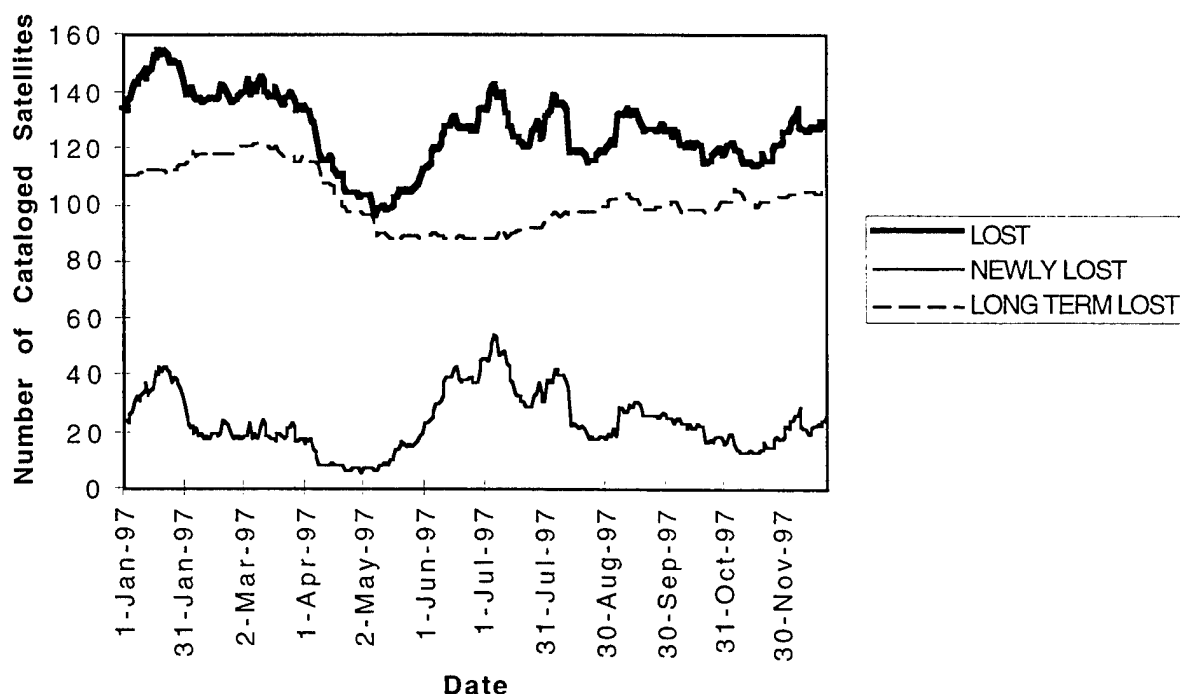
Figure 2. Lost Deep-Space Cataloged Satellites

Beginning in April 1997, the 1st Command and Control Squadron (1CACS) started a manually intensive effort to find lost satellites by attempting to correlate observations in SPADOC's unassociated observations (UOBS) file with element sets of lost satellites. Uncorrelated tracks (UCTs) from the SSN are routed to the UOBS file if SPADOC cannot correlate the UCT with a known satellite. From Figure 2 it is evident that 1CACS reduced the deep-space lost list to its lowest number in 1997 by this effort. The number of newly lost satellites was reduced rather quickly and remained low during the month of April. These lost satellites were easier to find. The number of long term lost satellites slowly declined during April. Due to manning constraints, 1CACS could not continue to expend the manual effort in UCT processing to find lost satellites. Beginning in May, the number of newly lost deep-space satellites increased rapidly due to the lack of attention to UCT processing. It is interesting to note that the number of long term lost deep-space satellites increased rather slowly beginning in May, and at the end of the year had not reached the level before 1CACS started its manually intensive effort to reduce the lost list.

The number of cataloged satellites on 1 December 1997 in each orbit class covering deep-space orbits is shown in Figure 3. The number of lost cataloged satellites on 1 December 1997 in these orbit classes is shown in Figure 4. It is interesting that there are no lost cataloged satellites in orbit class 51, which covers the circular semi-synchronous orbits. GPS and GLONASS satellites are in this orbit class. See Figure 5 for the definition of orbit classes. Geosynchronous satellites are in orbit class 63. This orbit class has the most deep-space satellites and the most lost deep-space satellites.
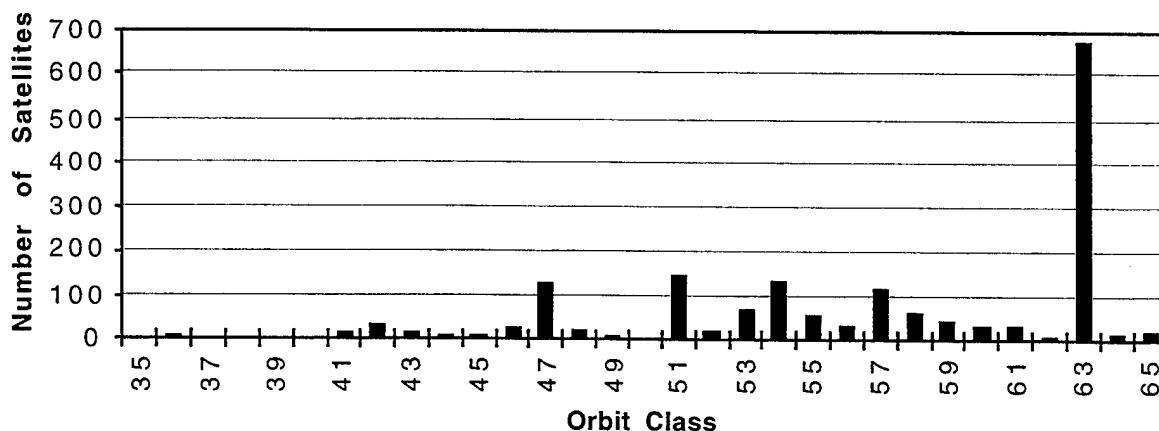
Figure 3. Number of Cataloged Satellites by Orbit Class on 1 Dec 1997
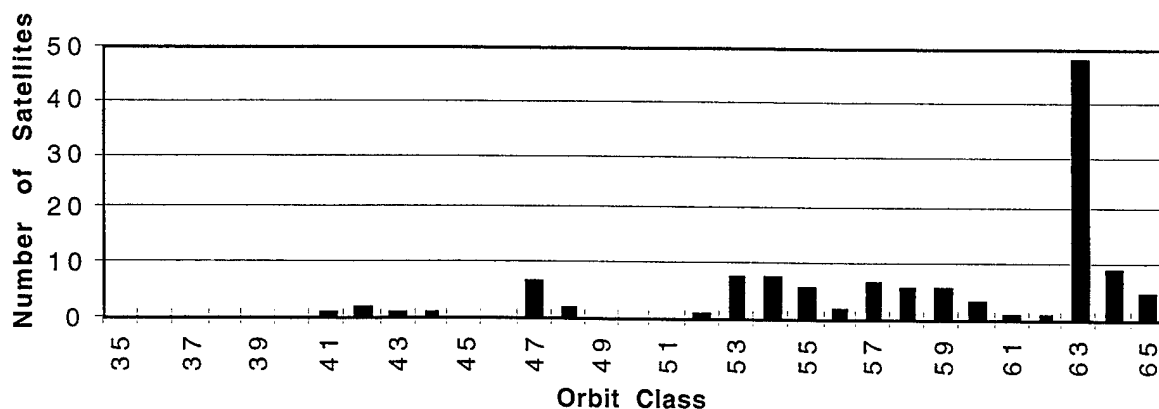
Figure 4. Number of Lost Cataloged Satellites by Orbit Class on 1 Dec 1997

13
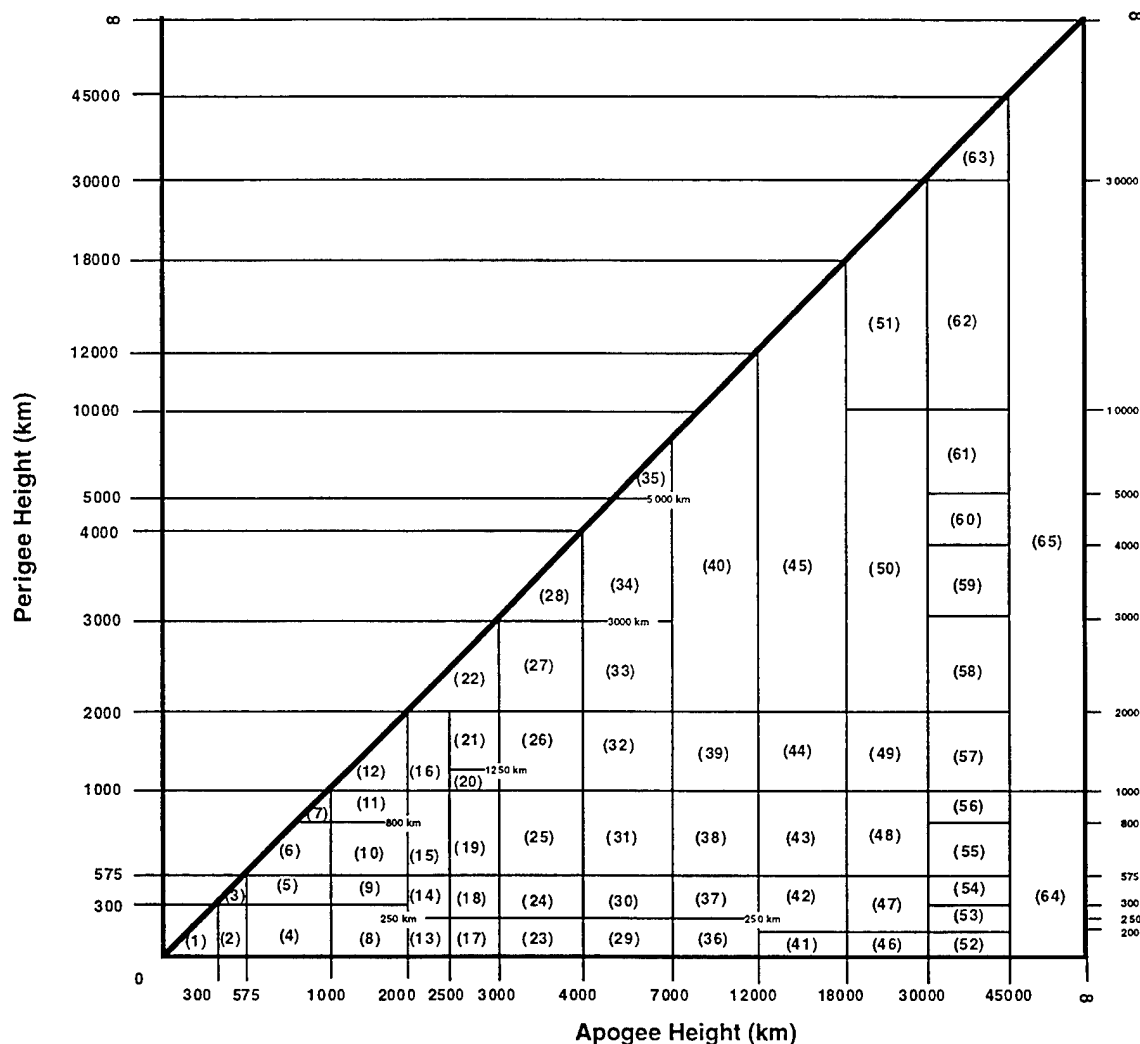
Figure 5. Definition of Orbit Classes

The average epoch age of near-earth cataloged satellites is about 0.4 days. The situation is much different for deep-space satellites. The average epoch age for 1997 of non-lost cataloged satellites in each orbit class covering deep-space orbits is shown in Figure 6. Orbit class 63 has the largest average epoch age, 5.3 days. The average for this orbit class for 1996 was 4.4 days. The average epoch age for orbit class 63 increased in 1997 because of the closure of the Pirinclik radar in February 1997. Pirinclik was used to track geosynchronous satellites in the eastern hemisphere. Figure 7 shows a histogram of the epoch age on 1 December 1997 of cataloged satellites in orbit class 63. The last bin, 9999, contains the lost cataloged satellites whose epoch age is greater than or equal to 30 days. The number of satellites in this bin, 48, is the same as the number in orbit class 63 in Figure 4. The epoch age distribution for orbit class 63 shown in Figure 7 illustrates how SPADOC maintains smaller epoch ages (less than 2 days) on high interest geosynchronous satellites than on low interest geosynchronous satellites. Table 1 shows that the observation rate is higher for high interest geosynchronous satellites than for low interest geosynchronous satellites. Tasking group 640 contains active geosynchronous payloads of high interest to U. S. Space Command (USSPACECOM). Satellites in tasking group 640 are tasked at the highest priority.

14
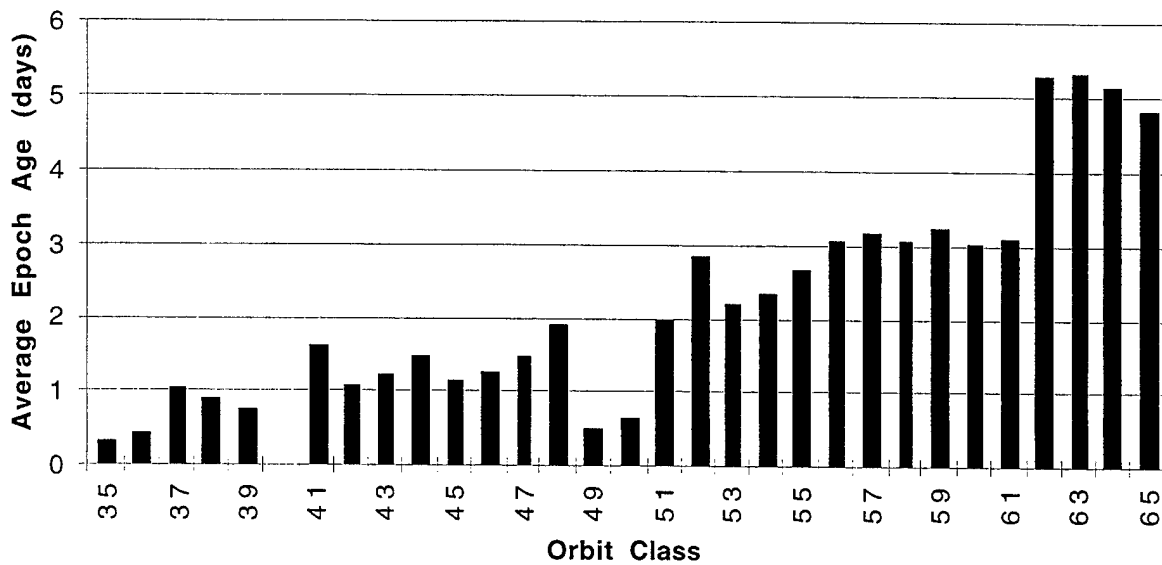
Figure 6. Average Epoch Age of Cataloged Satellites by Orbit Class for 1997
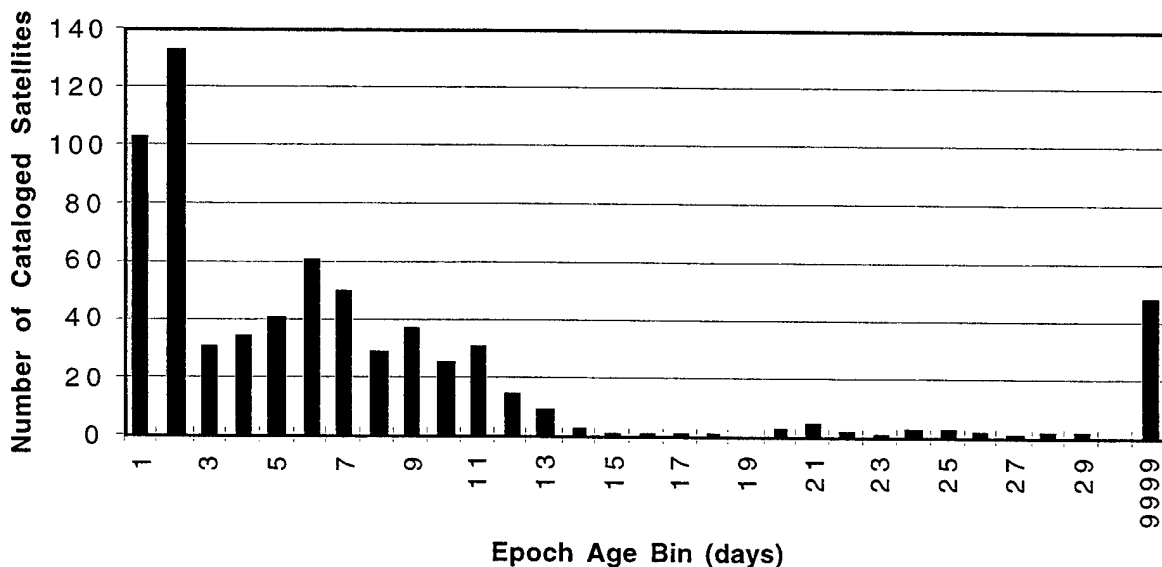
Figure 7. Epoch Age Histogram for Orbit Class 63 on 1 Dec 1997

Table 1. Average Number of Observations per Day per Satellite for Nov 1997

Geosynchronous Group	Description	Average Obs Per Day
Orbit class 63	All cataloged satellites	3.0
Tasking group 363	Rocket bodies	1.3
Tasking group 463	Dead payloads	1.4
Tasking group 563	Low interest active payloads	4.0
Tasking group 640	USSPACECOM high interest	8.2
Tasking group 963	1CACS high interest	4.9

Satellites are tasked at categories 1 through 5 with category 1 being the highest priority. Table 2 shows the tasking table for tasking group 463. The rows of the table correspond to categories, and columns to the level of tasking. The pairs of entries are the desired number of tracks and number of sensors to task at that category and level. The desired number of sensors may not be the actual number of tasked sensors due to a lack of sensors with visibility and capacity. The number in parentheses below the pair of numbers is the number of satellites at that position in the tasking table on 29 December 1997. The nominal position in the tasking table is row 5 and column 1, corresponding to 2 tracks from 2 sensors (one track from each sensor). If the SSN had more deep-space capacity, more of the satellites in this group would be maintained at the nominal position.

Satellites move away from the nominal position when the epoch adjustment threshold or element quality threshold is exceeded. Only a few of the satellites in this tasking group are at the nominal position. Most of the satellites are in column 8. The epoch adjustment threshold for tasking group 463 is 7 days. A satellite's category will decrease (priority increase) if its epoch age exceeds the epoch adjustment threshold. This will continue each day until either the element set is updated with an epoch age less than the epoch adjustment threshold, or the satellite reaches the highest priority tasking allowed by the populated entries in the tasking table (category 2 in this case). Once a satellite reaches the top row (category 2) and its epoch age stills exceeds the epoch adjustment threshold, it will move to the right (column increase) until it reaches the upper right-hand corner of the table. If the element set is updated with an epoch age less than the epoch adjustment threshold, the satellite's priority will decrease (category increase). This will continue each day, as long as the epoch adjustment threshold is not exceeded, until the lowest priority allowed by the populated entries in the tasking table is reached (category 5 in this case). Once a satellite reaches the bottom row (category 5) and its epoch age still does not exceed the epoch adjustment threshold, it will move to the left (column decrease) until it reaches the nominal position. Thus, each satellite moves up or down in the tasking table (and left or right if at a category boundary) depending on the epoch age of its element set. At category 5, a satellite in this group is not likely to be tasked to any sensor because the total SSN deep-space capacity will fill up with higher priority satellites. The epoch adjustment threshold of 7 days for this tasking group is correlated with the second local maxima at 6 days in Figure 7.

Table 2. Tasking Table for Tasking Group 463

Cat	Col 1	Col 2	Col 3	Col 4	Col 5	Col 6	Col 7	Col 8
1								
2	2/2	3/3	4/4	5/5 (2)	6/6	8/6	10/6 (2)	12/6 (39)
3	2/2	3/3	4/4	5/5	6/6 (1)	8/6 (3)	10/6	12/6 (36)
4	2/2	3/3 (2)	4/4	5/5 (1)	6/6	8/6	10/6 (1)	12/6 (21)
5	2/2 (24)	3/3 (2)	4/4 (6)	5/5 (5)	6/6 (6)	8/6 (5)	10/6 (12)	12/6 (55)

Table 3 show the same information for tasking group 640. The nominal position in the tasking table is row 2 and column 3. The epoch adjustment threshold for tasking group 640 is 1 day. More than half of the satellites in this group were tasked at category 2 on 29 December 1997; the others were tasked at category 1. Satellites whose epoch age exceeds 1 day at the time of the daily tasking run will be tasked at category 1. Satellites whose epoch age does not exceed 1 day will be tasked at category 2. The populated entries in this tasking table along with the epoch adjustment

threshold were defined by the user to obtain high priority tasking on this group of satellites and maintain element sets with epoch ages less than 2 days.

Table 3. Tasking Table for Tasking Group 640

Cat	Col 1	Col 2	Col 3	Col 4	Col 5	Col 6	Col 7	Col 8
1			2/2	3/3	4/4 (16)			
2			2/2 (6)	3/3 (9)	4/4 (11)			
3								
4								
5								

Figure 8 shows the average epoch age of the satellites in tasking group 640 (lower graph with scale on the left) and the percentage of satellites whose epoch age is less than 2 days (upper graph with scale on the right). Before Pirinclik closed in February 1997, the average epoch age was generally less than 1 day, and the percentage of satellites with epoch age less than 2 days was greater than 90 percent. Only row 2 of the tasking table was populated while Pirinclik was operational. After Pirinclik closed, the statistics in Figure 8 show more variations. Row 1 of the tasking table was populated after Pirinclik closed to attempt to keep the epoch age of these satellites as small as possible with the remaining sensors. The variations in the data after Pirinclik closed are attributed to the unreliable weather at the Diego Garcia GEODSS site.
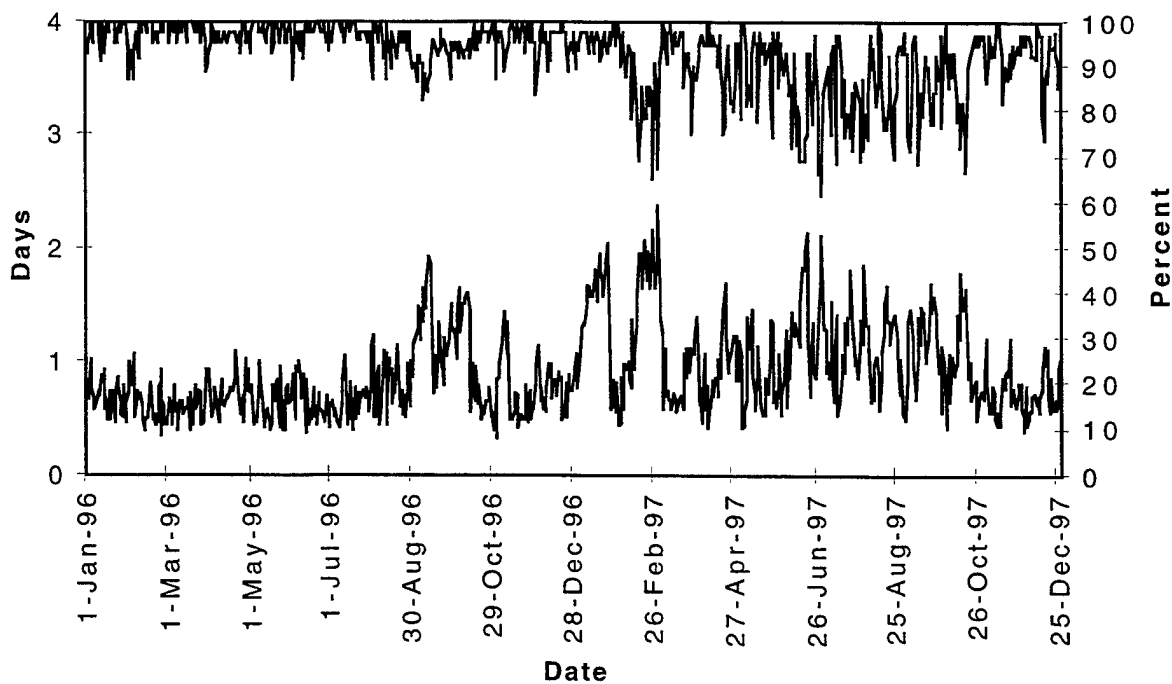
Figure 8. Epoch Age Statistics for Tasking Group 640

Figure 9 shows the average number of tasked sensors per satellite in tasking group 640 (upper graph) and the average number of sensors per satellite acquiring a tasked satellite (lower graph). Before Pirinclik closed, the average number of tasked sensors was typically 3 sensors. After Pirinclik closed, the number dropped to 2 sensors because most of the satellites in tasking group 640 were in Pirinclik's coverage and were tasked to Pirinclik as one of three sensors. The average number of sensors acquiring tasked satellites in tasking group 640 has dropped only slightly since Pirinclik closed due to increased tasking priority by populating row 1 in the tasking table. The user has attempted to continue to maintain satellites in tasking group 640 with current epoch ages after Pirinclik closed, at the expense of allowing the average epoch age of low interest geosynchronous satellites to increase.
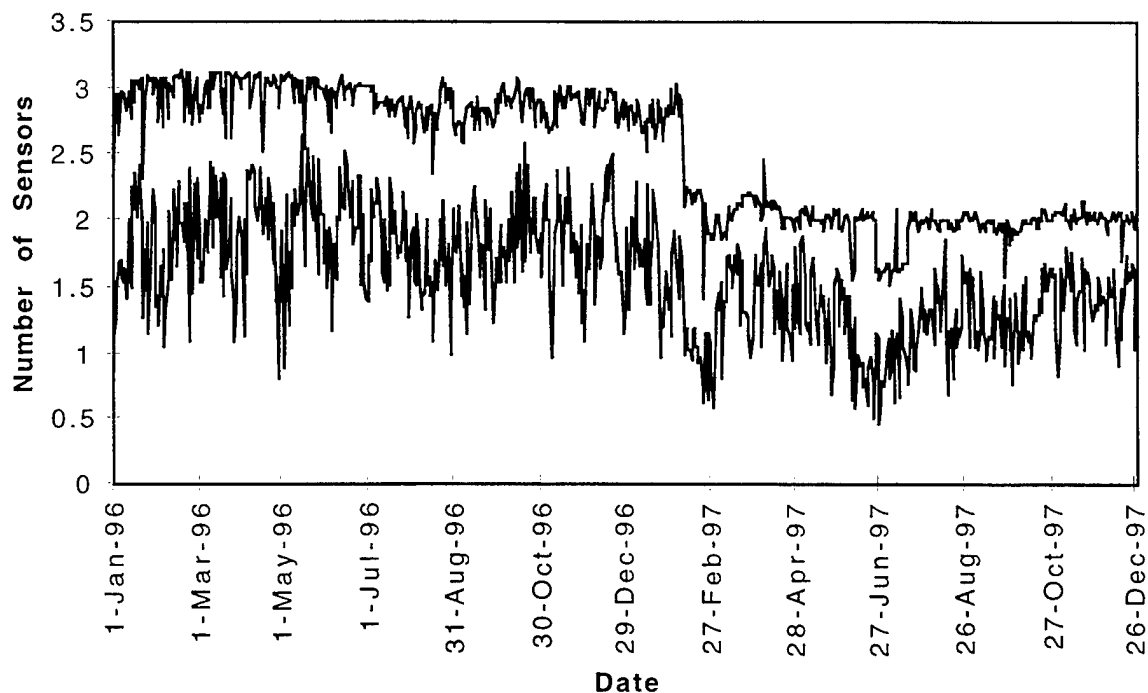
Figure 9. **Average Number of Tasked Sensors per Satellite and Average Number of Sensors Per Satellite Acquiring Satellites in Tasking Group 640**

SPADOC treats Maui GEODSS and the MSSS as separate sites for tasking purposes even though both sites are collocated on top of Mt. Haleakala in Maui and have identical coverage. Each site receives its own daily tasking message from SPADOC, and each site schedules its multiple telescopes to respond to the tasking. It has been noticed that a large number of satellites has been tasked to both sites by SPADOC. This is not the most effective utilization of the sensor resources at Maui. SSPAT was used to determine response rates on satellites tasked to both sites over an extended period of time. If a satellite was tasked to both sites more than 30 times, the site with the lower response rate was excluded from being tasked in the individual satellite tasking record in SPADOC. The data from SSPAT was written to tape and uploaded to SPADOC to avoid manually changing hundreds of satellite tasking records. Figure 10 shows the numbers of satellites tasked to each site and to both sites. The large drops in duplicate tasking on certain days correspond to the days data was uploaded from SSPAT to SPADOC. As of December 1997, 427 satellites have been excluded from Maui GEODSS and 938 satellites excluded from MSSS. Analyst satellites were not considered in this process because they are deleted and the analyst satellite numbers (SATNOs) are reused for different objects. Since July 1997 a steady state of approximately 150 satellites tasked to both sites has been maintained. Many of these satellites are analyst satellites created by NAVSPACECOM UCT processing or GEODSS UCT analyst satellites.
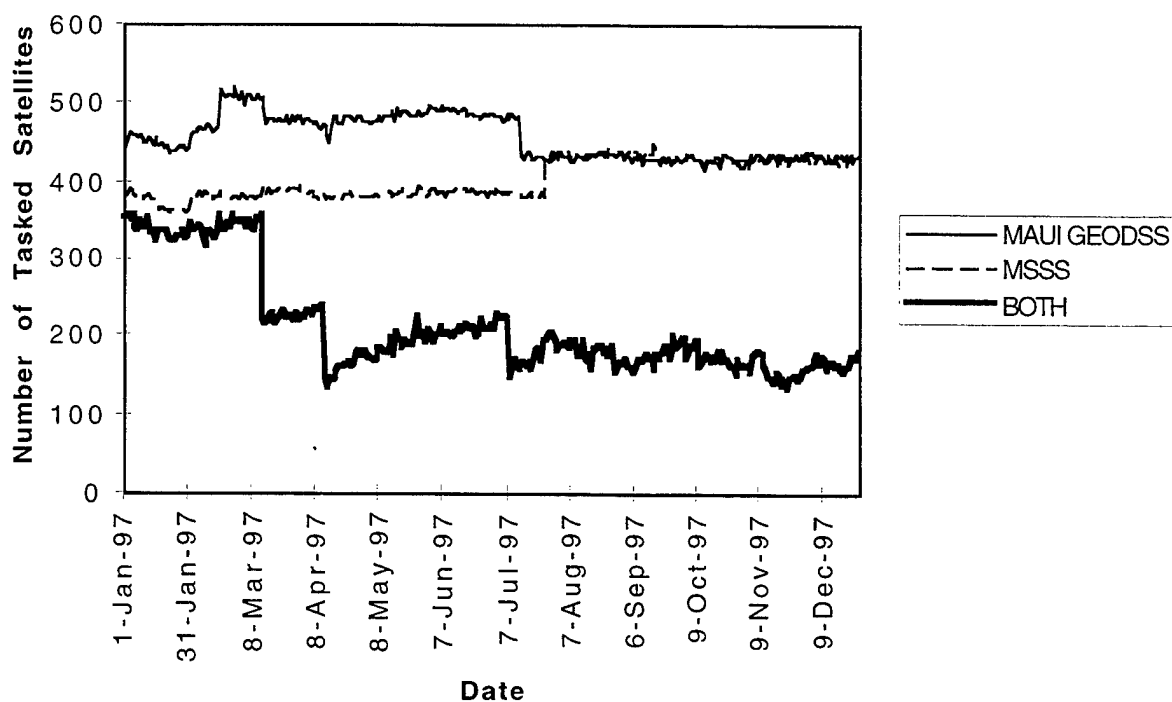
Figure 10. Duplicate Tasking to Maui GEODSS and MSSS

Figure 11 shows the number of satellites excluded from each site by orbit class. It is evident from the graph that many more satellites in non-synchronous orbits have been excluded from MSSS than from Maui GEODSS.
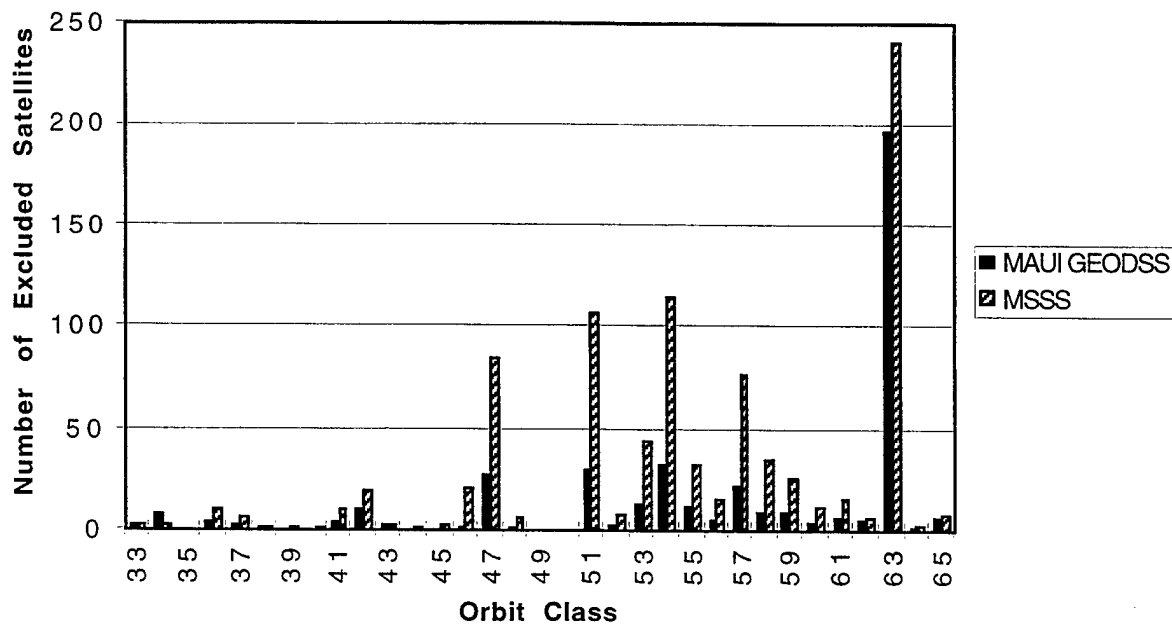
Figure 11. Excluded Satellites by Orbit Class

Tasking group 610 contains deep-space satellites whose epoch age exceeds 5 days and whose perigee is low enough to possibly have a conjunction with the Mir or Shuttle. The collision avoidance function in SPADOC is run against the whole satellite catalog to find conjunctions with the Mir, and with the Shuttle when it is up. The purpose of this tasking group is to obtain high tasking on satellites with potential conjunctions with the Mir or Shuttle, and hopefully update the old element sets. The tasking group is set up to task each satellite at category 2 to all deep-space sensors, all phased-array radars, and the NAVSPACECOM fence for every pass. The collision avoidance function's accuracy depends on the epoch age of the element sets since propagation errors grow as a function of time since epoch. The members of this group change daily as satellites are moved back to their regular tasking group after their elements sets are updated, and new satellites are added to the group as their epoch ages exceed 5 days. Figure 12 shows the number of tasked objects and acquired objects in tasking group 610 for each site for November 1997. Figure 13 shows the object response rate (objects acquired divided by objects tasked times 100) for each site. ALTAIR clearly has the highest percentage response rate for November 1997.
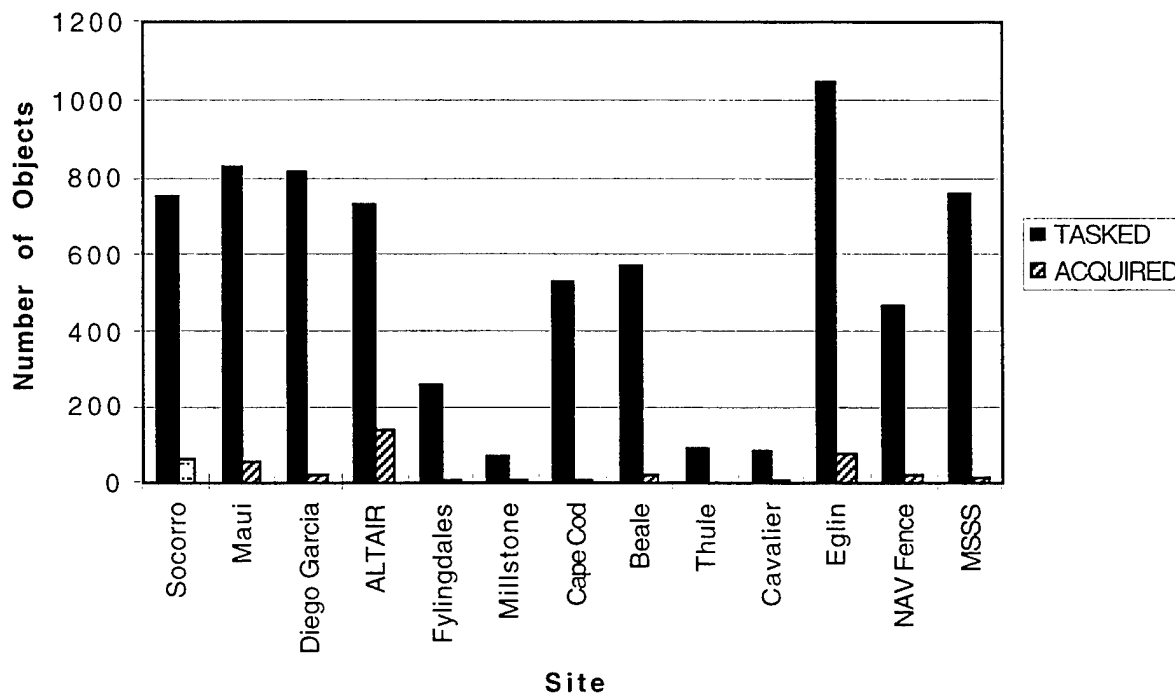
Figure 12. Site Response for Tasking Group 610 for November 1997

In conclusion, 250 to 400 deep-space satellites are not tasked by SPADOC each day because of insufficient deep-space sensor resources. However, for routine catalog maintenance, it is not necessary that these satellites be tracked every day. Tasking groups have been defined in SPADOC to manage the deep-space sensor resources for routine catalog maintenance of low interest satellites and to meet operational requirements for high interest satellites. Lost objects in the geosynchronous belt comprise the largest part of the deep-space lost list. Intensive manual effort in UCT processing reduced the deep-space lost list to its lowest size in 1997, but it began to grow again when the intensive manual effort subsided. Newly lost deep-space satellites are easier to recover by manual effort than long term lost satellites. The Space Based Visible (SBV) sensor may help reduce the long term deep-space lost list when it is added to the SSN in 1998. The SBV sensor has the unique capability to scan the entire geosynchronous belt.

Closure of the Pirinclik radar in February 1997 has severely reduced the coverage of the geosynchronous belt in the eastern hemisphere and made it more difficult to maintain current
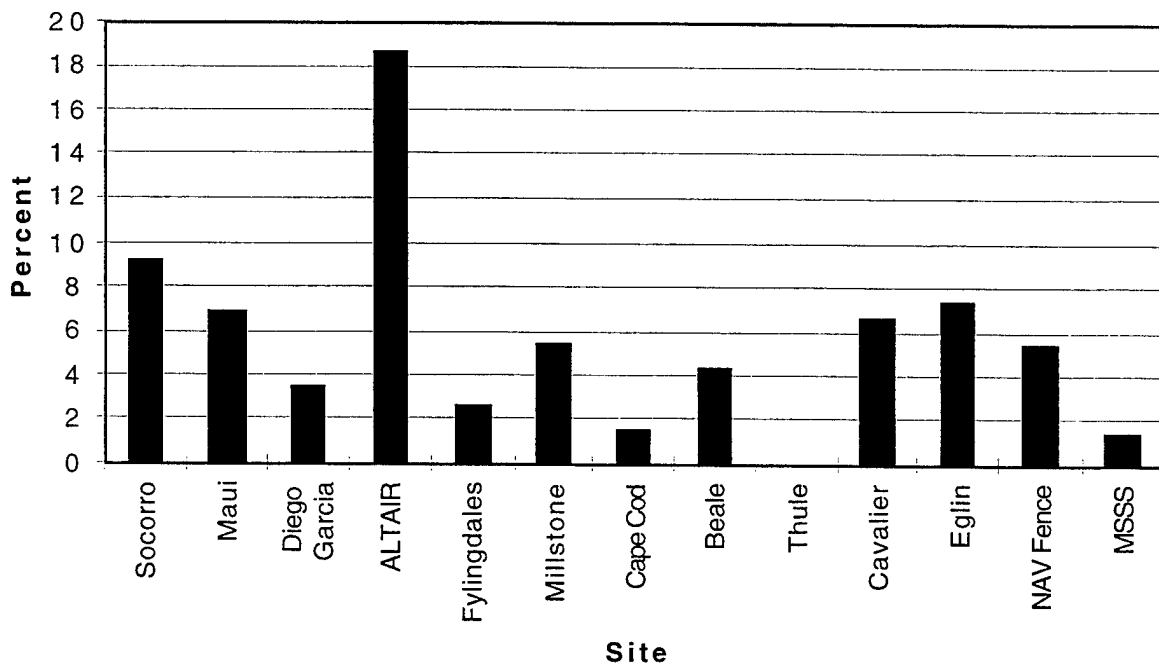
Figure 13. Site Response Rate for Tasking Group 610 for November 1997

element sets on high interest satellites in that region of the belt. The loss of Pirinclik has been mitigated by allowing SPADOC to dynamically adjust the tasking priority of these high interest satellites based on epoch age. Addition of the Transportable Optical System (TOS) to the SSN in Moron, Spain in 1998 will increase coverage of the eastern hemisphere.

Duplicate tasking to Maui GEODSS and MSSS has been greatly reduced but not eliminated through the ability to exclude individual satellites from being tasked to particular sites in SPADOC. The duplicate tasking problem can be eliminated when the MSSS comes under the control of the Optical Command, Control and Communications Facility (OC3F). However, the initial operational capability of the OC3F in 1998 will only control the three GEODSS sites.

The deep-space Mir and Shuttle conjunction tasking group heavily tasks the SSN for objects that are difficult to track. New techniques that best utilize SSN resources to intelligently search for these objects need to be developed.

THE COLLISION VISION PROTOTYPE ASSESSMENT SYSTEM

16th Space Control Conference at MIT Lincoln Laboratory
D.L. Oltrogge, R.G. Gist (The Aerospace Corporation)

Introduction and Background

This paper discusses the background, description, and prototypical application of The Aerospace Corporation's "Collision Vision" prototype system. Collision Avoidance (often referred to as COLA) is the process of determining when two space objects will be at some distance apart such that those objects are at risk of a collision (termed a "conjunction"); this process should provide a decision maker with all the data necessary to determine whether an evasive maneuver is required. Collision avoidance analysis has been utilized for many years. The first capability to perform Collision Avoidance was implemented at Cheyenne Mountain Operations Center (CMOC) in the mid-1960s.

Due to limitations in existing analysis systems, in January of 1996 The Aerospace Corporation proposed the utilization of (1) Ephemeris Reconstruction to address the lack of variable trajectory and powered flight modeling; (2) Using dynamic keep-out volumes based on realistic launcher and on-orbit dispersion data; (3) Probability Analysis to address lack of risk assessment; and (4) Automated display and integration of the analysis results. U.S. Department of Defense and National customers quickly became interested in such a system.

These customers tasked The Aerospace Corporation to create a prototype system demonstrating these approaches, since the anticipated minimum development time of three years for a similar operational capability was deemed unacceptable. Customers then procured an Silicon Graphics Maximum Impact R10000 workstation and a Windows NT Pentium Pro 200 MHz PC for The Aerospace Corporation to use while prototyping their proposed system, which was delivered in February, 1997. Collision Vision has been implemented on this prototype hardware and is currently being ported to other platforms. These implementations have been used to support real-time "shadow-mode" operational supports as well as more general, "global threat" assessments for various customers.

It has become useful to differentiate between COLAs for launching boosters/upper stages/payloads (termed "Launch COLAs") and COLAs for on-orbit objects (termed "On-Orbit COLAs"). Due to the customer emphasis and interest in Launch COLAs, Collision Vision has provided particular emphasis to correcting the inabilities of current Launch COLA analysis systems to model/perform (a) powered flight; (b) variable/RAAN-constrained missions; (c) vehicle dispersions; (d) risk assessment; (e) conjunction visualization; (f) orbital element-set age-dependent computations; and (f) integrated tool analysis able to produce a Mission Director-ready output product.

Overview of Components in a Full-Functionality COLA Analysis System

Through dialogue with our customers and investigations using the Collision Vision prototype system, the components which are required to provide the data a decision maker requires can be broken down into seven primary functional areas. If a decision maker's satellite(s) of interest are termed "primary objects" and the other objects which the primary object(s) may conjunct with are termed "secondary objects," these functional areas are defined as follows:

1) **Collision Avoidance Input Data:** Properly performing Collision Avoidance requires a number of inputs. These inputs include (a) information necessary to determine the state of all primary object(s) as a function of time (e.g. trajectories for each launching or on-orbit object or state vectors and thrust profiles for trajectory reconstruction); (b) information necessary to determine the uncertainties in the state of all primary object(s) as a function of time (e.g. covariances); (c) information necessary to determine the state of all secondary space objects (e.g. the complete Resident Space Object (RSO) SATFILE containing two-card element sets for all tracked space objects); (d) information necessary to determine the uncertainties of all secondary space objects (e.g., the RSO dispersion information obtained via the Air Force Space Command (AFSPC/DOY) funded Space Surveillance Performance Analysis Tool (SSPAT) effort at CMOC).

2) **Ephemeris Generation and/or Reconstruction:** For the primary object(s), the requirement to be able to model powered flight and handle variable trajectories drives the need to be able to generate and/or reconstruct an ephemeris. The Aerospace Corporation, drawing from many years of variable trajectory modeling using ephemeris reconstruction techniques, successfully applied this technique to COLA analysis. Since that time, The Aerospace Corporation has also demonstrated the value of using contractor-provided, in-line detailed guidance simulations to generate ephemerides.

For the secondary objects, analyses rely upon vectors provided by orbit determination techniques applied to Space Surveillance Network (SSN) space observations. As such, ephemeris generation must either use propagation algorithms (e.g., SGP4 or SP) which are consistent with the orbit determination methods originally used, or perform state vector epoch point conversion to obtain a corresponding element set for a different propagation model.

3) **Covariance Generation and/or Reconstruction:** For the primary object(s), the requirement to correctly detect conjunctions and perform risk assessment drives the need for the generation and/or reconstruction of dispersions as a function of time. The Aerospace Corporation, again drawing from launch support experience and an existing tool set, successfully applied covariance reconstruction techniques to contractor-supplied dispersion data for COLA analysis.

For the secondary objects, Collision Vision makes use of error information obtained from the SSPAT effort. This information is the best currently available for CMOC-derived RSO element sets. It assumes that real-time radar observations may be treated as truth; this assumption may need modification for deep-space objects. Also, the error information is a Root-Sum-Square error magnitude and must be coupled with another customer's analyses to determine how to derive a reasonable 3-dimensional error volume.

4) **Conjunction Assessment:** Conjunction assessment is the process of determining which close approaches exceed a user-specified close approach threshold and may result in a collision. The vast majority of tool development, other than the Collision Vision prototype system, has only concentrated in this one functional area. Such tools as COMBO (developed in mid-1960s, operationally used today), ORBWIN (developed in early 1990s to be able to model powered flight, but not transferred to CMOC primary operational computer system and no longer available), PVM-COMBO (developed in 1995 at Naval Research Laboratory to perform COLA analyses using parallel processing), and the new CALIPER tool (created by Kaman Sciences to analyze variable trajectories) all fall into this functional area.

5) **Risk Assessment:** Risk assessment is the process of taking conjunctions which have been found in the conjunction assessment functional area, coupled with information on the dispersions of the conjuncting objects, and determining their probability of collision. The need for this functional area, which is not implemented in current systems, should be readily apparent for predicted conjunctions between objects which have large dispersions about their nominal positions; such objects, in reality, have only a very remote chance of actually hitting each other. The lack of a risk assessment capability, as application of the Collision Vision prototype system demonstrates, results in lost launch opportunity.

6) **Conjunction Visualization:** Being able to visualize conjunctions has proven invaluable to determine how the objects and their dispersed volumes are interacting, providing insight into analytical results.

7) **Generation of Summary Information for Decision Makers:** Creation of COLA Summary Information is the final functional area of a complete system. These concise charts need to quickly convey the pertinent information to the decision authorities. Current systems make use of a separate organization to generate the summary information. The Collision Vision system has combined this functional area with the others, resulting in a single integrated analysis package run by a single organization.

Prototype System Description

The Collision Vision prototype system is comprised of software components which fall into each of the above functional areas. The system allows the user to perform end-to-end analysis of potential collisions and has been designed to support real-time use. This allows the user to perform preliminary assessments, followed by several update runs as launch time approaches. The full intent of Collision Vision is to provide the best set of tools in each functional area, allowing the user to compare and contrast the relative merits of the various algorithms the tools implement. The system is shown in Figure 1.

The prototype system utilizes realistic dispersion keep-out volumes for both launcher and Resident Space Objects (Figure 2). In general, this utilization results in fewer predicted conjunctions and therefore a reduction in launch window holds due to COLA assessment.
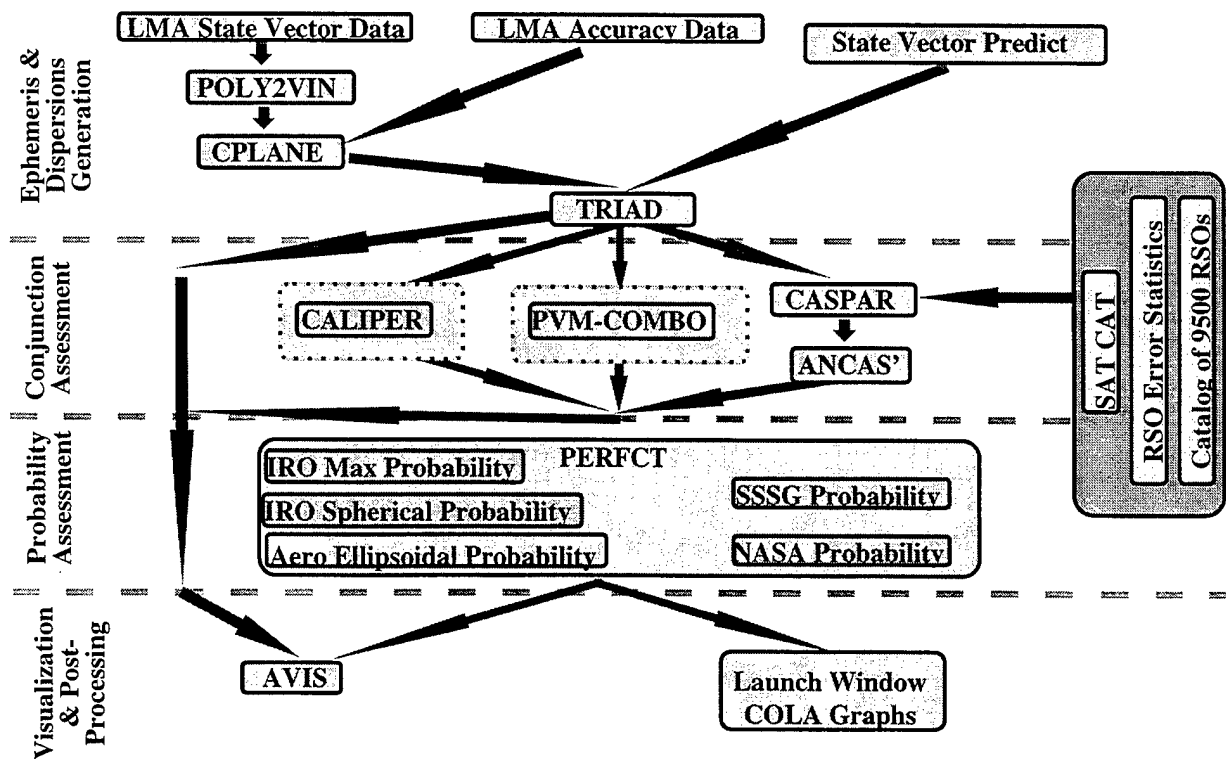

Figure 1: Components of the Collision Vision Prototype System

Software Component Validation Status:

The status of each of the prototype system functional areas is summarized in Table 2, and is as follows:

The ephemeris reconstruction functionality is addressed via software tools called CPLANE and State Vector Predict (SVP). CPLANE has been verified and validated by the Space Warfare Center/Analysis and Engineering (SWC/AE). SVP is used operationally for state vector and ephemeris generation/prediction

The testing which SWC/AE performed illustrated the benefits of both CPLANE and an Eastern Range tool called Theoretical Trajectory Generator (TTG). CPLANE was found to be approximately 5 times more accurate than TTG during powered flight segment reconstruction, while TTG was found to be approximately 2 times more accurate than CPLANE during coasting phases, but ran approximately 15 times slower. Both tools were demonstrated to be of sufficient accuracy for the COLA assessment role. The future intent is to investigate the addition of the TTG algorithm into the existing CPLANE tool, providing users with the best ephemeris reconstruction capability possible.

The conjunction assessment functional area has been rigorously tested (completed 22 July 1997) by SWC/AE as part of the test to ensure that the USSPACECOM Kaman Sciences CALIPER conjunction analysis tool was validated to support the Cassini mission last fall and to ensure that the CASPAR conjunction assessment tool is validated for Government use. The CASPAR conjunction assessment tool incorporates a well-established conjunction assessment module created by Col. Sal Alfano while stationed at Air Force Research Labs (formerly Phillips Labs).

In the probability assessment functional area, Collision Vision currently incorporates four distinct probability tools. These tools vary widely in methodology, precision and run time, and the prototype system facilitates making tradeoffs between the various models. Tests have been performed which demonstrated consistency between several algorithms and evaluations are on-going. Several in-house statistics and mathematics experts are reviewing not only the models currently implemented in the prototype system, but also other proposed probability models.

The visualization and post-processing functional areas are display and data reformatting tools. Based on standard Verification, Validation, and Accreditation practice, such tools are validated by ensuring that the tool's output matches the supporting input data. In addition, visualization tools have the added benefit that tool errors are typically readily apparent.

Tool Description	Validation Authority	Test Cases Run	Accepted?
Trajectory Generator	SWC/AE	33 Cassini trajectories (including both powered and coast phases)	Yes
Conjunction Analyzer	SWC/AE	Cassini trajectories for two days against 10 test objects and also against full catalog	Yes
Integrated Trajectory through Conjunction	Results agreed with SWC/AE approved results	Same as above	Yes
Probability Estimation Modules	SSSG, NASA, Aerospace, and others	Probability theory check and module result comparison for selected cases	Pending
Integrated Trajectory, Conjunction, and Probability	Pending	Pending	Pending

Table 1: Software Validation Status

CMOC Tool Descriptions

During the validation process the Collision Vision prototype was rigorously compared with results from CMOC. Though the tools used at CMOC have known limitations, they provide a starting point from which to measure potential improvements demonstrated by the prototype system. The first orbit conjunction tool used by CMOC was created in the mid-1960s and models spacecraft free-flight trajectories based on state vectors provided for the desired segments of flight. This tool, called COMBO, has the ability to create an Earth-fixed trajectory and apply this trajectory at any point across the launch window of interest. The tool rotates the trajectory through the continuous launch window (as opposed to discrete steps) and searches for close approaches to each RSO that falls inside a static elliptical keep-out region. The entry and exit times to this region (plus additional padding due to element set age) are then considered to be launch hold periods. Benefits of this software tool are that it is relatively fast and it models launch window holds to sub-second accuracy. Drawbacks are that it cannot model any type of variation in trajectories due to delay into launch window, in-flight steering, or powered flight. Additionally, the element set age padding algorithm appears to be of a coarse fidelity. Also, conjunctions for Titan launchers (which launch on the exact minute) are flagged based on missed distance corresponding to the worst-possible launch time, which may not be near an exact minute. Finally, there is no provision for estimating conjunction probabilities, trajectory dispersion, or dynamic keep-out region modeling.

The CALIPER tool was installed at CMOC prior to the Titan IV B-33 Cassini launch (Oct. 1997). This software was designed specifically for this single mission, but improved upon the existing tool, COMBO. CALIPER has the ability to utilize trajectories generated from an external source. This allows the option of having an external tool or agency model trajectory variability and powered flight portions of ascent. CALIPER is primarily a conjunction assessment tool which has compared very favorably with the equivalent portion of the prototype system. It has the drawback, however, of assessing conjunctions based on distance alone, and not based on the known dispersions of the launcher and the RSOs. In practice, these dispersions were used to determine a coarsely-defined keep-out distance relative to a pre-determined probability of risk threshold.

Results

The Collision Vision prototype system has been exercised in an operational environment for multiple launch attempts of four actual spacecraft launches. The results, while not used to make operational decisions, were rigorously compared with official COLA products generated by Cheyenne Mountain Operations Center (CMOC). In order to compare algorithmic differences alone, identical input data were used wherever possible. The principal input data set is the catalog of mean orbital elements (two-card NORAD element sets) representing the trackable RSOs (Resident Space Objects) in Earth orbit. The entire catalog used by CMOC in their COLA analyses (including classified element sets) was transferred to the prototype system at various time points prior to launch. The Collision Vision system was utilized at each of these times (launch time minus 48 hours, 24 hours, and 4 hours) and compared with CMOC results when available. The entire unclassified launch window was examined at the required discrete resolution. For Titan boosters, launch is initiated on the exact minute; for Pegasus, launch is possible on any second. For the Titan launches, delays of up to two seconds after the exact minute were also examined.

Individual Mission Results

Titan A-18

This mission provided an opportunity to emulate the CMOC tools and had the potential for close agreement. The mission profile included an ascent trajectory which was fixed in the Earth-relative frame. There was no trajectory variability due to delays into the launch window, no in-flight re-targeting, and since there was no upper stage, there was no thrusting being performed after injection into orbit. The only expected differences in the modeling were: (1) the ability of the prototype system to model a dynamically changing keep-out ellipsoid around the launcher and the RSOs (as opposed to CMOC's static keep-out region); and (2) CMOC's "padding" of the computed COLA due to RSO element set age. The Collision Vision system simulated both static and dynamic keep-out ellipsoids for

comparison purposes. The coarse-fidelity algorithm used to pad the COLA blackouts due to element set age was not modeled; the prototype system used instead the best-available error and error growth statistics to estimate RSO error due to element set latency.

Results from the mission were as expected. The prototype system found fewer conjunctions than did the CMOC system. Those conjunctions that were found were a proper subset of CMOC conjunctions. For those common conjunctions, the duration of the COLA launch hold was shorter for the prototype system when emulating the CMOC system due to discarding the element set age padding in favor of the error growth statistics. The durations were further reduced when using a dynamically changing ellipsoid keep-out region based on expected dispersions during flight. A typical comparison of COLA holds calculated by both systems is tabulated in Table 2 below, and a graphical illustration of the differences in COLA hold durations is shown in Figure 3. These mission results provided confidence that the prototype system was able to accurately emulate the COMBO program, and that precision refinements available from Collision Vision would indeed improve launch availability.

Time (sec):	2910.00	**Collision Vision**	A (km):	57.75
Altitude (km):	658.26		B (km):	6.75
Velocity (km/s):	7.48		C (km):	1.87

Westford Needles

Relative Range (km):	23.95
Closest Approach (km):	17.74
Closest Approach (sec):	2908.84
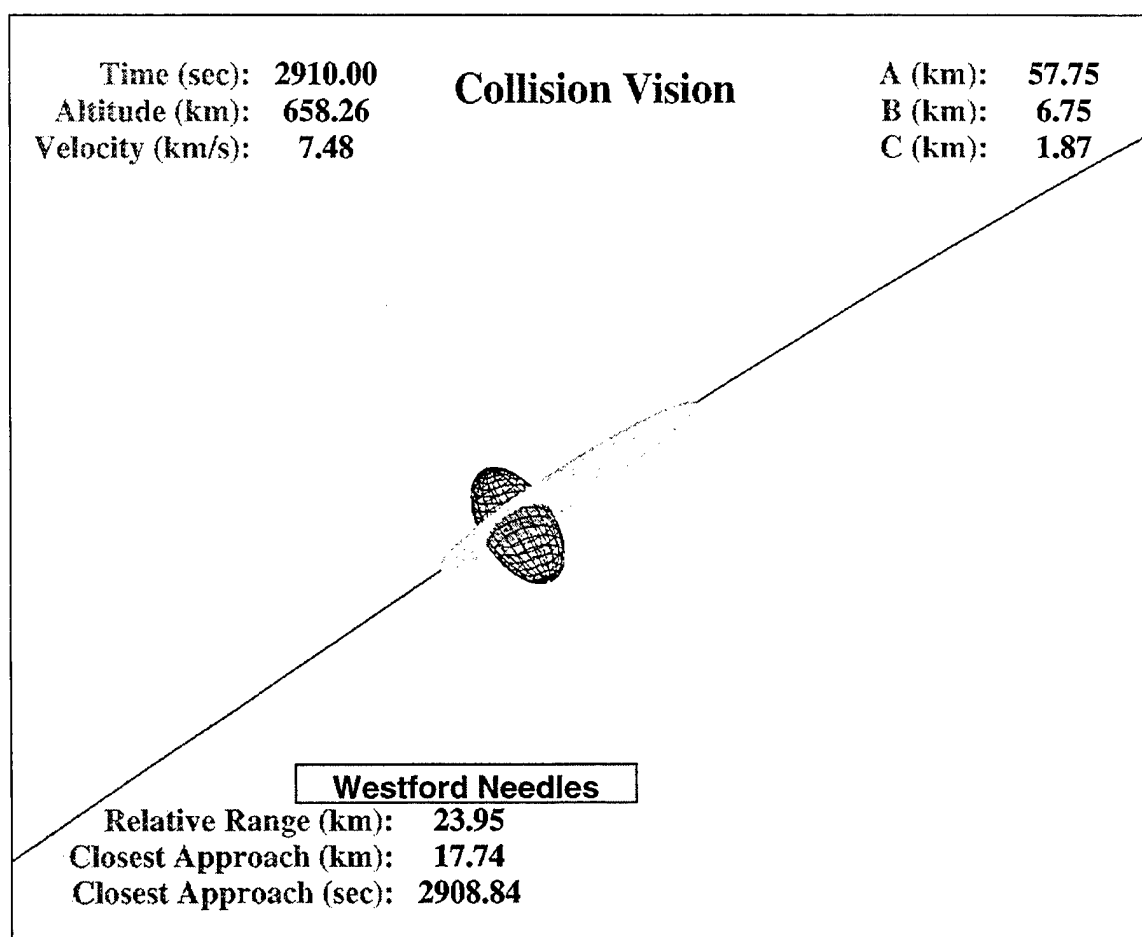
Figure 2 - Conjunction for Titan A-18 Mission Using Dynamic Dispersion Volumes

Case ID	Resident Space Object Number	Exact Minute Launch Time (hr:mn)	COMBO Off-Integer Minimum Time of Closest Approach Launch Delta Time (sec)	COMBO Time of Closest Approach (hr:mn:sc)	COMBO Miss Dist (km)	COMBO Bounding Miss Dist (Assumes 7.5 km/s closing velocity)	Collision Vision Miss Dist (km)	Collision Vision Time of Closest Approach (hr:mn:sc)
A	Unspec	02:32	- - - -	- - - - - -	- - - - -	- - - -	0.4	03:09:38
B	24135	02:35	+1	03:21:33	1.7	9.2	5.6	03:21:33
C	14631	02:38	-7	03:19:29	2.1			
D	01347	02:38	+10	03:10:01	3.1			
E	24965	02:40	+1	03:22:53	7.8			
F	24926	02:42	-6	03:30:05	7.8			
G	24847	02:43	-3	03:00:43	4.3	26.8	20.0	03:00:44
H	24979	02:46	-5	03:29:02	5.3			
I	24966	02:48	+5	03:30:37	3.0			
J	05400	02:55	-8	03:25:15	0.7			
K	21827	02:56	+7	03:14:33	1.5			
L vs P/L	16609 (MIR)	02:59	-6	04:34:40	72.9	117.9	81.6	04:34:42
M vs R/B	16609 (MIR)	02:59	-5	04:34:40	73.0	110.5	78.6	04:34:42
N	24387	02:59	-8	03:45:13	4.5			
O	23940	03:02	-2	03:30:25	7.4			
P	24583	03:03	-6	03:29:59	7.5			
Q	05021	03:03	-3	03:43:56	7.4			
R	18999	03:12	+6	04:00:31	1.8	46.8	18.8	04:00:29
S	24526	03:13	0 (+/- 0.5)	03:56:32	3.9	7.65	4.7	03:56:33
T	Unspec	03:18	+1	04:05:12	2.6			
U	16878	03:21	+4	03:40:26	7.6			

Table 2 - Typical Comparison Table for A-18 Mission (Obj #18999 corresponds to "Westford Needles" in Fig. 2)
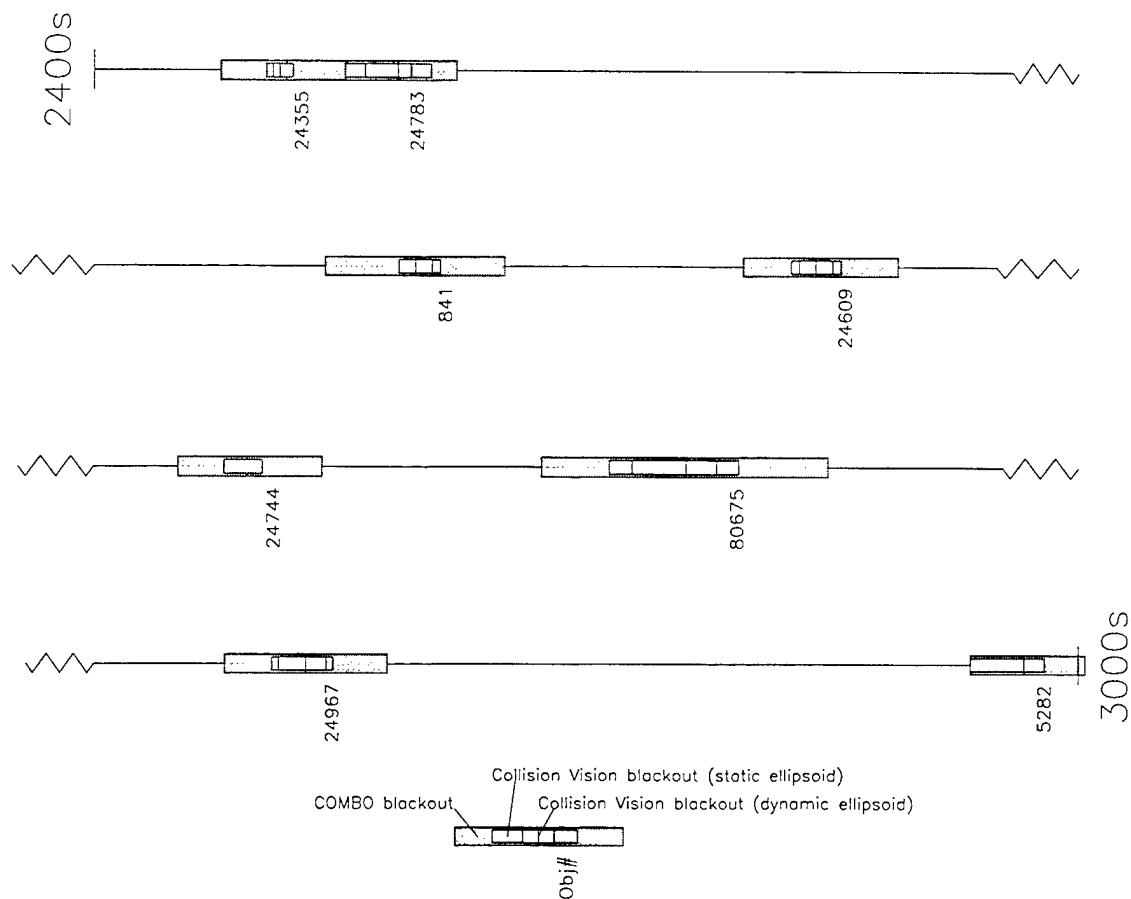
Figure 3 - Detailed Comparison of Ten Minutes of COMBO and Collision Vision for A-18 COLA Analysis at a Discrete One-Second Resolution

Titan A-17

This mission highlighted the differences resulting from a low-resolution modeling of trajectory variability across the launch window. The COMBO program was able to model the variability in only a limited way by using sparse (four) data points across the launch window and was unable to model powered flight. The prototype system used the contractor tool State Vector Predict (SVP) to generate a trajectory at each point of interest in the launch window. The discrepancies shown in Table 3 were therefore anticipated and can be observed to occur after the second stage burnout, at which time the trajectory variability becomes significant. The table shows no conjunctions in common between COMBO and the prototype system, illustrating the importance of correctly modeling variable trajectories.

Titan B-33 (Cassini)

CMOC used the CALIPER code to determine conjunctions for the Cassini mission in October 1997. This code is a conjunction analyzer which was validated concurrently with the prototype's conjunction analyzer CASPAR. During these validation tests, close agreement between CASPAR and CALIPER was observed. The trajectories for the Cassini mission were generated from launch polynomials used by both CMOC and the prototype system, and therefore were nearly identical. The only differences in results for this mission thus resulted from differences in how the probability of collision threshold was handled. The CALIPER program was designed to ensure identification of all conjunctions with a worst-case probability greater than a specified amount. As a result, a worst-case geometry was assumed for all conjunctions and a large spherical keep-out region was used. This approach is excessively

30

conservative if launcher and RSO covariances are available to enable analysis of the actual geometry as opposed to the worst-case scenario. Such covariance information is available in the prototype system, which enabled the calculation of actual probabilities of collision. Conjunctions at or above the given probability threshold were identified to determine launch holds. The comparison between CALIPER and Collision Vision B-33 results highlighted these differing approaches. As expected, the increased fidelity of the probability modeling in Collision Vision resulted in a significant decrease in launch holds determined for the Cassini launch.

Pegasus (STEP Mission)

The Pegasus launch analysis resulted in the severest test of the prototype system's computing resources. The STEP launch was analyzed using a much larger dispersion model than those used for Titan IV launches. This resulted in more identified conjunctions, thus slowing the conjunction assessment phase of the analysis. In addition, the launcher was available to begin ascent at any given second in the launch window (as opposed to exact minute Titan launches). This resulted in a larger number of trajectories to analyze, which increased both hard disk space requirements and computational time. These requirements exceeded the resources of the prototype system (see Table 4). As a result, the system was used only to examine the mission's interaction with manned objects (Mir and Shuttle). These limited conjunctions were determined accurately when compared with CMOC results.

Summary of Results

The following tables summarize some of the results of applying the Collision Vision system to launches using real operational data. Table 3 details collision avoidance launch holds determined by both systems and the degree of commonality between the differing approaches. These results reflect the analyses performed nearest to the launch time in each case. Table 4 illustrates typical computational requirements to perform a standard COLA analysis for each mission using Collision Vision. In some instances, requirements exceeded the capacity of the prototype system, in which case a limited analysis was performed and the resource requirements were estimated. Typically, a COLA analysis must be finished about an hour before launch; the prototype system hard disk is limited to 4 Gigabytes.

Mission	Total COLA holds	Collision Vision-only COLA holds	CMOC-only COLA holds	COLA holds in common
A-18 attempt #2	20	0	14	6
A-18 launch	11	0	8	3
B-33 attempt #1	24	0	18	6
B-33 launch	18	3	7	8
Pegasus launch (against manned objects only)	2	0	0	2
A-17 launch	5	3	2	0

Table 3 - Comparison of CMOC and Collision Vision COLA Holds

Mission	Ephemeris (min)	Conjunction Assessment (min)	Post-Processing (min)	Total Time (min)	Disk Space (GB)
A-18 (on exact minute)	5	10	10	25	0.1
A-18 (0,1,2 sec off exact min)	10	15	10	35	0.3
A-18 (on each second)	200	300	15	515	6.0
B-33 (0,1,2 sec off exact min)	25	35	15	75	0.7
Pegasus (0,1,2 sec off exact min;large disp.)	15	75	10	100	0.5
Pegasus (on each second;large dispersions)	300	1500	40	1840	9.0
A-17 (0,1,2 sec off exact min), Using SVP	100	15	10	125	0.3

Table 4 - Time and memory requirements

Conclusions

A prototype Launch Collision Avoidance system has been developed which uses state-of-the-art techniques to maximize launch window availability based on best available data. These data include accurate trajectories and expected launch dispersions and the latest available Resident Space Object element sets and the expected errors in their positions. From this information, the prototype system, Collision Vision, determines not only geometrical conjunctions but the associated probabilities. This is a critical factor in assessing the degree of risk for a given collision, and it is an item that is currently unavailable from any other source. Outputs include summary information to be used as a decision tool by launch directors and a 3-dimensional representation of the conjunction geometry for detailed analysis purposes. Multiple algorithms are available in some of its functional areas in order to exercise flexibility and evaluate different methodologies.

Validation of components of the Collision Vision system has been performed by CMOC support organizations and has advanced in parallel with certain tools used operationally by CMOC. The results of validation have shown that the examined portions of the prototype system perform accurately and appropriately. Validation of the probability functionality of the system is progressing.

Collision Vision has been used for COLA analysis in multiple launch attempts for four actual launches. Results from the system have been rigorously compared with operational outputs from CMOC. Differences in the two systems have been highlighted by the variety of the missions supported, and the anticipated improvement in COLA accuracy and precision due to the fidelity of the Collision Vision modeling has been demonstrated.

Existing COLA tools used by CMOC have an established heritage and validity. They have known limitations, but are currently the best tools being used operationally. It is anticipated that the Collision Vision prototype system described herein can be used to help focus and/or augment the current operational COLA capabilities at CMOC and improve their ability to provide accurate launch window availability advice in order to lower launch collision risk and assure improved access to space.

<u>The 488,006,860 Sources in the USNO-A1.0 Catalog</u>

D. G. Monet (U. S. Naval Observatory Flagstaff Station)

The USNO-A1.0 catalog, the largest star catalog ever compiled and the first in a new series of star catalogs being produced by the U. S. Naval Observatory, was designed for users with operational requirements for an all-sky catalog of star positions and brightnesses. It is available by request (see *http://www.usno.navy.mil/pmm/* for details) on 10 CD-ROMs, but quantities are limited and requests will be judged on their merit. No direct web access to the catalog is available yet, but several third parties serve portions of it. The needs of most users should be satisfied by the single CD-ROM "executive summary" catalog, USNO-SA1.0, which contains 54,787,624 entries and whose distribution is unlimited. In either catalog, each entry contains the right ascension and declination in the system of J2000, and the blue and red magnitudes.

INTRODUCTION

The U. S. Naval Observatory (USNO) is about 4 years into the production phase of the Precision Measuring Machine (PMM) program, and the first products are being released. The goal of the program is to produce deep (fainter than 18th magnitude), dense (beyond 10^5 sources per square degree when possible) star catalogs. The purpose of this paper is to discuss the usage of the first of these, USNO-A1.0, for computing the celestial coordinates of uncorrelated targets, and removing star clutter so that such objects can be identified from a single image. Only a brief introduction to the PMM program is presented here because the full discussion is available on the CD-ROMs or from the Web URL listed in the abstract.

The PMM program is based on the digitization and analysis of photographic sky surveys done by the Palomar Observatory, the European Southern Observatory (ESO), or the Anglo-Australian Observatory, depending on declination zone and epoch. North of $\delta = -30°$, the sky has been photographed in two colors (blue and red) at each of two epochs (mid-1950s and late-1990s). South of $\delta = -30°$, there are first epoch (mid-1970s) blue and red surveys but only a second epoch (late-1990s) red survey. The PMM has processed essentially all of these plates as well as those from several other surveys, and has produced an image database containing about 6 trillion pixels and a catalog database containing 52 bytes of data for each of about 6 billion objects. Because these databases are too large to serve and are quite difficult to manipulate, USNO is producing a sequence of catalogs intended to satisfy the needs of most users. When computing and networking technology is ready (and cheap!), USNO intends to make the entire archive available so that users with special needs can have access to it.

The first large PMM catalog is USNO-A1.0. It was generated by comparing the detection lists from the Palomar Observatory Sky Survey I (POSS-I) blue and red plates north of $\delta = -30°$ and the Science Research Council (UK) blue (SRC-J) and ESO red (ESO-R) plates south of $\delta = -30°$. Each coincidence between a blue and red detection within a 2 arcsecond aperture was deemed a real object, and no other image parameters (magnitude, color, shape, etc.) entered into the selection process. The resulting catalog contains 488,006,860

entries, and lists α and δ in the system of J2000, and m_{blue} and m_{red}. No information about the type of source (star, galaxy, etc.) is presented. The limiting magnitude is about $m_{blue} = 21/m_{red} = 20$ in the north, and about one magnitude fainter in the south (the southern plates are of higher quality). With 12 bytes per source, the catalog occupies about 6 GBytes and is published on a 10 CD-ROM set. The CD-ROMs also contain various READ.ME files, $tar()$ files of source and calibration codes, and a look-up table between USNO-A1.0 and the Space Telescope Science Institute's Guide Star Catalog 1.1.

At the request of members of the asteroid community, a spatially culled version of USNO-A1.0 was produced. This catalog, USNO-SA1.0, is a compromise between the size of the catalog and the need for reference objects, and was generated by sampling USNO-A1.0 to produce as uniform a surface density (about 1 per 2.5 square arcminutes) as possible. It contains 54,787,624 sources, fits on one CD-ROM, and is intended for systems with relatively large fields of view.

ABANDONING THE TELESCOPE MOUNT MODEL

A necessary but unpleasant task for essentially all astronomical observations is the computation of coordinates for objects of interest. In the past, a popular method was to equip the telescope with accurate encoders, to calibrate them using observations of "catalog stars" whose coordinates were known, and to determine the scale, rotation, and field distortions of the detector system. Such a "mount model" can produce astrometric accuracies of a few arcseconds, but extreme care is needed to do better than ± 1 arcsecond and typical accuracies are nearer ± 10 arcseconds. This method has not changed in the last century or so, and the prospects for significant improvements in astrometric accuracy are dim.

The need for a mount model astrometric algorithm disappears if there are many catalog stars in each image or field of view. Instead of using the telescope and detector to interpolate between known objects, the coordinates of the catalog and other objects can be measured and the transformation from (x,y) to (α,δ) can be computed from each image. When used in this differential manner, most image sensors are stable at sub-micron levels, and in most cases, the astrometric accuracy is limited only by the accuracy of the reference catalog. For most regions of the sky, the accuracy of USNO-A1.0 is about 0.25 arcseconds, and can approach 0.1 arcseconds over small areas.

The astrometric algorithm is as follows. A "star finder" algorithm examines the image and makes a list of sources. The telescope's pointing and field of view are used to extract a list of reference objects from the catalog. These lists are correlated, the transformation between image and catalog coordinates is determined, and the coordinates for all the other sources in the image are computed. The catalog-based astrometric algorithm offers the advantages of speed, accuracy, and autonomous operation over the mount model algorithm. The accuracy of the telescope's encoders enters as the size of the search radius for the list correlation, and has no effect on the astrometric accuracy of the solution.

Typical systems designed for searching for uncorrelated targets have fields of view that cover most of a square degree. In such fields, there can be hundreds or thousands of USNO-A sources, and the correlation of the lists is unambiguous. Optical systems designed for accurate analysis of faint objects may have fields of view of only a few arcminutes, and

USNO-A usually provides many tens of objects in these small fields. Usually, there are so many USNO-A objects that the effects of optical distortion, telescope flexure, and other problems can be recomputed from each image.

SEARCHING FOR UNCORRELATED TARGETS

The traditional method for searching for slowly moving uncorrelated targets is to take an image, wait an appropriate time, take another, and then identify objects that have moved. In many cases, USNO-A is deep enough and complete enough to identify and remove essentially all of the stationary sources (star clutter) in the image, thereby allowing for the identification of uncorrelated targets from a single image. The success of this approach is limited by the completeness of the reference catalog in the magnitude range of interest.

For a source to be included in USNO-A, it must have been detected on both the blue and red survey plates, and these detections must have been spatially coincident to within 2 arcseconds. The nominal limiting magnitude of the POSS-I O (blue) plate is 21 and that for the E (red) plate is 20. The requirement for blue and red detections means that the limiting magnitude of USNO-A depends on the intrinsic color of the source. Most stars have colors in the range of $0 < m_{blue} - m_{red} < 1$, so a reasonable estimate is that most objects brighter than $m_{blue} = 20$ are in the catalog. At the bright end, the onset of diffraction spikes occurs at about 15th magnitude, and by 10th magnitude the effects of saturation, spikes, and ghosting are severe.

Assuming that USNO-A goes faint enough for the application, the next concern is its completeness. A simple parameter is impossible to compute, primarily because of the complexity of the sky. The PMM detects and processes every object which exceeds a detection limit defined by the noise of the sky background, and it uses the same algorithm for all parts of the sky. In compiling USNO-A, no criterion other than the spatial coincidence of blue and red detections was used. Therefore, every effort was taken to make the catalog as complete as possible, but a large number special circumstances appear on the sky. The following is an incomplete list of why USNO-A may be incomplete.

1) Objects with extreme colors: As discussed above, the more bizarre the energy distribution of the object, the brighter its limiting magnitude for inclusion in USNO-A. As discussed below, USNO-B should address this problem.

2) Double and multiple star systems: Depending on the separation, difference in brightness, and the seeing and guiding during the observations, the object deconvolution algorithm can produce inconsistent results.

3) Bright stars: A 1st magnitude star saturates more than a square degree of the plate, and its ghosts saturate other areas. Entries for bright stars were left in USNO-A for the purpose of allowing automatic pointing algorithms to avoid them.

4) Galaxies and nebulosity: Extended object have lumps, lumps can be (incorrectly) detected as objects, and such spurious objects can correlate with spurious objects on the other plate.

5) The Milky Way: In some regions, the PMM's processing was limited by the confusion caused image crowding. One should be very careful in regions with more than 10^5 objects per square degree.

6) Plate overlap zones: The POSS plates are 6.5 degrees on a side but are taken on 6 degree centers. Due to difficulties in mapping the plate-to-plate systematic astrometric distortions, some plate overlap zones put multiple occurrences of the same star into the catalog. As discussed below, USNO-A2.0 will address this problem.

Although USNO-A is incomplete, most of the sky is relatively simple and USNO-A provides a reasonably complete list of known objects. Once these have been removed from an image, the task of finding new objects is much easier. In most of the cases pursued by USNO personnel, asteroids, comets, and other uncorrelated targets have been correctly identified using only a single image. This capability provides a significant improvement in telescope efficiency.

FUTURE PRODUCTS

At some level, the products generated by the PMM program are in direct response to the needs expressed by users. Currently, efforts are underway to fix two of the problems discussed above.

1) USNO-A2.0 will be the astrometric recalibration of USNO-A1.0. Major changes include the removal of references to the Guide Star catalog, adoption of the International Celestial Reference Frame, improved removal of the systematic astrometric distortions produced by the various telescopes, and a recalibration of the magnitudes.

2) USNO-B1.0 will combine the first and second epoch surveys so that proper motions and star/galaxy classifications can be computed. Part of this task will be the inclusion of objects found only on the red or blue plates, rather than limiting the catalog to objects found on both the red and blue plates. This should extend the limiting magnitude of the catalog for objects with extreme colors.

The schedule calls for completion of USNO-A2.0 in the summer of 1998, and for the first (probably internal) version of USNO-B1.0 by the end of 1998. The PMM program can respond to special needs, and inquiries should be addressed to the author.

ACKNOWLEDGMENTS

Potential Solutions for Enhanced Space Surveillance Network Capability

Eugene G. Stansbery, NASA/Johnson Space Center
Dr. Ramaswamy Sridharan, M.I.T. Lincoln Laboratory

1.0   Introduction/Background

U. S. Space Command (USSPACECOM) maintains a catalog of resident space objects (RSOs) which includes operational satellites, derelicts, and operational and fragmentation debris. In order to accomplish this, a network of radar and optical sensors called the Space Surveillance Network (SSN) has been established. Part of the space surveillance task is to perform collision warning for high value satellites such as the Space Shuttle, Space Station, and certain DoD assets. The current SSN routinely tracks and catalogs RSOs as small as 10 cm diameter. However, typical operational satellites can be seriously damaged or destroyed by collisions with orbital debris larger than about 0.1-1.0 cm. Several initiatives and studies have been undertaken in an effort to help close the gap in size between tracked and risk objects. These include:

> A 1992 NASA study (Ref. 1, 2, and 3) to determine if collision avoidance could be provided for the Space Station *Freedom* for objects down to 1-cm in size. The proposed network would have cataloged 1-cm objects to 600 km altitude.

> A 1996-97 study by the Space Debris Task Team (SDTT) (Ref. 4) consisting of NASA and the Air Force Space Command (AFSPC) personnel who were given the task to "Examine Space Surveillance Network capabilities to enhance orbital debris data collection and processing on objects (as small as 5 cm) not currently in the satellite catalog."

> A 1997-98 study (Ref. 5) led by Air Force Research Laboratory, Los Alamos National Laboratory, and Lawrence Livermore National Laboratory at the direction of the 1998 Senate Armed services Committee (SASC) authorization bill which, "directs the Secretary of the Air Force to undertake a design study of a system that could catalogue and track debris down to 1 centimeter in size out to 1,000 kilometers in altitude."

> A U. S. General Accounting Office (GAO) released report in December, 1997 on Space Surveillance (Ref. 6) which recommended that "the Secretary of Defense and the Administrator of NASA, in consultation with the Director of Central Intelligence establish a consolidated set of government-wide space surveillance requirements..." and that they "develop a coordinated government-wide space surveillance plan ..."

In addition to these activities, USCINCSPACE, Gen. Estes, requested that NASA formalize it's requirements for space surveillance. In August, 1997, the NASA Administrator delivered the new set of requirements (Ref. 7) to the SSN which included the requirement "to support the JSC (Johnson Space Center) ISS/STS (International Space Station/Space Transportation System) vehicle collision avoidance efforts, track resident space objects (RSO) and maintain a catalog for all objects with perigees less than 600 km and with size as specified in the Time Period column." The time period requirement is "Current: Enhance tracking such that catalog includes objects ≥5 cm; Mid/Far Term; with SSN upgrades, include all objects ≥1 cm."

2.0   The 1992 Space Station *Freedom* Study

2.1   Background

In August 1992, NASA was designing the Space Station *Freedom*. Plans for protecting the station from meteoroid and orbital debris (M/OD) included shielding it against penetrations from objects as large as 0.8 cm and performing collision avoidance maneuvers against objects in the USSPACECOM catalog which

then, as now, included objects as small as the nominal size of 10 cm. This left a gap in debris size to which the station was vulnerable. In August, the NASA Administrator directed that the Space Station Program Office undertake studies which would effectively eliminate this gap. Two study teams were formed in September. The first team studied enhanced or augmented shielding for the station. The second team studied improved tracking techniques.

The tracking team set out to answer the question "was performing collision avoidance for *Freedom* against objects ≥ 1 cm diameter within current technology?" The team reported to the head of the Space Station and the Associate Administrator for Space Flight on December 4, 1992 that it was within the available technology and they proposed a conceptual network of sensors which could perform the job. The estimated cost of $450-550 million to design and build the network was considered too high and no further work on the concept was performed. However, the team's methodology for studying the problem and the lessons learned from the study are still valid and applicable to the more recent initiatives.

2.2   Summary of Findings

2.2.1   Current vs. New Sensors

One of the significant findings, which shaped the 1992 study, was that the existing sensors of the SSN could not be readily upgraded or modified to meet the goals of the study. Radars in the SSN generally operate at UHF wavelengths of ~70 cm. At these wavelengths, objects ~12 cm and smaller are in the Rayleigh scattering regime. In the Rayleigh regime, the radar cross section (RCS) of an object falls off as the 6th power of the diameter. Therefore, in order to upgrade a radar so that it will have the same sensitivity for a 1-cm object that it currently has for a 10-cm object, the power/sensitivity of UHF radars would have to be improved by 60 dB. This was deemed to be an unacceptable solution. Similarly, existing optical sensors in the SSN were not capable of detecting 1-cm objects. Therefore, new sensors were needed to catalog 1-cm debris.

Having eliminated existing sensors, the team started from the ground up looking at the requirements that a new network optimized for the SSN collision avoidance network must meet.

2.2.2   Network Requirements and Tasks

A collision avoidance system (CAS) must perform three tasks: 1) it must generate the catalog of small debris objects; 2) it must maintain the catalog for all objects in the orbital space of interest; and 3) it must reduce the orbit uncertainty for the subset of objects predicted to collide with the high valued target. A fourth, non-mandatory task, is to provide imminent collision warning against objects for which a collision avoidance maneuver is not, or no longer, possible, but for which other mitigating options exist.

In order to generate a debris catalog, a search volume must be established. That volume must search all orbital space within a time period that is short when compared to the lifetime of the objects to be cataloged. In the 1992 study, the SSF was to have flown as high as 450 km altitude during periods of high solar activity. 600 km was chosen as the top of the altitude band of interest. Studies of area-to-mass of debris and orbital lifetimes indicate that some debris can reenter from 600 km in 13 days (area-to-mass of 1.0 m^2/kg) during periods of high solar activity. Therefore, the complete orbit space between these two altitudes should be searched in a time span that is shorter than 13 days. If the probability of detection is less than 100%, then it is desirable to search the volume more than once in the allotted time. Once an object is detected and identified as an "unknown," or uncorrelated target (UCT), the detecting sensor must be able to predict the orbit far enough ahead to be able to locate and track the object at the next track opportunity. The next track opportunity may be by the detecting sensor or by another sensor in the network. After a sufficient number of tracks are performed, an orbit can be determined and the object can be entered into the catalog.

When a sensor updates the location of an object, that location is known to within some error ellipsoid. Subsequent to the measurement time, the error ellipsoid grows due to such things as uncertainties in atmospheric drag or errors in the propagators until the next time that the object location is updated by another sensor. The lower an object is in altitude, the faster the error ellipsoid grows due to the increase in the effects of the atmosphere on the object. If the error in predicted position at the time of the next sensor observation approaches the mean distance between objects, the catalog will fail because re-identification will be impossible. In other words, to perform catalog maintenance, the orbital elements must be maintained well enough to correlate an observation. This is a much less restrictive requirement than the conjunction update task, which will be discussed next, but this requirement applies to all objects in the catalog. The study concluded that in order to maintain a catalog of 1-cm debris, the orbits would have to be updated at least daily. Since this had to be done for the entire catalog, capacity of the sensors was a driving issue. It was determined that one or more of the radars in the network needed to be either a phased array radar or an interferometer fence radar in order to accomplish this task.

A computer program called the Calculation of Miss Between Orbits (COMBO) determines close approaches between high valued targets and all other cataloged satellites including debris. The 1992 study called these close approaches "conjunctions." Simulations have shown that only a few objects per day would be predicted to come close enough to the SSF to cause concern. For these objects, it is necessary to update the orbit in order to decrease the uncertainty in predicted location at the time of the conjunction. One of the objectives of the SSF was to perform micro-gravity experiments. The SSF requirement was to have a 60% probability of achieving 6 periods of 27-30 contiguous days without maneuvering, giving a maximum number of 10 collision avoidance maneuvers per year. Given the number of objects of size >1 cm, this translated into an error ellipsoid of 400 m downrange and 8 m radial and crosstrack. At the low altitudes of SSF, the error ellipsoid would grow quickly due to atmospheric drag uncertainties. It was estimated that an observation would need to be made within two orbits of the predicted conjunction. Since there would only be a few objects per day with predicted conjunctions, these could be handled by lower cost "pencil" beam, dish antenna radars. Optical sensors were rejected because of the probability of not having the correct lighting or weather conditions when an observation was needed.

An observation too close in time to a predicted conjunction would not be useful for collision avoidance. There is a minimum time required to process the data, make the decision to move the station, prepare the station for the maneuver, make the maneuver, and for the maneuver to take effect. This time was likely to be from ½ to ¾ of the period of the SSF orbit.

2.3   Proposed Network

The conceptual collision avoidance network developed during the 1992 study utilized two radars that were being developed at the time. The first was the Ground Based Radar X-band (GBR-X) which was an X-band (3-cm wavelength) phased array radar that was planned for deployment on Kwajalein Atoll in the Marshall Islands. As a phased array radar, GBR-X would have been capable of erecting a debris search fence while simultaneously tracking several targets. Therefore, it could contribute to all three of the CAS tasks. GBR-X was never built as designed, but a variation of the design is still under development as the GBR-P (Ground Based Radar - Prototype) and will be discussed later in this paper.

The second radar under development was the HAVE STARE radar. This was also an X-band radar but was a mechanically steered, dish antenna design. As a dish radar, it could only track one object at a time and therefore was limited to the conjunction update task, which involved tracking a small number of objects. HAVE STARE was completed and is now temporarily located at Vandenberg AFB in California. HAVE STARE and GBR-X were being built by the same contractor and shared many of their major components, including transmitter tubes.

GBR-X and four HAVE STARE radars were to be located with roughly equal spacing within 180° of longitude and as close as practical to the equator. GBR-X was to be located at its planned site at Kwajalein while the HAVE STARE radars were to be located at South Point, Hawaii, Vandenberg AFB, California, Kennedy Space Center, Florida, and Kourou, French Guiana. With this arrangement, the five radars could see any low earth, near circular orbit on either its ascending or descending passage and guaranteed that an object could be seen at least once every 2 orbits (in fact, for most orbits, the objects could be seen on every orbit).

GBR-X would not, by itself, have the capacity to maintain the orbits of all of the 1-cm debris below 600 km. An additional sensor was planned. The Naval Space Command operates an interferometer radar, which erects a fan beam in an east-west orientation across the continental U.S. Orbits are determined by the location and time between penetrations of the fence. The interferometer concept can inherently handle a very large number of satellites. It also sets up a very large detection volume. If the fence covers 15°-17° of longitude (earth center angle) then each object is guaranteed of being detected at least once per day. The 1992 study proposed replacing the Naval Space Command VHF interferometer with an X-band system (called the Debris Interferometer Fence Radar [DIFR]) using as many components in common with GBR-X and HAVE STARE as practicable. The CONUS location limited the radar to detecting orbits with inclinations > 33°.

The DIFR would perform the catalog generation and maintenance tasks for objects with orbits > 33° inclination while GBR-X performed the same tasks for objects with orbits < 33° inclination. GBR-X and the four HAVE STARE radars would perform the conjunction update task.

3.0 Space Debris Task Team Study

3.1 Study Goals

The goals of this study were far less stressing than the other studies discussed in this paper. As such, it is also probably the most realistically achievable given the current fiscal climate.

The SDTT was given the task to "Examine Space Surveillance Network capabilities to enhance orbital debris data collection and processing on objects (as small as 5 cm) not currently in the satellite catalog." This task statement does not mention the purpose of the catalog, but the SDTT assumed that the eventual use of the system would be for collision avoidance. Also, the SDTT adopted an altitude limit of 600 km in order to keep the task manageable. Orbital Debris models indicate that ~5000 objects would be added to the current catalog.

3.2 The 1994 Debris Campaign

The SDTT was highly influenced by the members' experience with the Air Force's 1994 Debris Campaign (Ref. 8). During this campaign, 651 uncorrelated targets (UCTs) were detected. Of these, half were detected by the Eglin FPS-85 radar using a high elevation search fence dubbed the "NASA Debris Fence." The Cavalier radar detected another 32% of the UCTs. Optical sensors detected only 3%.

In addition to the intensive search for UCTs, the 1994 Debris Campaign made a large effort to retrack and catalog the UCTs. Of the 651 total UCTs detected, only 80, or 12.3%, were successfully retracked and only one remained in the catalog for any significant time after the campaign ended. UCTs detected by Cavalier stood a better chance of being retracked than UCTs detected by Eglin. It is believed that this was because of the higher latitude location of Cavalier and the fact that with its lower sensitivity, Cavalier detected larger objects than Eglin. All of the objects detected by Cavalier had inclinations detectable by Eglin and therefore both radars were available for retracking. But, Eglin detected many low inclination objects which would never pass within the coverage of Cavalier.

The low overall retracking rate is probably misleading. In 1995 the TRADEX (Target Resolution and Discrimination Experiment) radar located at Kwajalein performed a debris search using Stare & Chase techniques (Ref. 9). This mechanically steered dish antenna with a beamwidth of 0.6 degrees detected 37 total objects between October 29 and November 22, 1995, 25 of which were UCTs. TRADEX attempted to retrack 16 of the UCTs and 12 of the known objects. It was able to successfully reacquire 56% of the UCTs and 100 % of the known objects. The reason for the difference in retrack percentage is that Eglin and Cavalier were only operated in the special debris mode for a few hours each day and were not tasked to retrack the UCTs during the next available pass.

3.3 Recommendations of the SDTT

The SDTT recommended a phased approach to the task. Phase 1 would "operationalize" small debris tracking. This would involve routine operation of the NASA debris fence at Eglin with a corresponding fence at Cavalier, both existing sensors. Phase 1 would also assess the operational impact at both sensors and the Space Control Center (SCC).

Phase 2 would enhance Phase 1 capabilities by funding GBR-P (Ground Based Radar - Prototype) connectivity to the SSN and its use for space surveillance. Phase 2 would also use other existing sensors, which have demonstrated a capability to detect small debris. These sensors include TRADEX, Cobra Dane, the Experimental Test Site (ETS) and the Haystack Auxiliary (HAX).

Phase 3 would expand debris tracking by using an upgraded NAVSPACE fence operating at either S- or C-band. It could include other sensors currently in the planning stages if they are capable of detecting small debris.

3.4 Current Status

The USCINCSPACE has approved plans for upgrading the Space Surveillance Network for detection of 5-cm objects. The recommendations of the SDTT are being incorporated into the DoD/NASA Work Plan for Orbital Debris. Currently, funding is being sought for implementation of the "NASA" debris fence on the Eglin radar and for operation of the Cobra Dane radar.

4.0 The Senate Armed Services Committee Mandated Study

4.1 Study Goals

This study was conducted in response to Congressional language from the 1998 Senate Armed Services Committee (SASC). The SASC directed that the goals of the design study were to catalog debris down to 1 cm in size out to 1000 km in altitude. The SASC further directed that the study be coordinated between the Air Force Research Laboratory (AFRL), Los Alamos National Laboratory (LANL) and Lawrence-Livermore National Laboratory (LLNL). In additional to these laboratories, The Aerospace Corporation, Air Force Space Command, Jet Propulsion Laboratory, MIT Lincoln Laboratory, NASA/Johnson Space Center, and Navy Space Command also participated.

The goal of 1 cm at 1000 km is very stressing. The good news is that at higher altitudes, atmospheric drag effects are less pronounced and the orbits more stable than at low altitudes (<600 km). The bad news is that research by NASA using the Haystack radar indicates that there is a very large population of small debris with sizes typically less than 3 cm between 850-1000 km. These objects are most likely liquid metal Na-K coolant leaked from Russian RORSAT payloads (Ref. 10 and 11). Additionally, there appears to be a significant population of centimeter sized debris consisting of Aluminum Oxide slag from solid rocket motor firings (Ref. 12). Models indicate that up to 100,000 debris objects as small as 1cm may exist in orbits up to 1000 km.

The large number of objects has severe implications for the current method of cataloging. The report found that the current SCC is software limited to a catalog of 16,000 RSOs. This number can be extended to 40,000 with some hardware and memory upgrades. A novel concept was proposed to help alleviate this problem. The concept was to treat all small debris as UCTs and maintain a temporary catalog of only those objects which pose an imminent collision risk with the high value targets of interest.

4.2   Optical Systems

The SASC study took a close look at the utility of optical systems as a potential low cost alternative to radars. However, the report concluded that optical systems could not, by themselves, meet the stated requirements. Optics are not suitable for low altitude collision avoidance. All ground based optical systems are limited by weather. But, this limitation is compounded by the fact that for passive optical systems, the sensor must be in darkness while the debris is sunlit. For low or moderate latitude sites this only occurs for a short period near dawn or dusk. Although it is conceivable that given enough sites, optical systems could create a catalog of small debris, such a network would not be able to routinely provide timely orbit updates for collision avoidance against a low altitude target such as the Space Station.

The study did find that there were contributions to the network where optics could and should play a role. Optics could be well suited for high altitude orbits. High altitude orbits are lit for longer periods each night than low altitude orbits giving more opportunities for observation. Also, because the orbits at high altitude are more stable, they do not have to be revisited as often allowing some accommodation for weather outages. Similarly, optical sensors might also provide coverage for high eccentricity orbits where the object spends much of their time at high altitude.

Also, if an optical sensor/site is cheaper than a comparable radar, it might be cost effective to supplement a radar network with optical sites to handle special orbits such as Molniya orbits whose perigees are in the southern hemisphere (assuming that the object can only be detected at short slant ranges) or low inclination orbits (if all of the radars are located at high latitudes).

Other discussed uses of optics include the detection of objects which may be bright optically, but which exhibit small radar cross sections, space object identification, and high accuracy observations.

4.3.   Radar Systems
The principal finding of the study was that radar systems offered the best approach to detecting and cataloging debris at low altitudes. In particular, the study recommended that an upgraded NAVSPACE interferometer fence be designed and fielded. The upgrade primarily lay in the radar frequency – either S-band or C-band. Either of these would be able to detect 1-cm. debris out to 600 Km. altitude and 2-cm. sized debris at 1000 Km. altitude. However, the C-band, if designed with adequate power, could get down to 1 – 1.5 cm. size in debris detection. Further, the major advantage of the NAVSPACE fence was its guarantee of detecting debris in orbits above 33 deg. inclination at least 5 times a day. Thus, the major requirement of timeliness in cataloging could be satisfied. Additional radars were needed to track and establish precise orbits on debris that posed a threat to the International Space Station. These could consist of existing radars like Haystack, HAVE STARE, Millstone, TRADEX, TIRA in Germany and upgraded C-band radars like the ones at Kaena Point and Ascension.

4.3   Study Recommendations

In spite of the attention given to optical systems in the SASC study, the study concluded "to design an optical system to accomplish the 1 centimeter cataloging task alone would require hundreds of sensor sites around the world in order to deal with the limitations of optical sensors such as weather (inability to see through clouds), viewing time (twilight or night time) and field-of-view (a larger focal plane, which increases costs). Furthermore, the annual operations and maintenance cost of this optical system would very likely be large, even with extensive use of autonomous systems. Radar with its larger field-of-view and near all weather, 24 hour operation is well suited for the detection of orbital objects. We believe that

development of a complete system to detect, track and catalog space objects down to 1 cm in size should include both radar and optical surveillance systems."

The SASC study estimated costs for three systems. First it used the HICLASS system as a cost model for active optical systems. The study found that to build a comprehensive network would require at least 4 to 7 sites. Due to the extremely small field-of-view, each HICLASS system would require an acquisition capability such as the radar equivalent to Haystack in sensitivity. The estimated cost for this network was $1.5B to $2.5B.

Second, SASC study estimated the cost of a passive optical system. The system examined was comprised of a combination of search systems (one search telescope with a 2 to 3 m mirror and four chase telescopes of 1 m class) and catalog maintenance systems (1 m class). Global number of sites was estimated to be a minimum of 7 search sites and a minimum of 25 maintenance sites. It was noted that this system was not capable of performing the collision warning due to the "vagaries of both debris object orbits and weather" without adjunct radar systems. Acquisition costs of the optical sensors were estimated to be "on the order of $400M," but the report cautioned that there was large uncertainty in the number.

Finally, the SASC study used the 1992 Space Station *Freedom* Study network to estimate the radar systems costs. The study estimated that, with inflation, current costs of the radar network would be about $700M.

5.0   Discussion and Recommendations

The obvious first step to improving the Space Surveillance Network is to develop a unified set of well-defined requirements. The USCINCSPACE has begun this process by requesting and receiving the NASA requirements for space surveillance support.

Meeting any requirement for collision avoidance against 1-cm objects will require new sensors, which will take time to fund, design, build, and become operational. Therefore, a phased approach initially using existing sensors (as recommended by the SDTT) should be used. The phased approach will also allow operational strategies to be developed and refined as the catalog gets larger and the limiting debris size gets smaller.

Two radar systems have been identified in each study as being critical to creating and maintaining a 1-cm catalog. These systems are an upgraded GBR-P back to its original GBR-X capabilities and an upgraded NAVSPACE fence. GBR-P could simply be upgraded to GBR-X by populating its face with active transmitter elements. Yet, currently there are not any definitive plans for using either GBR configuration for space surveillance. Similarly, an upgraded NAVSPACE fence is in the planning stages. The Navy is currently planning to upgrade the fence to S-band. C-band would be a more appropriate frequency to detect 1-cm debris, but the Navy has no requirement that would drive them to the higher frequency. Steps should be taken to ensure that debris requirements are integrated into planning for both systems and that they are built and become operational for space surveillance in a timely manner.

Funding cuts for space surveillance in recent years have made it difficult for plans for improving the SSN to be taken seriously. Even the Phase 1 of the SDTT, which seemed very benign at the time, have run into problems. Eglin has upgraded to a new computer system, but because of lack of funding and requirements, the NASA debris fence was not implemented on the new computer system. Likewise the Cavalier radar faces possible closure because of funding cuts. Part of the problem appears to be that the Air Force is controlling the funding priorities while other agencies, such as NASA, have a large stake in the requirements. Therefore, it should be recognized that the SSN is a national asset. The SSN should not have to compete with other priorities in the Air Force for funding, but should be funded in accordance with its national importance.

References

1. "Debris Collision/Maneuver Avoidance." Presentation made to the Associate Administrator for Space Flight and the Associate Administrator for Space Station, NASA HQ. Dec. 4, 1992.

2. Stansbery, E. G. "Conceptual Design of a Sensor Network for Collision Avoidance." Proceedings of the 1993 Space Surveillance Workshop. M.I.T. Lincoln Laboratory Project Report STK-206, Volume II. 30-March-1 April, 1993.

3. Loftus, J. P., Jr., and Stansbery, E. G. "Protection of Space Assets by Collision Avoidance." IAA 6.4-93-752. 44th Congress of the International Astronautical Federation. Oct 16-22, 1993.

4. "NASA/AFSPC Space Debris Task Team Status Report." Presentation made to the USCINCSPACE and the NASA Administrator. October 22, 1997.

5. "Orbital Debris and the Environmental Restoration of Space: A Report to the Congressional Defense Committees." January 30, 1998.

6. "Space Surveillance: DoD and NASA Need Consolidated Requirements and a Coordinated Plan." GAO/NSIAD-98-42. U.S. General Accounting Office. December, 1997.

7. Memorandum from the NASA Administrator to the USCINCSPACE. August 27, 1997.

8. "1994 Space Debris Campaign: Final Report." HQ AFSPC/DOY. July 14, 1995.

9. Six, S. W. and LeClair, R. A. "TRADEX Autonomous Catalog Maintenance Experiment (TRACM)." Lincoln Laboratory Report 2813-02.

10. Kessler, D. J., et. al. "A Search for a Previously Unknown Source of Orbital Debris: The Possibility of a Coolant Leak in Radar Ocean Reconnaissance Satellites." IAA-97-IAA.6.3.03. 48th International Astronautical Congress. October 6-10, 1997.

11. Sridharan, R., et. al. "Remote Sensing and Characterization of Anomalous Debris." ESA SP-393. Proceedings of the Second European Conference on Space Debris. March 17-19, 1997.

12. Bernstein, M. D., and Sheeks, B. J. "Field Observations of Medium-Sized Debris from Post-Burnout Solid-Fuel Rocket Motors." SPIE Orbital Debris and Space Impactors II. July 28, 1997.

APPLYING ELECTRO-OPTICAL SPACE SURVEILLANCE TECHNOLOGY TO ASTEROID SEARCH AND DETECTION: THE LINEAR PROGRAM RESULTS

H.E.M. Viggh, G.H. Stokes, F.C. Shelly, M. S. Blythe, and J. S. Stuart
Lincoln Laboratory, Massachusetts Institute of Technology,
244 Wood Street, Lexington, MA 02173

Abstract

Lincoln Laboratory has a long history of developing electro-optical space surveillance technology for resident space object search, detection, orbit determination, and catalog maintenance of objects in Earth orbit. Recent advances in large format, highly sensitive CCDs make possible the application of these technologies to the detection and cataloging of asteroids, including Near Earth Objects (NEOs). When equipped with the new Lincoln Laboratory focal plane, camera, and signal processing technology, the modest sized (1-meter class) Air Force GEODSS telescopes have considerable capability to conduct sensitive, large coverage searches for Earth crossing and main belt asteroids. Field measurements have indicated that CCD-equipped GEODSS telescopes are capable of achieving a limiting magnitude of 22, over a 2-square degree field-of-view, with less than 100 seconds of integration. This is comparable to the sensitivity of considerably larger telescopes equipped with commercial CCD cameras. In addition to its high sensitivity, the Lincoln CCD employs frame transfer technology that is well suited to high coverage, high rate asteroid search operations since each frame can be readout while the next frame is integrating.

Technology development for asteroid search operations has been conducted at the Lincoln Laboratory Experimental Test Site in Socorro, NM over the past two years. Initial results, reported during the Space 96 meeting, indicated that the search system, now known as LINEAR (LIncoln Near Earth Asteroid Research), had considerable promise. Using the new large format 2560X1960 pixel frame transfer CCD camera mounted in a GEODSS telescope, forty-nine new asteroids were discovered over a period of several months, including one NEO (1996MQ). In addition, observations on seventy-nine known objects were collected and sent to the Minor Planet Center.

Since those initial attempts, LINEAR search operations have been considerably improved and automated. Data acquisition has been streamlined, detection algorithms have been updated, and the signal processing of the resulting data has been closely integrated with the data acquisition process. Field tests started again in January of 1997, with the objective of quantifying the capability of the system to conduct large area searches, detect new asteroids, and provide quality metric measurements to the Minor Planet Center. Since the large 2560x1960 pixel CCD camera was unavailable during this time, an older 1024x1024 pixel CCD camera was used. The smaller format camera has slightly less sensitivity than the larger camera and fills only about 1/5th of the field-of-view of the GEODSS telescope (which is filled by the larger chip). Observations were conducted over the dark of the moon periods during the months of March, April and May. Each search area was covered three times over a period of three to seven days to generate discovery observations of each new object that could be linked from day to day. The Minor Planet Center requires that newly discovered objects be observed over at least two nights before granting the object a designation.

Search productivity was quite high during each of the observing runs, in spite of the fact that a small format camera was employed. The main search strategy employed was to search near solar opposition and

near the ecliptic. A wide area search pattern for detecting NEOs was also briefly tested with promising results. Using the opposition search strategy, the LINEAR system was capable of repeatedly covering an area extending 15 deg. by 10 deg. over a period of a few days, to a limiting visual magnitude of approximately 21st. The following table provides statistics on the opposition search results:

MONTH	OBSERVATIONS TO MPC	KNOWN OBJECTS OBSERVED	NEW OBJECTS DISCOVERED	NEW NEO's
March	2,868	137	324	-
April	6,319	478	677	2
May	9,106	448	283	1
3 Mo Total	18,293	1,063	1,284	3

More recently, the large format CCD camera became available for use by LINEAR. Initial operations tests were conducted during the dark of the moon period spanning late October and early November 1997 and resulted in nearly an order of magnitude improvement in asteroid detection rates. Though results are still preliminary at the time of this writing, 52,542 observations were gathered over 10 nights of observing. These efforts resulted in the detection of 11 potential NEOs, 9 of which were successfully confirmed and new designations issued by the Minor Planet Center.

These series of observations validate that the large format 2560x1960 Lincoln CCD technology, originally developed for the Air Force GEODSS upgrade, is also quite effective when applied to the problem of discovering asteroids. Future development of this capability is planned to incorporate more highly automated operations so that they may be run remotely or in a fully unattended operations mode. These enhancements will increase the already high search productivity of the LINEAR program by providing considerably higher operations duty cycle.

Introduction

Recently there has been considerable discussion in both the press and in the Air Force regarding the detection and tracking of comets and asteroids. The interest has been generated by the collision of Shoemaker-Levy 9 with Jupiter and the realization that there are a large number of asteroids in orbits that will eventually lead to encounters with the Earth.

Figure 1a depicts the inner solar system, showing the main asteroid belt between the orbits of Mars and Jupiter. Asteroids in the main belt tend to have fairly circular orbits that do not threaten the Earth. However, some asteroids have orbits that cross the Earth's, and are referred to as Near Earth Objects (NEOs). Comets from the outer solar system can also cross the Earth's orbit.

The SpaceGuard Report[1] estimated the population of Earth crossing asteroids, or NEOs, to be 2100 objects with diameters larger than 1 km and 320,000 with diameters greater than 100 meters – see Figure 1b. Asteroids with diameters exceeding 100 meters can cause considerable regional damage in a collision with the Earth and asteroids with diameters exceeding a kilometer may cause global effects. Only a very small fraction of the NEO population is currently known. In order to assess the near term threat of such objects, the remaining population must be detected and cataloged. Therefore, the key enabling element of any "Earth defense" system is the detection capability that allows the discovery of such potentially threatening objects. This paper describes the performance of space surveillance technology originally developed for upgrading

the Air Force's GEODSS system, which, when applied to the problem of detecting and tracking asteroids, can provide this key capability.
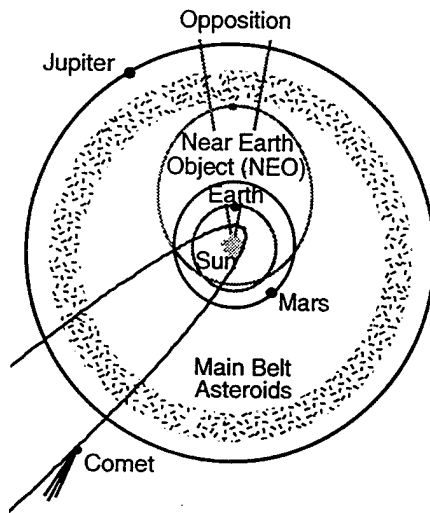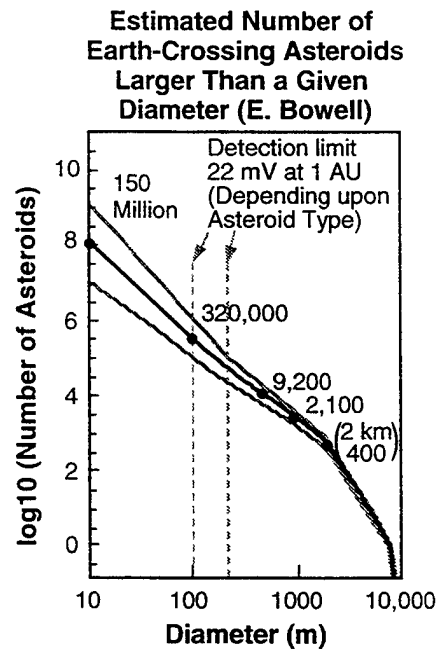

Estimated Number of Earth-Crossing Asteroids Larger Than a Given Diameter (E. Bowell)

Figure 1a, Orbits of asteroids and comets.

1b. Estimated population of Earth crossing asteroids with diameters above a given size.

Over the past several years, the US Air Force has been developing new devices and technology for the detection and tracking of Earth orbiting satellites. This technology has been targeted to provide an upgraded capability for an operational space surveillance system called GEODSS. Currently, a number of GEODSS systems are deployed around the world as part of the worldwide space surveillance system operated by the Air Force. Each GEODSS site is currently equipped with 1-meter class telescopes and EBSICON detector systems based on 1970's technology. The Air Force is now in the process of upgrading the GEODSS system to achieve the performance offered by state of the art detector systems. Under Air Force sponsorship, Lincoln Laboratory has developed a new generation of sensitive, large format, frame transfer CCD focal planes for GEODSS. These focal planes have been installed in a new generation of cameras and are currently undergoing testing at the Lincoln Laboratory Experimental Test Site (ETS).

When equipped with the new focal plane and camera technology, the modest sized GEODSS telescopes have considerable capability to conduct sensitive, large coverage searches for Earth crossing asteroids. Field measurements have indicated that the CCD equipped GEODSS telescope is capable of achieving a limiting magnitude of 22, over a 2-square degree field of view, with less than 100 seconds of integration. This is comparable to the sensitivity of considerably larger telescopes equipped with current cameras. In addition to the high sensitivity, the CCD is configured for frame transfer operations, which are well suited to high coverage, high rate asteroid search operations.

Detector Technology

Under Air Force sponsorship, Lincoln Laboratory developed CCD focal planes have been installed in a new generation of cameras which have undergone testing and validation at Lincoln Laboratory's ETS on

White Sands Missile range. The Lincoln focal plane and camera system provides considerably improved sensitivity, which reduces integration times and allows tracking of fainter objects, fast frame transfer readout which allows the integration of the next image to be started while the previous image is readout, and stringent blemish specifications, which minimize the loss of detections attributed to focal plane defects. The latest generation focal plane contains an array of 2560X1960 pixels and has an intrinsic readout noise of only a few electrons per pixel. In addition, these CCDs are constructed using a back illumination process, which provides peak quantum efficiency exceeding 90%, and solar weighted quantum efficiency of 65%. The CCD and the ETS field site are shown in Figure 2.
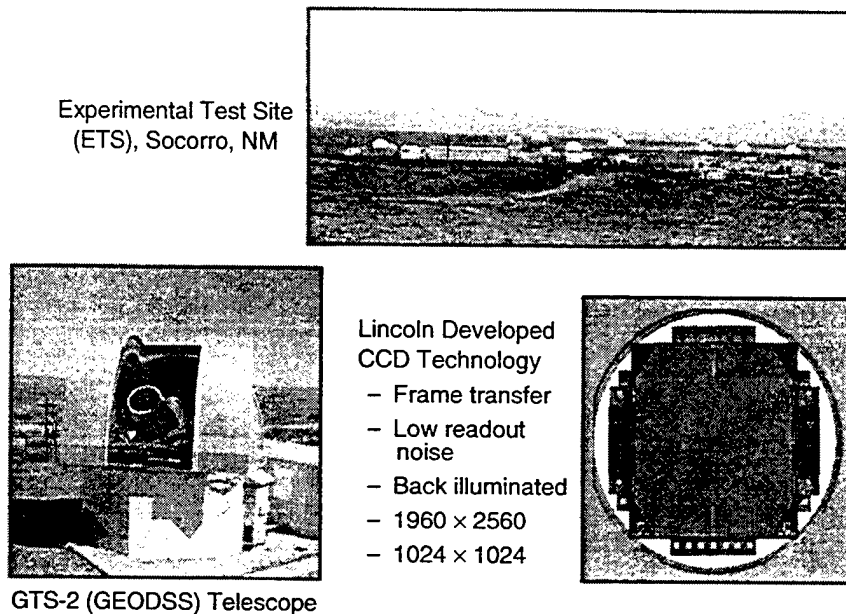

Experimental Test Site (ETS), Socorro, NM

GTS-2 (GEODSS) Telescope

Lincoln Developed CCD Technology
- Frame transfer
- Low readout noise
- Back illuminated
- 1960 × 2560
- 1024 × 1024

Figure 2. Lincoln Laboratory operated Experimental Test Site near Socorro, NM. & close-up view of 5 megapixel CCD chip.

The focal plane is equipped with 8 parallel readout ports to allow the 5-million pixel values to be read out in about 0.4 seconds. In contrast to most large format CCDs now on the market, which read directly out of the image array, the Lincoln CCD is equipped with frame store buffers. After an integration is finished, the resulting image is quickly transferred to the frame store buffers, freeing the active imaging area to conduct the next integration while the image is read from the frame store buffers. This feature also eliminates the need for a mechanical shutter to define the exposure, since the image transfer time from the imaging area into the frame buffer is only several milliseconds.

The CCDs described above have been constructed specifically to allow large portions of the sky to be searched for faint, moving targets. As such, they have the best combination of large format and detection performance of any CCDs that exist today. The detailed specifications for the CCD imager and the camera system are provided in[2].

Initial Field Tests

Initial field tests of the CCD and camera system were conducted over a period of several months, starting in August of 1995. These initial efforts were directed toward determining the capability of the system to meet its design specifications and the capability of the system to detect asteroids. Reference 2 contains the results of the initial characterization, which demonstrated that the CCD and camera are capable of meeting their specified performance requirements.

During these initial tests, conducted at the ETS in August 1995 and July 1996, a total of 75 hours of observing time were dedicated to searching for asteroids. That effort yielded a total of 177 observations of asteroids that were sent to the Minor Planet Center (MPC) in Cambridge MA. In the course of these observations, 49 new objects were discovered that received new designations from the MPC, including a confirmed Near Earth Object (NEO), which was given the designation 1996 MQ. In addition, observations of 79 known objects were also collected and used by the MPC to maintain their catalog. These results were reported in[2].

The LINEAR Program

The initial results were modest in terms of the amount of sky covered and the numbers of asteroids discovered, however, they were made with a preliminary camera and data system that provided only a small fraction of the possible discovery rate of an operational system using the same CCD technology. To demonstrate this, a new system was designed to achieve a much higher rate of search, processing, and discovery through the appropriate integration of existing real time hard disk storage, more tightly coupled signal processing, and automation of data management tasks. Thus, a small asteroid search effort, known as LINEAR (LIncoln Near Earth Asteroid Research), was started in early CY97.
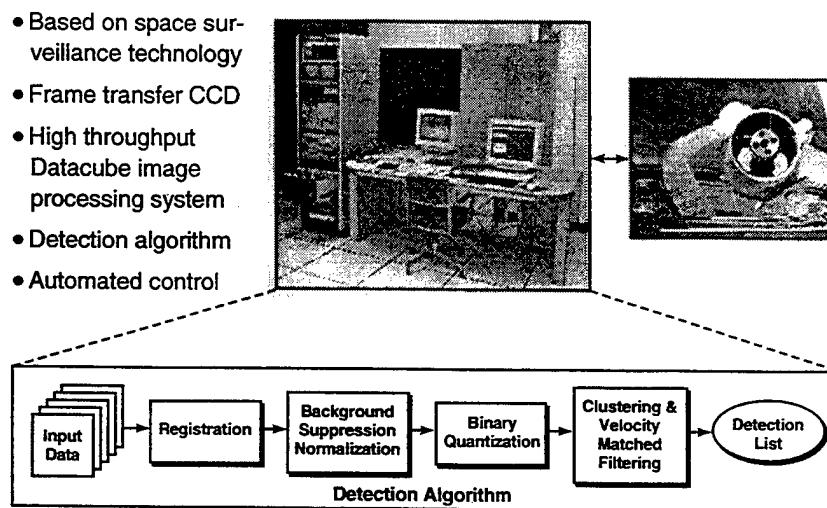

Figure 3. Block diagram of ETS system used to acquire asteroid data and detection algorithm.

Figure 3 provides a block diagram of the LINEAR system as operated at the ETS today. The detection algorithm employed has five major steps. The input data consists of three to five CCD images of the same location of the sky collected with an interval of 30 or more minutes between them. Image registration is performed to correct any pointing errors between the images by shifting the second through last frames as necessary to line up their stellar backgrounds with that of the first image.

Next, the registered images are normalized to remove background noise in the clutter suppression normalization block. Estimates of background mean and standard deviation are computed at each pixel, averaging over all the frames. The data are normalized on a pixel-by-pixel basis using the local background mean and standard deviation. The normalized data are then binary quantized with a simple threshold. A threshold value of 99.9% is currently used.

The binary quantized data are clustered on a frame-by-frame basis to group adjacent pixels into objects. The centroids and extents of the clusters are computed. Each cluster in the first frame is paired with each cluster in the last frame that falls within a specified radius, selected as an upper limit on asteroid rates of motion. These pairs form the list of candidate detections, or streaks. Each candidate streak is assigned a velocity by dividing the displacement from the beginning to the end of the streak by the time interval that it spans. For each candidate streak, intermediate frames are searched for clusters with the appropriate displacement to match the streak's velocity. These matching clusters are added to the candidate streak. Once all of the candidate streaks have been filled out, those streaks that have too few clusters are rejected. The streaks remaining are considered detections. Plate solutions are generated using a star matching algorithm and a star catalog, and then the precise locations of each detection in each frame is calculated. All detections are manually reviewed to identify and eliminate any false positives that have leaked through the system.

An example of the detection of an asteroid is shown in Figure 4. The data displayed is derived from five image frames made of the relatively bright asteroid 156 Xanthipe. Each frame was acquired by integrating for 0.5 seconds and the frames are each separated by 50 minutes. The top panel of the figure shows the full frame data. Below the full frame, the two panels on the left contain subsets of two of the full frames. It is obvious that there is an object that has moved during the four hours that have passed between the two pictures. The individual frames have been processed together using the automated moving object detection system discussed above to yield the output display, shown in the lower right corner of the figure. The end points of the moving object's streak are circled.

Detection Example

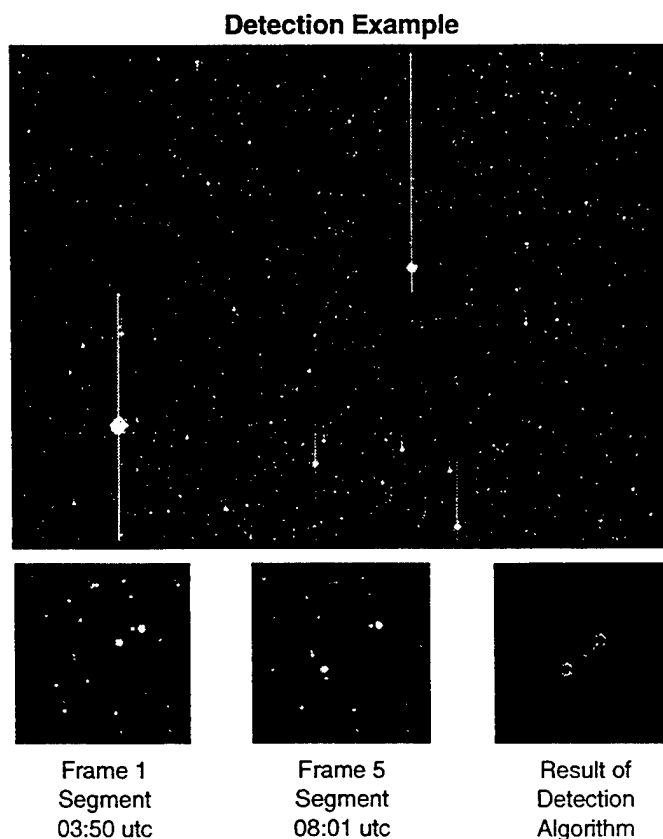| Frame 1 | Frame 5 | Result of |
| Segment | Segment | Detection |
| 03:50 utc | 08:01 utc | Algorithm |

Figure 4. Detections of moving objects resulting from processing a series of image frames. The top frame shows the entire field of view of the CCD. The two subframes on the lower left show subsets of the data containing an asteroid and the subframe to the lower right displays the processed result - an asteroid detection.

The LINEAR program has explored a number of search strategies intended to maximize the discovery of near Earth objects. The traditional search strategy is called an opposition search. Opposition searches are conducted in areas of the sky that are near solar opposition and near the ecliptic (shown in Figure 1a). The advantage of an opposition search is that the targets are in full solar illumination. In addition, a large fraction of the near Earth object population spends most of its time at large distances from the Earth, near the ecliptic.

The LINEAR system was tested with opposition searches March through July 1997. Because of limited equipment availability, a smaller 1024X1024 CCD was used (the smaller chip is 1/5th the area of the full-scale GEODSS chip). In spite of the fact that a small format camera was employed during the search operations, the productivity was quite high during each of the observing runs. The table in the abstract of this paper provides statistics on the search results with 1284 new asteroids being discovered in the three-month trial operations interval. The sky coverage achieved by LINEAR during those three months can be seen in Figure 5. During this series of search observations, the LINEAR system searched 1,211 square degrees of sky. Note that while large areas were covered, their remains a considerable portion of the sky not searched during the interval of our operations.
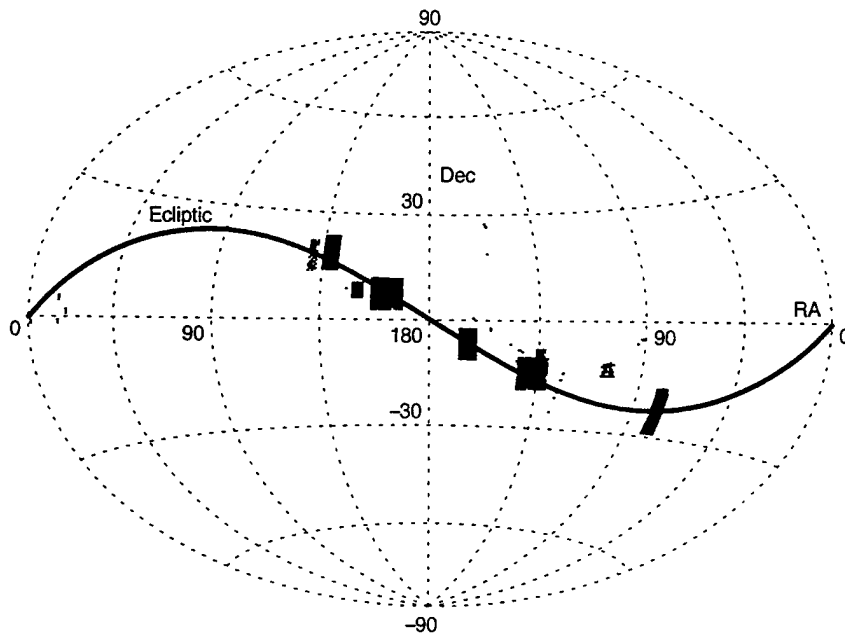

Figure 5. Equatorial plot of the sky covered by LINEAR in the three-month period of opposition search operations March-April 1997.

One of the problems with opposition searches is that NEOs are a relatively small fraction of the total asteroids detected. Most of the objects detected are in the main asteroid belt. Another possible technique for NEO searches is to search space nearby the Earth, hoping to find objects when they are closer to the Earth. This type of search will yield more small objects that can not be detected at opposition distances, however, nearby objects will not necessarily be concentrated in the direction of the ecliptic. This is because objects only slightly out of the ecliptic may be seen at essentially any Right Ascension (RA) and Declination (DEC)

as they past nearby the Earth as shown in Figure 6. This technique will also detect highly inclined objects that spend very little time near the ecliptic and would therefore be missed by an opposition search near the ecliptic.
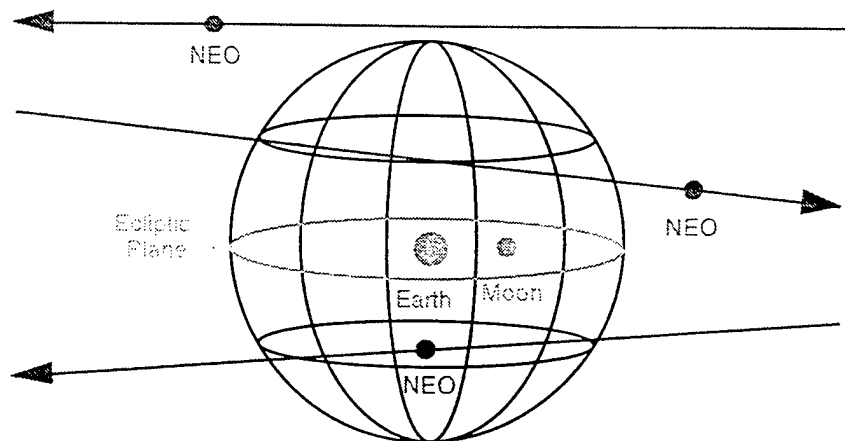

Figure 6. NEOs nearby the Earth may be observed at any RA and DEC.

Searching the entire sky visible to a given site in a single night and processing the data is a very stressing task, so stressing that it is beyond the capability of existing asteroid search programs. Therefore, the LINEAR program developed a method of searching large areas of the sky quickly by constructing a fence pattern along lines of fixed RA or DEC. For this pattern to be effective, it must be repeated many times a month to minimize leakage. Moving asteroids will eventually pass through one of the imaged lines, and by repeating the pattern often, e all NEOs below some velocity threshold will be detected. Even with the small percentage of the whole sky imaged by the fence, a large amount of data must still be collected and processed. Still, a large area of the sky must still be searched, so only three frames per field are acquired (versus five in the opposition search) and only fast-moving objects are fully processed and reported.

Initial results from this type of search are promising. During a period of seven nights of searching, one NEO and one classified by the MPC as an Unusual Object (UO) were discovered. The UO was originally though to be an NEO, but later confirmed to not come quite close enough to Earth's orbit. Still, it could threaten the Earth in the future if perturbed. Figure 7 indicates the fence search pattern used during these trial operations in June and July 1997. The lines shown in Figure 7 were repeatedly searched in such a way that the fence was leak-proof for object up to a certain angular speed.
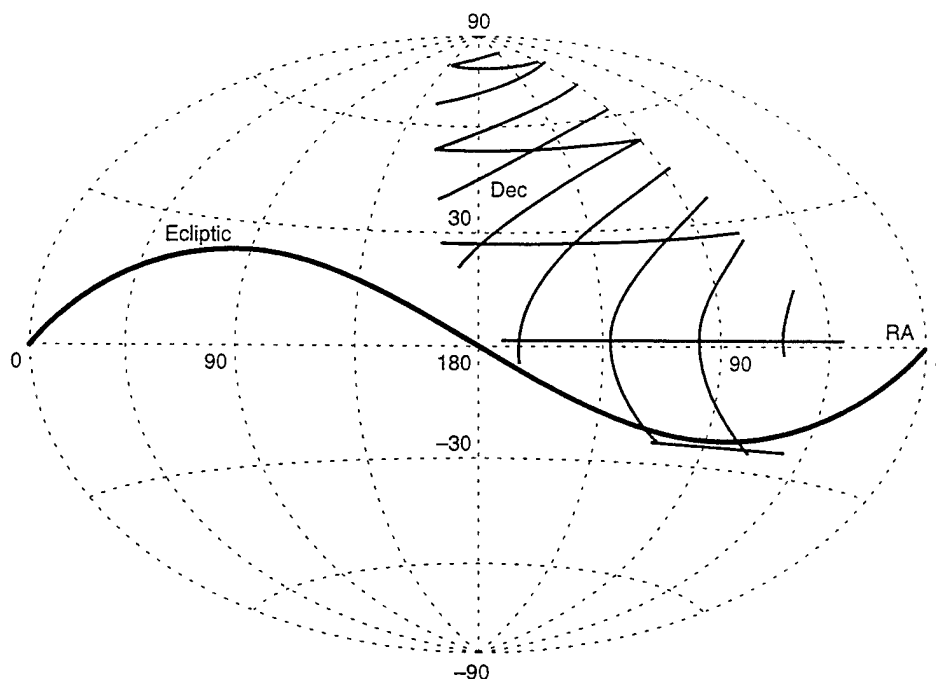
52

Figure 7. Equatorial plot of the sky covered by LINEAR during the period of trial operations of the leak-proof fence in June and July 1997.

LINEAR Program Results

The size distribution of asteroids detected by LINEAR is shown in Figure 8. The X-axis is the estimated diameter of the objects detected and the Y-axis is the number of asteroids in each size range. Diameters are estimated based on absolute magnitude assuming an average surface reflectance. Both the known population detected by the LINEAR search and the new discoveries are plotted. The distributions are based on those objects with MPC published element sets, while the totals include objects without published element sets. Note that the new objects discovered by LINEAR are generally dimmer than the known objects seen. By advancing the state of the art for detection sensitivity, LINEAR is sampling the steeply increasing population curve shown in Figure 1a. The peak of the population discovered by LINEAR is approximately two visual magnitudes dimmer than the peak for the known population.

Of course, the most interesting objects found by asteroid searches are the NEOs. Included in those discovered by LINEAR is a particularly interesting object (J97G03L) with an orbit that has the potential to come very near the Earth as shown in Figure 9. J97G03L is currently listed by the MPC as one of the most potentially dangerous NEO known. This object is one of 14 NEOs discovered by LINEAR through November of 1997. The orbits of all of the near Earth objects discovered by LINEAR – including those discovered most recently using the large format CCD, are shown in Figure 10.
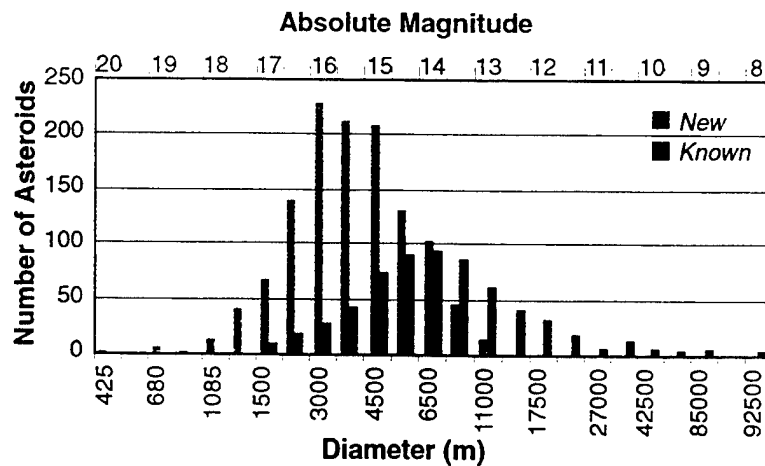
Absolute Magnitude

Figure 8. – Histogram of all asteroids detected by LINEAR, including new discoveries and known objects.

- NEO Asteroid 1997 GL$_3$
- Discovered 7 April 1997
- 21st visual magnitude at 1 AU
- Size: 170–370 m diameter
- Period: 3.43 years
- Close approach on 3 April 1997 of 0.03
- AU (5 × 10^6 km)
- Near top of MPC's list of "The Larger Potentially Dangerous Minor Planets"
- Closest potential approach: 0.002 AU

1997 GL$_3$ Discovery

Earth

Jupiter
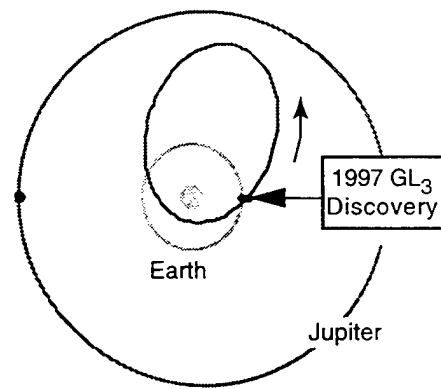
Orbit of 1997 GL$_3$
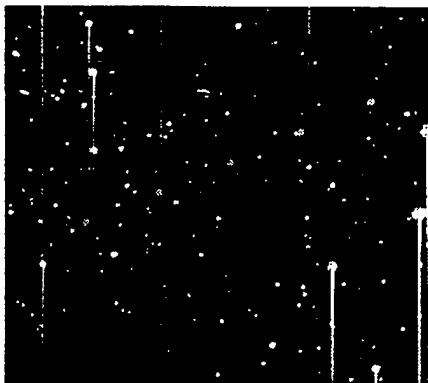
Composite of 5 Raw

Detection System Output

Figure 9. - Object J97G03L Discovered by the LINEAR Effort is listed on the Minor Planet Center's List of "The Larger Potentially Dangerous Minor Planets". Frames showing the detection of J97G03L are shown in the lower portions of the figure. A composite of the five raw data frames is on the lower left and the output of the signal processing system is shown on the lower right. The orbit of J97G03L is shown in comparison with the Earth's on the upper right with related information provided in the upper left. The object is on the 'The Larger Potentially Dangerous Minor Planets' list maintained by the MPC due to the very close potential approach to the Earth and the size.
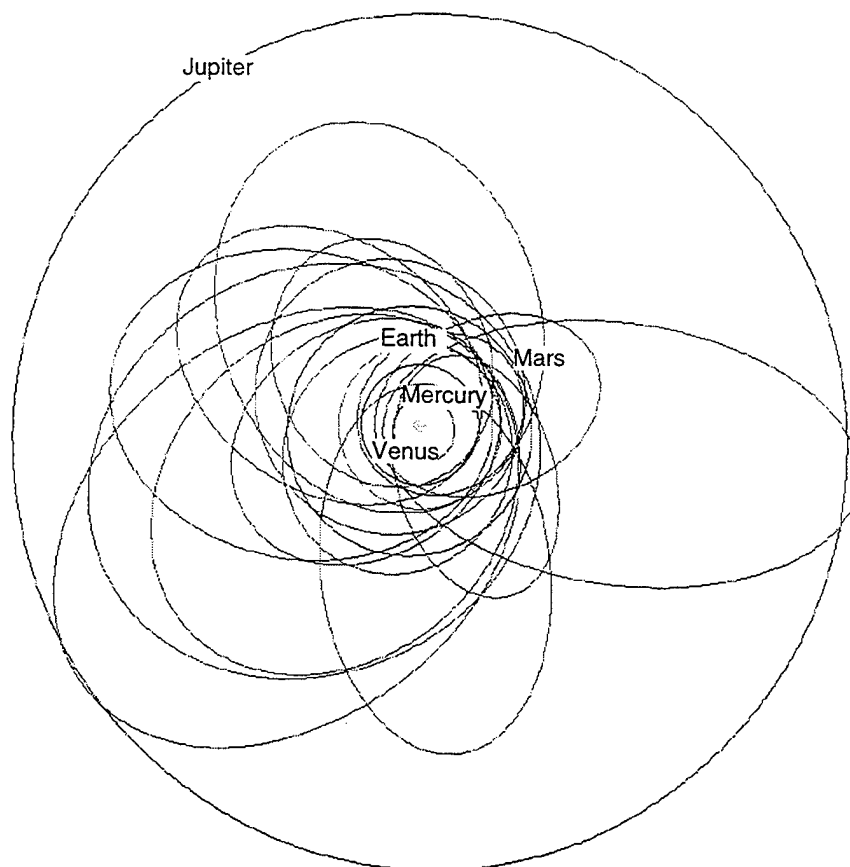
54

Figure 10. – The orbits of all of the NEOs discovered by LINEAR shown with respect to the inner solar system.

Figure 11 contains a histogram of the number of asteroids seen by LINEAR, both known and new discoveries, as a function of semi-major axis. As shown by this diagram, the majority of asteroids are in the main asteroid belt between Mars and Jupiter between 2 and 4 AU. Approximately only one out of 300 asteroids detected in an opposition search turn out to be near Earth objects.
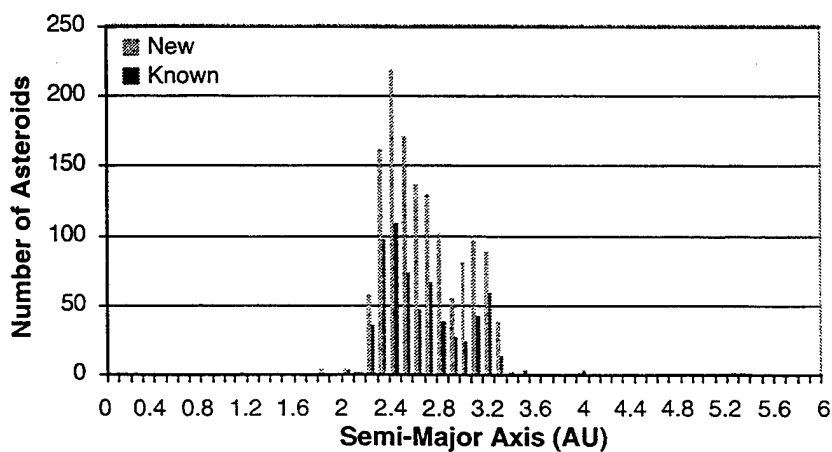

Figure 11. – Histogram of asteroids detected by LINEAR as a function of semi-major axis.

Figure 12 shows the eccentricity vs. semi major axis for the population seen by LINEAR. Again, both new and known objects are diagrammed. As can be seen from Figure 12, near Earth objects tend to have higher eccentricity than main belt objects. This causes their orbits to cross the Earth's orbit, as depicted in Figure 1a, yet their semi-major axis still brings them out to the main belt. This indicates that these types of NEOs may have been main belt asteroids that were perturbed into an Earth crossing orbit. Opposition searches tend to find this type of NEO.
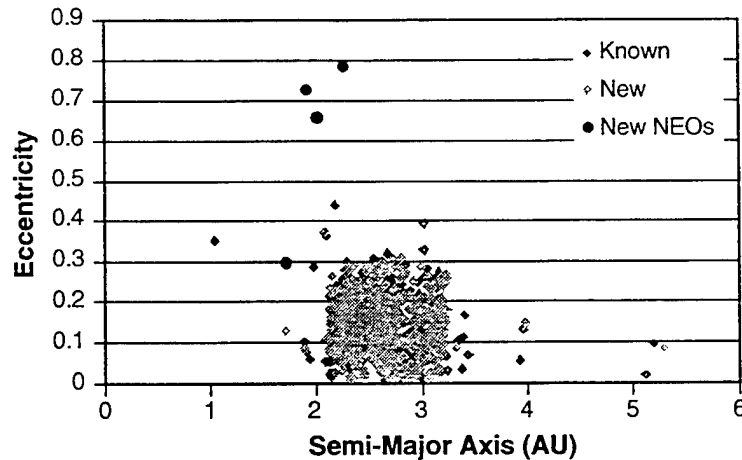

Figure 12. – Scatter plot of eccentricity verses semi-major axis for asteroid population detected by LINEAR.

Figure 13 diagrams the inclination of the population observed by LINEAR vs. their eccentricity. Note that the Unusual Object and one NEO are both highly inclined to the plane of the solar system. Both of these objects were detected by the wide area search technique, while the three low inclination NEOs were detected using opposition search. This indicates that both opposition and wide area search techniques should be used to find both low and high inclination NEOs. Note also that the Unusual Object, probably a dead comet, has an extremely high eccentricity and inclination. This UO, 1997MD10, was discovered June 29, 1997 and has a semi-major axis of 27 astronomical units, which indicates the its orbit extends out to between Neptune and Pluto. In addition, it has an extremely high eccentricity orbit (0.94). The absolute magnitude observed for this object indicates it is fairly large, placing its diameter in the range of 2 to 4 kilometers. Figure 14 depicts the orbit of this Unusual Object in relation to the planets and the NEOs discovered by the LINEAR program.
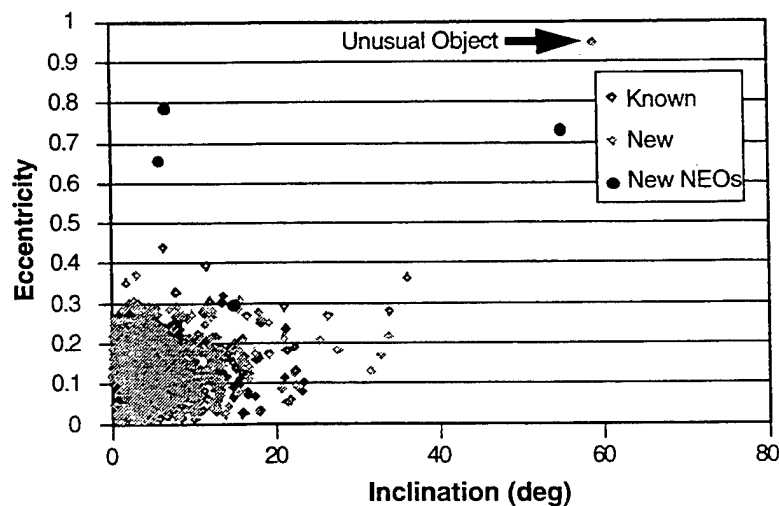

Figure 13. - Scatter plot of eccentricity verses inclination for asteroid population detected by LINEAR. NEOs and the unusual object clearly stand out of the general population.
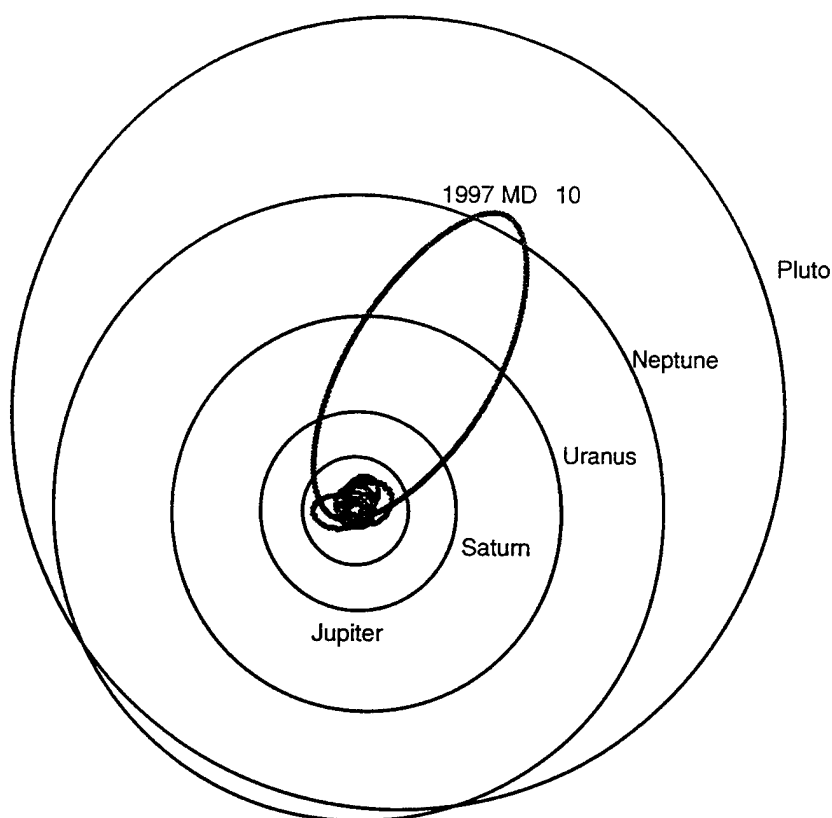
Figure 14. - The orbits of all of the NEOs discovered by LINEAR shown with respect to the entire solar system. Object 1997 MD10 has an extremely eccentric orbit that extends to between Neptune and Pluto.

Most Recent LINEAR Statistics

LINEAR began opposition search trials with the large format 1960x2560 pixel CCD on October 22, 1997. In the initial 10 nights of operations LINEAR generated 52,542 observations and detected 11 NEOs candidates – of which 9 were confirmed and received new designations from the MPC. Two of the NEO candidates, including one moving 17 degrees per day, were lost in subsequent follow-up attempts. The previous LINEAR monthly average of observations sent to the Minor Planet Center during the April-May 1997 opposition searching was 6,098 observations per month. Thus, the use of the large format CCD increased the observation rate generated by LINEAR by almost an order of magnitude. Table 1 contains the numerical data for our opposition search observations over the past year including both small format and large format CCD operation.

TABLE 1
Recent LINEAR Observation Statistics

PERIOD	CCD	OBS GENERATED	OBS/MO	NEW DES	NEOs
3/97 – 5/97	1024x1024	18,293	6,098	1,284	3 confirmed
10/22/97-11/7/97	1960x2560	52,542	52,542	Pending	9 confirmed

Future Plans

The LINEAR team intends to continue operating with the large format CCD and camera as available. The large format camera allows larger areas of the sky to be searched and provides more detections per processed field. We will continue to experiment with different search strategies including continuing the development of the wide-area search fence technique. Such search approaches should be highly productive for detecting NEOs, as opposed to objects in the main asteroid belt. In addition, we intend to experiment with deep and slow searches intended to detect more distant objects such as long period comets. Comets are of interest because they arrive in the inner solar system with the least warning time, and with very high velocity and kinetic energy. Finally, we believe that the LINEAR system can be modified to allow for detection across multiple nights of observations, with the intent of finding very slowly moving objects such as distant comets or other trans-neptunian objects.

Summary

In conclusion, the LINEAR program has been quite successful in demonstrating the capability of state-of-the-art Air Force space surveillance technology when applied to searching for NEOs. The search productivity of LINEAR has been quite high. The 1024x1024 CCD results compare favorably with other ongoing search programs. Using this small format CCD, 18,293 observations were sent to the Minor Planet Center over three months, resulting in 1,284 new MPC designations, including four near Earth objects. Initial experience with using the large format 1960x2560 pixel CCD in wide area searches promises substantial improvements over all search programs. In late 1997, 10 days of operations with the large format CCD camera system generated 52,542 observations, with 9 confirmed NEOs, bringing LINEAR's total to 13 NEO discoveries.

References

1. Morrison, D., Binzel, R.P., Bowell, E., Chapman, C.R., Friedman, L., Gehrels, T., Helin, E.F., Marsden, B.G., Maury, A., Morgan, T.H., Muinonen, K., Ostro, S.J., Pike, J., Rahe, J.H., Rajamohan, R., Rather, J.D.G., Russell, K.S., Shoemaker, E.M., Sokolsky, A., Steel, D.I., Tholen, D.J., Veverka, J., Vilas, F., and Yeomans, D.K., 1992. The Spaceguard Survey: Report of the NASA International Near-Earth-Object Detection Workshop (Washington, D.C., NASA).

2. Stokes, G., Weber, R., Shelly, F., Beatty, D., Viggh, H., Rork, E., and Hayes, B., "Air Force Planetary Defense System: Initial Field Test Results", Space V Proceedings of the Fifth International Conference on Space '96, Volume I, pg. 46-54.

Contributing Sensor Operations of the Space-Based Visible (SBV)

G. Stokes and R. Sridharan, MIT Lincoln Laboratory

Introduction and Objectives

For the past two years, the Space-Based Visible (SBV) sensor, onboard the BMDO Mid-Course Space Experiment (MSX) spacecraft has been operating as a technology demonstration of space-based space surveillance. During this time, the Space Surveillance Principle Investigator (SPI) has been charged with gathering sufficient data with the SBV to validate the concept of space space-based surveillance and to allow independent confirmation of the accuracy of the data. This successful technology demonstration effort has shown that the SBV sensor could provide significant operational capability to Space Command. In fiscal 1998, the transition of the SBV/MSX to contributing sensor status was initiated. This transition is being accomplished as an Advance Concept Technology Demonstration (ACTD) program.
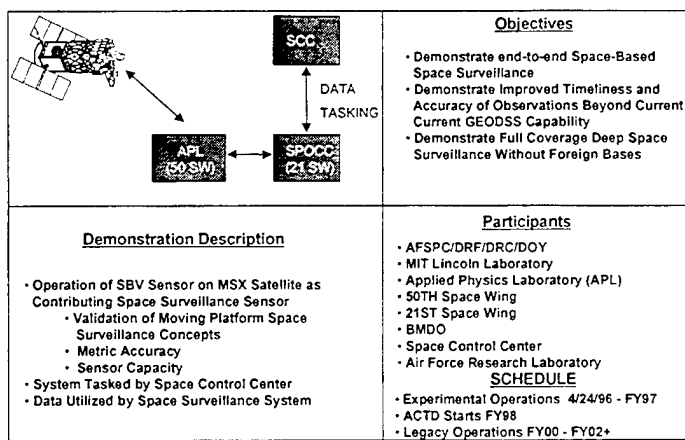
This paper will provide an introduction to the Space-Based Visible sensor, its operations and, the results achieved during the technology demonstration. In addition, the transition to operations as a contributing sensor and the current status of the effort will be described.

The Space-Based Visible program has a number of program objectives:

1) SBV is a technology demonstration program where three primary new technologies are incorporated. These technologies include:
   a) High off axis rejection optics, to allow observations of faint targets near the sunlit Earth limb;
   b) Advanced staring focal plane arrays to allow sensitive search of large areas of the sky;
   c) On-board signal processing capability to reduce the large volume of focal plane data to a manageable set of target data.

2) SBV is a demonstration of space-based surveillance. This objective includes:
   a) Technology demonstrations of space surveillance, such as demonstrating that faint targets could be detected and that high metric accuracy data could be obtained.
   b) Functional demonstrations, including responding to standard Space Command tasking and demonstration of search operations.
   c) Acquisition of raw full frame background and phenomenology data for advanced signal processor development.
   d) Operational experience and lessons learned, which are to be transitioned to space-based space surveillance sensors.

3) SBV is resident on the BMDO MSX satellite and has been involved in number of ballistic missile defense tests. Thus, SBV has gathered target phenomenology data on a broad range of missiles and other targets, as well as broad band visible data including a variety of backgrounds.

Figure 1 is the official Space Command "quad chart" for the Space-Based Space Surveillance Operations (SBSSO) ACTD. The chart highlights the objectives of demonstrating end-to-end space-based space surveillance; demonstrating improve timeliness and accuracy of observations beyond the current GEODSS capability; and demonstrating full coverage deep space surveillance without foreign bases. Also highlighted on the chart is the large number of participants in the program.

Space-Based Space Surveillance ACTD

		Objectives
	DATA TASKING	• Demonstrate end-to-end Space-Based Space Surveillance • Demonstrate Improved Timeliness and Accuracy of Observations Beyond Current Current GEODSS Capability • Demonstrate Full Coverage Deep Space Surveillance Without Foreign Bases

Demonstration Description
 	
• Operation of SBV Sensor on MSX Satellite as Contributing Space Surveillance Sensor
  • Validation of Moving Platform Space Surveillance Concepts
    • Metric Accuracy
    • Sensor Capacity
• System Tasked by Space Control Center
• Data Utilized by Space Surveillance System
		Participants
		• AFSPC/DRF/DRC/DOY
		• MIT Lincoln Laboratory
		• Applied Physics Laboratory (APL)
		• 50TH Space Wing
		• 21ST Space Wing
		• BMDO
		• Space Control Center
		• Air Force Research Laboratory
		SCHEDULE
		• Experimental Operations 4/24/96 - FY97
		• ACTD Starts FY98
		• Legacy Operations FY00 - FY02+

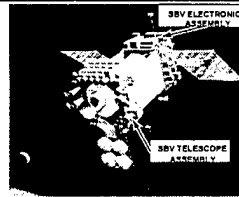MIT Lincoln Laboratory

Figure 1

More specific objectives related to the demonstration of end-to-end operations include integration of the SBV sensor as part of the space surveillance network. This includes the objective of exercising SPADOC with real space-based space surveillance data while helping to address the current deep space capacity shortfall. As part of the process of exercising SPADOC with real space-based space surveillance data, the fusion of space data with the ground network is required. The demonstration of routine space surveillance tasking response and geosynchronous belt searches are also program goals. The overall goal of SBV contributing sensor operations is to establish a legacy for future space-based space surveillance systems, and to affect a technology transfer to the eventual operational system.

SBV Overview

Figure 2 details the technologies included in the SBV for demonstration. First, in the lower left corner of the figure, is the high stray light rejection telescope. A high stray light rejection capability allows the detection of faint targets in high backgrounds near the lit Earth limb. In order to accomplish this objective, the SBV employs an off axis optical design and was kept extremely clean during integration, launch and operations. The second major technology included in the SBV is a low noise CCD focal plane. The focal planes included in the SBV are 420 by 420 pixel, frame store arrays. A total of four of the CCDs were included in the SBV focal plane. Each frame store CCD has an active pixel area and a frame store area. During space surveillance operations, the satellite is stabilized in a sidereal track and a sequence of integrations is gathered. A typical sequence would include as many as 16 frames, resulting in almost 3 million pixels of information. The quantity of raw data generated by this process is far too much to be downlinked on the 1 Mbit/sec communications available to the MSX on a timely basis. Thus, the final technology that is demonstrated on the SBV is on-board signal processing. The on-board signal processor takes the three million pixels of information per field area and compresses them by a factor of about 2000, extracting a few stars used in pointing and the streak signatures of moving
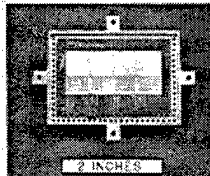
Space-Based Visible (SBV) Program

- SBV launched 24 April 1996

- SBV sensor meeting or exceeding all goals

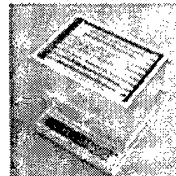- Successful demonstration of space-based space surveillance

MSX Satellite
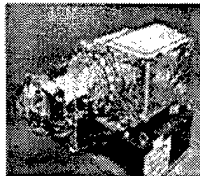
High Straylight Rejection Telescope

Low Noise CCD Focal Plane Array

Automatic Target Detection Signal Processor
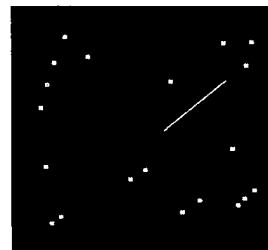
MIT Lincoln Laboratory

Figure 2

RSOs. The effect of the signal processor is shown in Figure 3. On the left panel is a raw frame set consisting of 16 individual frames (the frames have been added for this diagram). In this frame the stars are stationary and the streak represents the satellite. The signal-processed result is shown on the right frame of Figure 3. Here, a small subset of the stars has been extracted for use in determining the attitude and the signature the satellite has been extracted.

SBV Signal Processor
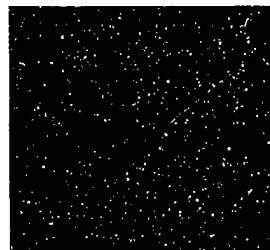
Raw SBV frameset

- 2-16 frames per frameset
- 0.4 - 1.6 sec integration per frame
- Sidereal track (staring)
- Ephemeris track
- Process on-board and on ground

Signal processor image

- Signal processor functions
  - Target detection
  - Star detection
  - Clutter rejection
  - Data compression
  - Signature generation

MIT Lincoln Laboratory

Figure 3

Figure 4 outlines the metric data processing implemented for the SBV. The goal of the SBV program has been to produce 4 arcsecond metric observations of target satellites. That goal is shown as the inner circle on the lower panel of Figure 4. For comparison, the 10-arcsecond A-spec accuracy requirement for the GEODSS system and the 12-arcsecond pixel size of SBV focal plane are shown. In order to accomplish 4 arcsecond metric results, three inputs are required. First, the sensor data, as described above, is used to determine the end points of the satellite streak. Each such streak produces two observations of the satellite. The signatures of several stars are also included in the signal processor report. The star positions are extracted from the signature

data and template matched against a Star catalogue to determine the attitude and distortion of the SBV telescope. The attitude determination is routinely accomplished with an absolute accuracy of a few tenths of an arcsecond. The final piece of information required is the station position of the MSX, or the MSX ephemeris. Lincoln Laboratory has maintained the MSX ephemeris, to the accuracy of plus or minus 15 meters, by processing the S-band ranging data supplied by the SGLS network.
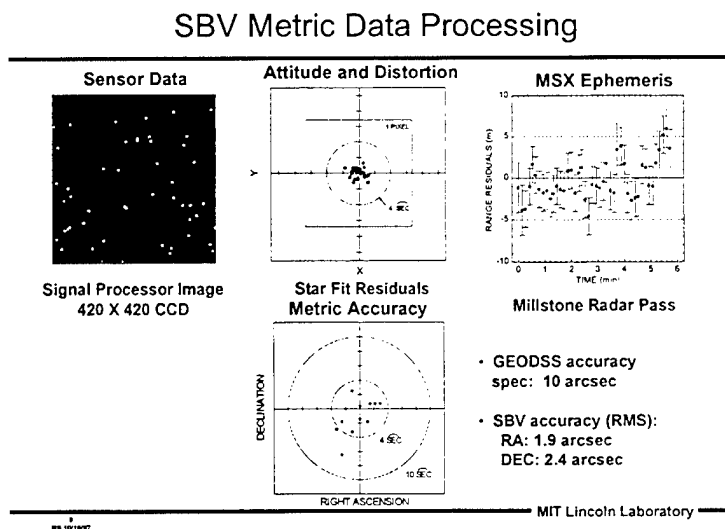
SBV Metric Data Processing

Figure 4

SBV Operations

The control network for the SBV when operated as a contributing sensor is shown in Figure 5. The First Command and Control Squadron (1CACS) generates tasking at the Mountain and forwards it to the SBV Processing Operations and Control Center (SPOCC) located at Lincoln Laboratory. The SPOCC schedules operations in response to the tasking and generates SBV/MSX commands that will implement the operations on the satellite. The SPOCC mission planning process is highly automated and it takes into account all of the constraints, capabilities and issues related to resources on-board the spacecraft. The commands are sent via electronic link to Johns Hopkins Applied Physics Laboratory for inclusion in the MSX upload and are uplinked to the MSX spacecraft. Data are then acquired by the SBV and the results are stored in a RAM buffer on-board the SBV instrument, until a 1 Mbit/sec downlink is available. Downlinks can be accomplished via the APL dedicated station or the SGLS network. Data are returned to the SPOCC at Lincoln Laboratory for processing into observations in the standard type 8 format. The observations are delivered to the Mountain via the existing link connecting Millstone to the SCC. A goal of 100 tracks per day has been established for each 8-hour operations day of the SBV. The SBV is operated 7 days/week, with one day/week allowed for routine maintenance and development

**MSX / SBV Contributing Sensor
Control Network**

**Contributing Sensor Operations
December 1997**

100 tracks / day

MIT LL
SPOCC

1 CACS
21 SW

Tasking

SBV

MSX

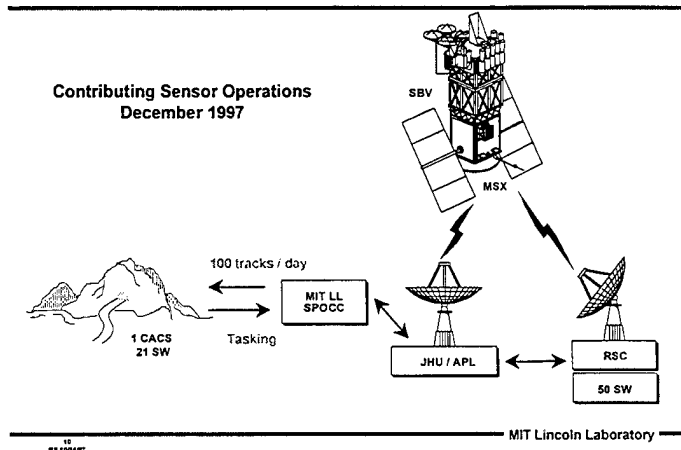JHU / APL

RSC

50 SW

MIT Lincoln Laboratory

Figure 5

The SBV Processing, Operations and Control Center, located at Lincoln Laboratory, has successfully demonstrated space-based space surveillance operations during the technology demonstration phase. Functions of the SPOCC include the reception of tasking from 1CACS, event planning, SBV command generation, data reduction, MSX ephemeris generation and SBV health and status monitoring. The SPOCC is highly automated and is operated by a minimal staff.

The operational timelines that have been established for contributing sensor operations of the SBV/MSX are shown in Figure 6. The timeline starts with reception of 1CACS tasking in the SPOCC. Within four hours the commands to execute the event have been generated in the SPOCC and forwarded to Applied Physics Laboratory in a format called EDF. Four hours later is the first contact in a cluster of contacts between the MSX and the APL station. Commands are uploaded and during this contact and execution of the events to gather the data starts immediately. During a subsequent contact with APL, additional commands are upload as required and data is downloaded from observations that have executed. The MSX is operated for a dedicated eight-hour block of time. Once that eight-hour time has been completed, the final set of data is downloaded at an AFSCN station. Observations are supplied to the SCC within a 24-hour cycle time after receipt of tasking.

MSX / SBV Operations Timeline

APL contact cluster

MSX surveillance data
acquisition

| 0 | 4 | 8 | | | 16 | | 24 |

HOURS

SSC
tasking to
SPOCC

EDF
to
APL

Upload
contact

Upload and
download
contacts

AFSCN
download

Observations to SSC

SBV has access to all space
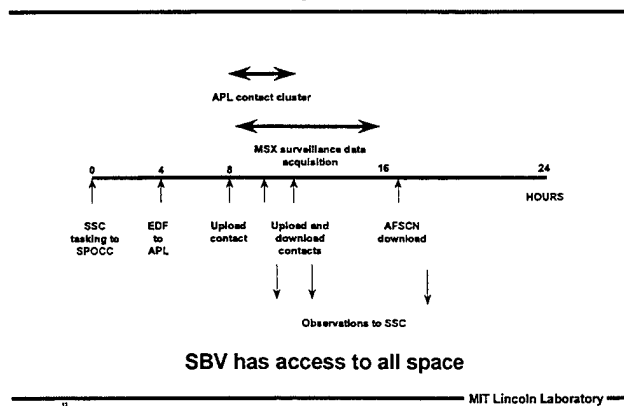
MIT Lincoln Laboratory

Figure 6

The contribution that is expected from the SBV sensor is 100 tracks per 8-hour day during full operations. As of this writing, the SPV is supplying 70 tracks per 8-hour day, and a number of improvements are being undertaken to increase this number to meet or exceed 100 tracks per day. These improvements to the SBV are summarized near the end of this paper and discussed in detail in another paper at this Workshop. In addition to the capability for tasked response, the SPV has a broad area search capability. Each of the 4 CCDs has a field-of-view of 1.4 by 1.4 degrees. We believe this capability will allow the search of 1/3 of the geosynchronous belt +-3 degrees in longitude per eight-hour day using the SBV in a GEO-belt search mode. This capability will allow true surveillance of space, seeing not only currently catalogued objects, but also adding new and lost objects to the catalogue. In addition, in the area of the geosynchronous belt, the productivity of the sensor is increased because multiple objects are often seen in a single field.

Overview of SBV Results

Figure 7 contains a histogram of the entire set of correlated resident space object (RSO) observations made by the SBV during the technology demonstration period. As can be seen, the SBV has detected objects in all orbital regimes including objects in Low Earth Orbit (LEO), objects in semi-synchronous orbits and geosynchronous objects. As can also be seen, the SBV has focused on high altitude and geosynchronous objects. This is because of the current network capacity constraints in this regime and also because the SBV is unique among all space surveillance sensors when applied to the geosynchronous belt. As shown in Figure 8, the SBV is the only space surveillance sensor that has access to the entire geosynchronous belt. Also shown in Figure 8, is the result of a single frame set taken at a field position in a geosynchronous belt. The figure shows the 4 objects detected in a single frame set.
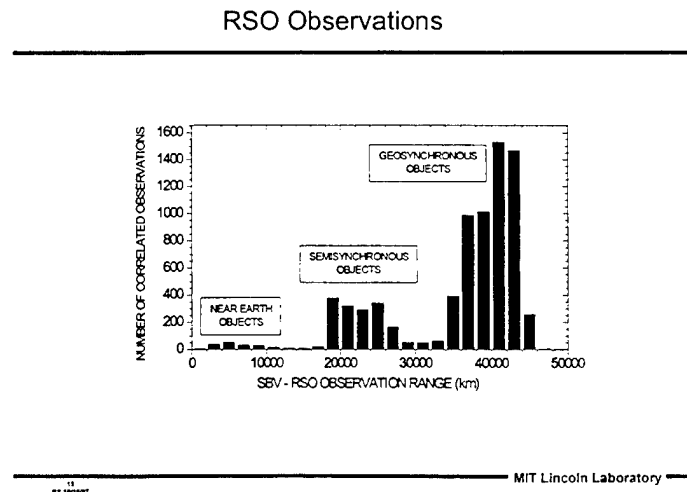
RSO Observations

Figure 7

Geosynchronous Belt Surveillance

Four Geosynchronous Targets in Field of View

GEO Surveillance of Entire Belt is Unique Capability of SBV
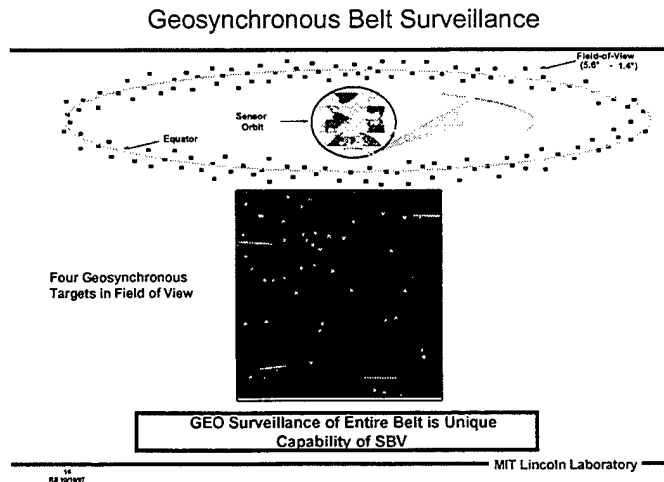
MIT Lincoln Laboratory

Figure 8

The capability of the SBV wide field view for search applications is also shown in Figure 9. These data were gathered in a single data acquisition (frame set) by the SBV. Signatures of 5 satellites are present in the data on the right panel, and the detected positions are plotted along with the predicted detections on the left and panel. These five satellites represent members of all orbital regimes including the geosynchronous, LEO and geosynchronous transfer orbits in a single SBV data set.

SBV Wide Field of View Application

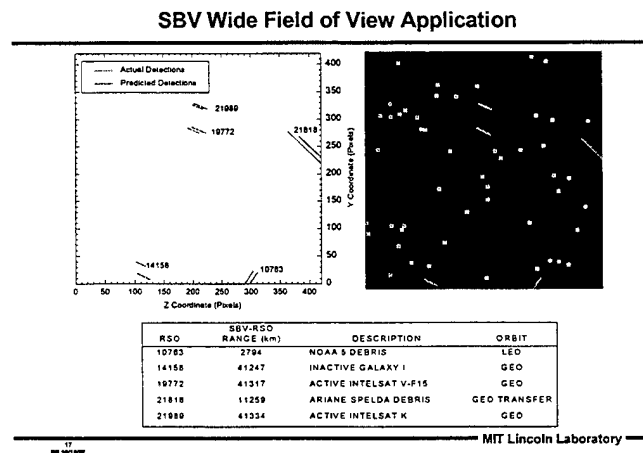| RSO	SBV-RSO RANGE (km)	DESCRIPTION	ORBIT
10763	2794	NOAA 5 DEBRIS	LEO
14158	41247	INACTIVE GALAXY I	GEO
19772	41317	ACTIVE INTELSAT V-F15	GEO
21818	11259	ARIANE SPELDA DEBRIS	GEO TRANSFER
21989	41334	ACTIVE INTELSAT K	GEO

MIT Lincoln Laboratory

Figure 9

The detection sensitivity of the SBV is demonstrated in Figure 10. Figure 10 is a histogram of all of the correlated observations that the SPV has made as a function of magnitude of the target observed. The SBV was originally designed as a 14.5 magnitude sensor, but has capability exceeding 15th magnitude.
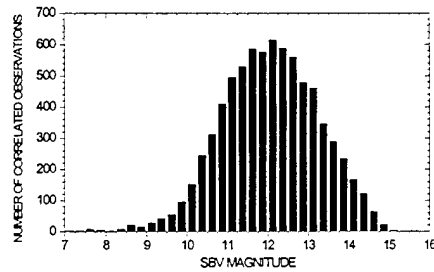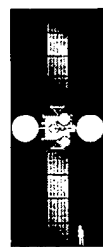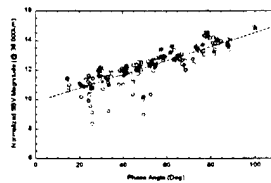
Figure 10

Most of the discussions above have focused on the metric observations gathered by the SBV. As part of the observation process, rudimentary signature data are also acquired on the target satellites. One of the uses of this photometric signature data from SBV is shown in Figure 11. The data on the right side of the figure are signature observations plotted as normalized SBV magnitude as a function of phase angle. The satellite objects from which the data were gathered are Hughes 601 communications satellites. The bottom panel on the right represents data from satellites that were not stabilized and thus are tumbling. These satellites show a flat magnitude trend with phase angle. Data for satellites that are stabilized are shown in the panel on the upper right. For these objects, the photometric data shows a definite trend toward getting much brighter at low phase angles. This is because of the large solar arrays, which are maintained pointing toward the sun. Thus, the time history of observations using the SBV can be used to determine some information on the operational state of the target satellites. More information on this application is contained in another talk at this Workshop.
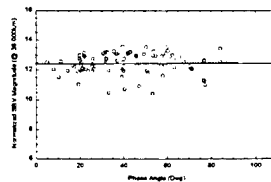
Large 3-Axis Geosynchronous Payloads

Figure 11

Transition to Contributing Sensor Operations

As of the writing of this paper, the SBV is in transition toward contributing sensor status. The SPOCC is responding weekly to tasking from 1CACS and is returning correlated observations via email to the Space Warfare Center. Close coordination with the user communities is being maintained via the Tasking and Data Utilization Working Group (TDUWG). The objectives of the TDUWG are to make sure that the SBV is both tasked efficiently and that the resulting data are used to good effect. A series of off-line testing has been completed successfully. Online testing is scheduled for late December 1997.

One result that has become obvious in the process of demonstrating the SBV is that the SBV is more productive when tasked to search the geosynchronous belt than when responding to tasking for specific objects. Figure 12 shows SBV tracking performance over 14 months of operations. When tasked against specific objects the SBV performed a mean of 18 looks or fields per hour. When used in a geosynchronous search, the SBV executed over 26 looks per hour. In the case of tasked operation, the timelines are dominated by maneuver time of the MSX satellite. In the geosynchronous surveillance case the timeline is dominated by the signal processing time.

SBV : Tracking Performance

Number of looks/hour based on 14 months of operation
(each look = 2 observations/satellite)

Event Type	Mean	Min.	Std. Dev.	Comment
Tasking	18.04	17.0	0.47	Dominated by maneuver time
GEO Surveillance	26.44	9.77	10.0	Dominated by signal processing time

MIT Lincoln Laboratory

Figure 12

A number of tasking tests has been accomplished between the SPOCC and 1CACS. An example set of tasking received from 1CACS is shown in Figure 13. This was received for testing the week in September 15 1997. Figure 14 shows the response to that tasking over the week. The objects are shown as a function of category: those that are tasked, those that were scheduled, and those that were acquired. Far more objects are tasked to the SBV than SBV can possibly observe. This was done to make sure that the satellite never had to wait for a target to become visible. Thus, the number of scheduled objects is far smaller than the number of tasked objects. The numbers of objects having been scheduled and acquired are shown in the last column to the right. As can be seen, the performance of the SBV is at about the 70 percent level. The fact that not all scheduled objects are detected is largely due to radiation events seen in the focal plane which effect the signal processor performance.
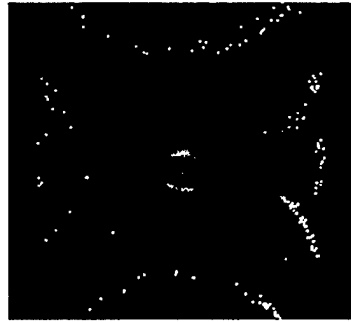
New Tasking : Week of Sept. 15 97

MIT Lincoln Laboratory

Figure 13

Test # 1 Extension : Week of Sept. 15 97

Category	Tasked	Scheduled	Acquired
1C	40	15	10
2C	825	161	99
2D	25	17	4
3C	335	80	86
# of tasked objects	1225	273	199
Bonus objects			31
Uncorrelated tracks			82

MIT Lincoln Laboratory

Figure 14

Capability Enhancements

There are a number of development activities intended to increase the capability of the SBV. Each of these, when accomplished, will lead to increased observation rate. The first is the implementation of the conjunction scheduler. Since a large number of objects are tasked to the SBV on any given day, more than one tasked object is in a field of view at any given time. The new conjunction scheduler will make use of this effect to increase the capacity of the SBV by preferentially scheduling observations during these conjunctions. As of this writing, testing on the new scheduler was beginning and initial results are promising.

The second development activity is the implementation of a new maneuver model, which removes a number of the constraints on MSX pointing and operations imposed during the interval of the technology demonstration. Initial test results have been encouraging.

The third development activity is intended to address the effects of the radiation events on the signal processor performance. A new software upload to the on-board signal processor of the SBV is being created. The new software contains modifications to the signal processor algorithms, which should help eliminate both false streaks and radiation induced corruption of

real streaks. These radiation events and methods that we are using to help eliminate their effect are discussed in another paper in this Workshop.

Together, these enhancements and upgrades to the SBV are expected to increase the productivity to meet or exceed the 100 track/8-hour day goal.

Summary

SBV on MSX has been performing quite well and has met or exceeded its design goals. Operations during the technology demonstration phase have shown performance that will make it an asset to the space surveillance network. On the basis of these tests and independent validation of the metric accuracy by the Space Warfare Center, the SBV is transitioning to operations as a contributing sensor. Full contributing sensor operations are expected in calendar year 1998.

Performance Improvements of the SBV
R. Sridharan, Bill Burnham and Andy Wiseman, MIT Lincoln Laboratory

1. Introduction

The SBV on MSX is transitioning from being an experimental sensor to an operational contributing sensor to the deep space surveillance part of the Space Surveillance Network. Two months of simulated operation have yielded adequate experience to state the following:
1. The sensor provides accurate and useful data on deep space RSOs.
2. The productivity of the sensor has met or exceeded expectations.
3. The data from the SBV are useful to SCC in its Space Control/Space Surveillance mission.

This paper traces the various improvements in the SBV and SPOCC over the last year that have contributed to the current level of productivity and performance of the sensor. The aim of these improvements has been to:
1. increase the quantity of the data from the sensor;
2. improve the quality of the data from the sensor;
3. assess sensor performance both on a daily basis and to trend its performance;
4. and, last but not least, to automate the use of the sensor so that ground operations cost can be controlled.

The SBV today routinely produces 120 tracks per 8-hour day on deep space RSOs – a comparable performance to that of a GEODSS site consisting of two one-meter class telescope systems. Further, the metric accuracy (4 arcsec. in RA and dec.) of the data from the sensor is a factor of three better than that of the GEODSS.

2. Productivity Enhancements

Four significant steps have been taken in the last six months to enhance the productivity of the sensor and the consequent usefulness of the SBV as a contributing sensor:
1. 7 days/week operation
2. A revised spacecraft maneuver model
3. The introduction of the COLA scheduler
4. Modifications to the Signal Processor software.

The impact of these steps is the major theme of this paper and will be described in the following sections

2.1. Full-time operations

Space Surveillance operations depend on timely and reliable data flow on RSOs. Hence, it is vital to have 7-day/week availability of sensors. The SBV, under previous paradigm as an experimental sensor, was operated 5 days/week. But as a contributing sensor to the SSN, it is being operated 7 days/week with one of those days reserved

71

for maintenance and developmental activities. A companion paper in the Space Control Conference[1] describes the methods of monitoring the performance of the SBV. The SBV collects data on RSOs in a sidereal stare mode where the stars are kept stationary in the focal plane and the satellite moves across part of the focal plane over several exposures or frames called a frameset. Detailed planning for a day's events is carried out in SPOCC and the commands are sent to APL to be uploaded to the spacecraft. The performance monitoring system collects statistics on how many framesets have been commanded for each day's events. Typically, two framesets are collected per RSO, which should yield four observations, constituting a track, spanning ~1 – 2 minutes in time. If there is a satellite streak detected in every frameset, at least 200 framesets/day must be planned to achieve 100 tracks/day that is called for by the funding agreement for the sensor.

Fig. 1 shows the recent history of the mission planning results for the SBV. The first noticeable improvement in the productivity occurs when the sensor started operating 7 days/week – the dips due to weekends are gone! The number of framesets per 8-hour day increased to ~120.
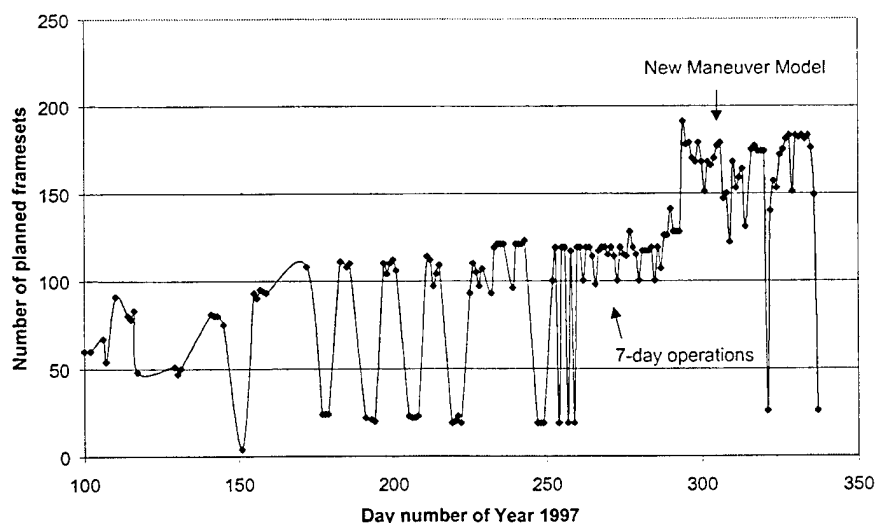

Fig. 1: Effects of two productivity enhancement techniques

2.2. Revised Maneuver Model

The mass of the MSX satellite is approximately 6000 lbs. The SBV is co-pointed with all the other sensors on the MSX along the +X axis of the spacecraft and is not separately gimbaled. Thus, to point the SBV, the entire spacecraft has to be maneuvered in attitude. Since the MSX is not a system controlled in real-time from the ground, the planning process has to account for the MSX attitude control delays in collecting data for every frameset (the step-and-settle time). A typical frameset may involve 12.8 secs. for 8 frames of 1.8 sec. each, followed by 35 seconds for the signal processor to reduce the data and an additional 3 – 5 minutes for the spacecraft to maneuver to and settle at the next pointing. A conservative model for the step-and-settle time has been

---

[1] G. Zollinger and R. Sridharan : "Peformance Monitoring of the SBV", 1998 Space Control Conference

in use in SPOCC mission planning since the early days of spacecraft life, as productivity was not the issue. However, once the transition to a contributing sensor mode was decided upon, tuning of the maneuver model was necessary to reduce the dead time between exposures. This was achieved by analyzing high rate attitude sensor data from the MSX during sample experiments. As a result, the second step change of ~40% in number of planned framesets per month shown in Fig. 1 was achieved – from 120 to 170 framesets per 8-hour day.

2.3. The COLA Scheduler

The SBV is an inherently wide field-of-view instrument with each CCD covering approximately $1.4^0 \times 1.4^0$ and all four together covering a total field-of-regard[2] of $6.6^0 \times 1.4^0$. It is immediately evident that the SBV can exploit clusters in the geosynchronous belt to enhance productivity, defined as the number of RSOs tracked/day. However, a small study indicated that there is a substantial number of transient, temporal clustering of non-geosynchronous objects too as Table 1 below shows.

Table 1: Available conjunctions

Time (min)	Geosynchronous clusters	Geosynchronous-nonsynchronous	Nonsynchronous-nonsynchronous
0	56	10	11
2	56	11	12
4	56	8	9
6	56	7	10
8	55	9	10
10	66	11	10
12	79	8	15

Table 1 was generated by the following procedure. A set of 612 deep space RSO's were chosen from the catalog (232 geosynchronous, 380 other). Beginning at an arbitrary time on an arbitrary day, the number of conjunctions visible to th SBV every two minutes was calculated. Two satellites were said to be in conjunction when they were within 2.8^0 (or two CCD fields-of-view) in angular position of each other as viewed by the SBV. The results are remarkable in that apart from the known geosynchronous clusters, there is at any given time a significant number of mostly transient clusters involving non-geosynchronous satellites with either GEO or non-GEO satellites. An example of actual data is also shown in Fig. 2 wherein the SBV detected a LEO, a HEO and three GEO satellites within the same FOV – all in an apparent conjunction.

---

[2] The total field-of-regard is larger that four times the individual FOV per CCD because of the considerable distortion inherent to the off-axis design of the telescope. Also the SBV can process data from only one CCD at a time.
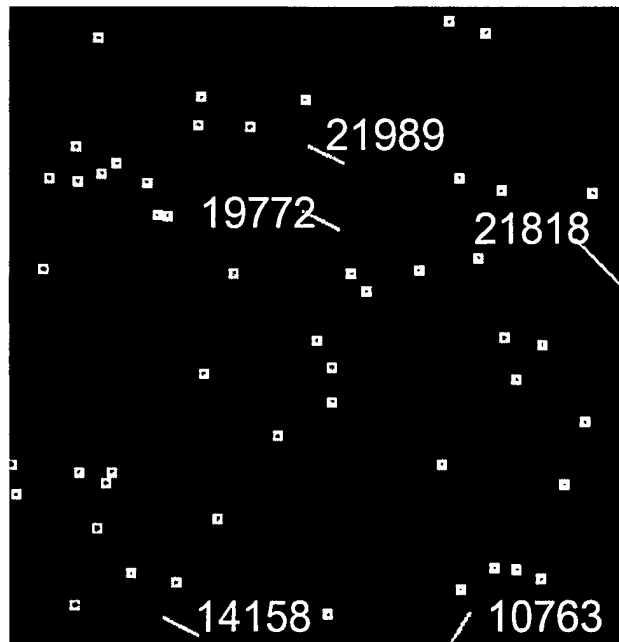
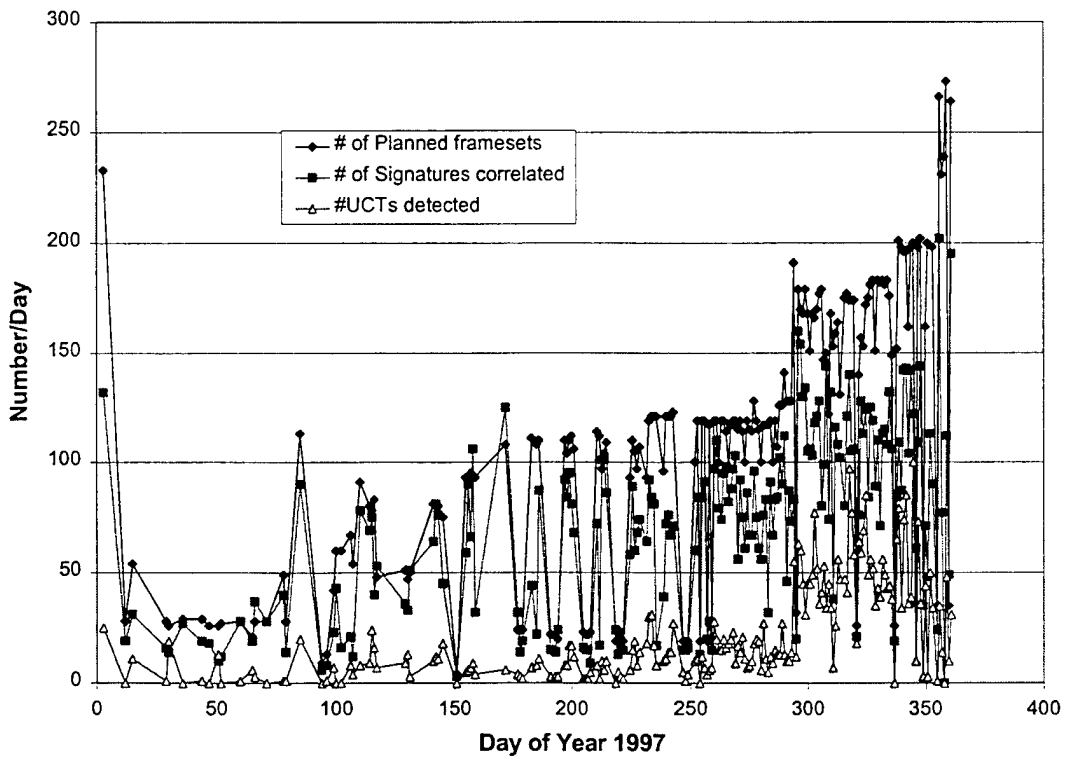Fig. 2: Apparent Conjunction of LEO, HEO and GEO satellites

Fig. 3: Recent Performance of the SBV showing impact of COLA

A new scheduler was designed to operate the SBV. Called the **Conjunction-Optimized-Look-Ahead** or **COLA** scheduler, it takes advantage of the large field-of-

view and available conjunctions to schedule satellites. The result is a significant increase in the productivity of the sensor as evidenced by Fig. 3. In this figure, the number of correlated streaks is the actual output of the SBV after filtering out false streaks (see Sec. 2.4 below). Each streak yields two observations per RSO. On the basis that a track is 4 observations per RSO, or equivalently two streaks, it is clear that the SBV is generating over 100 tracks/day as called for by the ACTD[3] agreement. Note that there are two steps due to COLA: the first when the short event of the day was converted to COLA and the next when both events of the day were converted to COLA. While the use of COLA is still in its early stages, the following results are already evident:

1. Use of temporal, apparent conjunctions of satellites in a large field-of-view is an effective technique for enhancing the productivity of the SBV and, by inference, any wide field-of-view sensor.

2. The tasking of the SBV should take advantage of the availability of COLA. In particular, over-tasking of the sensor is required so that conjunctions may always be availed of. It is even conceivable that "wide-open" tasking of the entire deep space catalog to the sensor may be an effective technique as long as COLA is designed to accept and process such a large number of satellites.

3. Many techniques are available for the optimization of the COLA-generated schedule subject to the constraints of the spacecraft and sensor. These have yet to be investigated.

2.4. Signal Processor software enhancements

The SBV has an on-board signal processor that compresses several frames of full-bandwidth CCD data into a few stars and a few satellite streaks. The process is shown schematically in Fig. 4. The CCD camera collects a series of raw frames or exposures
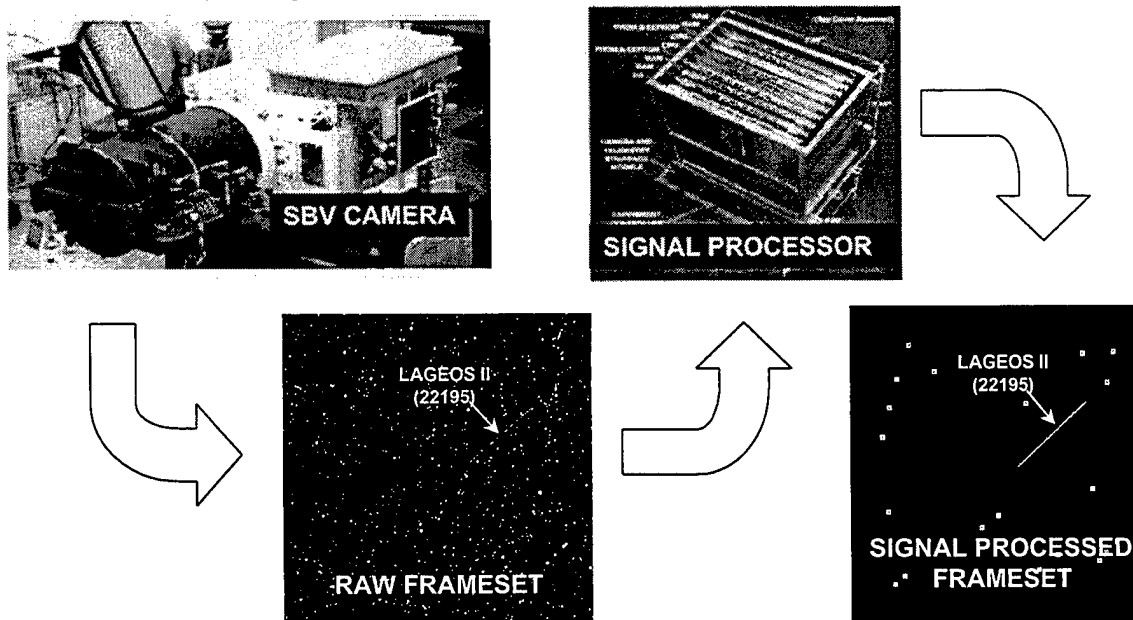

Fig. 4: Data flow on-board the SBV

and transmits them to the Signal Processor. The frameset is processed by the SP to retrieve the streaks of moving satellites against a background of fixed stars. The streak information along with a short list of the stars is sent to the ground as the compressed output of the SP. The stars are matched against a star catalog in ground processing to elicit the boresite pointing of the SBV. The streak endpoints are then determined in angular coordinates. This process works well in general. However, very often, there are proton events – bright, temporally short flashes – that either corrupt the streak or, in some cases, look to the signal processor like a streak. An example is shown in Fig. 5.
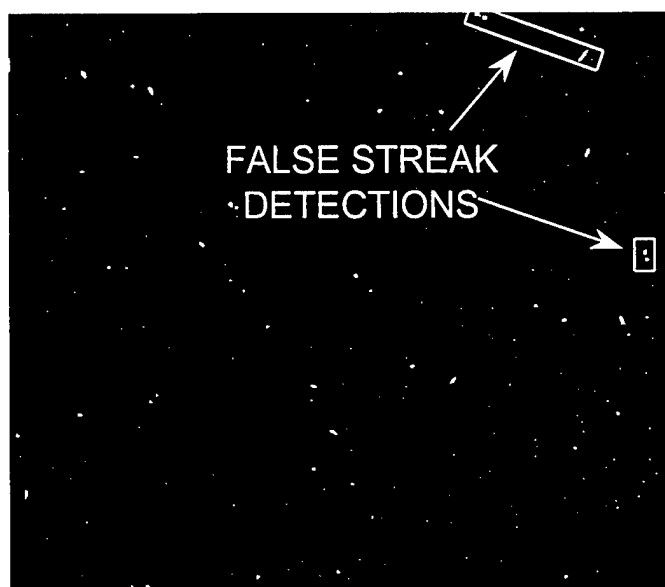
Fig. 5: A frameset with the SBV cover closed showing false streaks
caused by proton events

The frameset in Fig. 5 was taken with the cover of the SBV telescope closed (note that this frameset was taken outside of the South Atlantic Anomaly, a high radiation environment region, wherein the SBV is 8% of the time). Thus all star- and streak-like apparitions in the frameset are caused by proton or radiation events on the focal plane. The number of such events varies from ~30/frame to as many as 900/frame depending on the geographical location of the satellite. Hence, fully 32% of the framesets collected by the SBV show false streaks due to such radiation events.

Filtering out the false streaks due to proton events is presently done on the ground. Fig. 6 shows a comparison between a false streak due to a radiation event and a valid streak from a RSO as seen in the data. It is clear that the proton event is a temporally short, very bright event unlike the signature of a typical RSO. Software has been added to the ground-based data reduction process to detect and remove false streaks based on the characteristic difference in signature.

Fig. 6. Signature characteristics of a false streak (left) and a valid streak (right)

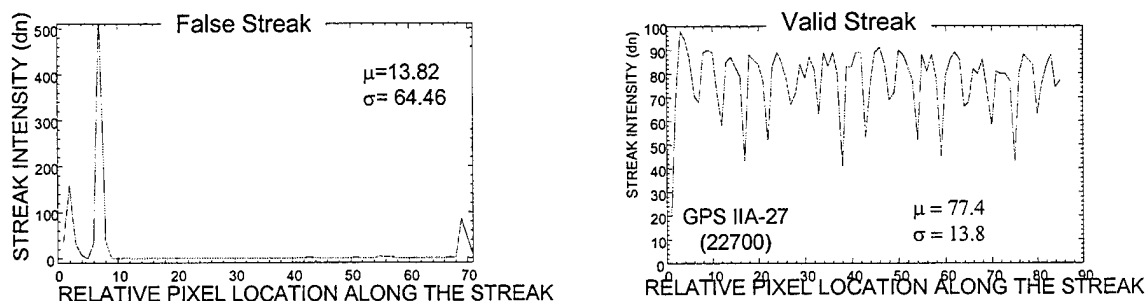Tests on the ground have shown that there are two additional problems with the proton events. Proton events may overlay valid streaks in which case the detected streak gets corrupted and the algorithm described above fails. Also, a high density of proton events could cause an overload on the signal processor rendering it unable to detect any streaks. These problems can only be corrected by modifications to the on-board processing software in the signal processor. Such software has been developed and tested on the ground. The results are shown in Table 2 below. 195 framesets (or looks) were examined with both the old SP code and the revised SP code. The

	#Looks	#Streaks	False Streaks	#Valid streaks	#Valid streaks corre-lated	#Valid UCTs	#Visible objects detected
Old SP code	195	298	41%	177	90%	10%	68%
New SP code	195	241	15%	204	88%	12%	79%

number of detected streaks actually decreased – but entirely because of the reduction in the percentage of false streaks detected. The actual number of valid streaks increased. Both of these are desirable performance characteristics. The software is going through the process of upload and test. The revised code should offer significant increase in the number of valid streaks detected by the SP and, consequently, in the productivity of the SBV.

4. Quality of Data Improvements

Two activities are proceeding to improve the quality of data from the SBV:
1. Modeling of RSO brightness
2. Modeling of attitude drift of the spacecraft

4.1. RSO Brightness modeling

The SBV, being in orbit, can cover a wide range of phase angles. In fact, in principle, it can make measurements from 0^0 to 150^0 in phase angle, the latter limit being the closest one can get to the sun and still make valid measurements without saturation. In practice, however, high phase angles have been limited to ~110^0 because of safety concerns of other instruments on board. An example of such measurements is given on the left-hand side in Fig. 7. These measurements are translated to the detection intensity in digital numbers on the focal plane of the CCD in the right-hand figure. In both cases, the magnitude scale has been normalized to a distance of 36000 Km.
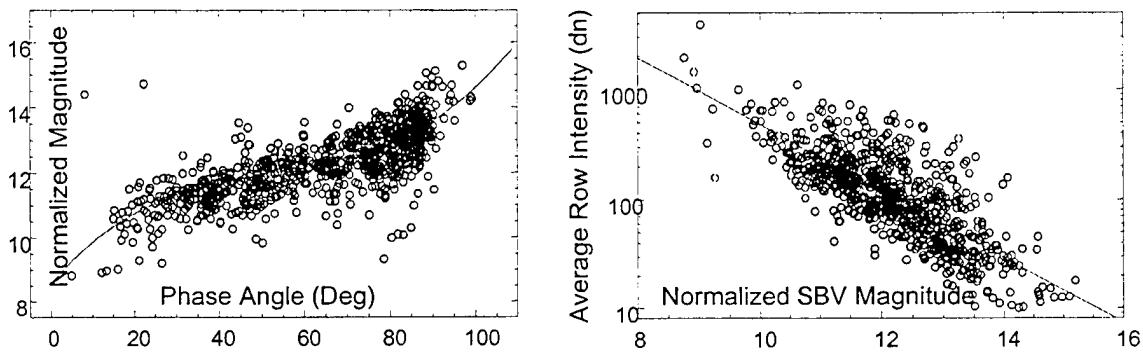

Fig. 7: RSO brightness modeling example: GLONASS satellites

The Scheduler will utilize models built on the basis of such measurements to ensure that a RSO is bright enough to be always detectable. The database in SPOCC will be populated with these measurements at 10^0 phase angle (or other appropriate angle) intervals. Where such data are not available, a brightness function for a class of targets is used. This procedure should ensure that the RSO is always detectable in the focal plane.

4.2. Spacecraft attitude drift modeling

The SBV has met its goal of metric accuracy of 4 arcsec. However, given the number of cataloged stars detected and the consequent precision of the boresite estimation, an effort was undertaken to assess whether the metric accuracy can be improved. As a companion paper[4] demonstrates, the metric accuracy can be enhanced by modeling the drift in attitude of the spacecraft during a frameset. Results indicate that a metric accuracy of 2 arcsec. for SBV data is achievable. These results will have a significant impact on the capability to determine initial orbits and also produce higher accuracy orbits on all RSOs.

5. Sensor Performance Modeling

A detailed assessment of the detection performance of the SBV is being made. Early results are given below:

---

[4] C. von Braun : "SBV metric accuracy modeling", Space Control conference 1998, M.I.T. Lincoln Laboratory, April 1998.

Detection method : Sidereal track, on-board SP
Geosynchronous RSOs in catalog : 493
Small GEO RSOs : 18
GEO RSOs detectable by SBV : 475
  Detected by SBV : 300
  Not detected by SBV : 38
  Not attempted : 137

The reasons for the lack of detection of a significant number of GEO satellites are under analysis. It is suspected that the causes are radiation events on the focal plane, inappropriate phase angles and occasional close clustering of RSOs within the resolving capability of the signal processor. Such results are being analyzed with all appropriate variables to ascertain the sensor's limits of performance.

6. Operations Cost and Automation

The SBV Operations and Control Center is a large software system. The SPOCC operates 7 days/week, 8 hours/day. However, the typical timeline for operations on a given day spans approximately 16 hours. Thus it is essential to automate operations in SPOCC so as to ensure reliable and repeatable performance of the SBV as a contributing sensor. The typical operations scenario is as follows (approximate times):

0700 UT : Tasking received from 1CACS
0800 UT : Tasking automatically processed
  Mission planning software initiated
1300 UT : All mission planning products ready
  Operators arrive in SPOCC
  Key outputs are checked to ensure experiments will be performed without compromising safety of sensor or S/C
  All command compliance products from previous day's experiments checked
  Health and status of the sensor checked
1500 UT : Commands for experiments transmitted to APL
1600 UT : APL verifies experiment commanding as safe
1800 UT : Upload of experiment commanding to spacecraft
2300 UT : First download of data
2400 UT : Data processed and metric data transmitted to 1CACS from first download
0500 UT : Second download of data
0600 UT : Metric data from second download processed and transmitted to 1CACS

All operations in SPOCC are automated. A substantial number of performance points are monitored for errors and the operators automatically paged for serious errors that may compromise the mission. The software system is shown in Fig. 8.

79

The command compliance and performance monitoring systems are described in a companion talk in this conference (see footnote 1). Several levels of alarms from warnings to severe are created by the command compliance system. The operators have insight through checkpoints/displays as shown by the smiling faces. In general
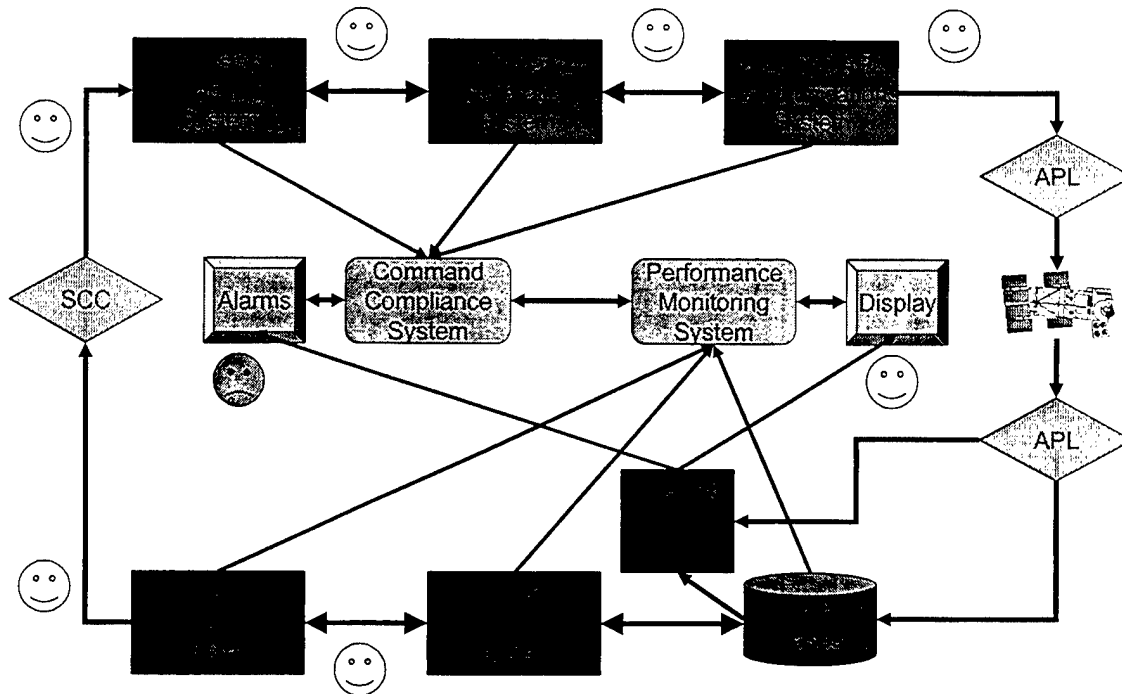
Fig. 8: Automated SPOCC software system showing operator checkpoints

the system runs itself once triggered by the arrival of tasking or by the receipt of downloaded data from the satellite.

7. Summary

The SBV is becoming a contributing sensor to space surveillance under agreement between BMDO and AFSPC. One of the requirements is to produce 100 tracks/day on deep space targets. Several steps have been taken to meet/exceed this goal. It seems quite likely that a single SBV (15 cm. telescope) operating 8 hours/day will equal or exceed the productivity of a GEODSS site with two 1.2 meter telescopes while at the same time producing data of better quality.

SBV Space Surveillance Performance
Jayant Sharma, MIT Lincoln Laboratory

Abstract

The Space Based Visible (SBV) sensor package on the Midcourse Space Experiment (MSX) satellite has been conducting space surveillance for nearly one and half years. This paper will describe the long term detection sensitivity and metric performance of SBV using onboard signal processed data. This data is also used to illustrate unique capabilities of the SBV sensor. SBV has access to the entire geosynchronous belt, and its wide field of view allows data to be collected on multiple resident space objects (RSOs) simultaneously. The large field of view also allows data to be collected on uncorrelated targets (UCTs). Use of SBV observations to detect and identify UCTs is also presented.

Introduction

The goal of SBV is to demonstrate the ability to make observations of resident space objects (RSOs) from a space based platform. The description of the data processing is provided in a previous paper [Ref. 1]. Sensor characteristics relevant to routine space surveillance are summarized in Table 1. This paper describes how the unique properties of the SBV sensor can be exploited for space surveillance. First, the SBV sensor is on an orbiting platform and has access to the entire the geosynchronous belt. Second, the wide field of view of the sensor allows multiple RSOs to be detected simultaneously.

Table 1. SBV Sensor Characteristics

Spectral Range	0.3 - 0.9 μm
Spatial Resolution	12.1 arcsec/pixel
Field of View per CCD	1.4 x 1.4 Deg
Aperture, f/no	15 cm, f/3
Number of Frames per Frameset	4 – 16 frames
Frame Integration Times	0.4, 0.625, 1, 1.6 sec
Frame Sizes	420x420 pixels

Surveillance Data Summary

This section describes the quality of SBV surveillance data. SBV has been observing RSOs since its launch in April 1996, and this data is used to describe the quality of the space surveillance observations. Unless noted otherwise, all the SBV data used in this study is routine space surveillance data. This data is collected in a sidereal track mode, where the stars appear as point sources and the RSOs appear as streaks. Routine surveillance data is then processed through the onboard signal processor to extract the star and streak information as illustrated in Figure 1.
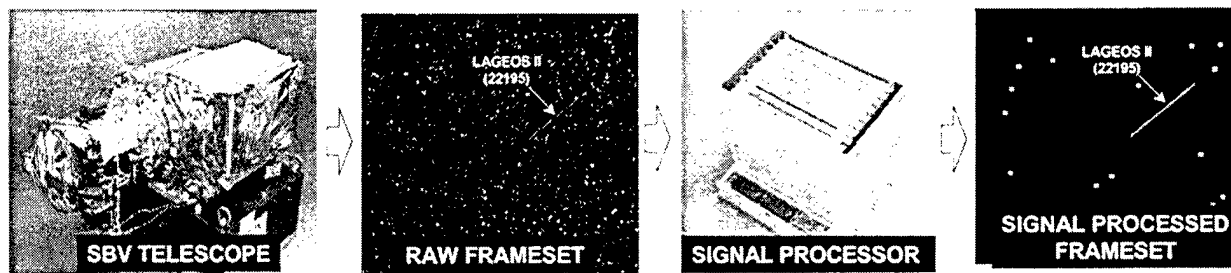
Figure 1. Routine Surveillance Data

The ability of SBV to detect a large range of objects, and the metric accuracy of those observations will also be illustrated. Over 10,000 observations of RSOs have been collected, and the histogram of the observed SBV magnitude of these detections is shown in Figure 2. Since the primary focus of SBV is deep space surveillance, over 95 percent of these observations are on deep space objects. SBV magnitude closely approximates the visual magnitude scale, but is a function of the sensitivity of the SBV CCD over its spectral range. Figure 2 clearly demonstrates a detection sensitivity down to 15th SBV magnitude for the sidereal mode of data collection.

Figure 2. SBV Magnitude of Correlated Objects

Figures 3 and 4 illustrate the histogram of observed magnitudes for selected RSOs. These two non stabilized geosynchronous satellites illustrate the range of detections due to different viewing angles of a large and small RSOs.

Figure 3. Observed Magnitude of 22927 (Telstar 401)
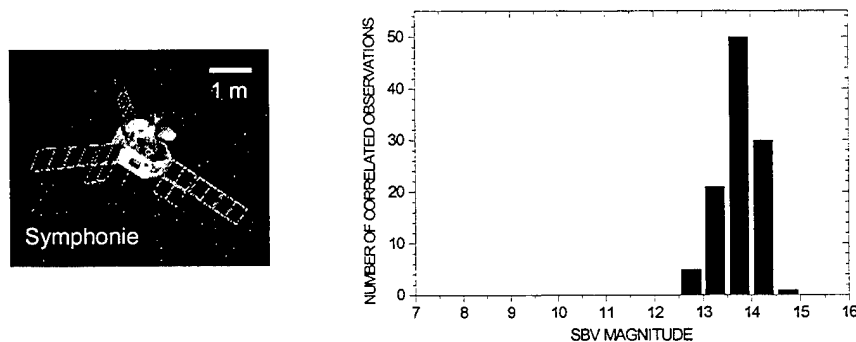
Figure 4. Observed Magnitude of 7578 & 8132 (Symphonie A & B)

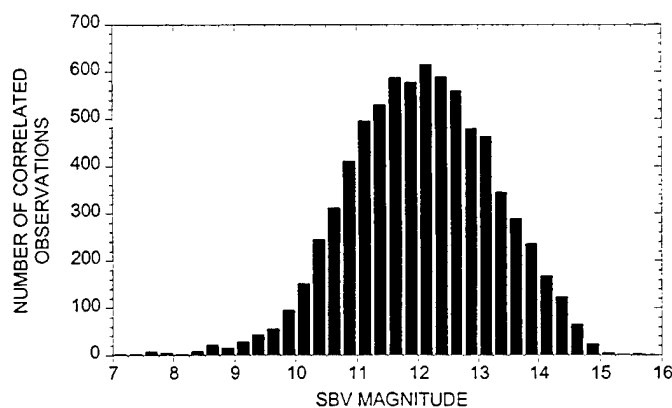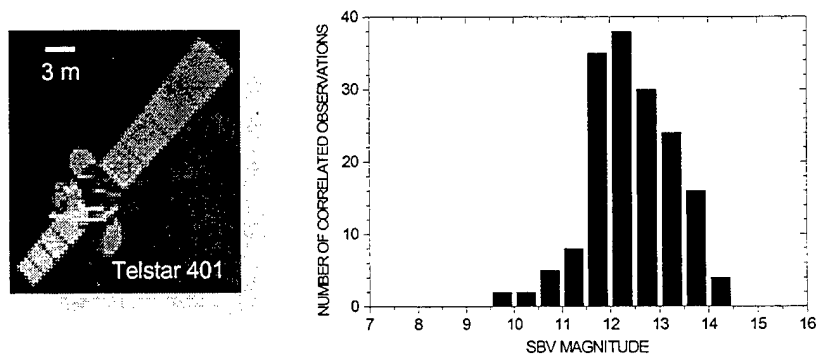The goal of the SBV sensor is to produce metric observations that have a 4 arcsecond metric accuracy. This is accomplished in three primary steps. First the pointing of the sensor is accurately estimated. This is done by centroiding the detected star location, and matching them with stars from a catalog. The second step involves precisely determining the location of streak endpoints on the focal plane and mapping them back into right ascension and declination [Ref 1]. Finally, the position of the SBV platform must be accurately determined. This is accomplished by performing precise orbit determination of MSX [Ref. 2]. Figure 5 shows the quality of the SBV pointing and the MSX orbit for the first 500 days of SBV operations. Figure 5a shows a histogram of the RMS star fit residuals per frameset, and indicates that the average star match with a catalog star is performed with a precision of 0.8 arcsecond. Since the pointing is determined by a least squares estimation process, the pointing accuracy can be approximated by dividing the star match quality by the square root of the number of stars matched. With an average of 12 stars being matched per frameset, the resulting pointing accuracy is approximately 0.2 arcsecond. Figure 5b is a histogram of the Millstone Radar RMS range residuals and illustrates that the orbit is known to better than 10 m. The radar data is not used to estimate the orbit and serves as an independent assessment of the orbit quality [Ref. 2].
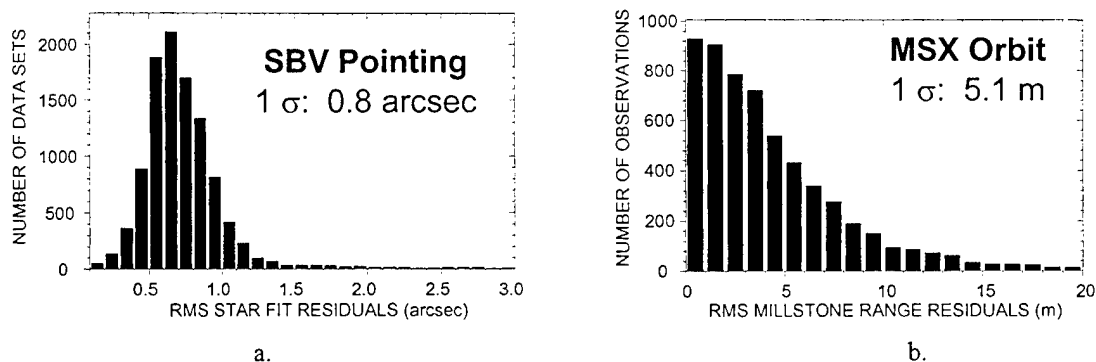
Figure 5. SBV Pointing and MSX Orbit Quality

The updated SBV pointing is used to map streak endpoints from focal plane coordinates to right ascension and declination coordinates, which are then combined with the MSX location to create space based observations. The accuracy of these observations is assessed by calculating the difference between the observed location and an accurate predicted location. The predicted location is based on an orbit using the ground based Space Surveillance Network (SSN) observations[Ref. 3]. This assessment relies on an accurate orbit using SSN data, which is not always available due the quality and/or quantity of tracking data. For this analysis, SBV observations of Russian navigation satellites (GLONASS) were used for the accuracy assessment. These are noncalibration satellites that are routinely tracked by both optical and radar sensors. A histogram of the SBV RMS observation residuals for GLONASS satellites is shown below in Figure 6, and indicates that the accuracy of the observations is approximately 4 arcseconds.
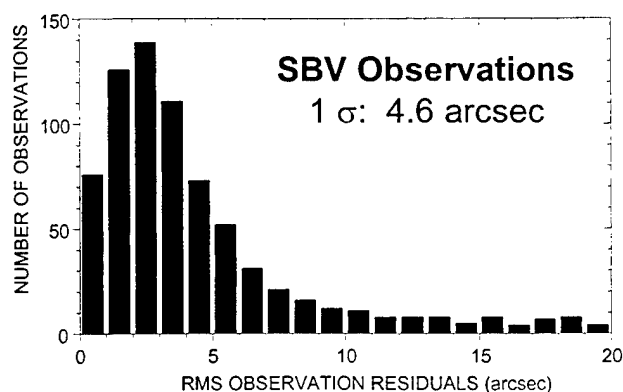
Figure 6. SBV GLONASS Observation Residuals

The temporal behavior of orbit and observation quality is shown in Figure 7, and shows no degradation over the time period indicated.

MSX Orbit
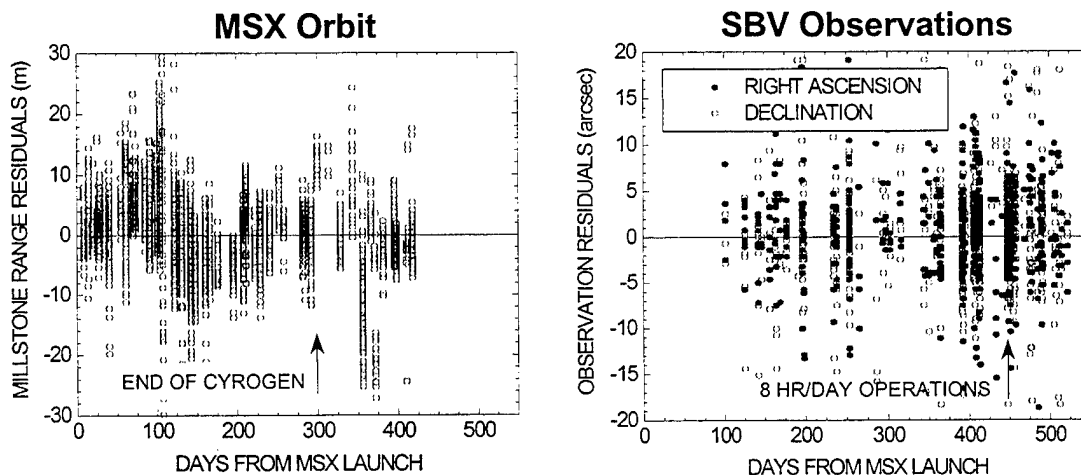
SBV Observations

Figure 7. Temporal Variation of Orbit and Observation Quality

Geosynchronous Belt Surveillance

The quality and sensitivity of the SBV data has been demonstrated in the previous section. This section will look at some of the capabilities of SBV in performing space surveillance. In particular this section will look at exploiting the wide field of view (1.4x1.4 Deg) and the ability of the SBV to view the entire geosynchronous belt. Access to the entire geosynchronous belt is illustrated by Figure 8, which shows a plot of all station kept geosynchronous satellites observed by SBV through November 1997. The tick marks indicate location as a function of east longitude on the geosynchronous belt.
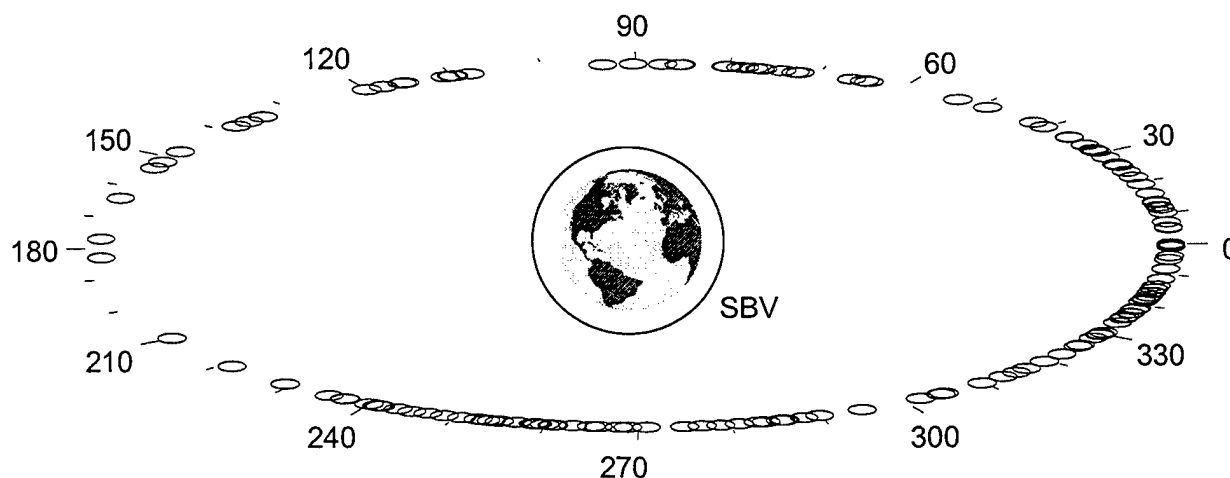
Figure 8. All Station Kept Geosynchronous Satellites Observed by SBV (as of 11/97)

This plot shows that SBV has access to the entire geosynchronous belt. The wide field of view allows multiple objects to be detected. This is particularly advantageous for surveillance of the geosynchronous belt, where

85

satellites are stationed close together. The wide field of view also allows for the detection of nonstation kept RSOs in the geosynchronous belt. This capability is illustrated in Figure 9a, which shows a cluster of five commercial communication satellites located at 259 E longitude as well as a drifting RSO. Figure 9b. shows an histogram of the observed location of the satellites in this cluster over several hundred days, and clearly shows the small station keeping bounds used by these satellites. The location on the geosynchronous belt is calculated by converting the observations directly to longitude. The position vector of the RSO relative to SBV is calculated by multiplying the unit vector of the observed direction by the range to the RSO, as determined from the correlated element set. The inertial position vector of the RSO relative to the center of the earth is determined by adding the precise position of SBV to the SBV-RSO position vector. This geocentric vector is then rotated into an earth fixed frame and converted to longitude and latitude. By relying on the element set for only the range value, additional position errors in the element set are not mapped into longitude or latitude.

a.   b.
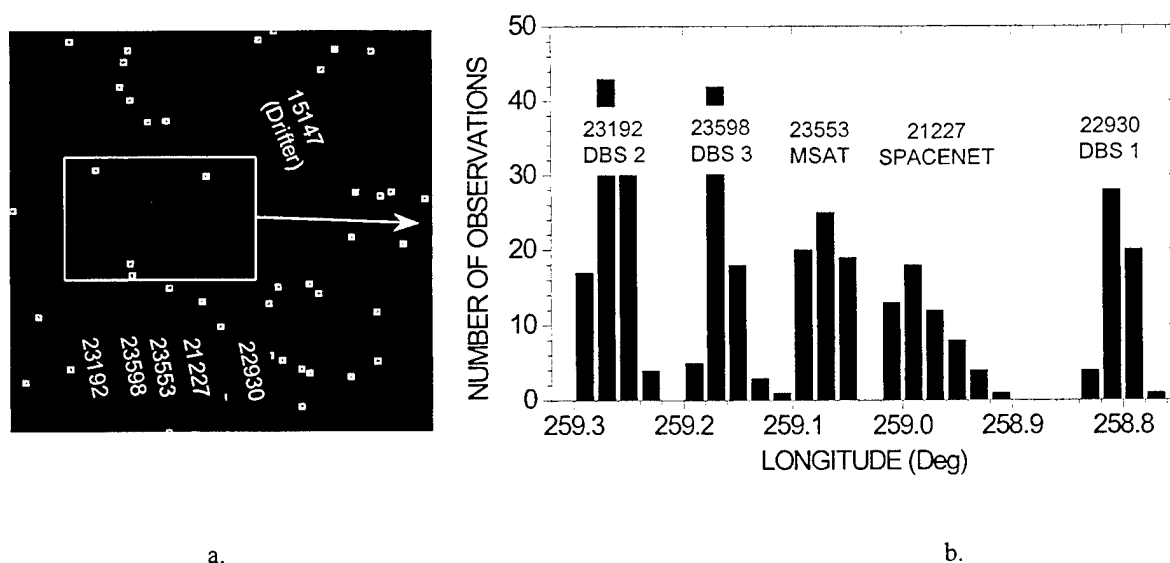
Figure 9. SBV Observations of Geosynchronous Cluster

The observed location of geosynchronous satellites is also useful in detecting station keeping maneuvers of the satellite. If the satellite is observed frequently, then a maneuver can be detected by looking at the change in longitude. Figure 10a shows a cluster of two Russian geosynchronous RSOs located at 12 E longitude, with two additional drifters in the field of view. Figure 10b shows a plot of the observed longitude as a function of time, and longitudinal station keeping maneuvers are visible. Two maneuvers for object 22269 are evident at an interval of approximately 50 days. Similarly, two maneuvers are visible for object 22557 but are separated by 80 days. Knowledge of the maneuvers can be utilized to restart the orbit determination process and so improve the orbit accuracy, or can be used to estimate the size of the maneuver if precise orbit determination procedures are used.
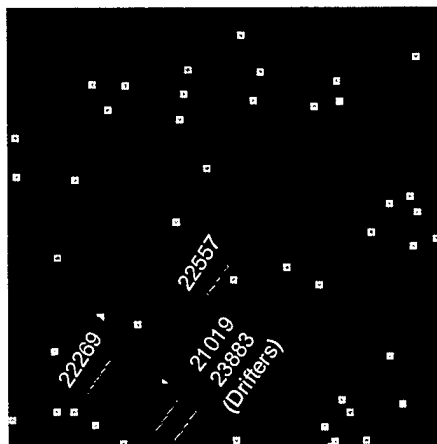
a.
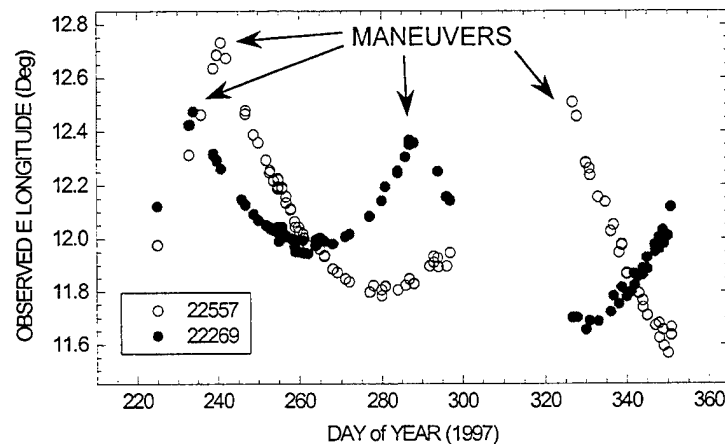
b.

Figure 10. SBV Observations of Maneuvering Geosynchronous Satellites

Uncorrelated Target Analysis

This section looks at another benefit of a wide field of view sensor. Its ability to collect data on lost objects, and objects whose element sets are not well known. In addition to collecting data on known objects, a wide field of view also facilitates the detection of uncorrelated targets (UCTs). Before the SBV UCT data can be utilized, it is necessary to first determine if the detected streak is a valid streak. The current algorithms on the onboard signal processor will occasionally connect a sequence of radiation events to form a streak, a false streak. A false streak will typically go through the data reduction process without being correlated, and be identified as an UCT. It is necessary to separate the valid streaks from the false streaks. An algorithm has been implemented in the data reduction process to analyze streak data and identify valid streaks.

The streak detection algorithm relies on the analysis of the intensity and temporal information of the streak. Once a streak is detected by the signal processor, a five pixel wide swath encompassing the streak, as shown in Figure 11, is sent to the ground.

DETECTED STREAK   **STREAK SWATH**
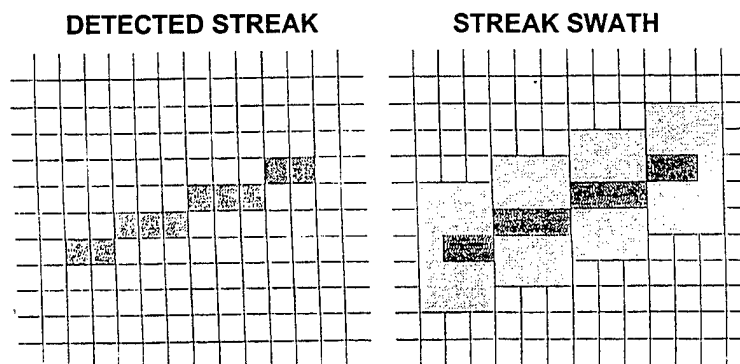
Figure 11. Illustration of Streak Swath

For each pixel in the swath, the maximum intensity value above the background average is determined, and the frame number in which it occurred is reported. Figure 12 shows a raw frameset with six valid streaks and one false streak and plots of the streak intensity along their lengths. In this case, the false streak consists of two radiation events being connected together. One discriminent is the variability of the intensity information, which is quantified by dividing the standard deviation of the streak intensity by its mean. This quantity is referred to as a scintillation index. Valid streaks show less variability than false streaks.
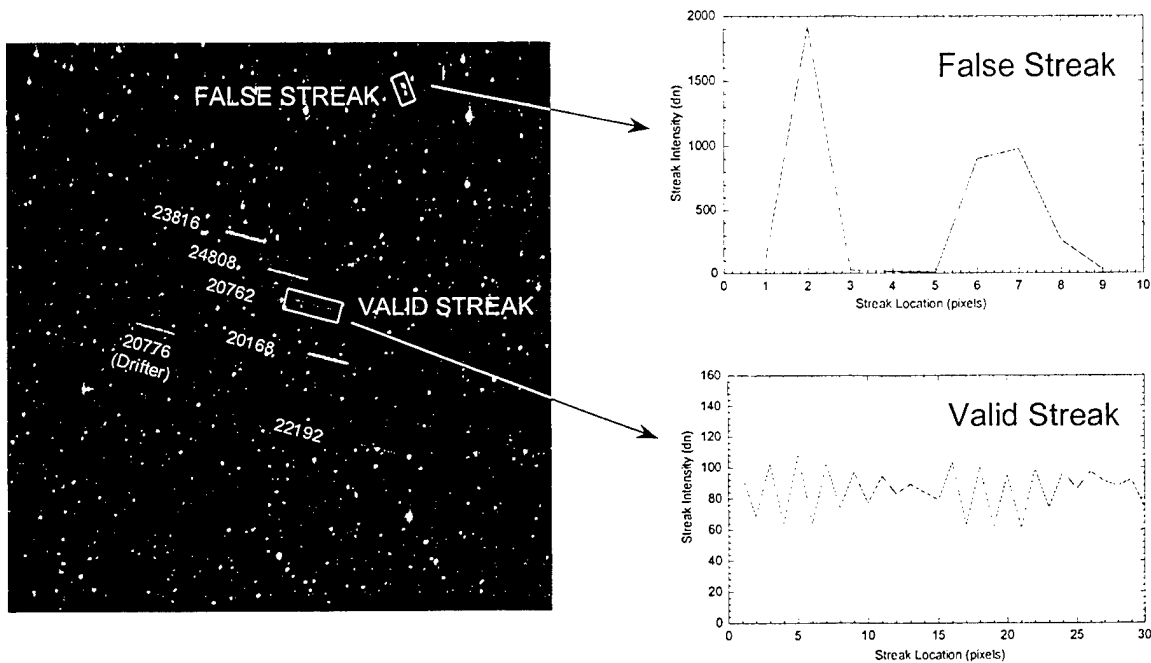
Figure 12. Determination of Valid Streaks

A scintillation index for the temporal information is also used, and it consists of looking at the statistics of the frame numbers occupied by the brightest pixel for each row of the streak swath. Again, valid streaks show less variability than false streaks. The intensity and frame indices are combined to form a streak quality index, which is then used to separate valid and false streaks.

Once a UCT detection has been determined to be valid, further steps are taken in an effort to identify it. The first step is to determine if the streak can be correlated with something nearby. RSOs with old or poor quality element sets will typically not correlate. Figure 13 illustrates the case of a RSO with an old element set. It shows a plot of the detected and predicted locations of three RSOs that were in the field of view.

RSO	DESCRIPTION	OBSERVED SBV MAGNITUDE	AGE OF ELEMENT SET
23118	METEOSAT ROCKET BODY	14.5	38 Days
15391	NATO IIID	13.3	7 Days
23528	INTELSAT VII	11.7	< 1 Day
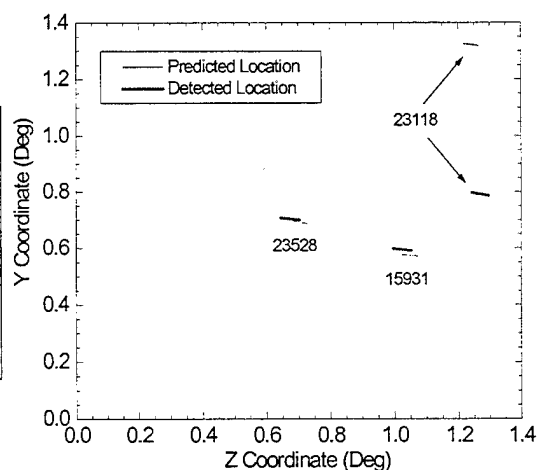
Figure 13. Correlation of Lost Objects

The two objects near the center readily correlated to objects in the RSO catalog, but object 23118 did not initially correlate due to the age of the element set. It was eventually correlated by fitting the SBV observations with ground based observations on 23118.

The final example describes the first confirmed discovery of a lost object by SBV. On day 295 (1997), while observing the geosynchronous object 21821 (at 36 degrees east longitude), SBV detected an UCT drifting through its field of view as shown in the two plots in Figure 14 taken 47 hours apart. No apparent catalog objects were candidates for its identity. Further observations indicated the object had stopped drifting, and an element set was created using initial orbit determination techniques. This element set was then refined with additional observations.
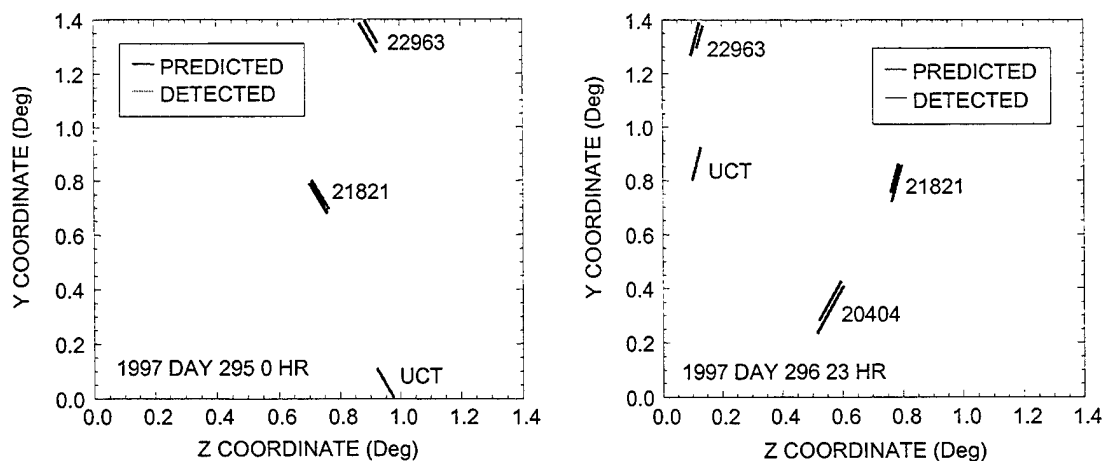
Figure 14. SBV UCT Observations

89

The photometric data for this object was analyzed for clues to its identity. Figure 15 shows a plot of the normalized SBV magnitude as a function of the phase angle. All observed magnitudes are normalized to a constant range of 36,000 km to remove the effect of range from the data.
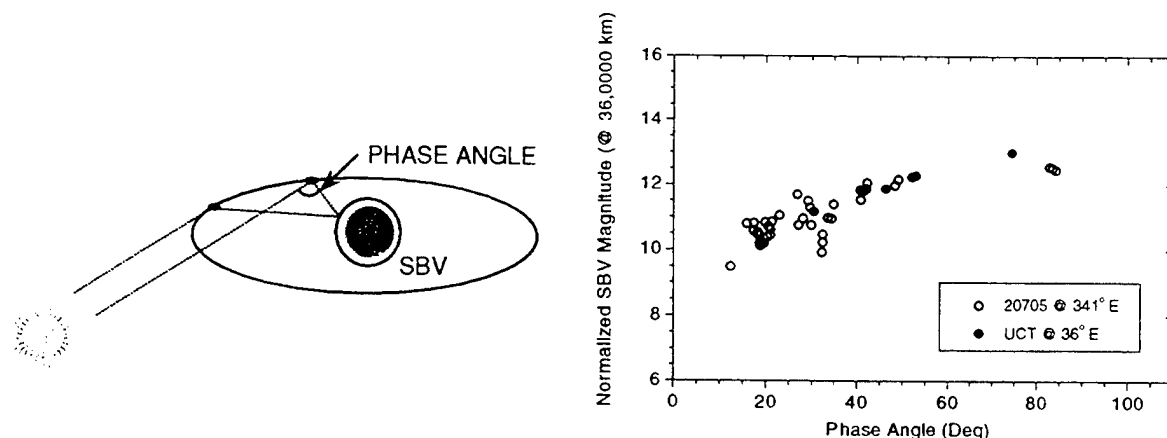
Figure 15. UCT Photometric Data

The curve that describes the shape of the photometric data is referred to as a phase function. The data on the UCT describes a linear phase function which is consistent with that of a large 3-axis stabilized satellite whose solar panels are tracking the sun. Also shown in Figure 16, for comparison, is the suspected identity of the UCT. This UCT was suspected of being object 20705, the French TDF 2 satellite (3-axis stabilized), which was being relocated from 341 degree east longitude. The First Command and Control Squadron (1CACS) was notified of the UCT, with its element set and possible identity. The object was subsequently observed by ground based sensors, and its identity was confirmed as object 20705.

Summary

Signal processed surveillance data collected over the first 500 days of SBV operations has been used to demonstrate the sensitivity and metric accuracy of the SBV sensor to 15th magnitude and 4 arcseconds respectively. The capability of the SBV to perform space surveillance of the entire geosynchronous belt has also been shown. The wide field of view of the SBV sensor permits simultaneous observation of geosynchronous satellite clusters, and also aids in the detection of UCTs. The photometric data has proven useful in the identification of UCTs.

1. Sharma, J., et al., *SBV Data Reduction*, Proceedings of the 1997 Space Control Conference, Report STK-249 Vol. 2, MIT Lincoln Laboratory, Lexington, MA, 25-27 March 1997.

2. Abbot, R. I. et al., *MSX Precise Ephemeris*, Proceedings of the 1997 Space Control Conference, Report STK-249 Vol. 2, MIT Lincoln Laboratory, Lexington, MA, 25-27 March 1997.

3. von Braun, C., et al., *SBV Metric Accuracy*, Proceedings of the 1997 Space Control Conference, Report STK-249 Vol. 2, MIT Lincoln Laboratory, Lexington, MA, 25-27 March 1997.

SBV Performance Monitoring
G. Zollinger and R. Sridharan, MIT Lincoln Laboratory,

1. Introduction

M.I.T. Lincoln Laboratory has built, and continues to operate, a space-based visible wavelength optical sensor (SBV) for space surveillance. Launched in April 97 on board the BMDO-sponsored MSX satellite, the SBV has been performing its mission successfully (as companion papers in this session demonstrate). Unlike ground-based space surveillance systems, the SBV does not afford the luxury of real-time control. All planning and scheduling of resources has to be done a day ahead at the SBV Operations and Control Center (SPOCC). The collected data flow down from the satellite to the SPOCC only at the end of each day's data collection event thus precluding any near-real-time response to any features or anomalies in the data.

SPOCC is not a round-the-clock operation. Consequently, when operators arrive on site they need the ability to quickly ascertain the success of the previous day's experiments. Hence, a suite of software tools has been developed to aid in assessment of the data collection events. These tools condense large amounts of mission planning and experiment data into easily comprehensible form by extracting key information out of a large volume of data. A key function of the software is not only to assess the success of a given mission but also to provide enough information to troubleshoot potential problems. These tools take the form of report generation, user defined queries, plotting utilities, signal processor analysis, and three-dimensional representations of experiments. All these tools use Netscape as a backbone, making the software easily accessible and portable. This paper describes these tools and illustrates their utility.

2. Command Compliance

The first tool developed for understanding the SBV's performance is a software package called Command Compliance. Command Compliance is a simple program that compares the experiment results with the experiment as planned. A series of tests are performed on every signal processor image (or look[1]) to answer questions like: What was the object tasked? Was it in the field of view? Did the detected streak correlate with the object? A set of summary statistics is also generated including the number of looks, the number of objects tasked and acquired, and the amount of memory used. These reports enable the operators to comprehend the results of the previous night's experiments.

Command Compliance reports are automatically generated for every experiment. They are written in HyperText Markup Language (HTML), which is a Netscape standard for Web pages, thus making them extremely portable. Such portability is vital in an op-

---

[1] Description of the modes of data collection, signal processor image, look, etc. can be found in the companion papers at this session.

erational environment with multiple computer platforms such as DEC Alphas, SGIs and PCs. All computer platforms are able to access and display these reports.

A key use of the Command Compliance software is for troubleshooting because it provides an independent analysis of the spacecraft data, mission planning and the data reduction processes. One of the first major bugs that Command Compliance uncovered was discrepancy in the databases both in the volume of data and in some key values such as the CCD or the integration time used for the look[2]. Missing data obviously affect the throughput of the sensor, but if the CCD number or Integration Time is mislabeled then the tasked object will not correlate or may not even be the field of view. Investigation revealed that a software bug and error handling in the decommutator[3] were responsible for the problems.

3. The Command Compliance Query Engine

Command Compliance software has evolved over the last year to encompass a battery of tests to track attributes. However, a Command Compliance report represents assessment of the performance of a single experiment. In order for us to assess the performance of the SBV, we need to evaluate multiple experiments at a time (the big picture). With this requirement in mind, a new set of tools has been developed using Command Compliance as the underlying engine.

The first tool developed is a query engine, wherein the user is able to specify a set of queries with user-defined limits for any set of attributes from the Command Compliance reports. A sample Command Compliance report has about thirty columns, all of which are important attributes but may not be relevant when looking for specific patterns or trends in experiment data The program uses a Web based interface in which PERL is used to handle the queries. A sample query might involve the South Atlantic Anomaly (SAA). The SAA is a high radiation environment wherein the SBV is exposed to several hundred proton events per second. The Signal Processor on the SBV is unable to detect any valid satellite streaks amidst such a dense background of false events. Command Compliance can be used to show that the SBV spends about 8.2% of its time in the SAA. So a sample query, designed to discover trends in performance, can be designed to filter out cases where the SBV is in the SAA. For example, the GLONASS satellite catalog number 23511 is a bright object even at high phase angles but is not always detected by the SBV. The query engine can be used to generate the following results (Table 1) about why the SBV did not correlate 23511. This set of queries can be executed in less than half an hour.

---

[2] The SBV has four abutted CCD's with contiguous fields-of-view of $1.4^0 \times 1.4^0$, only one of which can be used per look. Two integration times per frame are possible (0.4 sec. and 1.6 sec.) with 4-16 frames per look.

[3] The decommutator converts the telemetered science data from the satellite into engineering units and stores them into the databases.

Number of Looks	Percent	Category
178	100	Looks made to acquire 23511
101	56.7	Looks with streak correlated to 23511
77 out of which	43.3 out of which	Looks without streak correlated to 23511 out of which
21	11.8	Looks with one UCT (probably 23511)
8	4.5	Looks with "data missing problem"
8	4.5	Looks in the SAA
12	6.7	Looks with no detectable streaks
23	12.9	Looks without a valid streak
3	1.7	Looks with zero UCTs
2	1.1	Looks with <5 stars detected or matched

Table 1: Statistics on why 23511 did not correlate

An uncorrelated target (UCT) is a streak that is deemed valid but does not match anything in the catalog within the correlation bounds used in the data reduction algorithm. The next two reasons that 23511 did not correlate were described earlier. If there are no detectable streaks then no object can be correlated. A valid streak is a streak where the number of pixels that a streak occupies in each frame and the intensity of the streak are reasonably consistent. Proton events can create false streaks, and those false streaks meet neither criterion. Data Reduction relies on star matches to generate an accurate measurement of the SBV pointing and so low star matches leads to limited accuracy in pointing, affecting object correlation. Each of these statistics describes a distinct problem to be addressed in improving SBV operations.

As another example, the query engine has been useful in reporting instances of major anomalies such as the Signal Processor Anomaly. This anomaly results from a (software) failure of the on-board signal processor and results in "blank" looks with no stars and streaks being detected. All other housekeeping information is still transmitted.

4. Graphical Capabilities

Along with the query engine, a sibling plotting package has been developed. The plotting package can generate graphs involving many of the attributes tracked by Command Compliance enabling an analyst to identify key changes in spacecraft operations. The program uses another Web based interface, this time relying on PERL and GNU-PLOT for handling data manipulation. A key difference between with this program and the query engine is that the software can plot one variable as a function of another. An example plot might show the number of planned framesets (or looks) /day that the SBV has collected since Jan 1 1996 (Figure 1). The SBV operations have changed from a handful of events per week to a contributing sensor mode with experiments lasting 8 hours/day, 7 days/week. This plot show three key changes in the SBV operations. The first is the beginning of the seven-days-a-week SBV operations, during which the number

of planned framesets per day reached a higher plateau. Recently a new maneuver model has been put in place, which reduces the amount of time necessary for tracking an object. This modification increases the number of objects that can be tracked per day. The third change is the effect of the new scheduler COLA that takes advantage of fortuitous conjunctions of satellites within the SBV field-of-regard to enhance the productivity of the sensor.
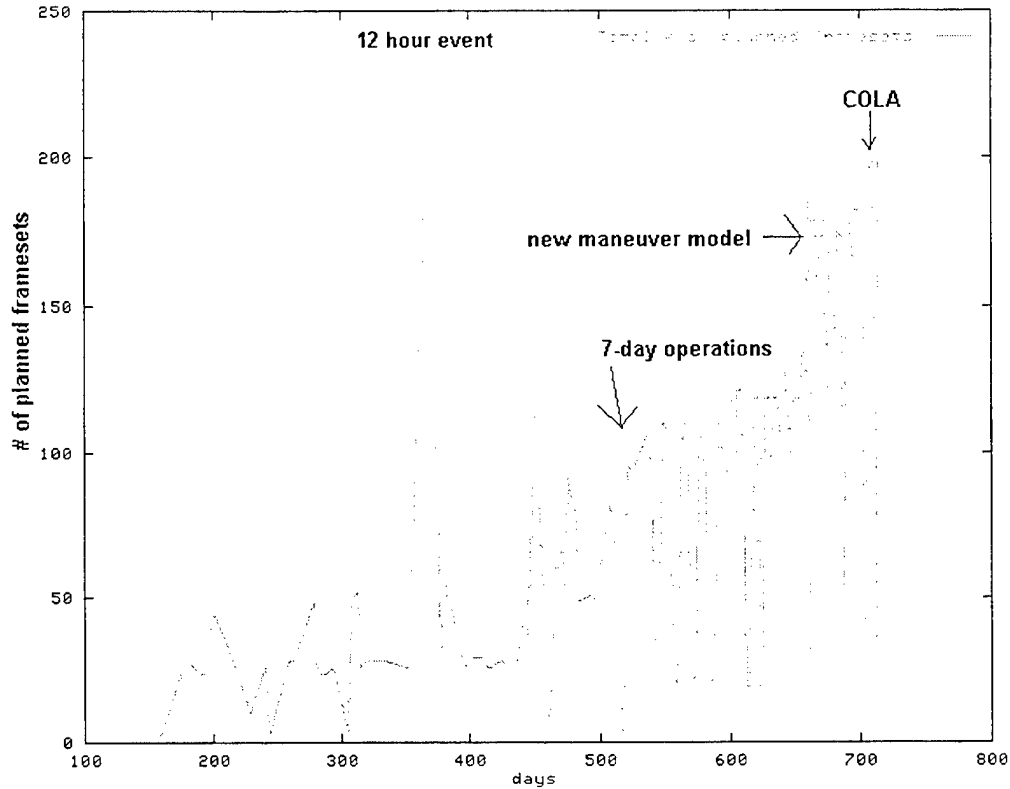
Figure 1: plot of planned framesets a function of days since Jan 1 1996

5. Signal Processor Image Tool

The SBV is an optical sensor that transmits Signal Processor images consisting of a collection of stars and streaks, which on the ground are converted into metric observations of satellites. A tool has been developed to combine into a simulated image the star and streak information along with the data reduction products such as predicted location of streaks, correlated streaks, and UCTs. Figure 2 is a sample Signal Processor image generated by this tool. Every streak reported by the Signal Processor is classified as one of three things: a valid correlated target (dark blue), a UCT (green), or as a false streak (red). The image also displays the predicted location of every object (light blue) within the field of view of the CCD. The field of view calculation considers an area that is wider than the 420 by 420 pixel region of the CCD, which is necessary because uncertainties in an element set can alter the expected location. The image also shows a typical star field distribution.

96
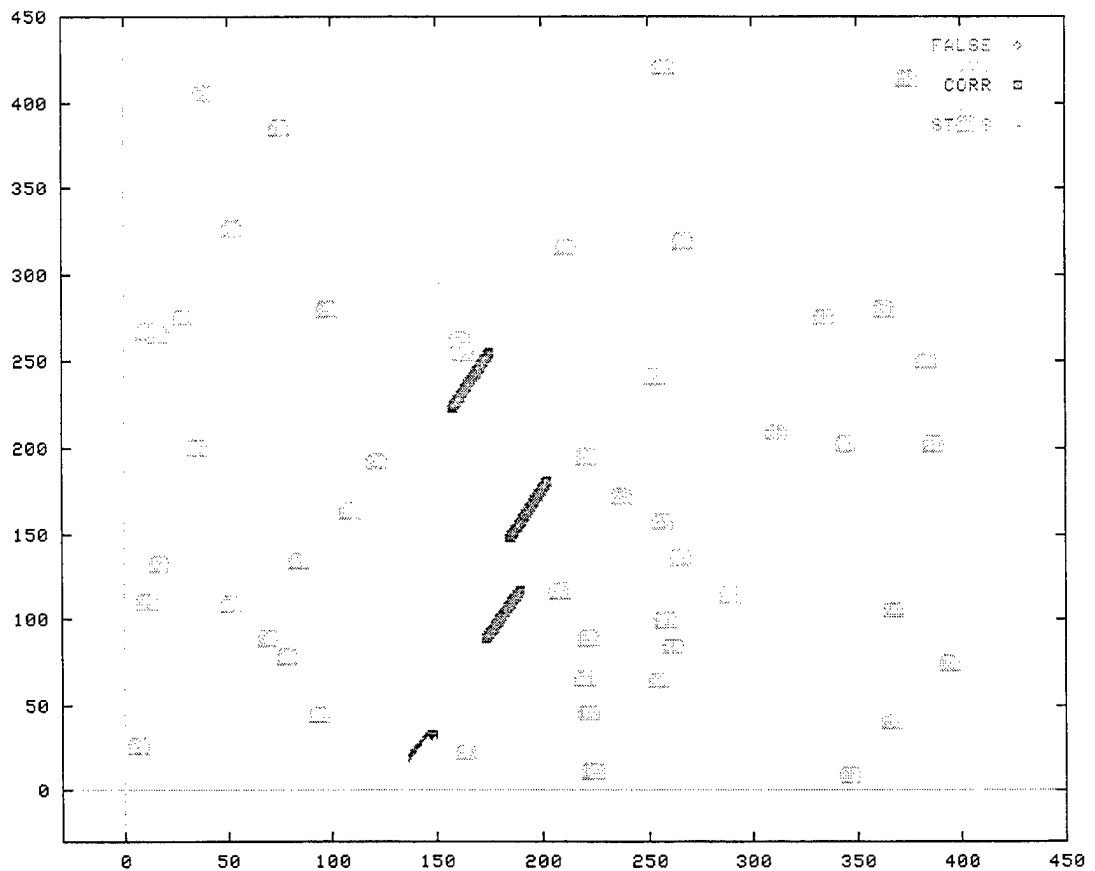
Figure 2: Sample Signal Processor Image

Figure 3 shows a second type of image that this program generates with each streak labelled by an object identification number. This is useful when dealing with UCTs because it shows the predicted location of every streak in the field of view and sometimes the UCT will match one of these predicted streaks. Therefore to assist this process, the program also provides information such as the age of element sets, tools for displaying individual streak attributes, and the element sets used in the catalog on that day. But the most important piece of information that this program provides is table that contains all other looks where every object in the field of view was seen before. This table also mentions whether or not the object correlated or if there was a UCT. The user can splice the observations from several looks and then matching the element set becomes considerably easier. This feature asisted in the rediscovery of 23118, a METEOSAT rocket body that had not been tracked for thirty eight days.
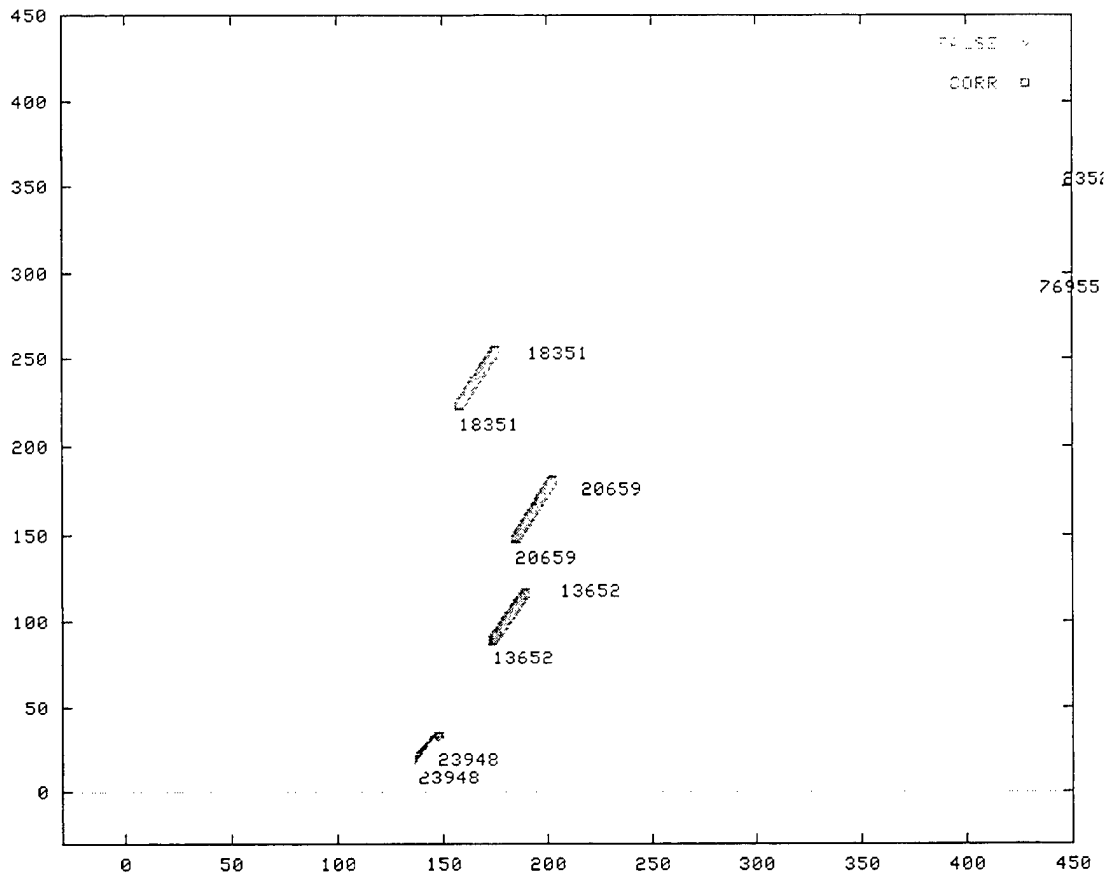
Figure 3: Sample Target Identification Image

This software tool has perhaps the best interface out of all the tools described in this paper. It ties in with Command Compliance query engine, Compliance Reports and the user can asses whole experiments with just a few mouse clicks. This is done by viewing the *photo proofs* of an experiment, which display signal processor images of every look from a given event.

6. 3-D Models of SBV Experiments

A 3-D experiment visualization tool serves two major needs: first to understand how the mission planning software's scheduling algorithms work; and second to help understand the nature of tasking from Space Command.

Displaying a Space Command tasking list in three dimensional space is not especially difficult. However, displaying an SBV experiment which involves a great deal of animation is considerably harder. Fortunately, the San Diego Super Computing Center (SDSC) and Silicon Graphics invented a HTML variant called Virtual Reality Modelling Language (VRML). Using VRML, the user can set up complex models and animation, all

of which can be viewed via Netscape. VRML also allows interaction and manipulation of user created three dimensional environments.

In Figure 4, a sample Space Command tasking list is displayed. This particular set has a majority of objects on one part of the geosynchronous belt. However, the SBV spends a portion of its orbit on the other side of the Earth from where it cannot see this part of the belt. Consequently, typical SPOCC operational procedure is to augment any tasking list to ensure that the sensor time is used effectively.
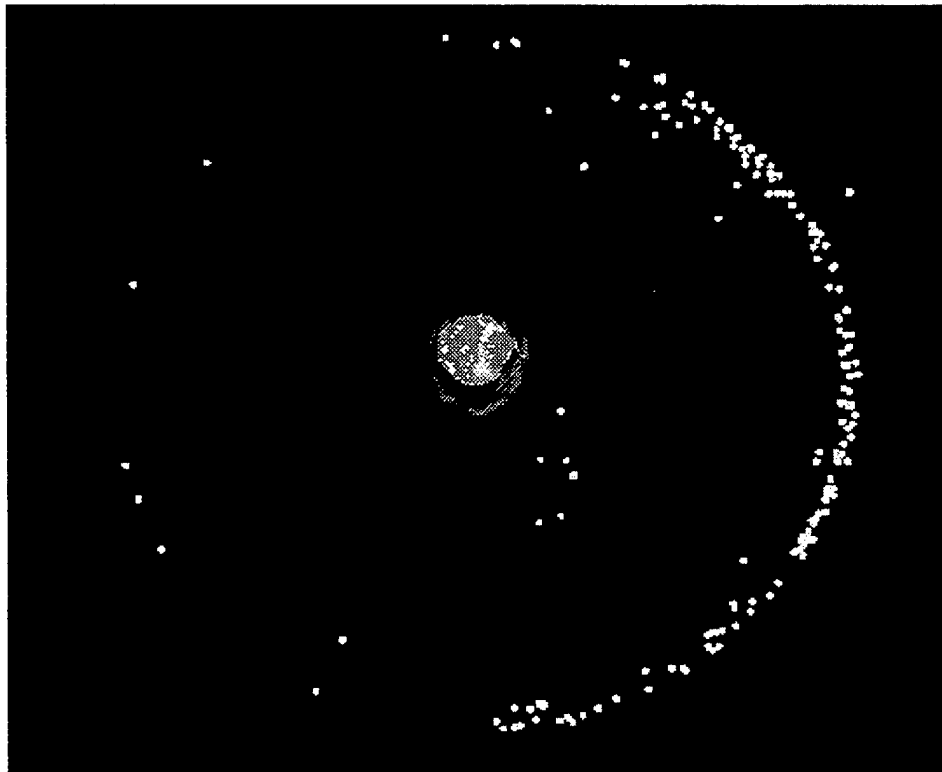
Figure 4: VRML display of tasking list

In Figure 5, a sample SBV experiment is shown. This picture is just a snap-shot out of the full VRML animation which will be shown in the talk. In this picture, the SBV is "under" the Earth. Thegreen beam is the field-of-view (1.4°x 1.4°) of the SBV "illuminating" a satellite. The satellites are shown as spheres: the blue spheres are satellites that at this point in the experiment have not been tracked; and the red spheres are objects already looked at by the SBV. Each object's orbit path during the experiment is shown with the white lines.

Figure 5: VRML display of an SBV experiment

By moving the mouse the user can travel inside this environment and perform actions such as object identification (placing the mouse on an object), zooming in/out, walking, and rotating the viewpoint. Another interesting feature is the ability to quickly change viewpoints. In Figure 6, the view point has changed from that of Fig. 5 to one where the observer is riding on the space craft.

One of the most important lessons this visualization tool offers is a deeper understanding of the performance of the scheduling algorithm. While viewing the animation, we were able to infer that the scheduler did not weight satellite attitude maneuvers adequately as compared to tasking priority. Maneuvers are of concern because they typically require considerable energy and also may affect spacecraft life. This led to modifications in the weighting scheme to ensure efficient utilization of the spacecraft.

gravity Walk Slide Look Examine Point ◀ View ▶ Straighten (?) COSMO
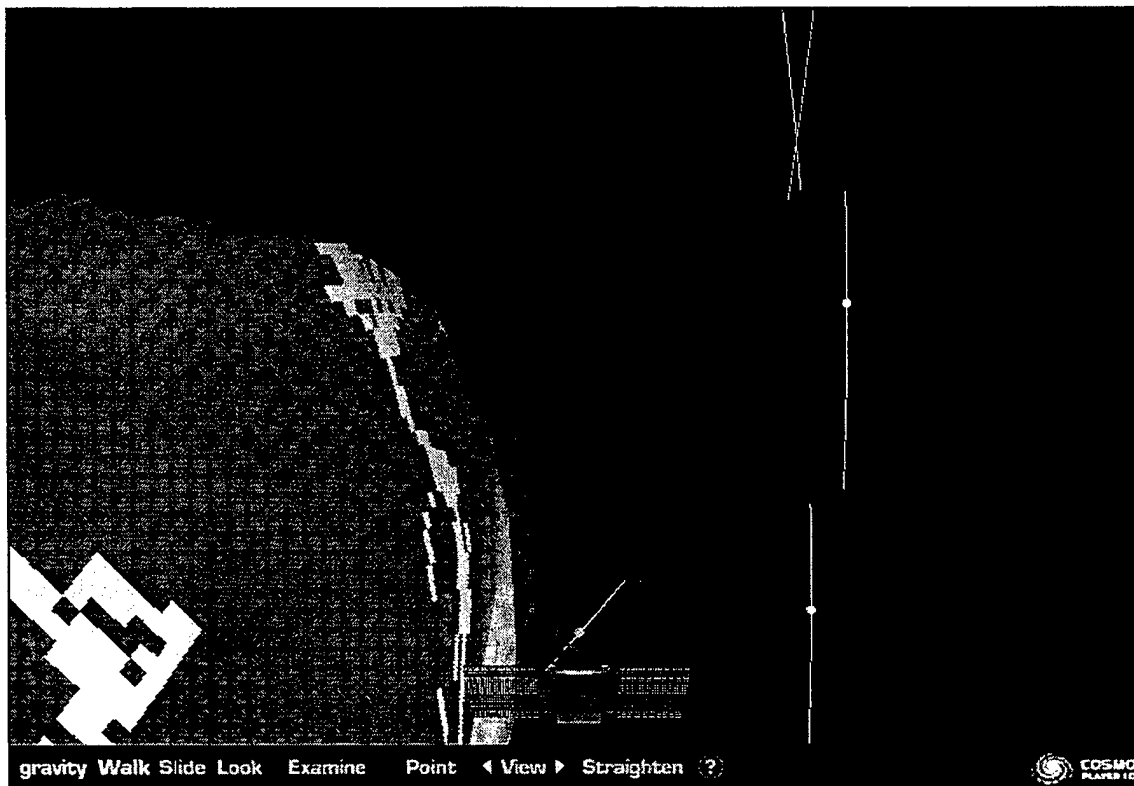
Figure 6: VRML file showing the SBV point of view

7. Summary & Future Plans

We have developed a suite of software tools that are useful for monitoring the performance of the SBV. These tools take many forms: reports, plots, queries, signal processor images, and 3-D models. The interface for these tools guarentees that users can access and interpret large amounts of data with a minimum amount of effort. These tools are extremely effective for trouble shooting known and unknown problems. NETSCAPE serves as an underlying theme in all these tools for two main reasons: accessiblity and portability. These tools have become an intergral part of SPOCC and will continue to be developed and refined as needs arise and as more COTS tools become available.

SBV Space Object Photometry: Initial Results

R. Lambour, R. Bergemann, C. von Braun, and E. M. Gaposchkin
M.I.T. Lincoln Laboratory, Lexington, MA 02173

Abstract

One of the objectives of the MSX surveillance experiments is to collect photometric and radiometric data on a selected set of resident space objects (RSO) from the LWIR to the short wavelength UV using the SPIRIT III, SBV, and UVISI instruments. Analysis of these data will primarily emphasize: 1.) construction and validation of phenomenological models for a broad range of RSO classes (*e.g;* spin-stabilized, three-axis stabilized) over a wide range of solar phase angles, and 2.) discrimination between classes of RSOs and identification of discriminating characteristics within an RSO class. This paper concentrates on the initial results from the Space-Based Visible (SBV) instrument. We will provide an overview of the surveillance data collected to date, discuss its limitations, and present examples of the data.

Introduction

Photometry refers to measurement of the light flux from an object, usually in multiple wavelength bands. In the astronomical community, multispectral photometric measurements provide a powerful remote sensing tool to determine the size, shape, rotational period, temperature, and some surface properties of asteroids and comets from reflected sunlight. The same concept can be applied to glean information about Earth-orbiting satellites. The optical signature of a satellite consists primarily of sunlight reflected from various surfaces toward an observer. The reflectivity of the surface depends upon wavelength, surface roughness, incident and reflected angles, and temperature. The total signature of the satellite is a function of the satellite configuration, surface material properties, sun-target-observer (phase) angle, and satellite orientation. Satellite photometry has been pursued with varying degrees of enthusiasm since the 1960s, concentrating mainly on the visible wavelengths. These observations have determined quantities of interest such as position, spin period and variation of brightness with phase angle (phase curve). These quantities can also shed light on the orientation of the satellite, given some *a priori* knowledge of its configuration[1-3].

One of the goals of the Midcourse Space Experiment (MSX) surveillance experiments was to collect multispectral photometric data on RSOs for Space Object Identification (SOI) and to investigate its utility for space surveillance. These data are useful for a number of tasks, notably establishment of RSO brightnes models to facilitate space surveillance mission planning (scheduling), discrimination, and monitoring. Discrimination refers to the ability to distinguish one RSO from another. Monitoring refers to the task of determining the location and operational status of an RSO. This paper will present additional detail on these concepts, and the initial analysis of data from the Space-Based Visible (SBV) sensor which operates in the visible region of the spectrum (hence the name).

SBV Overview

The SBV sensor was launched on board the MSX satellite on 24 April 1996. MSX resides in a 888 km altitude, sun-synchronous orbit. The goal of the SBV was to demonstrate the ability to make observations of RSOs from a space-based platform. The SBV sensor consists of a 15-cm aperture off-axis telescope with a thermo-electrically cooled CCD focal plane (FP). In addition, a signal processor and supporting electronics are also contained aboard the spacecraft. The SBV focal plane consists of four abutted frame transfer CCDs, each with 420x420, 27 μm pixels. Additional characteristics of the instrument are presented in Table 1 and in Ref. 4.

The SBV employs two tracking modes to observe RSOs. The primary tracking mode is to track the background stars so they appear as point sources on the FP. The RSOs will appear as streaks in the FP due to their relative motion with respect to the star field. This mode is known as sidereal tracking. The

second mode is to track the RSO so that it appears as a point source while the stars streak on the FP; this is known as ephemeris tracking. Most of the data presented in this paper were obtained in sidereal track mode.

A typical SBV RSO observation consists of 6-16 420x420 frames of data. These frames can be stored with the onboard tape recorder and downlinked as raw images, or the images can be processed through the onboard signal processor (SP). The SP extracts relevant information from the raw frames and forms a SP report to be downlinked. The report contains data (position and intensity) on the FP detections which appear as streaks or as point sources. The data presented in this paper were obtained from SP reports rather than reduction of raw images.

A comment on the photometric accuracy mentioned in Table 1 is necessary. The stated accuracy of 0.2-0.3 SBV magnitudes (M_{SBV}) was derived using raw images of Landolt stellar calibration fields[12] obtained in sidereal track mode. Therefore, the photometric accuracy refers strictly to *point sources* on the FP. When the object of interest appears as a streak on the FP, as is the case with RSO observations in sidereal track mode, the photometric accuracy probably degrades, but the extent of the degradation is not yet known. In addition, it is not yet known if processing the raw data through the SP results in an additional loss in photometric accuracy. Therefore, we must be conservative in drawing conclusions from the data.

MSX/SBV SOI Data Collection Goals and Experiments

The primary goals for SBV SOI data collection were: 1.) collection of a comprehensive data set for use in definition and validation of phenomenological models of RSOs for space surveillance mission planning and SOI; 2.) SOI characterization of a number of different RSO classes and identification of sensor discriminants between and within classes; and 3.) collection of data on RSO clusters to investigate the use of SOI data in discrimination and catalog maintenance. Consequently, data is being collected on a number of different RSO classes at a variety of phase angles (0-140°), including phase angles which cannot be observed from the ground. Table 2 summarizes the principle RSO classes on which data are being collected, and Figure 1 presents a pictorial comparison of some of these RSO classes. Table 3 presents a summary of the SBV space surveillance experiments; each of these experiments returns some RSO photometric data either through SP reports or raw images. The data discussed in this paper were collected during the SP experiments (SU02, 03, 04, 09, 10).

As an example of the utility of SBV photometric data, consider the Specular Search (SU 15) experiment. The reflection of sunlight from an RSO consists of two types of reflections characterized as diffuse and specular. The diffuse reflection refers to the omnidirectional reflection of sunlight from the surface and is generally a result of the roughness of the surface. The specular reflection refers to a mirror-like reflection from the surface which tends to be highly directional and significantly brighter. It is the diffuse reflection that permits routine optical detection of RSOs whereas the specular reflection can be observed at a particular location only when the Sun-RSO-observer geometry is appropriate. Specular reflections are observed when the sensor, the normal to the reflecting surface (usually a solar panel), and the Sun are in the same plane, and the angle between the sensor and the normal to the reflecting surface is equal to the angle between the Sun and the surface normal. The 0.5° angular width of the Sun is the theoretical width of the reflected ray, but for solar panels, misalignment of the cells broaden this width to a few degrees[5-7].

For the solar cell covered, spin stabilized, cylindrical RSOs shown in Figure 1, the symmetrical distribution of solar cells results in a conical locus of specular reflections about the spin axis, having an angle from the equatorial plane equal and opposite to the Sun's declination angle, as shown in Figure 2. Previous work also indicates that the brightness of the specular reflection varies relatively weakly with phase angle, which means that the specular return can be observed at relatively high phase angles[7].

The SBV can observe the specular return from each of this type of RSO once per orbit when the solar declination is equal or less than the parallax angle, ψ, from the geosynchronous belt to the orbit tangent at the MSX polar crossings. The parallax angle ranges between ±10°. This geometry permits observation of specular returns for ~50 days, twice per year, centered on the spring and autumnal equinoxes.

The situation is different for the three-axis stabilized payloads. Their solar arrays are essentially flat plates which track the sun; therefore, the phase angles at which the specular reflection from these RSOs

can be observed should be extremely limited and dependent upon the offset angle between the solar panel normal and the RSO-to-Sun vector. Thus, SBV will observe specular returns from these RSOs only at specific phase angles, and not necessarily on every orbit.

The utility of the specular data is obvious; for example: 1.) spin stabilized and three-axis stabilized payloads can be distinguished from one another based on where and when the specular returns are observed; 2.) the misalignment of a spin stabilized RSO spin axis from the equatorial plane can be discerned with multiple observations, since the time/location of the peak specular return will be different from the aligned case; 3.) solar array offset angles can be determined for three-axis stabilized RSOs allowing determination of available power and age of the spacecraft; 4.) tracking of small, otherwise unobservable, RSOs becomes possible.

Initial Data Analysis

The SBV photometric database contained 15102 observations of unclassified cataloged objects in mid-December 1997. These data represent observations on 994 different objects (payloads, debris, and rocket bodies). In our initial survey of the SBV observations we chose to examine the data as a function of phase angle and solar declination angle (i.e., season) as was originally done with earlier ground based observations. Whether or not this is appropriate will become apparent as the data is analyzed. We also chose to consider the data as organized by RSO class. We will present results for several RSO classes.

The brightness data will be presented as SBV magnitude (M_{SBV}), where magnitude has the same meaning as it does in the astronomical literature. However, most visible-band astronomical observations are transformed to Johnson V-band magnitude (M_V), which represents the amount of light flux collected over a wavelength range defined by a Johnson V-band filter: 480-700 nm[8]. The SBV, which has no filter, is responsive to light over the 300-900 nm region; therefore, magnitudes calculated from SBV measurements are representative of the light flux collected in this waveband. M_{SBV} and M_V correspond only when the reflection from the RSO has the same spectrum as the Sun. Beavers [Ref. 3, 9] has shown that this is not the case for some RSOs; therefore, exact correspondence between M_{SBV} and M_V should not be expected. The difference has not yet been determined.

HS-376 Spin Stabilized. Figure 3 (top) shows the M_{SBV} normalized to a range of 36,000 km versus phase angle for all observations of HS-376 satellites. Active satellites are represented by a blue +, and inactive satellites by a red circle. There are 45 HS-376 on orbit. The distribution of observations in phase angle is shown on the bottom of the figure. The observations range in magnitude from M_{SBV} = 8 –15, a range of about 7 magnitudes. Note the observation of specular reflections at phase angles of ~80°. These data suggest that specular data collection on spin stabilized cylinders need not be restricted to low phase angles during the equinoxes. Beavers [Ref. 3, 9] reported a brightness range of about 6 M_V, so it appears that these data are consistent with the previous ground-based measurements. It is interesting to note that very few of the observations of inactive satellites are brighter than M_{SBV} ~ 11. The inactive satellites tend to have orbital inclinations greater than 0°; for the set of spacecraft considered here, the inclinations range from 1-9°. Additionally, these spacecraft, since they are not being station-kept, may no longer have their spin axes aligned normal to the orbital plane. Both of these effects will move the specular cone to a different location, perhaps ensuring that SBV cannot observe the specular reflection.

There appears to be no well defined dependence of brightness on phase angle for either the active or inactive cylinders; a wide range of M_{SBV} is observed for any particular phase angle. Several factors may contribute to this; first, we have plotted data from many spacecraft in Figure 3. However, even if we consider a single spacecraft, a large amount of scatter remains in the data, as shown in Figure 4. Second, as mentioned earlier, Beavers [Ref. 3, 9] noted a 6 M_V variation in brightness over the course of a year for some of the HS-376 spacecraft due primarily to the change in solar declination. We plotted the data as a function of solar declination angle (δ_{sun}) to examine seasonal dependencies in brightness. Figure 5 (top) shows the M_{SBV} as a function of δ_{sun} and Figure 5 (bottom) shows the distribution of data points as a function of δ_{sun}. Based on the previous ground-based observations, we would have expected to see the brighter points (M_{SBV} < 10) fall within δ_{sun} = ±10°, and the dimmer points at larger angles. In addition, we would have expected some of the inactive payloads to be brighter at δ_{sun} > 10° due to non-zero inclinations and/or spin-axis misalignment and more scatter in the inactive payloads data for the same reasons. Figure 5

(top) shows that some of the brighter points for the active payloads do fall within $\delta_{sun} = \pm 10°$, but many do not. In addition, the data on the inactive payloads show much less scatter than the active payloads data, and no evidence of being brighter than the active payloads at $\delta_{sun} > 10°$. Figure 5 (bottom) shows that we do not yet have an even distribution of data over season, which may explain why we fail to see the expected pattern.

In Figure 6, we present the brightness versus δ_{sun} curve for 20762 (Thor). It is interesting that we do appear to observe the expected variation of M_{SBV} with δ_{sun} for this individual spacecraft. However, there is much more scatter in the data at negative δ_{sun} (fall and winter) than for positive δ_{sun}. If our observing platform were on the ground, we would probably attribute this scatter to glints or reflections off the main antenna of the spacecraft which is mounted on the top. However, the MSX should be able to observe reflections from the main antenna at any time of the year. Obviously, these trends in the HS-376 data bear further investigation.

The data from the SU15 experiments also proves to be very interesting. In Figure 7, we present M_{SBV} versus time (UT) for a specular search experiment run on April 10, 1997. These data are observations of an RSO cluster consisting of 23877 (Galaxy-9) and 19484 (SBS-5) both of which are HS-376 spacecraft, but of significantly different age (Galaxy-9 was launched in 1996, SBS-5 in 1988). The data show both spacecraft start out fairly bright and then dim by 1-2 M_{SBV}. The spacecraft then brighten again, reaching approximately the same magnitude (~9.5 M_{SBV}) at the same time, and subsequently dim. The amount of time between the two bright points was ~20 minutes. Observation of two specular brightenings during a single pass was unexpected; previous models predict a single peak in brightness as the MSX moves through the parallax angle corresponding to δ_{sun}.

What produced the two peak structure in the data? On April 10, $\delta_{sun} = 7.96°$ which is ~2° below the theoretical maximum solar declination at which SBV can observe specular reflections. We believe that MSX passed over the south pole during the time the data were collected and passed through the locus of peak specular brightness (ref. Fig. 2) twice. Figure 8 is a cartoon which facilitates interpretation of the data. Although we did not have the spacecraft ephemeris available at the time of this writing, we did have the MSX orbital element set for April 10, and we propagated the orbit to the appropriate UT. At the beginning of the data collection (04:44 UT), MSX was beginning a pass over the south pole. A simple geometrical model can be constructed assuming that MSX is in a circular orbit with 90° inclination and that the RSO spin axes are aligned with the Earth's spin axis. The parallax angle is then: $\psi = \tan^{-1}(0.17237\sin(\lambda))$, where 0.17237 is the ratio of the MSX orbital distance (1.1411 R_E) to the geostationary distance (6.62 R_E) and λ is latitude. When the parallax angle (Fig. 2) is equal to 7.96°, MSX was at south latitude of 54.2°. The spacecraft must travel through a 71.6° arc of its orbit before encountering the second specular peak. Using the circular orbital velocity at 888 km altitude the model predicts that the specular peaks should be 20.4 minutes apart, in excellent agreement with the data. A more realistic model will be constructed when we have the MSX ephemeris.

Also worthy of mention is the difference in magnitude between SBS-5 and Galaxy-9 before and after the passage through peak brightness. Although we do not yet know the size of the error bars on the data points, this difference could be indicative of an ability to discriminate between RSOs of the same class based on their age (assuming there are no differences in configuration).

HS-601 Three-Axis Stabilized. Figure 9 presents the SBV observations of HS-601 spacecraft in the same format as Figure 3. Note the dearth of observations on inactive spacecraft; there are 32 HS-601s on orbit and only one of these is inactive. We have three observations on the inactive satellite, making them difficult to distinguish in Figure 9. Most of the observations (738 of 983) in Figure 9 are of the DBS cluster at 259° E longitude which contains 4 HS-601s: 22930 (DBS-1), 23192 (DBS-2), 23553 (MSAT-2), and 23598 (DBS-3). This composite phase curve is well ordered compared to that for the HS-376 class. There is a definite linear trend with respect to phase angle, indicating that it is best to observe these spacecraft at low phase angles. The range of magnitudes observed is $M_{SBV} = 7.5 - 15$. The specular reflection from the relatively large HS-601 solar arrays is expected to be much brighter than the $M_V \sim 8$ reported by Beavers for the HS-376 class, possibly down to $M_V = 2-3$. The SBV saturates for objects brighter than about $M_{SBV} \sim 8$, therefore the bright points on the phase curve in Figure 9 (top) may or may not represent specular reflections. Regardless, there is a general brightening of the class near 30° phase angle. This could be indicative of a solar array offset angle of ~15°. This brightening implies that data

collection for the purposes of determining solar offset angles and thus power and age should take place at low (20-30°) phase angles for this RSO class.

There appear to be two branches in the phase curve which parallel each other and separate at higher phase angles. Since most of the observations are of the DBS cluster, we examined the data from each of these four spacecraft individually to determine if any of them was responsible for the brighter branch. These data are shown in Figure 10. The top plot shows the observations of all three DBS satellites and the bottom plot shows the observations for MSAT-2 and MSAT-1 (MSAT-1 is not a member of the DBS cluster but is of the same configuration as MSAT-2). Obviously, the MSATs are distinguishable from the DBS satellites, having a much flatter phase curve. Why this is so might be due to their radically different configurations; the DBS satellites consist of a 2.2 m^3 box with two 4-panel solar arrays (total area of 43.89 m^2) and two 2.14 m diameter antennas, whereas the MSAT satellites have smaller 3-panel solar arrays (total area: 32.92 m^2) and two graphite mesh antennas which measure 4.9 m x 6.7 m[10]. A diagram of each satellite is shown in Figure 10. The MSAT observations are indeed responsible for the brighter branch in the composite phase curve at higher phase angles.

The observations of this spacecraft class may be quite valuable for investigation of sensor discriminants within an RSO class. There are two main configurations for the HS-601, one with 3-panel solar arrays and one with 4-panel arrays. The difference in area is more than 10 m^2. In addition, the antenna configurations differ significantly for the various satellites[10]. We currently are examining the data for other solar illumination dependencies, differences in brightness based on configuration, and we are constructing a theoretical brightness model for the "box and panels" satellite configuration to facilitate examination of the data.

Gorizont/Raduga Class. We have just begun to examine the SBV data on the Russian Gorizont and Raduga satellites. These satellites are believed have the same configuration[10,11]. The SBV observations are presented in Figure 11 in the same format as the top of Figure 3. The phase curves show a linear dependence on phase angle and are very similar for the two types of spacecraft. For both classes, there appears to be significant amount of scatter in the data, but a clear trend toward lower magnitudes at low phase angles. Analysis of this data is ongoing.

Summary and Conclusions

We have presented an overview of the SBV sensor, the experiments and methods used to collect visible-band photometric data on various classes of RSOs, and the limitations of these data. Although the photometric error budget remains undetermined for the signal processed data, we have begun to analyze the data, and presented examples with preliminary interpretations.

These data are being used to construct and validate RSO models for use in space surveillance mission planning and SOI. We touched very briefly on the utility of the data for future surveillance scheduling. The spin stabilized cylinders specular reflections can be observed at phase angles of 0-80° near the equinoxes which provides a wide window for scheduling observations. Conversely, the three-axis stabilized payloads should be observed at low phase angles to enhance detectability and probability of observing specular reflections from the solar arrays; this provides a more narrow window for scheduling observations. Study of the impact of these data on future mission planning is ongoing.

Preliminary comparisons between the HS-376 model developed by Beavers [Refs. 3, 9] and the SBV data look good, and the SBV data displays similar dependencies with respect to phase angle and season as does the earlier ground based data. We have not yet compared the SBV HS-376 specular reflection data with the model of Beavers [Refs. 3, 9], but the SBV data shows a peak brightness comparable to the older model. The SBV data on three axis stabilized satellites (HS-601, Gorizont/Raduga) appears well behaved and construction of theoretical brightness models to facilitate examination of the data is underway.

These data will also be used for SOI characterization, identification of sensor discriminants and monitoring tools. The SBV HS-376 specular data and the HS-601 phase curves showed some utility for discrimination and monitoring. The HS-376 specular data was particularly interesting in that we observed a significant difference in the magnitude of two cluster members of identical configuration, but differing ages. In addition, we noted a double peak in the light curve for HS-376 specular data taken near the pole when the solar declination was near the maximum observable from the MSX orbit. The ability to obtain

two specular returns separated by 0-30 minutes on every orbit could prove to be a powerful tool for monitoring and maneuver detection. The HS-601 phase curve demonstrated the ability to discriminate between different satellite configurations.

Future work will concentrate on collection of additional photometric data, determination of the photometric accuracy of signal processed data, and continued analysis of the data and application to space surveillance mission planning. In addition to the signal-processed data, the SBV has taken a large amount of raw photometric data on RSOs which has yet to be analyzed. Addition of this data to the database will also be a priority.

References

1.) Kissell, K. E., Diagnosis of spacecraft surface properties and dynamical motions by optical photometry, *Space Research IX*, pp. 68, 1969.
2.) McCue, et al., Optical Characteristics of Artificial Satellites, *Planet. Space Sci., 19.*, pp. 851, 1971.
3.) W. Beavers and L. Swezey, personal communication, 1995a.
4.) Harrison, D. C., and J. C. Chow, The Space-Based Visible Sensor, *John Hopkins APL Technical Digest, 17*, #2, pp. 226, 1996.
5.) Krag, W. E., Visible Magnitude of Typical Satellites in Synchronous Orbits, Technical Note 1974-23, MIT Lincoln Laboratory, 1974.
6.) Friedman, A. S., personal communication, 1974.
7.) Bergemann, R. J., personal communication, 1992.
8.) Allen, C. W., *Astrophysical Quantities*, The Athlone Press, London, 1983.
9.) Beavers, W., L. W. Swezey, personal communication, 1995b.
10.) *Jane's Space Directory*, Andrew Wilson (ed.), Jane's Information Group, Alexandria, VA, 1996
11.) Demechenko, B. I., *et al.*, *Zone Catalogue of Geostationary Satellites*, V. G. Fesnekov Astrophysical Institute, Ministry of Science-Academy of Sciences of Kazakhstan, pp. 80, 1996.
12.) Landolt, A. U., UVBRI Photometric Standard Stars Around the Celestial Equator, *Astron. J., 88*, pp. 439, 1983.

Table 1: SBV Characteristics

Spectral Range	$0.3 - 0.9$ µm
Spatial Resolution	12.1 arcsec/pixel
Field of View	1.4 x 6.6 degrees
Apeture, f/#	15cm, f/3
Frame Integration Times	0.4, 0.5, 0.625, 1.0, 1.6, 3.125 seconds
Frame Sizes	420x420, 357x420, 178x420 pixels
Quantum Efficiency	28 %
Point Source Sensitivity @ SNR=6.0	15.7 SBV magnitude
Photometric accuracy (point sources)	0.2-0.3 magnitudes at $M_{SBI}=14$

Table 2: Principle Classes of RSOs Observed by SBV

Low Altitude	Radar Calibration Spheres Stabilized: *e.g.,* DMSP, NOAA
Intermediate Altitude	Lageos/Etalon Spheres GPS Glonass Molniya
Deep Space	Spin-stabilized cylinders: *e.g.,* HS-376, HS-393, GMS 3-Axis stabilized: *e.g.,* HS-601, Gorizont, GE-3000, GE-5000

Table 3: SBV Experiment Descriptions

SU02	RSO Detection in High Backgrounds
SU03	SBV Metric Calibration
SU04	Joint SPIRIT III/OSDP and SBV Metric Calibration
SU09	Routine Space Surveillance Tasking
SU10	Geosynchronous Belt Search
SU11*	Unknown Object Detection and Characterization
SU12*	Ram/Anti-Ram Debris Observations
SU14*	Space Object Photometry (joint SPIRIT III/SBV or UVISI/SBV)
SU15	Search for Specular Reflections from Geosynchronous RSOs
SU17*	Space Object Photometry in Stressing Backgrounds
SU33*	SBV-only or joint SBV/UVISI PI Experiment
SU35*	Joint SBV/UVISI PI Experiment

* denotes raw data collection event
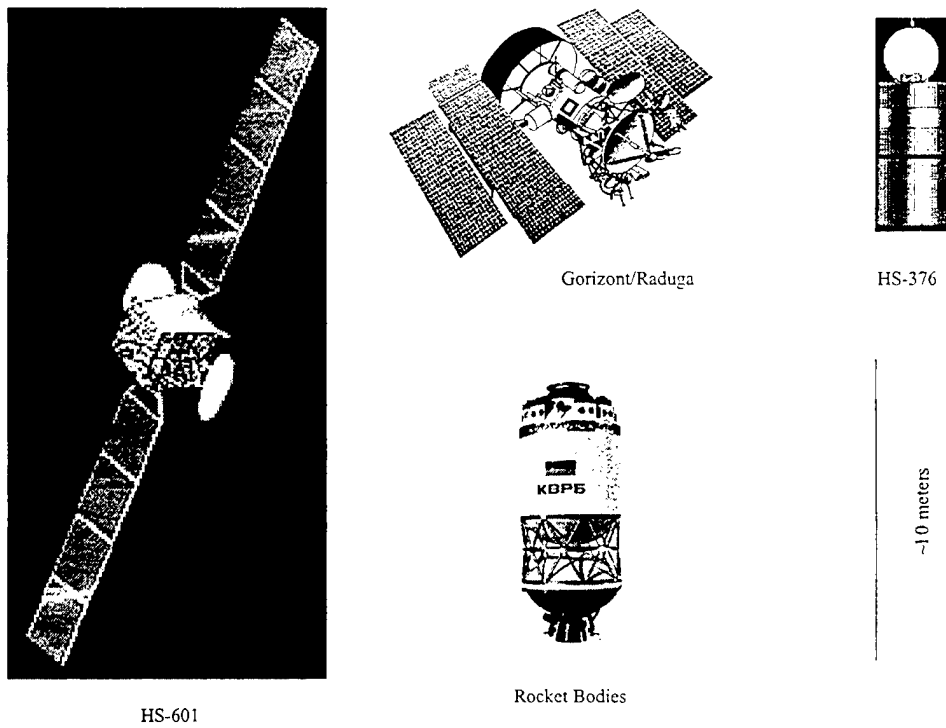
Figure 1: Pictorial representation of RSOs observed by SBV (roughly to scale). The bar on the right represents ~10 meters.
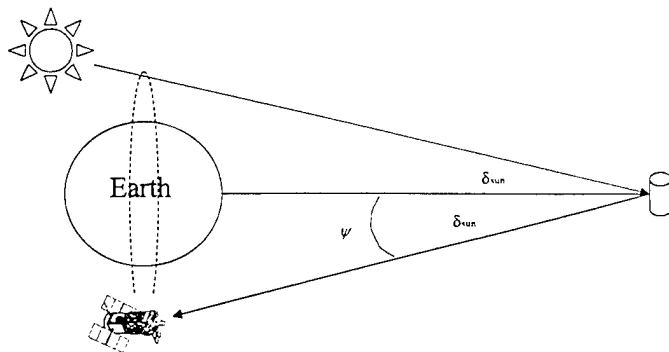
Figure 2: Cartoon of specular reflection geometry for spin stabilized RSO (not to scale).
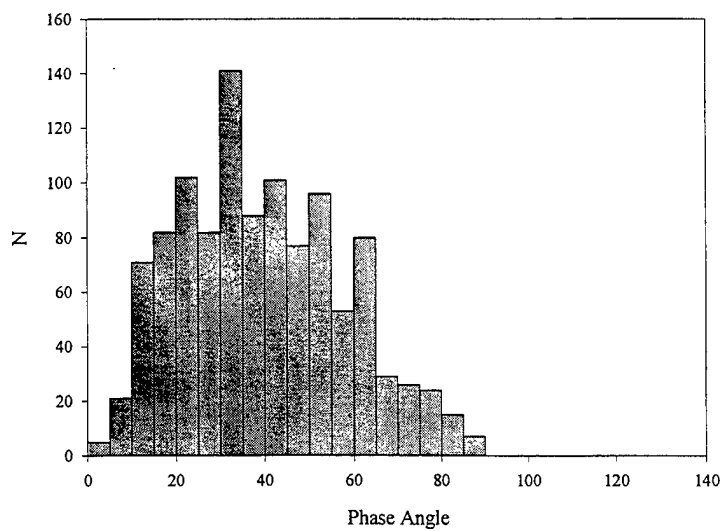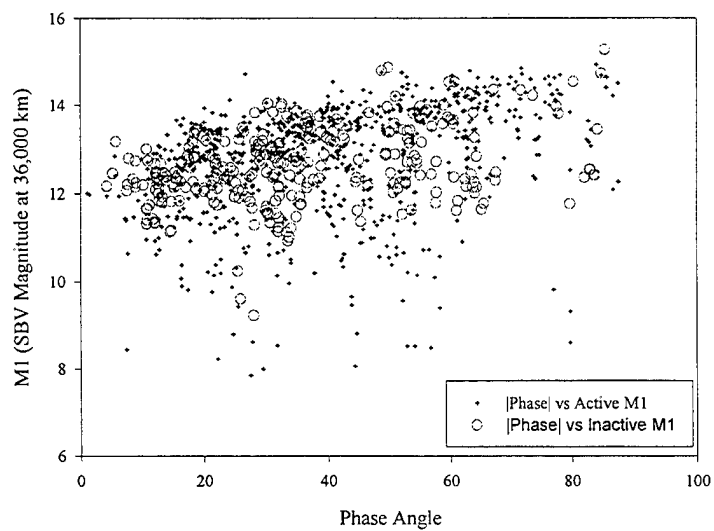
Figure 3: SBV magnitude as a function of phase angle for HS-376 satellites (top). The distribution of these observations in phase angle is shown on the bottom. The total number of observations is 1100.
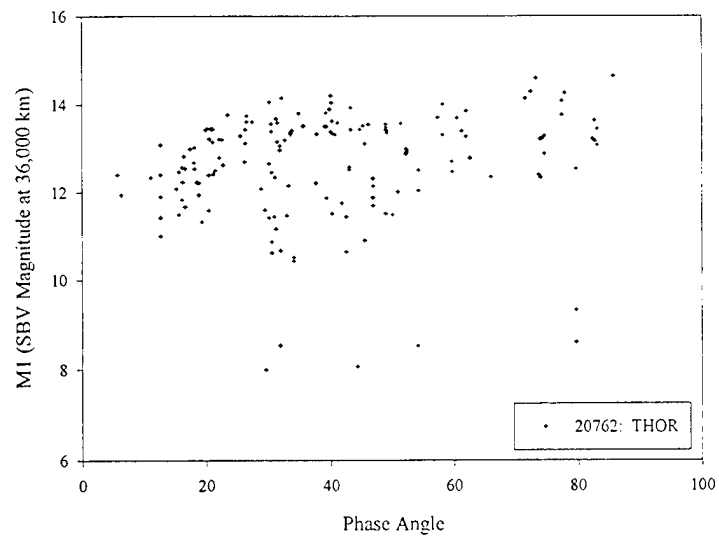
Figure 4: Phase curve for 20762 (Thor), an HS-376 spacecraft operated by Norway. Note the bright points at high phase angles.
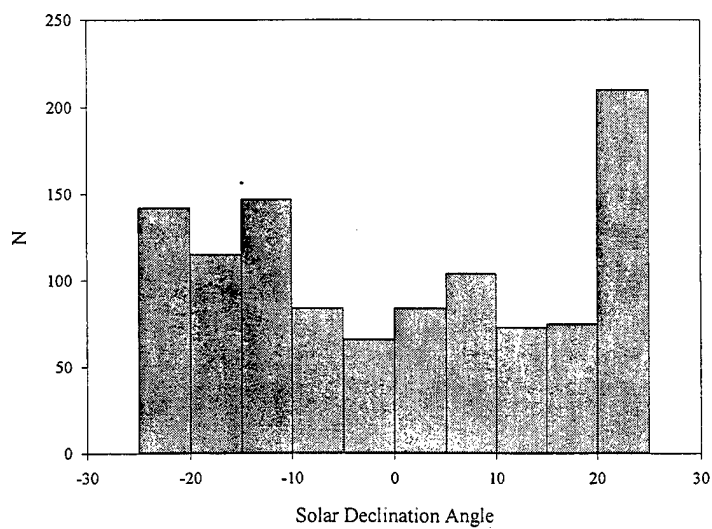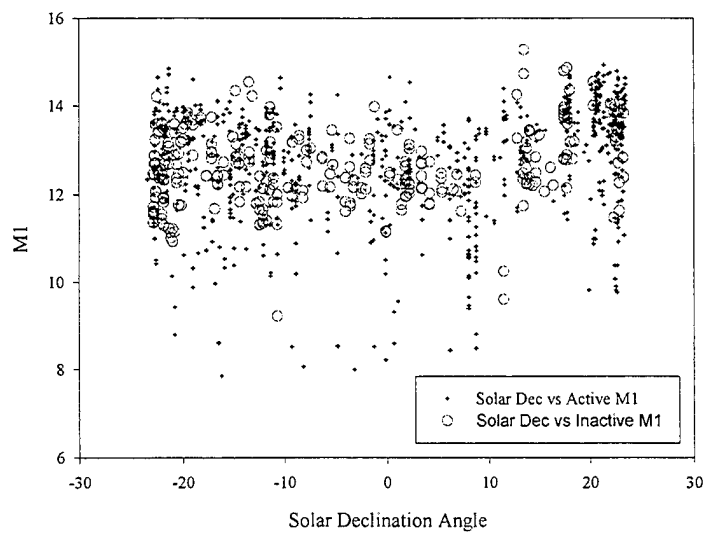
Figure 5: SBV magnitude as a function of solar declination for HS-376 satellites (top). The distribution of these observations in solar declination is shown on the bottom. The total number of observations is 1100.
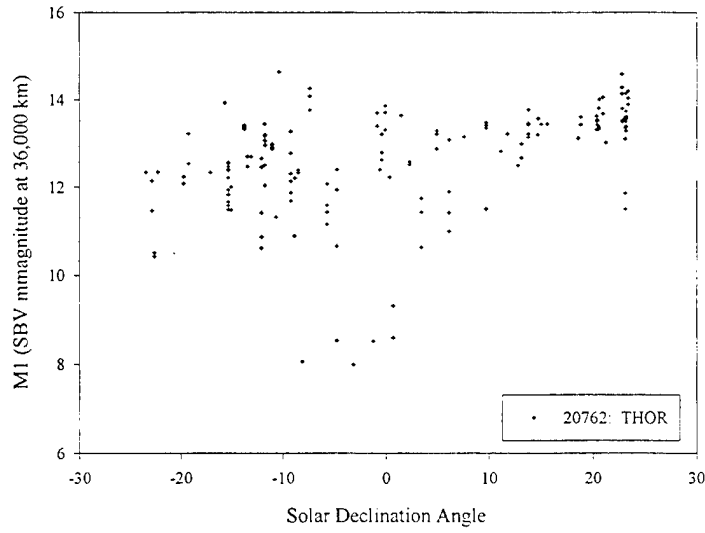
Figure 6: M_{SBV} versus δ_{sun} for 20762 (Thor), an HS-376 spacecraft .
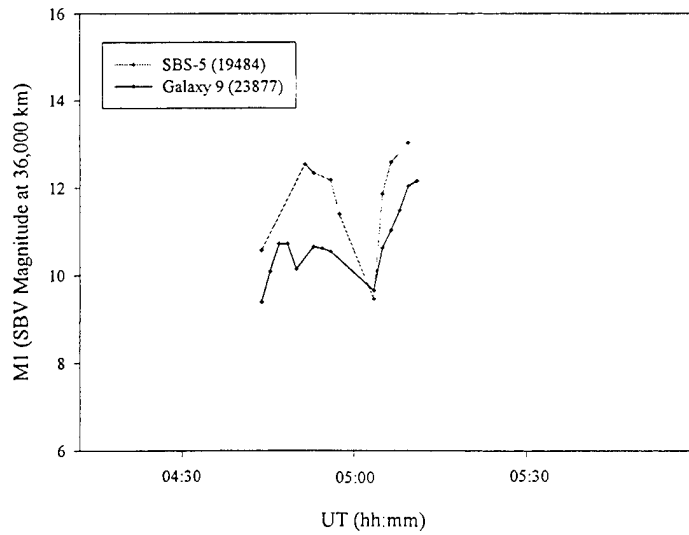
Figure 7: M_{SBV} versus UT on day 100 (April 10) of 1997 for 23877 (Galaxy 9) and 19484 (SBS-5), two HS-376 spacecraft.

Locus of Peak Specular for Cylindrical Geostationary RSO

MSX Orbit

Earth
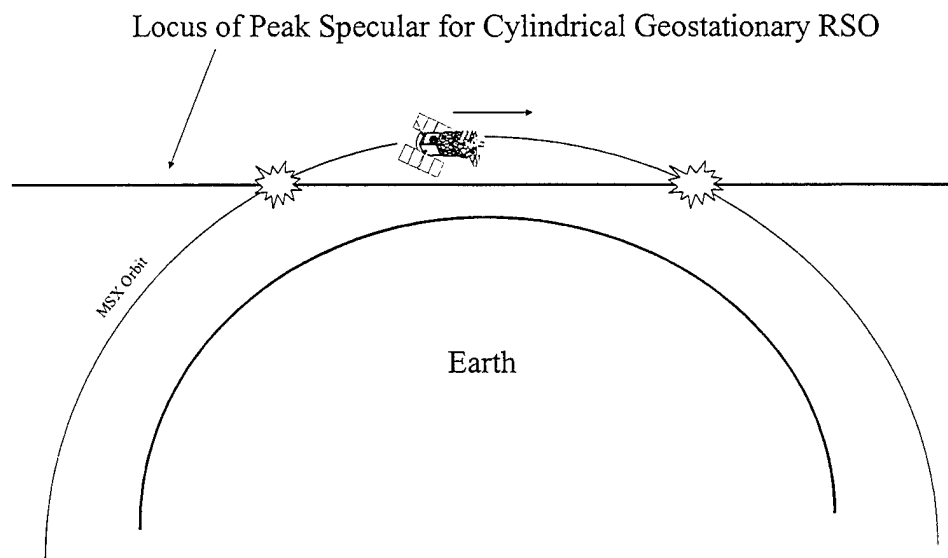
Figure 8: Cartoon of the geometry which would produce two brightness maxima during the observation of a specular reflection from a cylindrical geostationary RSO. A maximum in the RSO light curve occurs at each point where the MSX orbit intersects the locus of peak brightness.
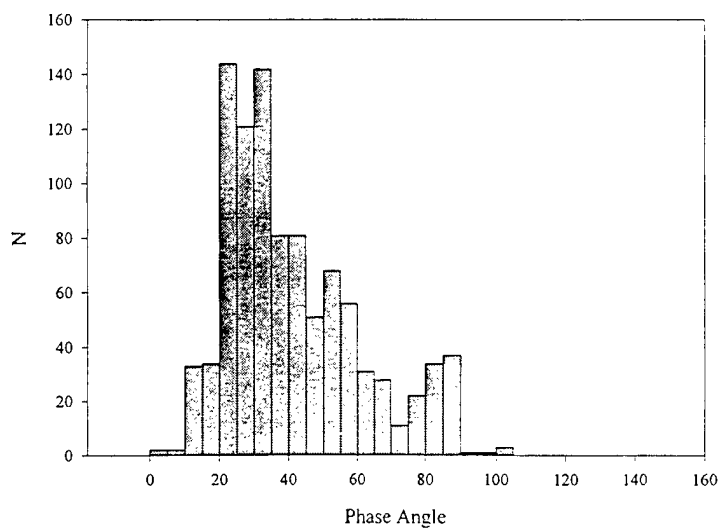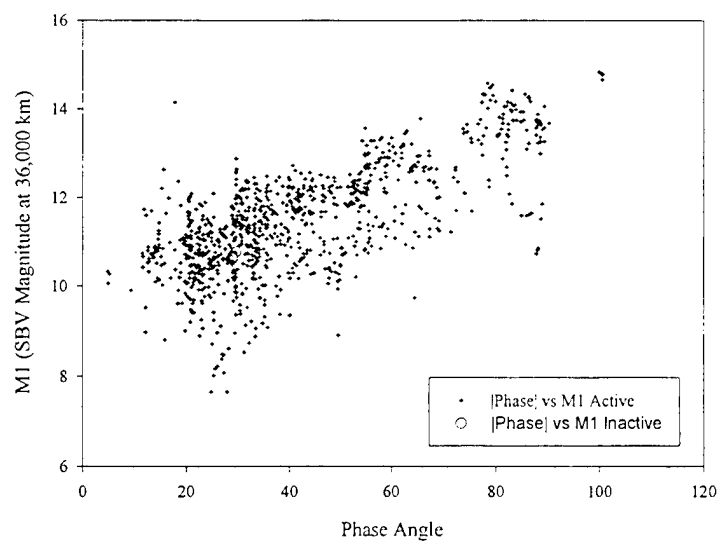
Figure 9: SBV magnitude as a function of phase angle for HS-601 satellites (top). The distribution of these observations in phase angle is shown on the bottom. The total number of observations is 983.
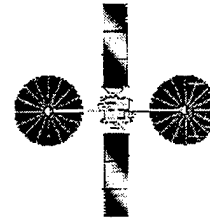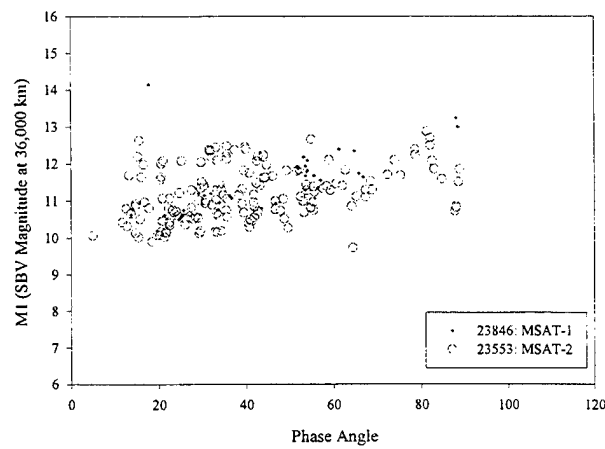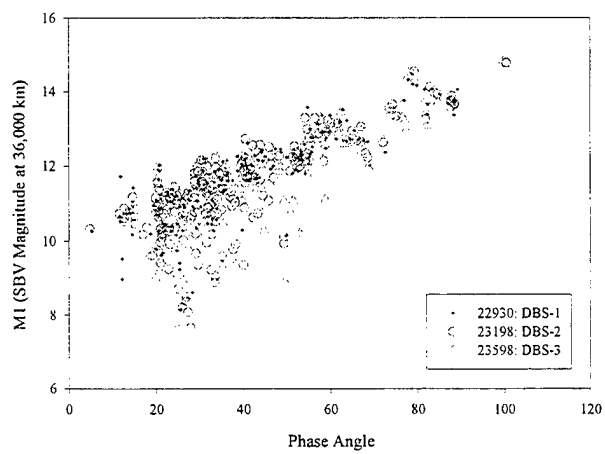
Figure 10: Comparison of phase curves for satellites in the DBS cluster. Top: Observations of the three DBS satellites. Bottom: MSAT-1 and MSAT-2.
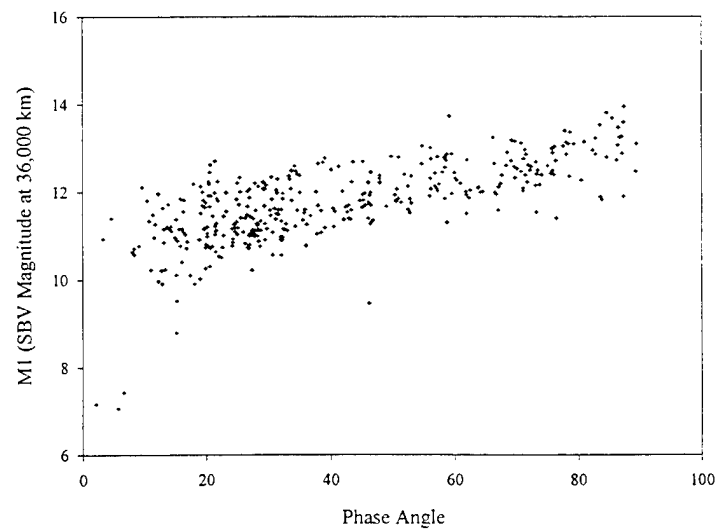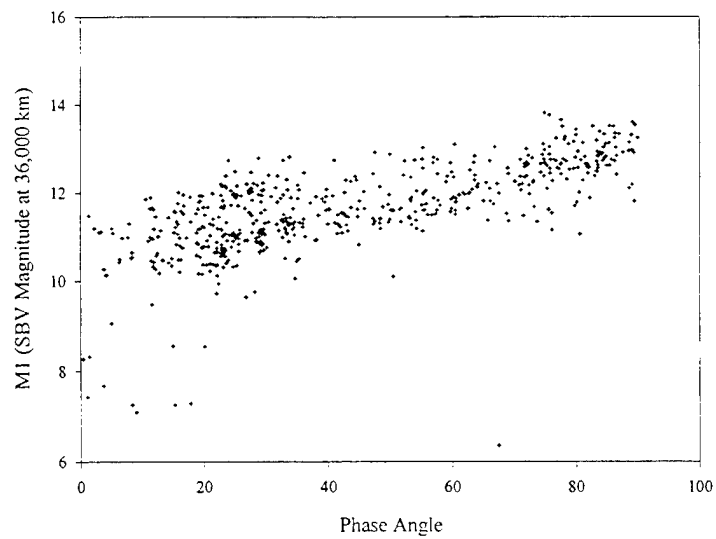
Figure 11: SBV observations of Russian Gorizont (top) and Raduga (bottom) communications satellites. Note the similarity in the phase curves.

Space-Based Space Surveillance: Thoughts on the Next Step

Grant Stokes and Ronald Sayer, MIT Lincoln Laboratory

The SBV program has successfully demonstrated space-based space surveillance. Thus, it is natural to ask what is the next step in building a space-based space surveillance capability. One answer of course, is to assume that SBIR LOW will provide the required capability as a byproduct of the missile warning capability. Another is to look at the job of space surveillance alone, and decide what needs to be done to satisfy specific space surveillance needs. Following the second approach, this paper discusses concepts for future implementations of space-based space surveillance systems tuned for space surveillance.

One intriguing approach to space based space surveillance is the use of electro-optic sensors in a coordinated optical fence configuration. The optical fence would accomplish space surveillance by repeatedly searching the orbital plane of the sensors and detecting all objects above some detectability threshold as they pierce the plane (see Figure 1). The payoff of such a system is full coverage of Low Earth Orbiting (LEO) and Deep Space (DS) populations, including an assured 1/2 revolution timeliness for high altitude, low eccentricity satellites (High altitude, high eccentricity objects are detected at least once every revolution). In addition, such a system has no weather outages, is amenable to automated operations and is robust to the failure of a single sensor/satellite.
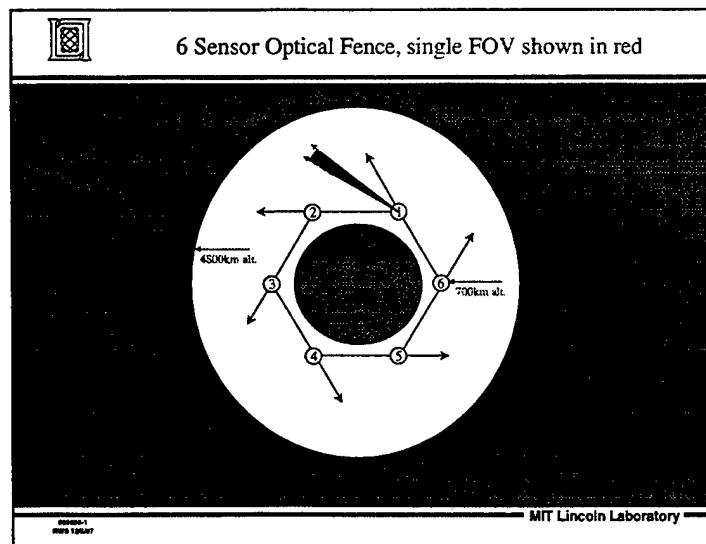
Figure 1.

The sensors postulated for use in the fence are based on the SBV sensor. For purposes of our system design, the aperture of the satellite borne telescopes would be 10 inches and each sensor would be equipped with a modified GEODSS upgrade CCD. This configuration will supply sensitivity considerable in excess of that achieved by the SBV system. In order to provide high search rate, the field-of-view of each sensor would be 6 degrees by 6 degrees and the telescope

would be gimbaled to allow quick movement to the next field. A fast, but achievable, onboard signal processing system would be needed to process the high data rates produced by such a sensor.

The optical fence would be constructed from between 2 and 6 sensors, each on a host satellite in a circular, sun synchronous, always sun-lit ring at an altitude of about 700 kilometers. Each sensor is responsible for scanning its portion of its orbital plane. Figure 1 shows a diagram of a six sensor optical fence. The field-of-view of a single sensor is shown. That field-of-view is swept in a step stare fashion to cover the area between the two lines emanating from satellite 1. Likewise, the other satellites search their areas of responsibility. The leak-proof portion of the coverage is shaded. The fence is leak-proof because satellites with orbital altitudes above 4800 kilometers cannot cross the field-of-view of the ring of sensors faster than the field-of-view can be searched. Most lower altitude objects, those with altitude's under 4800 kilometers, are tracked every few hours.

A statistical estimate of the fence system performance is shown in Figure 2, as a function of the number of satellites included in the space surveillance constellation. The average number of sightings per day is shown on Y-axis as a function of target altitude on the X-axis. The various lines indicate capability for constellations of varying size. The sightings per day were calculated by multiplying the chance a target stays in the field-of-view of the ring long enough to be detected by twice the number of revolutions per day. The target is assumed to be in a circular orbit, and is assumed to be in an orbital plane perpendicular to the sensors' orbital plane. This choice of a target's orbital plane is the most stressing. If the target's orbital plane is not perpendicular to the sensor's orbital plane, the target is more likely to be detected since it will spend more time in the ring of sensors' field-of-view. The leak proof altitude and the LEO performance degrade slowly as the number of sensors is reduced, with the exception of the transition between 2 sensors and 1. Since the sensors are in a single orbital ring, as long the number of sensors is greater than 2, significant performance can be maintained if one sensor fails.
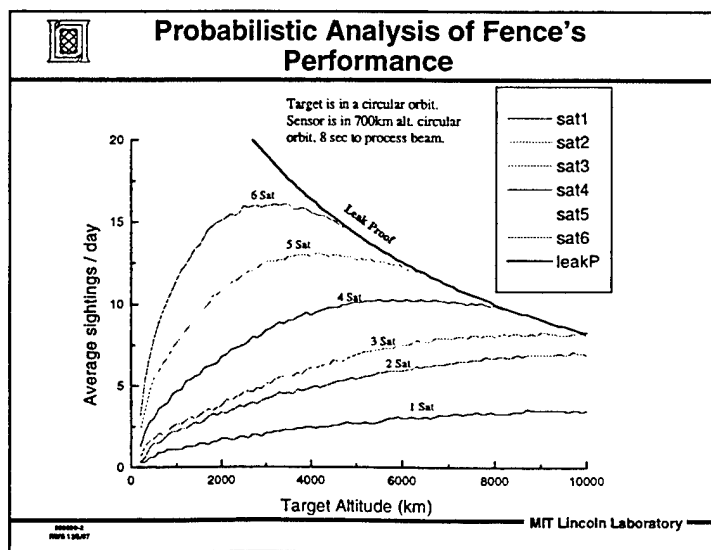
Figure 2

Another method for determining the capability of the fence system is to measure the maximum gap time; defined as the maximum time a given satellite can go without being seen by the sensor system. Figure 3 illustrates the maximum gap time for LEO and DS targets for a given six-sensor configuration of the ring. These results were obtained from a 4 day simulation using the entire unclassified catalogued, which contains 7998 targets. The figure is a histogram of the number of targets that have given gap times. Note that almost the entire population of satellites has gap times less than 12 hours, with only a few, mostly those in orbits very similar to the space surveillance constellation, having gap times exceeding 30 hours. This is true for both the deep space and low altitude populations.
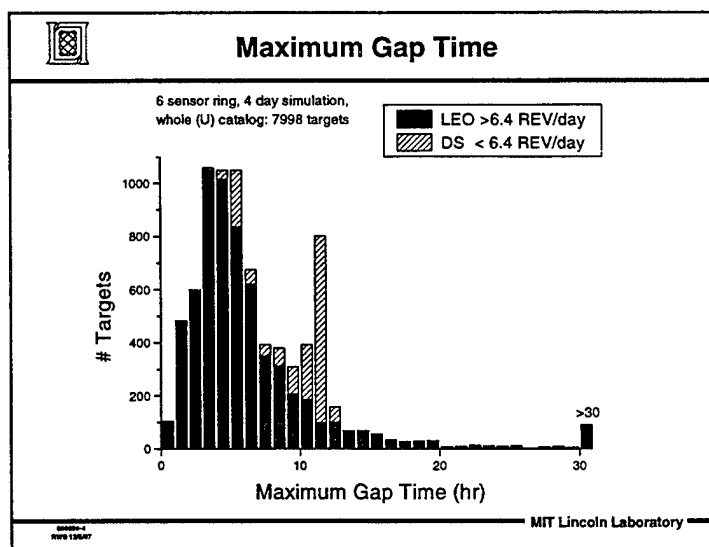
Figure 3

The sensitivity of the EO fence sensors is expected to provide 1.5 to 2 visual magnitudes improvement over the SBV capability. This yields a 17.3 visual magnitudes detection limit in the average case, with a 15.4 visual magnitude detection limit in the worst-case (highest phase angle in worst seasonal case). Even in this worse-case scenario, a half a revolution later the target is at a favorable solar phase angle and the detection limit is 17.3 visual magnitudes or better. The average case indicates for a reflectivity phase angle product of 0.01 (a conservative estimate), the system will detect an 80-cm diameter object at geosynchronous altitudes and a 20-cm diameter object at a range of 10,000 kilometers.

In summary, the space-based optical fence has considerable capability for space surveillance. Only 2 to 6 satellites are required, operating in a coordinated constellation. Each of the sensors requires a relatively modest satellite payload containing 10-inch optics. Deep space objects will be detected every half revolution with a few highly eccentric orbits detected every full orbit. Most low altitude orbiting objects will be detected every few hours, and the sensitivity will be considerably better than GEODSS or SBV.

Given that an electro-optic space-based fence appears to be a credible instrument for space surveillance, we have considered what steps can be taken with available technologies to advance in that direction. In our view, the first step towards an optical fence system is the demonstration of "up to date" technology on a single spacecraft. To that aim, we have generated a system

design for an autonomous space surveillance vehicle we call ASSET (Autonomous Space SurvEillance Technology). ASSET is intended to build on the SBV experience by employing the technology available in the late 1990s, which represents a major improvement from the late 1980s as used in the SBV.

Fundamental technological advances between the SBV era and the current time will provide considerably more capability for ASSET. Two specific areas of technological advance have been focal planes and space qualified processors. When the SBV was designed, we were starved for pixels on the focal plane. We desired to accomplish both wide field-of-view operations for search applications as well as high metric accuracy for improved orbit determination. Then current focal planes provided for 420 by 420 pixels. For ASSET to achieve a larger field-of-view and greater metric accuracy than SBV, more pixels on the CCD would be required. In the intervening time since the SBV technology freeze, focal planes have improved considerably. Current state-of-the-art 2560 by 1960 pixel, frame transfer focal planes have been fabricated for the GEODSS upgrade program. These focal planes contain enough pixels to improve on both SBV's field-of-view and metric accuracy. In addition, the quantum efficiency of the focal planes has increased from 27 percent solar weighted quantum efficiency for the SBV to 66 percent solar weighted quantum efficiency for the current focal planes. This provides an increase in sensitivity of more than a factor of 1.5, in the background-limited case.

Space qualified processors have also increased considerably in capability since the late 1980s. The SBV contained a custom build signal-processing unit with a capability of 10 MIPS and containing a few megabytes of RAM memory. Currently general-purpose space qualified computers in the 100 MIP range are available. These processors contain hundreds of megabytes of memory. While the SBV processors were programmed in assembly language, the current generation of space qualified processors are programmable using standard languages such as C.

The objective of the ASSET program is to demonstrate autonomous maintenance of the geosynchronous belt population. To that aim, ASSET is intended to combine mission autonomy plus spacecraft autonomy, with the end objective of reducing operations costs. The concept of operations for ASSET is in the construction of a leak-proof optical fence in the geosynchronous belt. Since ASSET is only to be a single satellite "constellation", the concept of operations will be considerably different than that suggested for the optical fence system discussed above. The intended output of the ASSET system is a geosynchronous catalog "on demand" and the observations of the satellites seen. In addition, ASSET will be able to flag previously unknown objects that have appeared, thus, providing new object notification and determing that catalog objects are not in their expected location, thus, providing maneuver notification.

The current system design for ASSET has the satellite in an about 700 kilometer altitude, circular, Sun synchronous orbit. The ASSET focal plane would include a charge couple device of 1024X2048 pixels, yielding a field-of-view of 4 degrees by 2 degrees. Metric accuracy attainable from the system is approximately 2 arcseconds. Figure 4 diagrams the orbit of the ASSET system around the Earth in a sun synchronous, circular orbit. ASSET will search the portion of the geosynchronous belt with solar phase angles < 90 degrees. This configuration allows the telescope to be constructed with minimum baffling, thus reducing weight and cost.

ASSET's Sun-Sync Orbit
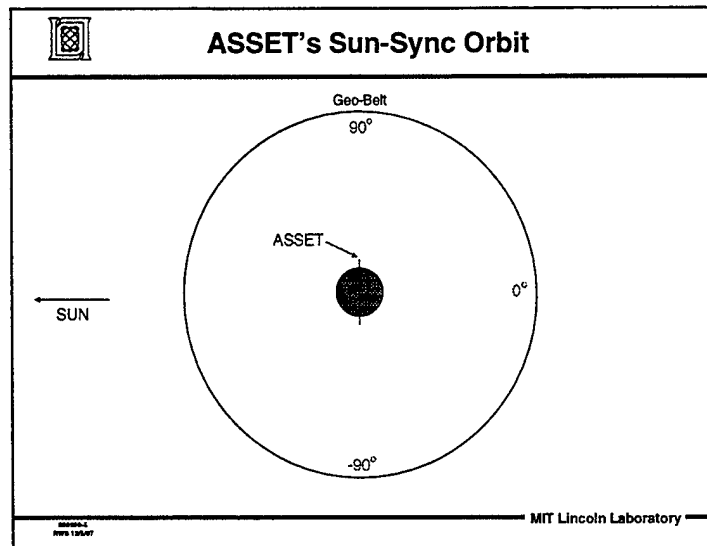
Figure 4

In order to assess the capability of ASSET against the geosynchronous population, we have estimated the number of fields of view that can be collected per orbit. ASSET would function in a step stare mode by tracking the stars and taking a series of frames. Fixed objects are stars, while moving objects are RSOs. This process is very similar to the operations of the SBV sensor. Each set of frames would contain eight frames, each with a 1/2-second integration period. We assume a time of 30 seconds/field position as a baseline for discussions; this includes the time to collect eight frames, process the data, and step and settle time to the next location. Based on available signal processing capability we believe that this is a conservative estimate. The orbital period of ASSET (at an altitude of 700 kilometers) is about 99 minutes, enough time for scanning 197 30-second fields. The scanning scheme invasion for ASSET a shown in Figure 5. The 195 overlapping fields are used to cover plus and minus 4 degrees latitude and 140 degrees of longitude every orbit of the ASSET spacecraft. These fields of view are arranged in an overlapping grid of 39 by 5 fields.

Scanning Scheme

Scanning fence for GEO from phase angles ~0° to ~70°

Equator

39 X 5 (2° X 4°) = +-4° lat. X 140° long.

Scanning Fence
  195 overlapping pointings to cover +-4° lat. X 140° long. every ASSET rev
    39 groups of 5 stacked pointings
  Observe most targets 4-6 times per day
    Targets with inclinations > 4° will be seen less often
    Targets with inclinations > 15° may NOT be visible sometimes
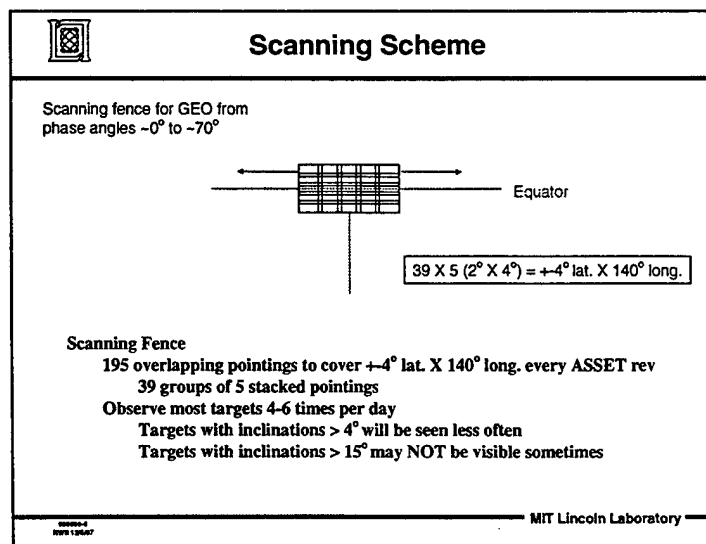
Figure 5

In order to quantify the performance of ASSET when operated in the manner described above, a 4-day numerical simulation was run against the entire unclassified RSO catalogue. The 4 days of observations yielded 4470 satellite detections per day, with each detection yielding two observations. Of those detections, 2500 detections per day were geosynchronous objects, 660 detections per day were deep space (non-Geosynchronous) objects, and 1310 detections per day were low Earth orbiting objects. The total of almost 9000 observations/day, each with a metric accuracy of 2 arcseconds represents a significant space surveillance capability.

Since ASSET is intended to provide a leak-proof fence in the geosynchronous regime, it is instructive to examine the number of sightings per day expected for objects in the geosynchronous catalog. This information is provided in Figure 6, which contains a histogram of the number of RSOs as a function of the number of sightings per day. All of the RSOs in the unclassified geosynchronous catalog are sighted by the ASSET system. In fact, most of the objects in the catalog are seen many times per day. Figure 7 displays the simulation results in a slightly different way. Here, the maximum gap times between observations are histogramed. As a result of the scan pattern chosen for ASSET, low inclination objects in the geosynchronous belt are seen several times over a period of a few hours and then approximately 17 hours elapse until the next cluster of observations. Most active satellites in the GEO-belt have low inclination. Objects with inclinations greater than 4 degrees have larger gap times. In just a few cases, for objects with very high inclinations, there are gap times above 28 hours.

Figure 6

**GEO Objects
Maximum Gap Times**

ASSET 4 day simulation, 1 sensor: 700 km orbit
checkerboard scan pattern: 5 stack
493 GEO objects

MIT Lincoln Laboratory
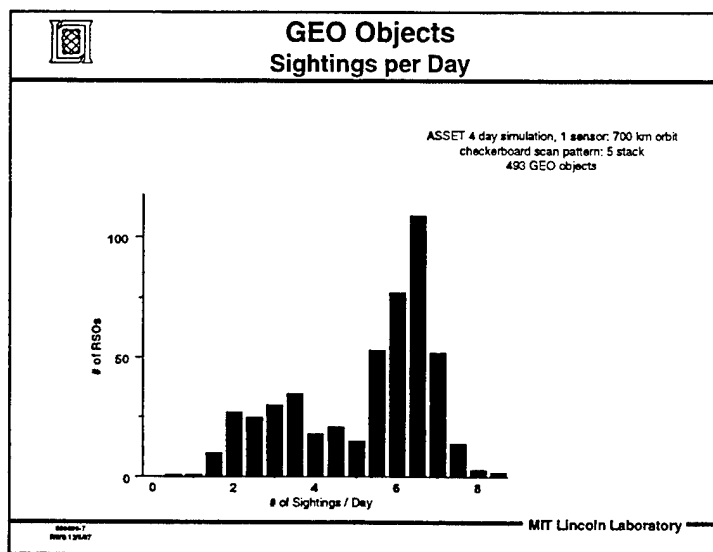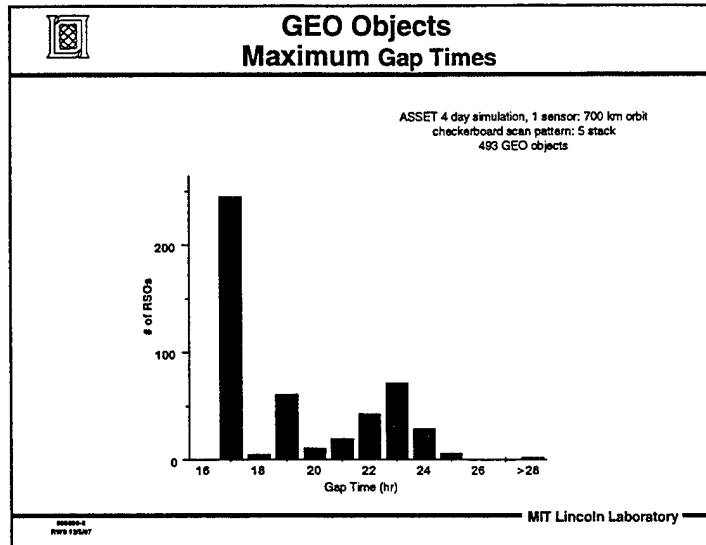
Figure 7

Figure 8 shows an example of an ASSET system implemented as a free flyer on a MIGHTYSAT bus. The MIGHTYSAT bus is actually a fairly restrictive bus to design against. It provides only 100 pounds of payload capability, less than 100 watts of power and is not stable to the desired level. The maximum sized optic that could be designed given such constraints is an 8-inch effective aperture on-axis system (9-inch physical aperture with some obstruction by the secondary and supports). A diagram of this telescope is shown in Figure 9. This telescope combined with the CCD discussed earlier provides approximately a 16.8 visual magnitude detection capability.

ASSET Implementation on MIGHTYSAT Bus

MIT Lincoln Laboratory

Figure 8

125

Asset Telescope Concept

Multi-Layer Insulation (MLI)

OTCCD

Thermal Strap

Thermo-Electric Cooler (TBD)

MLI

To Radiator

Thermally Insulated S/C Interface

MIT Lincoln Laboratory
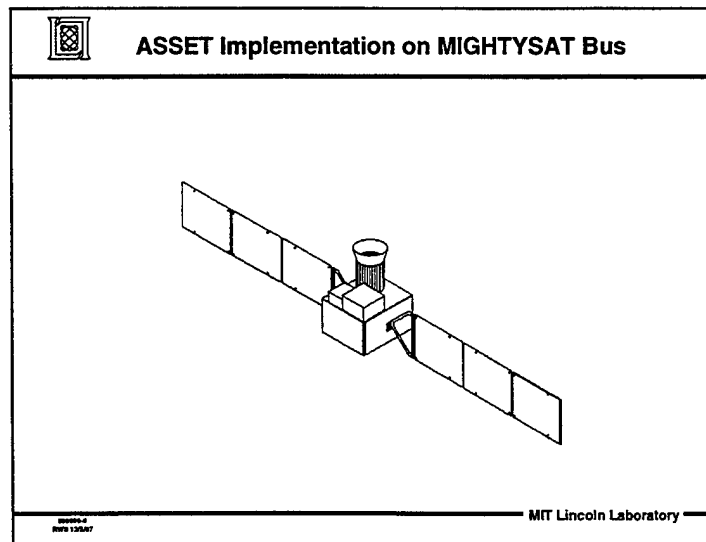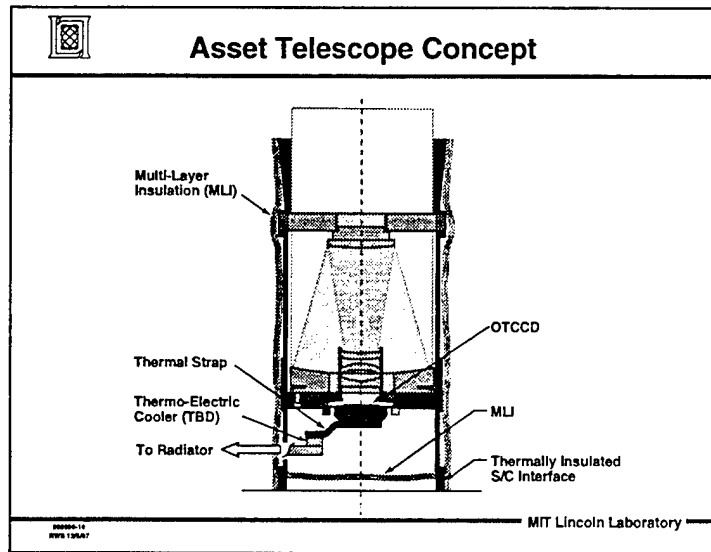
Figure 9

Another engineering challenge of placing such a payload on a small satellite is that of jitter. In order to obtain high metric accuracy observations, very low jitter is required. Generally small lightweight buses have considerably more jitter than is acceptable to the ASSET instrument, which has a metric accuracy goal of 2 arc-seconds. Thus, the system needs some active stabilization. Rather than use the standard solution, which is a mechanically steered compensation mirror, we have chosen an advanced focal plane technology. This technology is based on our orthogonal transfer CCD structure or OTCCD. Generally CCDs are intended to transfer information on the pixels along a single axis for readout purposes. In OTCCD, transfer along both axes, rows and columns, is enabled. This allows the compensation of motion of the image on the focal plane during the integration period, assuming that the pointing of the system is known very accurately during that time. In the ASSET as currently designed, we intend to take the 400 Hz output of the attitude determination system on the MIGHTYSAT payload and use that information to drive the compensation system on the OTCCD. A picture of the OTCCDC structure is shown in Figure 10, along with the layout of the chip we have designed for ASSET. The OTCCD is 1024 by 2048 pixels; each pixel is slightly larger than 20 microns. The chip, which is a conservative design, includes four output ports. The rates of the 4 parallel readouts have been matched to the 1/2 second integration period. Thus, 1 Mbit per second per readout port is required. This is readily achievable given current technology that has been developed for the GEODSS program. Noise of less than 6 electrons per second is expected at an operating temperature of -40 degrees Centigrade. OTCCD structures such as these have been demonstrated at Lincoln Laboratory for atmospheric compensation purposes.

Figure 10

In summary, space-based optical fence systems offer very capable solutions in the area of space surveillance. The relatively small number of sensors, each requiring modest payload budgets, are needed to construct a system that provides true surveillance of space. Figure 11 shows the evolution of technology from the SBV era to a possible operational system in the 2005 time frame. Currently, 1998 technology allows construction of a capable first step system, which will pave the way for the eventual transfer of the space surveillance mission to space.

Figure 11

127

Focal Plane

- OTCCD Structure
- Specification
  - 1024 x 2048 pixels
  - >20 μm pixels (21?, 24?)
    - Larger pixels increase f/#, ease optics design
    - Yield not seen as an issue
  - 4 output ports
    - 0.5 Mpix/port
  - 1 Mpix/sec/port
  - 0.5 sec read time
  - Noise < 6 electrons
  - Operating Temp -40 °C

Output Port 512 x 1024 · OTCCD Electrodes · Storage Area 1024 x 1024 · Image Area 1024 x 2048 · Storage Area 1024 x 1024 · OTCCD Electrodes

MIT Lincoln Laboratory

Sensor System Evolution

Development of Operational Capability

	SBV	Evolutionary Demo	Operational System
		GEO Fence	Full Fence
Year	1989	1998	2005
# of payloads	1	1	4
Sensitivity	15.5 Vmag	16.8 Vmag	17.3 Vmag
Telescope	6 inch	8 inch	10 inch
Quantum Efficiency	27%	66%	66%
Search Rate	100sq °/hr	960sq °/hr	64,800sq °/hr
CCD	420X420	2048X1024	2560X2560
FOV	1.4°X1.4°	4°X2°	6°X6°
Processing	10 MIP	100 MIP	1000 MIP/sat
Tasking Response	12.5 trk/hr	120 trk/hr	960 trk/hr

MIT Lincoln Laboratory

Figure 11

127

Cheyenne Mountain Operations Center (CMOC) Space Control Improvement Initiatives

D.W. Deist, Major, USMC

Introduction

This paper briefly presents some details of the space operations that occur in the Cheyenne Mountain Operations Center (CMOC) and current initiatives to improve operations. CMOC contains elements from the North American Aerospace Defense Command (NORAD), United States Space Command (USSPACECOM), and Air Force Space Command (AFSPC). The Space Control Center (SCC) in CMOC is the USSPACECOM operational center responsible for ensuring freedom of action in space and, if required, denying any enemy that same freedom of action. Two of the functional areas included in that mission are space surveillance and protection. Within these functional areas are the tasks of launch, maneuver, and reentry processing, pre-launch conjunction analysis, on-orbit conjunction analysis, and anomaly resolution. Within CMOC there are efforts underway to improve operations in each of the above areas. This paper will only discuss current CMOC initiatives, it will not discuss long range goals, planning, or policy of USSSPACECOM.

A hollowed-out mountain in the Colorado Rockies is the location of the U.S. nerve center that would sound the first alarm of an attack against North America. The 100-million-year-old Cheyenne Mountain was tunneled out in the early 1960s to make room for a complex of 15 steel buildings. Some 7,000 tons of steel was trucked in for use in fabricating the buildings which house everything needed to perform the mission--people, supplies, computers, display screens, and communications equipment. In the mid-1960s, the early warning function was moved from an above-ground vulnerable building in Colorado Springs to the granite-shielded security of Cheyenne Mountain. The heart of the underground complex is the unit's command center, which began operations under NORAD in Cheyenne Mountain in 1966.

Today, CMOC serves as the command and control center for the nation's Integrated Tactical Warning and Attack Assessment (ITW/AA) system. The ITW/AA system is made up of radars and other types of sensors around the world and in space that provide warning information, as well as the communications and computer systems inside Cheyenne Mountain that process the raw data from the sensors for use in evaluating a potential attack. All the communications equipment, computer systems, software, and individual operational centers in Cheyenne Mountain used by the North American Aerospace Defense Command (NORAD) and United States Space Command (USSPACECOM) in providing warning of air, space, or missile attack are part of the ITW/AA system. CMOC is comprised of operational centers which include the Missile Warning Center, the Space Control Center, the NORAD/USSPACECOM Command Center, and the NORAD Battle Management Center.

NORAD, USSPACECOM, and Air Force Space Command are responsible for operating and maintaining the ITW/AA system. Air Force Material Command's Electronic Systems Center is responsible for its acquisition, integration, and sustainment (including system upgrades).

CMOC Space Control Operations

The CMOC Space Control Center (SCC) helps to provide the foundation for all U. S. space operations by accomplishing space surveillance and space protection support for a variety of users. Between 1958 and 1960, the tracking of space objects was divided between three organizations: the US Air Force Air Research and Development Command, the Advanced Research Projects Agency, and the US Navy Space Surveillance Network. The Air Force argued for a single integrated network, the Space Detection and Tracking System (SPADATS) to consist of Air Force and Navy efforts to be placed under the operational control of NORAD. The Army and Navy favored a tri-service agency to control surveillance while NASA wanted space surveillance under its authority. SPADATS was established, and in October 1960, the SECDEF assigned its operational control to NORAD. Eventually, separate centers for space defense (SPADOC) and space surveillance (SSC) were established in Cheyenne Mountain Air Station. In 1994, these centers were combined to form the current Space Control Center.

Mission

The space control mission is to ensure the freedom of action in space and, if required, to deny any enemy that same freedom. It is analogous to sea control or air superiority. This mission can be broken into three areas of responsibility: *surveillance, protection, and negation.* Surveillance and protection will be discussed herein. Negation is a wartime mission. Due to treaty restrictions, it is mostly theoretical, and it involves no day-to-day operations. Therefore, it will not be discussed here.

The SCC reports to the NORAD/USSPACECOM Command Center, primarily in support of its ITW/AA mission. An example of this support is ensuring that a space event, such as the routine reentry of space debris, is not misinterpreted as a hostile event. The SCC also interfaces with several other CMOC centers: Missile Warning (ex: launch detection data); Air Defense (ex: radio frequency interference resolution); Intelligence (ex: upcoming launch data); and Weather (ex: solar conditions).

An integral part of the SCC is the members of the 1st Command and Control Squadron (1CACS), which reports to AFSPC's 21st Space Wing. 1CACS handles all routine space surveillance activities, and maintain and implements the maintenance schedule of the space surveillance network (SSN). Although the SCC is a unique center, it is not the only one that can perform the space control mission. The Navy operates an alternate space control center in Dahlgren, Virginia to provide a backup or augmentation capability. This alternate center

employs different manning, equipment, and procedures. Each week, they conduct a 10-hour proficiency shift, where the alternate is prime and CMOC SCC is in "hot shadow."

Manning

CMOC centers are divided into 5 crews (Alpha through Echo) which work 3 shifts to provide 24-hour coverage. Within the SCC, there are 7 USSPACECOM crew members:

1. *Space Control Center Commander (SCCC)*: responsible for overall crew coordination and interface with Mission Director (CMOC Command Center)
2. *Deputy SCCC (DEP)*: responsible for overall crew operations, message preparation, and interface with other CMOC centers
3. *Space Control Analyst (SCA)*: responsible for conjunction assessment and laser clearing analyses, and high interest surveillance tasking
4. *Orbital Analyst (OA)*: responsible for sensor tasking and processing observations for maneuvers, reentries, and launches (2 per crew)
5. *Space Control Officer (SCO)*: responsible for processing radar frequency interference events, and ground attack/sabotage and anti-satellite threats
6. *Space Control Technician (SCT)*: responsible for launch processing, anti-satellite threat support tasking, and maintenance of center log.

In addition, the 1CACS provides crew members to process routine observations, and other missions which are discussed in other workshop briefings. The SPADOC 4C computer system is the "brains" of the SCC. It provides a data and communications capability to monitor space activities, to provide warning of threats or attacks against satellites, and to protect satellites by identifying threats and providing information necessary to avoid or counter them. Its support contractor provides a dedicated technical representative for each crew to conduct database maintenance, troubleshooting, and exercise support as required.

Surveillance

The primary objective of space surveillance is fourfold: to *detect, track, identify, and catalog* all manmade objects in space. The end product of this effort is the satellite catalog (SATCAT), an unclassified product which is openly available. In order to maintain an accurate SATCAT, maneuvers (changes in orbital parameters) and launches (introduction of new space objects) must be processed in a timely manner. There are three basic categories of launches: *domestic, cooperative, and foreign. Domestic* launches occur within the US; *cooperative* launches occur outside the US, but the launch agency provides launch parameters to the SCC prior to launch; *foreign* launches occur outside the US, and no launch parameters are provided in advance of the launch.

Maintaining an accurate SATCAT minimizes the risk of NORAD or the Commonwealth of Independent States (CIS) misinterpreting routine space activity as a hostile event. In this regard, the SCC supports risk reduction treaties in three specific areas: breakups, errant launches, and reentry assessment objects (RAs). A *breakup* is what its name implies -- a single space object that breaks into more than one space object. If the breakup meets criteria for RA (discussed later), and can reasonably be expected to reenter over the CIS, the SCC must prepare a message to report this event to national authorities. An *errant launch* is a space launch that diverges from its nominal launch profile and is not terminated by range safety. If the predicted flight path might appear as a threat to the CIS, then a message must be sent.
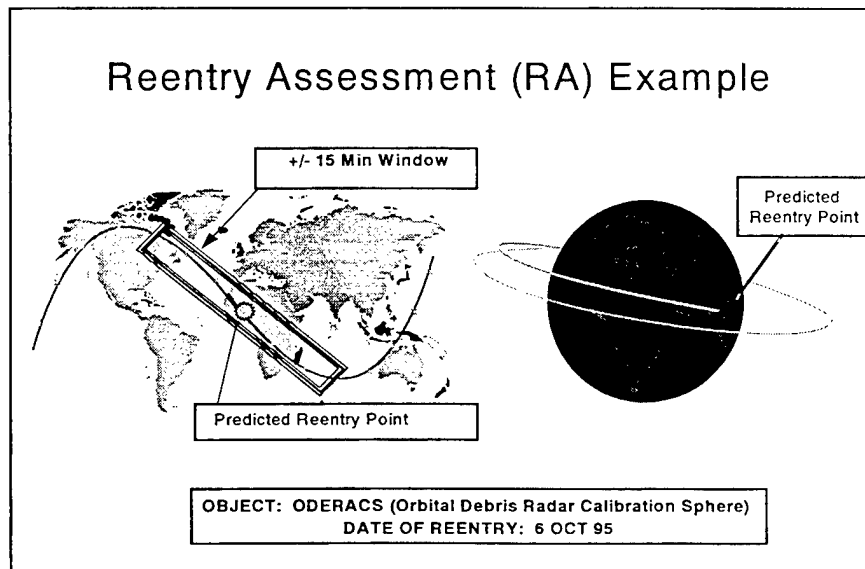
Figure 1. Reentry Assessment (RA) Example

A reentry assessment (RA) object is defined as a decaying manmade space object that has a greater than 5 percent chance of surviving reentry. For practical purposes, the SCC clarifies this to be all payloads, rocket bodies, or platforms, and any debris with a radar cross section greater than 1 square meter. The normal processing of an RA object is as follows (based on time before predicted impact):

- 10 days out: 1CACS hands processing moves to the SCC
- 10 to 4 days out: SCC updates RA at least once per day
- 4 days out: SCC updates RA once per shift; start providing ground traces to Command Center
- 2 days out: Sensor tasking priority increased for RA object
- 1 day out: Sensor tasking priority increased again
- 6 hours out: Reportability determined
- 2 hours out: Reportability reevaluated

An RA object is reportable if its predicted impact is on or within 15 ground track minutes of the CIS, or if it breaks up any time after 6 hours prior to predicted impact. The example shown in Figure 1 was the decay of an ODERACS (a small radar calibration sphere released by the space shuttle). Since the critical segment of its groundtrace (-15 minutes to +15 minutes from its predicted impact point) did not overfly the CIS, it was non-reportable.

New foreign launches (NFLs) present a challenge to the SCC. Since there are no launch parameters provided to the SCC prior to such launches, it is critical that the SCC process launch information in a timely manner to ensure the new space objects are cataloged. In the event of such an unannounced launch, the SCC must:

- Receive and interpret launch data provided by CMOC Missile Warning Center (MWC)
- Determine the initial orbital inclination of the object(s)
- Alert appropriate sensor sites that may see the object(s)
- Coordinate the detection, tracking, and cataloging of the objects

The surveillance mission is accomplished through the tasking of the space surveillance network (SSN). The SSN consists primarily of 17 optical and radar sensors deployed worldwide (7 in the continental US) that contribute to the detection and tracking of near-earth and deep-space objects. Deep-space sensors are categorized as sensors capable of tracking objects with orbital periods of 225 minutes or greater. There are several types of sensors in the SSN:

- *Mechanical radars* are the classical dish-shaped antennae that can track only one object at a time (Altair, Antigua, Ascension, Clear, Kaena Point, Millstone).
- *Phased array radars* use hundreds of individual radio frequency elements, each of which can be individually controlled to form a composite radar signal. It can track multiple objects simultaneously (Beale, Cape Cod, Cavalier, Eglin, Fylingdales, Thule).
- The US Navy Space Surveillance Network (NAVSPASUR) is the only *continuous wave radar* in the SSN. It consists of 3 transmitters and 6 receivers that form a radar "fence" approximately 2,000 miles long, 2 miles wide. Although it can look 6,000 miles into space, it cannot be moved or adjusted to track.
- The majority of deep space tracking is performed using ground-based *electro-optical* deep space sensors (GEODSS) or other optical trackers (AMOS, Diego Garcia, MOTIF, Socorro). The performance of these sensors is limited by weather and lighting conditions.

Figure 1 shows the location of the 17 SSN sensors. There are three mission categories for these sensors:

- *Dedicated*: sensors that have a primary mission of space track in support of the SCC
- *Collateral*: sensors that have a primary mission other than space track, but can support the SCC on a non-interference basis. Most collateral sensors have a primary mission of missile warning.
- *Contributing*: sensors under contract to provide space track support to SCC. Some of these sensors may have limitations on their times of operation.
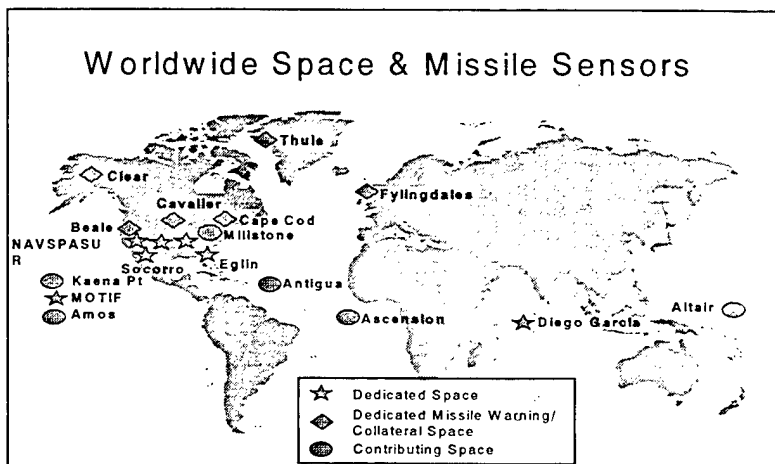
Figure 2. Worldwide Space and Missile Sensors

Protection

The SCC performs several protection functions as part of its ongoing mission. One such function is *laser clearing*. Research lasers often radiate into space. Using the SPADOC 4C computer database, the SCC ensures that these lasers do not accidentally illuminate an active payload, thus preventing inadvertent damage.

Protection against *radio frequency interference* (RFI) of communications between satellites and ground stations has become more challenging with the increasing number of payloads in space. When notified by owner/operators, the SCC, with the help of other CMOC centers and outside agencies, supports the identification and resolution of such interference. The source of interference may be manmade or natural. If manmade, the RFI may be accidental or intentional, the latter being termed *electronic warfare* (EW). *Solar conditions*, and their interactions with the

Earth's geomagnetic environment, cause most of the natural RFI. Solar phenomena can affect satellites in other ways, also. Increased solar activities, caused by solar flares, can cause changes in the geomagnetic and atmospheric characteristics of the Earth. Major effects to the satellites include computer bit flops, overheating, communications problems, and increased drag on low-orbiting objects.

The SCC also has wartime protection missions against *intentional threats*. This includes alerting space system elements of any potential or actual threat against other elements, or whole space systems in general. Ground attacks or sabotage at ground sites are considered the most probable threats. The SCC also processes direct anti-satellite attacks (co-orbital, direct ascent, directed energy, and nuclear detonation); the details of these missions are beyond the scope of this paper.

To perform the protection mission, the SCC must communicate with a number of space system owner/operators. As previously mentioned, the SCC coordinates closely with the NORAD/USSPACECOM Command Center in support of their ITW/AA and risk reduction missions. Satellite operations squadrons (SOPS) and the Air Force Space Control Network (AFSCN) together accomplish telemetry, tracking, and control (TT&C) for many space systems. The SCC supports protection actives for these SOPS and AFSCN sites, along with those of the SSN. The SCC also supports protection processing for launch activities out of the Eastern and Western Ranges, as well as smaller ranges, such as Wallops Island and White Sands. This processing consists of launch window screening to ensure the nominal flight window does not intersect with any cataloged space objects. The SCC supports NASA space activities, the most important of which are manned space flight missions.

The SCC supports the Space Shuttle throughout its entire mission profile. To protect the Space Shuttle when it is on orbit, the SCC performs a conjunction assessment analysis at least three times each shift (see Figure 3). The current concept of operations for manned space flight safety is to screen 36 hours into the future for any objects entering a 100km sphere surrounding the Space Shuttle. An on-duty SCA manually reviews the list for any object that enters a box around shuttle or ± 5km radially, ± 25km in-track, and ± 5km cross track (5x25x5). If any object intersects the box, it is termed a *conjunction*. A conjunction will receive a higher tracking priority and it's track will be maintained at a higher accuracy. If the object then enters 2x5x2 box, NASA Johnson Space Center will be notified and given information necessary to make a maneuver decision. Similar procedures apply daily for Mir, with information being passed from NASA Johnson Space Center to the Mission Control Center - Moscow (MCC-M).
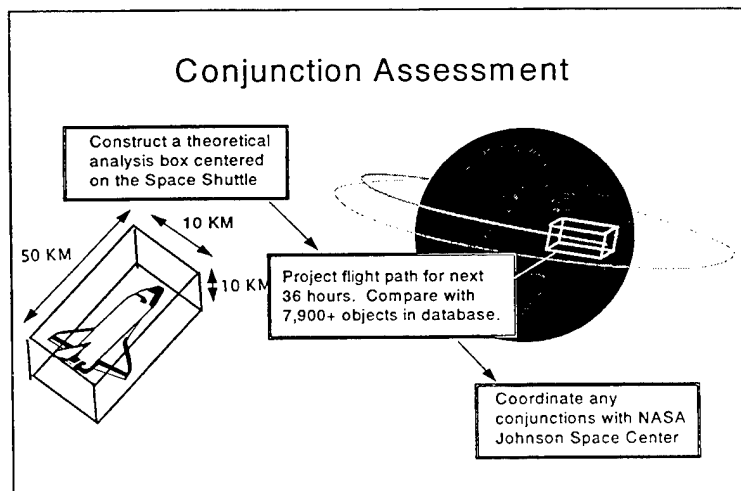
Figure 3. SCC Space Shuttle Conjunction Assessment Processing

Improvement Initiatives

Current improvement initiatives focus on protection. The task of EW/RFI resolution is one which has taken on increased importance recently with the increased proliferation of space and subsequent increase in reported interference. The first area of improvement in EW/RFI resolution is in the reporting stage. Due to a historic lack of meaningful feedback to users reporting interference, the current prevailing attitude of many users is "why report it?" To overcome that attitude, CMOC has increased efforts to get information out to users concerning CMOC capabilities and provide feedback to users when interference is reported. These increased efforts have been through attendance at Frequency Management Working Groups, various conferences and the draft of a new USSPACECOM regulation establishing standards for anomaly reporting, processing, and feedback.

In the area of EW/RFI processing, efforts have been focused on improved training for the SCO. The SCOs have received increased training on worldwide satellite communications capabilities and the science behind satellite communications and interference. They have also been given updated references to better allow them to understand and receive reports and accurately process anomalies.

Determining the general location of the offending emitter is often the key to interference resolution. CMOC access to geolocation capabilities has historically been limited only to cases determined to be of critical nature. CMOC has initiated submission of broader reaching geolocation requirements in an attempt to gain greater access to geolocation capabilities. Those requirements are currently in the approval phase, likely to be approved by Spring 1998.

136

Once the general geographic location for an interfering emitter is determined, CMOC searches databases of known emitters and conducts an analysis to identify the specific interfering emitter. The database search and analysis is done using the Prototype Workstation for Electronic Warfare and Frequency Interference Resolution (POWERR). This workstation is designed to search a database for potential emitters, do a link analysis, and identify potential interfering emitters. It has been plagued, however, with a lack of sustained funding, and adequate access to needed databases. In spite of it's drawbacks, POWERR has demonstrated the utility of an EW/RFI tool for the SCC. USSPACECOM has joined with the Joint Spectrum Center, US Naval Space Command (NAVSPACE), Air Force Space Command (AFSPC), NSA and other government agencies, to develop an analysis tool that takes advantage of many of the analysis features of POWERR and incorporates them into a user friendly platform capable of doing database searches, interference analysis at all frequencies to include lasers, and various other space oriented analysis functions. This new platform which has community wide support is called SATPRO. The first version of SATPRO was delivered to CMOC in February 1998 and will reach IOC in FY2000. The goal in CMOC is to sustain funding for POWERR and continue to improve database access, until it can be replaced by SATPRO.

Another area of satellite protection receiving attention is the arena of orbital safety which involves two distinct areas for the SCC; launch collision avoidance (COLA) and on-orbit conjunction analysis (CA). Launch COLA involves screening the launch vehicle against the SATCAT of approximately 9000 objects. The SCC computer system was designed to project a vector for ballistic flight of a launched object against the SATCAT. It cannot model powered flight, variable flight azimuths, or in-flight yaw steering. A workstation, CALIPER, was developed for the Cassini spacecraft launch which models powered flight and variable flight azimuths. However, it requires trajectory polynomials that represent the flight path, something not currently routinely received from launching agencies. Although the probability of a collision during the launch phase is extremely low, space will continue to get more crowded and the likelihood of collision will increase. Recognizing that, USSPACECOM has drafted a regulation requiring any agency launching from a U.S. launch site to provide the information necessary for CMOC to perform a COLA. They have also begun an evaluation of the current capability in an effort to identify areas of needed improvement. The new emphasis on launch COLA should provide the needed support to further develop the workstation started by Cassini into an operational launch COLA workstation capable of processing all launch platforms using the launch nominals currently sent to CMOC for tracking purposes, modelling powered flight, variable flight azimuths, yaw steering, and providing associated covariance (measure of accuracy) data for users needing to calculate probabilities of collision.

The launch of the first element of the International Space Station (ISS) will mark a significant increase in the quantity and quality of support to NASA manned space flight. NASA requirements for ISS are for a screen 72 hours into the future for any manned or mannable object. They also require associated covariance data with any flight vector sent from CMOC. CMOC does not currently have the ability to provide accurate covariance data. Software is under development to be delivered in summer 1998 that will give the SCC that capability. The new software is in two parts. The first part uses laser data available on the Internet to calibrate the data received in CMOC from the Space Surveillance Network (SSN). The second part maintains approximately 1000 objects from the SATCAT at the highest possible accuracy, calculates potential conjunctions, and provides covariance data and needed vectors for any objects conjuncting with manned objects. This new software will be hosted on a single workstation, possibly along with the launch COLA software, and operated by a new SCC crew position, the Orbital Safety Analyst (OSA). The OSA will still manually screen for objects entering a 100km sphere around ISS, just as for Shuttle, but once a conjunction is identified, he will not have to wait for tasking to be increased to establish a more accurate track, it will be resident on the workstation. Conjunctions within the 2x5x2 box can immediately be identified and associated vectors and covariance data can be sent to NASA.

CMOC has increased the use of modern information dissemination systems to improve operations. Information is now gathered from numerous sources, classified and unclassified and disseminated to theater commanders, component commands, and national decision makers through various processes. Unclassified information is readily accessible to crews over the Internet. Secret information is shared through the SIPRNET. And Top Secret information historically only available to and distributed by the intelligence community is available to operational centers through Intel Link. The installation of platforms with access to each of these webs has provided a quantum leap in the timeliness of information to crews and crew situational awareness.

Summary

Through increased cooperation with other agencies and use of state-of-the-art processing, CMOC is attempting improve it's ability to accomplish space surveillance and protection. Efforts in the areas EW/RFI reporting, training, geolocation and analysis, launch COLA, and on-orbit CA are beginning to have a significant impact on operations. These efforts have not been without vision. Each of these has been labeled as a prototype and example of where the SCC is headed in the future as it migrates to a distributed architecture. CMOC is aware of the increasingly important role it will play in space surveillance and protection, possibly for commercial as well as military users of space and is positioning itself now for the future.

Advanced Techniques for Estimating and Refining Orientation Vectors of Space Object Imagery

Xun Du, Stanley C. Ahalt (Ohio State University), Capt. Bruce Stribling (PL/OL-YY)

Abstract

We describe three advanced techniques incorporated into the design of a model-based image analysis system which automatically estimates the orientation vector of satellites and their sub-components. The system, implemented in Khoros, operates on images obtained from a ground-based optical surveillance system. Features of each satellite image are first extracted by partitioning the image and constructing a model representation. Second, pose estimates are obtained from model-matching across a model database. Finally, pose refinements are derived from photogrammetric or geometric information.

We discuss three advanced techniques: eigen-indexing, robust affine point matching, and random edge sampling. Eigen-indexing is a novel indexing method which constrains the number of model candidates and significantly improves the overall system speed by providing an efficient way to access the model database. We include a theoretical analysis of the eigen-indexing technique. Robust affine point matching significantly improves pose-refinement performance on degraded imagery. Finally, random edge sampling is a novel pose estimation technique used on those satellites which are difficult to partition and therefore violate nominal requirements for affine point matching. We demonstrate these techniques on estimating orientation vectors from challenging satellite imagery.

Introduction

The Maui Space Surveillance System (MSSS) at an elevation of 3000 meters on the island of Maui, serves as a test-bed for new and evolving electro-optical sensors, and supports state-of-the-art measurement for a wide variety of government agencies and general scientific community research and development programs. Presently, the primary MSSS instrument is a closed-tube Cassegrain f/16 1.6-meter telescope (1.596-meter clear aperture, 25.10 meter Cassegrain focal length and 8.25 arc seconds/mm plate scale at the Cassegrain focus).

Because of the exceptional nature of the site, which is characterized by dry, clear air with visibility exceeding 150 km, seeing is typically on the order of one arc second. Thus, the major source of image degradation for the telescope is atmospheric turbulence. However, measurements of Fried's atmospheric turbulence coherence length, r_0, averages 12 cm in the summer and 10cm in the winter, exclusive of "doom seeing" (phase shifts due to internal and external temperature differences). Here the Fried parameter, r_0, is interpreted as the effective calibration of a diffraction limited telescope that would yield the equivalent resolution in the absence of the atmospheric turbulence, and is independent of the physical dimensions of the telescope.

Because of the site, telescope characteristics, and unique post-processing techniques, the MSSS facility can collect photographs of orbiting satellites (and space debris) with outstanding clarity in spite of atmospheric turbulence. We refer to these images as Space Object Imagery (SOI). Notably, the cost of collecting SOI at the MSSS facility is considerably less than the cost of collecting similar images from monitoring satellites.

SOI's primary utility is in supporting assessments of the operational status of particular satellites. Using satellite imagery anomalous behavior can be detected, and nominal configuration can be confirmed. Additionally, estimation of satellite pose (orientation) serves as a method of confirming alternative pose information.

Estimating the 3-D orientation vector for a satellite and its sub-components plays a central role in the function of the MSSS facility. However, estimating the 3-D orientation vector of any object from its 2-D image is difficult because the various 2-D images which can be formed from a 3-D object can be quite different from different viewing angles, and because ambiguities can result for objects with symmetries. As we explain later, additional ambiguities can occur when image degradation arises due to, for example, atmospheric turbulence.

SOI has characteristics which allows us to take advantage of certain techniques which have been developed in other computer vision applications. Accordingly, we have developed a SOI Image Processing Architecture (SOI-IPA) which is designed to automatically estimate satellite orientation from its 2-D images. In our problem formulation, we have constructed the architecture so that 3-D orientation vectors are estimated from a single image of known satellites.

However, we anticipate that the system will be modified in the future to handle multiple views and a large number of satellites.

Our architecture employs two steps: pose estimation and pose refinement. Pose estimation attempts to determine the rough pose of a given satellite image by matching the image pose with previously observed (and truthed) images - usually derived from synthetic models. Pose refinement estimates the 3-D orientation vector for each component of the satellite by extracting features and analyzing the photogrammetric information which can be gleaned from the image.

The paper is organized as follows. In Section *SOI Data* we describe the SOI data. In Section *Architecture* we present an overview of the system architecture, which is followed in Section *Pose Estimation* and *Pose Refinement* with greater detail regarding pose estimation and pose refinement. In Section *System Performance* the performance of the system is evaluated, and in Section Conclusions we summarize our results and indicate possible future improvements.

SOI Data

SOI imagery has certain unique characteristics, some of which pose challenges, but others of which can be effectively exploited to simplify the design of an SIO-IPA system. The most important characteristics are: 1) satellites are imaged in a large variety of poses, 2) potentially both high- and low- resolution imagery can be encountered, 3) backgrounds are not cluttered and the object is always prominent in the image, 4) rectangles are reasonable primitives for use as descriptors of many satellite sub-components, and 5) most satellites are symmetric with respect to their major axis.

Further, because some measured SOI images are degraded substantially by atmospheric turbulence and sensor miscalibration, we assume here that only an identified subset of the collected images are sufficiently detailed to realistically allow for orientation-vector processing, e.g., see Figure 1.

HST image: pose 1   HST image: pose 2
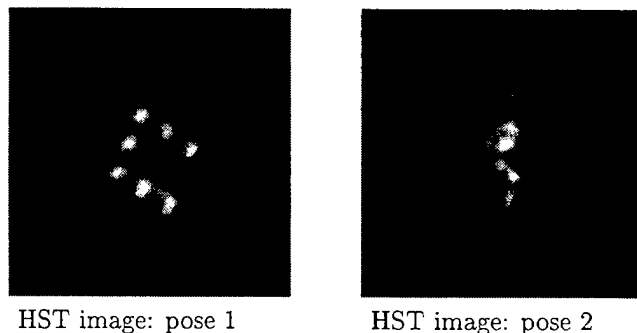
Figure 1: Measured images of satellites.

Because of the difficulty in truthing large amounts of measured imagery, which is required in a model-based system such as the one discussed here, our system development has been based on the use of synthetic images. These images, or models, do not suffer from distortion as compared to their real counterparts, as shown in Figure 2. Here we report tests in which these synthetic images are realistically degraded to stress the system. Moreover, we are currently testing measured images, as well as collecting additional images combined with ground truth which can be used to test the system under operational conditions.

Architecture

As noted above, our model-based object recognition system uses a two step approach. Figure 3 shows the system-level block diagram.

The system consists of a number of modules. The image pre-processing, feature extraction, model-representation, eigen-indexing, and model-matching modules draw from pre-computed models in the model database to perform

Synthetic HST image: pose 1   Synthetic HST image: pose 2
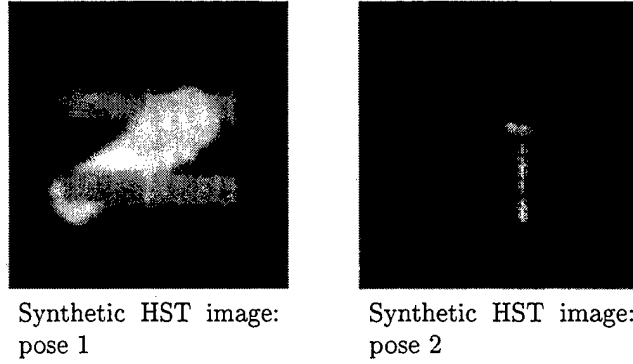
Figure 2: Synthetic images of the HST satellite
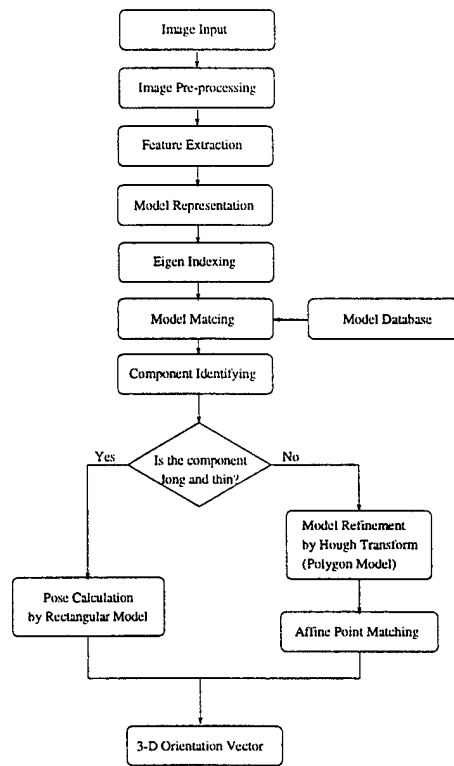
Figure 3: System block diagram

pose estimation. Component identification, model refinement, affine point matching and pose calculation are used in the process of pose refinement - making use of the results obtained from pose estimation. The model refinement and affine point matching are only necessary if the sub-component is shaped, degraded, or oriented such that the simplifying assumption of a rectangular model is violated.

The modules, such as model database, image pre-processing, feature extraction have been already described in detail in previous papers [2, 3, 8]. The model-database is constructed off-line and we employ an indexing technique called *eigen-indexing* which is described in the next Section. The image pre-processing module uses non-linear histogram stretching to expand the range of the pixel intensities of the image over the entire available range of intensities. The feature extraction module partitions the image into segments, where our basic segmentation method is a local peak picking process on the image histogram after texture analysis.
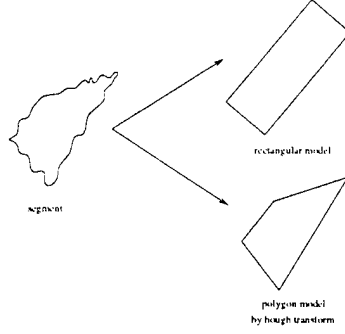
Figure 4: The polygon model Vs. the rectangular model

The model representation we are using includes rectangular models [2, 3, 8] and a newly developed polygon model. To extract the rectangular model for each segment, the centroid and central moments of each segment is calculated. From these moments, we derive the principal axes of the region. We use these two principal axes to represent the best fit rectangle. This set of rectangles is used as a model representation of the satellite if the segment is long and slim. Otherwise the polygon model is employed. Figure 4 shows the differences between the rectangular model and the polygon model.

The polygon model is constructed by using a *Hough Transform*. The Hough transform is a technique which can be used to isolate features of a particular shape within an image. In our case, since the satellite panel has a polygonal shape, we are using the Hough Transform to detect straight line edges.
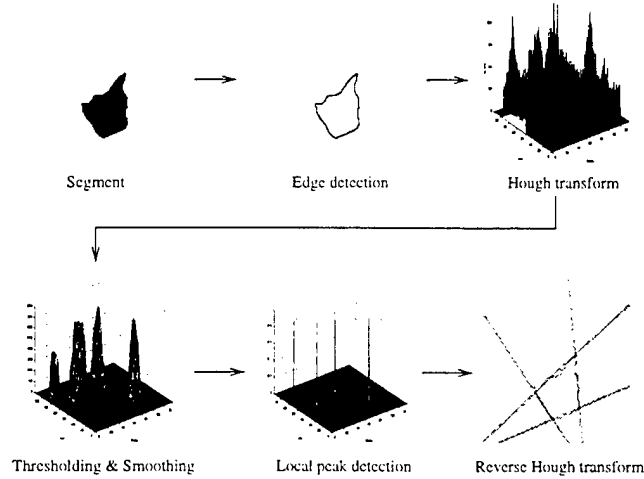
Figure 5: Polygon Model by Hough Transform

Figure 5 shows the process of extracting the polygon model by using Hough Transforms. First, the edge pixels are obtained by using a contour detector. Note that the edge image may be noisy. Then, the transform is implemented by quantizing the Hough parameter space into finite intervals or accumulator cells, i.e., a multidimensional array. As the algorithm proceeds, each (x_i, y_i) on the edge image is transformed into a discretized (r, θ) curve and the accumulator cells which lie along this curve are incremented. Peaks in the accumulator array represent strong evidence that a corresponding straight line exists in the image. In the Figure 5, four such peaks are extracted and correspond to the four lines in the image plane which can be obtained by using a reverse Hough Transform. In this case, the polygonal model is a better representation of the satellite segment than a rectangular model.

Pose Estimation

142

As mentioned earlier, the pose estimation module determines the rough pose of the satellite. The rough pose should tell us 1) how many components are presented in the image, 2) how these components are organized, and 3) roughly how the components are oriented.

Feature-based model matching is a conventional method for 3-D object recognition and can be used to find the satellite's rough pose. Each entry in the model database corresponds to a particular pose of the satellite, and features extracted from the image are matched with those of the model in the database. The best match tells us the rough pose of the satellite. However this is a graph matching problem and is known to be NP-complete. Thus, model matching across the whole model database is computationally expensive.

To circumvent this problem, a number of indexing techniques have been proposed. [6, 5] The basic idea is to associate a numerical key with each model in the database, and find the matching candidates by comparing the key for the feature representation of the image with the key of each model in the database.

Because each model in the model database corresponds to a particular pose of the satellite, in order to apply this indexing idea to our pose estimation problem we need to find some viewpoint dependent features. Such features will, hopefully, uniquely characterize the model for a given viewpoint. The most obvious feature is the number of geometric primitives (rectangles). Other features, such as the areas of the rectangles and the distances between these rectangles, are also good viewpoint dependent variables.

Based on these arguments, we define a N-by-N matrix where N is equal to the number of rectangles in the model. The entry (i, i) is equal to $\frac{a_i}{a_{max}}$, where a_i is the area of the ith surface and a_{max} is the area of the rectangle with the largest surface area in the model. The entry (i, j) is equal to $1 - (\frac{d_{ij}}{d_{max}})^2$, where d_{ij} is the distance between the center of the ith rectangle and the center of the jth rectangle and d_{max} is the maximum distance between any pair of the rectangles. Thus entry (i, j) approaches 0 if the ith rectangle and the jth rectangle are far away from each other and approaches to 1 if they are close to each other. Consequently, the off-diagonal elements of the matrix encode adjacency information of the rectangles in the model.

Eigenvalues as Feature Set

After the primitive matrix is constructed, the eigenvalues of this matrix is computed as our feature set. The use of eigenvalues and eigenvectors has also been employed in other computer vision applications like face recognition and edge detection. We choose eigenvalues as our features for the following three reasons:

1. **Spectrum representation of the graph.** In graph theory, the eigenvalues of the adjacency matrix of the graph are also known as the spectrum of the graph. It has been shown in [1] that various important graph characteristics can be captured in the spectrum.

2. **Permutation invariance.** We note that the eigenvalues are *permutation invariant*. In other words, the eigenvalues are invariant with respect to ordering of primitives, i.e., the ordering of the rows and columns of the primitive matrix. This property is very useful because it allows us to perform a gross comparison between two objects without solving the computationally expensive correspondence problem between the primitive sets of the two objects.

3. **Lipschitz property.** Denote the characteristic polynomial of a matrix $A \in M_n$ as $p_A(t)$. Then the n zeros of this polynomial of degree $n > 1$ will depend continuously upon the coefficients. Consequently, satellite poses that are visually similar also have eigen-indices that are numerically close.

The Lipshitz property of the eigen-index can be [4] most readily proved using complex analysis. For a polynomial with complex coefficients

$$p(x) = a_n x^n + a_{n-1} x^{n-1} + ... + a_1 x + a_0, a_n \neq 0, \tag{1}$$

where $n \geq 1$, given any $\epsilon > 0$, there exists a $\delta > 0$ so that for any polynomial

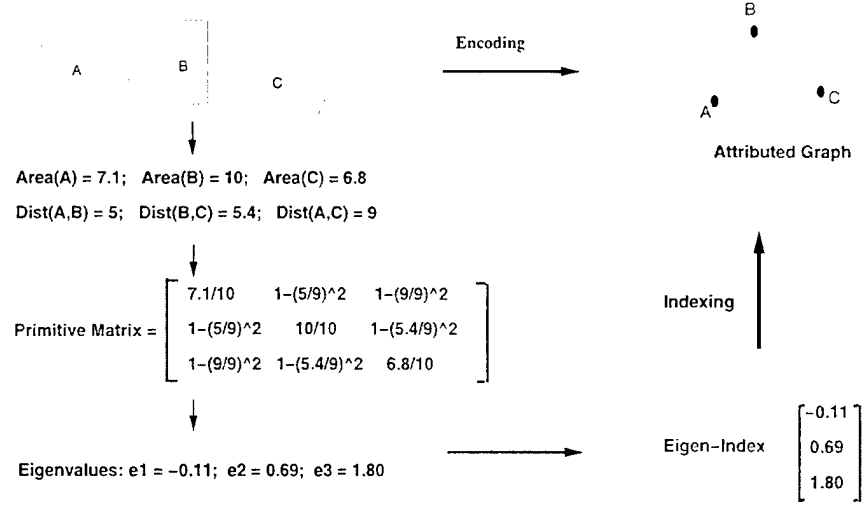$$q(x) = b_n x^n + b_{n-1} x^{n-1} + ... + b_1 x + b_0 \tag{2}$$

Figure 6: Procedure to form eigen-index

which satisfies $b_n \neq 0$ and

$$\max_{0 \leq i \leq n} |a_i - b_i| < \delta, \tag{3}$$

we have

$$\max_{0 \leq j \leq n} |\lambda_j - \mu_j| < \epsilon \tag{4}$$

where $\lambda_1, ..., \lambda_n$ are the zeros of $p(x)$ and $\mu_1, ..., \mu_n$ are the zeros of $q(x)$ in the same order. For example, both are arranged in descending order.

This implies the zeros of a polynomial is continuous with respect to the coefficients. The zeros will not change abruptly if the changes in the coefficients are small enough. Using the fact that the zeros of the characteristic polynomial $P_A(t)$ are the eigenvalues of A and the coefficients of $P_A(t)$ are continuous functions of the entries of matrix A, we can reach the conclusion that the eigenvalues of a square matrix are continuous with respect to the entries of the matrix.

Among the entries of our primitive matrix, the area a_i is continuous as the satellite change its pose slowly. That is, small changes in the satellite pose results in a small change in the a_i. And with the continuity of each a_i, it is not hard to show that a_{max} is continuous. This argument is also true as for d_{ij} and d_{max}. Thus, all the entries of our primitive matrix are continuous. Consequently, the eigenvalues are continuous or Lipschitz. This property also implies that two similar primitive matrices have similar eigenvalues.

Eigen-indexing

The discussion on the eigenvalue properties above shows that the eigenvalues or eigenvector is a good feature set to use in representing the satellite. Now we discuss how we use these eigenvalues as an index key in the matching process.

We calculate the eigenvalues of the primitive matrix and store them in a vector in ascending order. As mentioned before the resulting ordered eigenvalue vector is permutation invariant, i.e., it is not affected by the ordering used to construct the primitive matrix. This vector is used as the index key to this particular model. These procedures are demonstrated in Figure 6.

The eigen-indexing process is completed by calculating the Euclidean distance between the index of the model-representation of the image and those of the models in the model-database and choosing the model with the smallest distance. For two indices with different dimensions, the index with the smaller dimension is zero padded to make

the dimensions equal. Effectively, we assume that the indices with missing dimensions are projections of those with larger dimensions, as would occur with occluded sub-components.

Pose Refinement

The pose refinement module determines the 3-D orientation vector of each component of a satellite, namely the body and sub-components of the satellite. To do so we need to use the rough pose information extracted from the pose estimation module which tells us how many components are present in the image, and roughly how these components are organized. The pose refinement module then 1) identifies each of these components, 2) discriminates the major and minor principal axis of each component, and 3) calculates the 3-D orientation of each component.

To identify each satellite component, we use a simple technique based on moment calculation. Because each component is represented by a rectangle, the question now becomes which rectangle represents the body and which represent the sub-components. To identify the body, we use the fact that the body typically is in the center of the other components. We calculate the centroid of the satellite by taking the average of the areas of all the rectangles and calculate the distance between this centroid and the center of each rectangle. The rectangle which represents the body is selected by the shortest distance. The remaining rectangles are thus sub-components. From these sub-components we further find the sub-component which has least occlusion by choosing the rectangle with the largest area. This least occluded sub-component is used to calculate the orientation vector of the collective sub-components.

Affine-invariant Point Matching

After the components are identified we use affine point matching to refine the 3-D pose of each component. Affine-invariant matching [7] is an appropriate technique for recognizing flat or nearly flat objects in a 2D perspective projection image. This technique assumes that: model(s) of object are known in advance; objects in a scene may overlap and/or may be partially occluded; points-of-interest *on a plane* can be located; and object depth variations in the plane are relatively small. Fortunately, SOI data satisfies these assumptions in most cases.

Under these assumptions, perspective projection is well approximated by a parallel projection with a scale factor, so two different images of the same flat object are in affine correspondence. Hence, there is a non-singular 2×2 matrix $\mathbf{A}$ and a translation vector, $\mathbf{b}$, such that each point, x, in one image is translated to $\mathbf{A}x + \mathbf{b}$.

Model:
a = A(c11 - c00) + B(c01-c00) + c00

IMAGE:
Ta = A(T(c11-c00)) + B(T(c01-c00)) + T(c00)
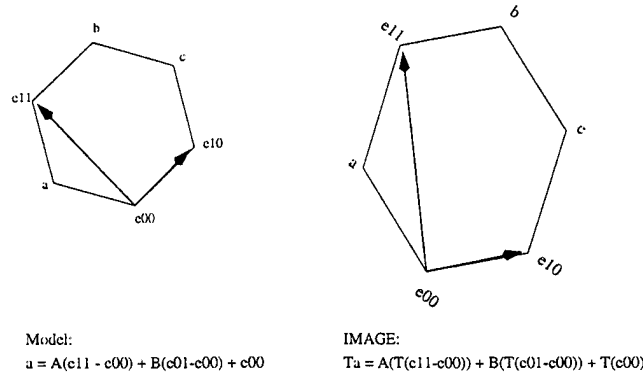
Figure 7: A simple example of an affine transformation.

Interest points can be selected at polyhedral vertices or at points of sharp convexities. Any three interest points on a plane form a *basis set* for the description (transformation) of the remaining interest points on the same plane. The problem then becomes to match, in the face of noise, a particular basis set with all of the corresponding points of the model. As shown in Figure 7, in a transformed image the interest points expressed in terms of an affine basis have the same affine coordinates. In some of the literature, this techniques is referred to as geometric hashing.

The algorithm we use for Geometric Hashing is as follows:

1. build affine coordinate database off-line,

2. extract interest points from input image,

3. using 3 interest points as a basis function, transform other interest points in scene to affine coordinates (H(coord) = (object, basis)),

4. vote for (object,basis) pairs,

5. if one (object,basis) has sufficient votes, continue, else try new basis (return to 3),

6. find best least-square match (to ameliorate noise and occlusion effects),

7. verify object edges
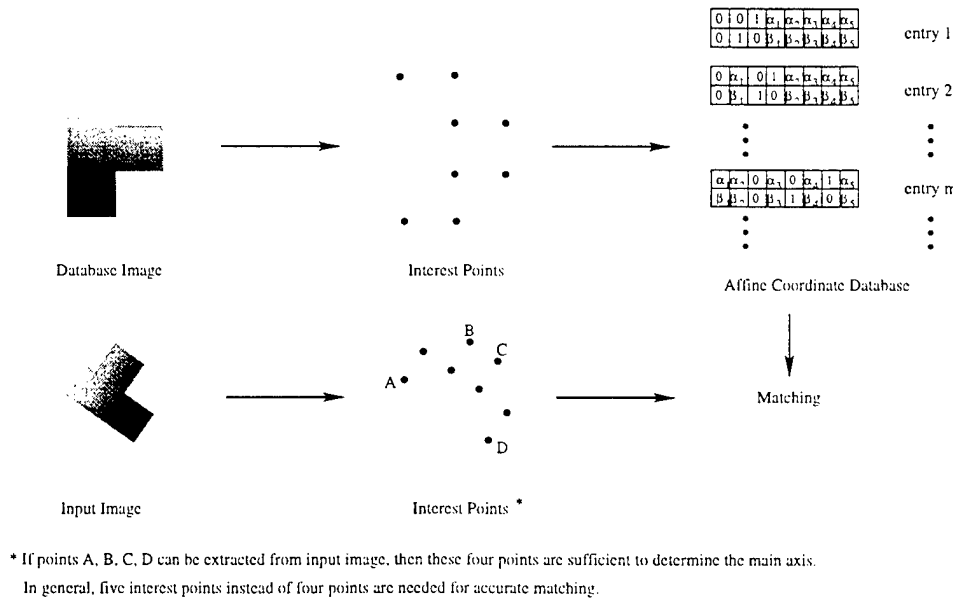
Figure 8: Matching procedure for GORZ image.

For an example GORZ image, the procedure is shown graphically in Figure 8. We observe in this case, as is true for many satellites, that occlusion of both panels will never occur because the two panels of the GORZ satellite are parallel and at least one panel is always visible. This implies that we can reduce the number of interest points in the database since redundancy is not required for occluded panel matching. In general the more points in the database, the more accurate the matching results. In the extreme, if we include all the points on each edge as interest points, then we will have a database with a full description of each boundary. In such cases, even if severe occlusion occurs in the input image, we will still have sufficient information to provide an accurate match. However, in realistic implementations, such a complete representation is computationally prohibitive.

As the number of points retained in the database are reduced, perhaps only keeping the polyhedral vertices of the boundary, the computation costs will drop significantly while the possibility of error increases. However, we observe that for degraded imagery, excess points in the database can actually result in an unexpected error.

As shown in the Figure 9, for a blurred panel image ($\sigma^2 = 20$), no matching error results when using a six-point database. However, a 90 degree error can occur when using an eight-point database. The only difference in the two examples is that the two interest points located at boundary concavities are not included in the 6-point database. It
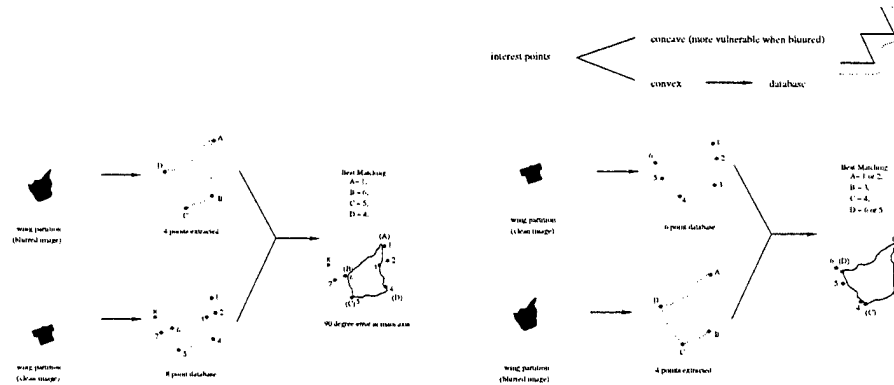
Figure 9: Comparison of matching accuracy.

is easy to show that the concave points are more vulnerable to blurring, and are consequently hard to extract from the input image. Furthermore, the redundant concave points interfere with other points in the database in certain circumstances. Thus, for our system implementation, we use only convex points as interest points, and our results indicate that no matching errors are found for the blurred images we have tested.

We note that while geometric hashing is used to calculate the orientation of the panel of GORZ satellite, the simple rectangular model can still used for many other satellites. This observation is based on the fact that we can always discriminate GORZ, or similar satellite images (having complex sub-component geometries) from others at the pose estimation phase due to the construction of the primitive matrix. The primitive matrix relies on the segment area and the centroid distance rather than the shape of the segment. Consequently, our system is able to implement different pose refinement schemes according to the satellite identity provided by the pose estimation module.

Pose Estimation of a complex satellite

In this section, we discuss pose estimation of images that are hard to partition. The methods discussed before are dependent on the assumption that all the satellite sub-components can be reasonably well partitioned, and thus isolated for analysis. However, some satellite images are hard to segment because the complexity of the satellite structure. Figure 10 shows the image of one such satellite, the OCNR satellite.
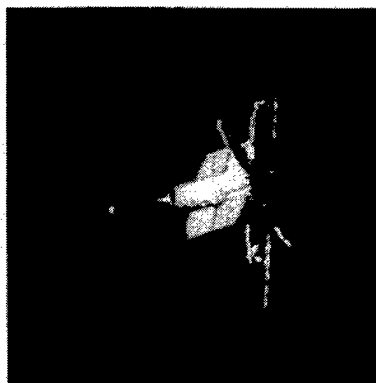
Figure 10: An OCNR image

Satellites like the OCNR have characteristics that make more conventional processing problematic - namely very few "flat" sub-component surfaces that can be isolated and analyzed using, e.g., texture analysis and nominal affine matching. We observe that satellites like this are optically "stealthy". This is NOT because they offer a reduced signature, but - to the contrary - they offer a veritable wealth of detail (due to scintillations and other such

147

phenomena) which is extremely difficult to automatically resolve and register if the pose is altered even slightly. A simplistic explanation of the origin of this problem is that the bright spots can shift considerably across even small aspect changes.

In order to aggressively attack the most challenging satellite images, such as OCNR, we have been experimenting with a new method which employs edge detection, clustering, and affine transforms.

The clustering method we are now using is a random sampling of the edge-map produced from the (robust) edge-detection that is produced from our edge-detection algorithm. The resultant clusters form a rough sketch of the input image. The sketch is used as a set of possible interest points in the affine point matching process.
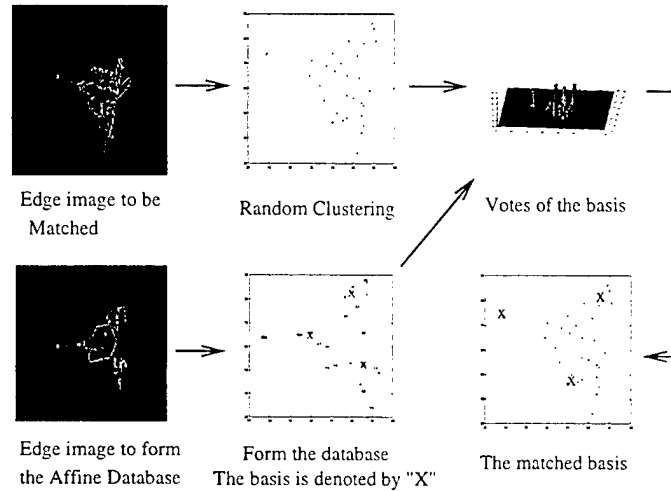
Figure 11: A 32 interest-point matching example.

Figure 11 shows the matching process for this new method. Instead of partitioning, we just perform a common edge detection to obtain the edge images. Then we randomly pick 32 points from the edge point set. The affine point matching is the same as before - we count the votes to determine the matched basis. The result shows a rational pose change between the two images.

We hope that this technique can also be of some benefit when the system is called upon to perform pose estimation of unknown satellites. Since no prior geometric information will be available, an accurate absolute pose is impossible to obtain in theory. However, using this new approach, we can at least calculate the relative pose change to one reference image. Additionally, the relative pose change can be used to predict the movement of the unknown satellite.

System performance

By studying measured satellite images we find that image distortion which is due to seeing and telescope diffraction is more prominent than sensor noise. Thus, for the tests we report here we vary seeing conditions and telescope diffraction to determine the affects on the orientation vector estimation. The image distortion due to seeing and telescope diffraction can be characterized by a point spread function (PSF). In the following test, a Gaussian mask is used to blur the synthetic images to obtain distorted images. We use the clean images to form the model database and the blurred images to test how image distortion affects the pose estimation and pose refinement.

Evaluation of Matching Accuracy

First we evaluate the matching performance on pristine synthetic HST images. The experimental procedure is as follows:

- construct the model-database by using a set of clean images, each of which corresponds to a particular pose of the HST satellite.

- blur the clean images with a blurring mask to form a set of distorted images which are used as testing images.

- apply the testing image to the pose estimation module and find a model in the model-database.

- generate the confusion matrix.

Figure 12 shows how the synthetic HST image is distorted by a Gaussian blurring mask with $\sigma^2 = 20$.

Clean synthetic HST image   Blurred with $\sigma^2 = 20$
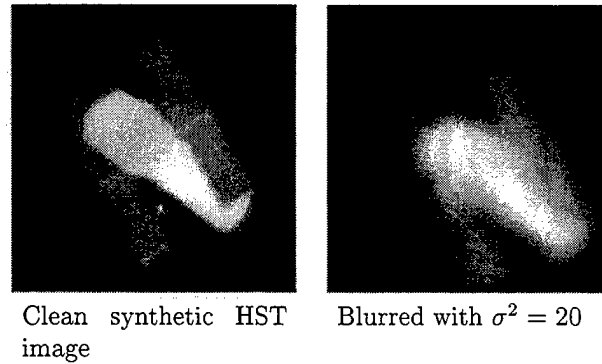
Figure 12: Comparison of clean and blurred synthetic HST images

Evaluation of Pose Refinement

We have also studied how image distortion affects the final orientation vector estimation. The experimental procedure is as follows:

- construct the model-database by using a set of clean images, each of which corresponds to a particular pose of a satellite.

- calculate the orientation vector via the pose refinement module for each model in the database.

- blur the clean images with a blurring mask to form a set of distorted images which are used as testing images.

- apply the testing image to the pose estimation module and find a model in the model-database.

- do model matching to find the feature correspondence between the model of the testing image and the model from the model database.

- use pose refinement module to find the orientation vector.

- compare this vector with the ground-truth vector, which we know because we know the image from which the distorted image originated.

Figure 13 shows the RMSE of the estimated orientation vector verses σ^2 for the four different angles of the satellite components, namely, (θ, α) of the body and (θ, α) of the solar panel. For this figure, the performance is averaged across 4 satellites using a total of 226 images.

Conclusions

We have developed a 3-D orientation vector estimation system for Space Object Imagery. This system uses model-based techniques to realize orientation vectors for major satellite sub-components by employing a two-step approach: pose estimation and pose refinement.

Our tests show that the overall system performance is reasonably robust. Of course, further testing and development is needed, in particular considering a larger database of measured images, more sophisticated noise models, and multiple-frame data.
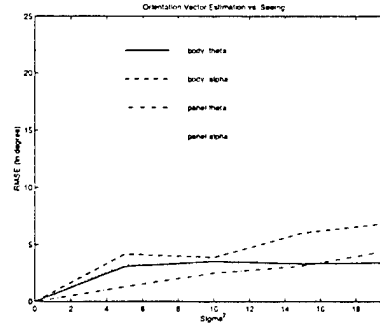
Figure 13: Performance of the orientation estimation at varying σ^2 levels

References

[1] D.M. Cvetkovic, M. Doob, and H.Sachs. *Spectra of Graphs*. New York: Academic Press, 1979.

[2] Xun Du, Stanley C. Ahalt, and Bruce Stribling. 3-D Orientation Vector Estimation for Sub-Components of Space Object Imagery. In *Proceedings of the 1997 MIT/LL Space Control Conference*, volume 1, pages 110 – 128, Lexington, MA, March 1997.

[3] Xun Du, Stanley C. Ahalt, and Bruce Stribling. 3-D Orientation Vector Estimation for Sub-Components of Space Object Imagery. In *Proceedings of the 1997 Signal Processing, Sensor Fusion, and Target Recognition Conference*, pages 395–405, Orlando, FLA, April 1997.

[4] R. A. Horn and C. A. Johnson. *Matrix Analysis*, pages 539–540. Cambridge University Press, Cambridge, England, 1985.

[5] K. Sengupta. *Object Recognition Using Large Modelbases*. PhD thesis, The Ohio State University, March 1996.

[6] H. Sossa and R. Horaud. Model indexing: The graph-hashing approach. *Proc. of Computer Vision and Pattern Recognition*, pages 811–814, 1992.

[7] H.J. Wolfson. Model-based object recognition by geometric hashing. *Computer Vision, ECCV90*, pages 526–536, 1990.

[8] J. Zhao, S. C. Ahalt, and B. E. Stribling. 3-D orientation vector estimation from satellite imagery. In *Proceedings of the 1996 SPIE conference on Applications and Science of Artificial Neural Networks V*, volume 2755, pages 472–483, Orlando, FL, April 1996.

Improvements to the MIT Radar Calibration System (MRCS) at the FPS-85

Anthea J. Coster, Karl P. Buchmann, Lorraine E. Thornton, and E. M. Gaposchkin
MIT Lincoln Laboratory

ABSTRACT

The MIT Radar Calibration System (MRCS) was developed by MIT/LL in 1991 and installed at the FPS-85 radar on Eglin AFB in March 1994. It has been operating successfully at the radar since that time. The MRCS was the first system to use the Global Positioning System (GPS) for real-time ionospheric monitoring. The MRCS has three major functions: the calculation of atmospheric corrections for use in the real-time satellite tracking program; the provision of a quick-look calibration capability which enables an operator to assess sensor performance in near real-time; and the computation of sensor calibration coefficients using a software sensor model. This paper will provide examples of how the MRCS has aided in the detection of software and hardware problems at the FPS-85. In addition, selected operational capabilities of the MRCS will be presented.

Current improvements to the MRCS include the procurement of hardware spares for enhanced reliability, the replacement of obsolete equipment with more dependable hardware, and the development, testing, and delivery of a new version of the MRCS code by MIT/LL. This last item features year 2000 compliance, new Kalman filter algorithms for ionospheric modeling, and enhancements to the system's graphics and stand-alone operation.

1.0 INTRODUCTION

This paper will describe the planned upgrades to the MIT Radar Calibration System (MRCS). The MRCS was developed by MIT Lincoln Laboratory in 1991 and installed at the AN/FPS-85 radar on Eglin AFB in March 1994. The AN/FPS-85 radar is situated on Eglin Air Force base, located on the panhandle of Florida. The FPS-85 is a phased array radar, operating at UHF frequency (442 MHz), and is used primarily for near earth space surveillance. It is capable of detection and simultaneous track on multiple satellites in low earth orbit (LEO) and deep space. Azimuth, elevation, range, and range rate observations are provided by the FPS-85 on those tracks. The primary function of the MRCS is to ensure that the FPS-85 observations are of consistent high quality and accuracy.

The MRCS was the first calibration system to use the Global Positioning System (GPS) for real-time ionospheric monitoring. This paper will provide examples of how the MRCS has aided in the detection of software and hardware problems at the FPS-85. In addition, selected operational capabilities of the MRCS will be presented.

On-going improvements to the MRCS include the procurement of hardware spares for enhanced reliability, the replacement of obsolete equipment with more dependable hardware, and the development, testing, and delivery of a new version of the MRCS code by MIT/LL. This last item features year 2000 compliance, refined algorithms for ionospheric modeling, and enhancements to the system's graphics and stand-alone operation.

The next section of this paper will provide the background material for understanding the MRCS as it now exists. This includes a description of the elements of a metric data calibration system and a brief discussion of the Improved Radar Calibration System (IRCS), which the MRCS replaced. Following this, the developmental history of the MRCS at the FPS-85, up to its present

incarnation, is discussed. The component functions of the MRCS are then described in greater detail. Next, an example of the utility of the MRCS in diagnosing large-scale problems in the FPS-85 metric data is presented. The current upgrades to the MRCS are described, and, finally, suggestions for future enhancements, and the motivations behind them, are briefly considered. The paper is summarized in the last section.

2.0 BACKGROUND

2.1 Metric Data Calibration

The objective of radar metric calibration is to make a sensor's observations as accurate as possible. Every sensor has bounds on its accuracy due to physical limitations of its tracking hardware. In theory, proper modeling of the system biases inherent to the sensor can enable that sensor's observations to approach the physical limits of its accuracy. The system biases must be monitored continuously because they can change over time due to alterations or failures in the hardware or software.

A standard method of calibrating a sensor is to develop models that can be tuned to remove any biases observed in the radar tracking data. In order to determine these biases, however, a source of accepted truth must be available for comparison. Given a precision orbit for a resident space object, the sensor can track that particular object and a comparison can be made between the radar observations and the high-quality orbit. The results of this comparison are metric residuals. Residuals collected over a reasonable time span can be used to build a model for a given sensor. Subsequent residuals can be used as input to that model. When performed carefully and properly, the radar system biases can be all but eliminated by modeling in this manner, down to the limits of the sensor's accuracy.

Real time corrections for both atmospheric delays and the effects of atmospheric refraction are another important component to successful metric calibration. By observing the refraction in transit through the atmosphere of dual-frequency electromagnetic signals, the total electron content (TEC) of the ionosphere can be measured. Using this information, a map of the TEC around a radar site can be generated, and, from this map, ionospheric corrections for radar observations can be provided in real-time. Further improvement to accuracy can be achieved for very low elevation angles by measuring certain meteorological values (pressure, temperature, and humidity) and computing the refraction due to the troposphere.

The final element of metric data calibration is the provision of a quick-look ability that enables an operator to see in near real time how the sensor is performing subsequent to tracking a specific calibration target. This allows the radar personnel to rapidly assess the effects of system changes such as hardware modifications or updates to the sensor model biases.

In summary, the components required in any system to perform proper metric data calibration include both the software and hardware necessary to perform the following tasks:

1) The calculation of the atmospheric refraction corrections for the real time satellite tracking program;

2) the provision of a metric quick-look ability; and,

3) the computation of sensor calibration coefficients using a sensor model program.

Both the MRCS, and the original IRCS, have these elements in their design.

2.2 Improved Radar Calibration System (IRCS)

In the mid-1980s, the MITRE Corporation installed the Improved Radar Calibration System, or IRCS, at the FPS-85. The IRCS was designed as a complete calibration system, supplying not only estimates of the delay due to the ionosphere, but also providing both a sensor model and quick-look capabilities. In reality, due to lack of adequate initial testing on site, the sensor model provided with the original system never worked.

The IRCS utilized the constellation of Navy TRANSIT satellites. These satellites broadcast at two UHF frequencies, allowing estimation of the TEC around the FPS-85 site. Typically only one TRANSIT satellite was in view at a time. In addition, each TRANSIT satellite broadcast its ephemeris, and final precision orbits on these satellites were available on a weekly basis from the Defense Mapping Agency. Thus a source of truth was available with which the FPS-85 could compare metric tracks of the TRANSIT satellites, both in a quick-look fashion and in post-processing.

The IRCS sensor model was debugged, modified, and then ported to a personal computer by Lincoln Laboratory staff (Gaposchkin, 1997) near the end of the 1980s. As input to the model, personnel at the MIT/LL Millstone Hill Radar provided satellite residuals derived from precision orbits on specific LEO and MEO laser calibration spheres. These calibration spheres are tracked by a worldwide network of NASA-run laser tracking stations which provide very high precision ranging data. These ranging observations, and radar tracks of these targets, are input into the orbit computation program, DYNAMO, at Millstone. By running DYNAMO with these observations as input, orbits are produced that are precise, generally, to within 30 cm in each X-Y-Z coordinate. Residuals generated by comparing FPS-85 observations to these orbits provide a high fidelity input to the sensor model.

Thus, the elements necessary for radar metric calibration existed at the FPS-85 in the late 1980s. However, by the early 1990s, the IRCS was experiencing difficulties. The most pressing of which was the planned decommissioning of the TRANSIT satellites, which finally occurred in January 1997. Without the TRANSIT constellation, the IRCS would be completely inoperative. Furthermore, the HP1000 workstation on which the IRCS was built was becoming increasingly difficult to maintain. For example, a disk failure in mid-June of 1993 disabled the IRCS for eight weeks.

Though the FPS-85 had a fairly simplistic ionospheric model on which to depend, it was clear that a more reliable and comprehensive method of calibrating the radar was necessary. MIT/LL personnel developed a proposal for the MIT Radar Calibration System, or MRCS, which would include and supersede all of the functionality of the IRCS. The MRCS would utilize the Global Positioning System (GPS) for real-time ionospheric modeling and would incorporate the sensor bias model. Work on the MRCS was begun in 1992.

3.0   M.I.T. RADAR CALIBRATION SYSTEM (MRCS)

3.1 History of the MRCS

In March 1991, the GPS Real-time Ionospheric Modeling System, or GRIMS, was integrated into the tracking software at the Millstone Hill radar (Coster, et al., 1992). The GRIMS used a TI4100 GPS receiver, which was capable of tracking up to four satellites at a time, as the source for dual

153

frequency signal delay measurements. GPS broadcasts at two frequencies, L1 (1575.42 MHz) and L2 (1227.6 MHz). By computing the difference in delay between the L1 and L2 signals, the ionospheric refraction component can be calculated along the line of site to the particular GPS satellite being tracked.

At any given time, the delay measurements for the GPS satellites in view would be input into a Kalman filter in the GRIMS software. The Kalman filter then predicted the coefficients of a simple model of the Total Electron Content (TEC) around the site. The advantage to this model was that it preserved the azimuth, elevation, and time information available in the GPS signal. For any observation made by the Millstone Hill radar at a given azimuth, elevation, and range, the model would compute a ionospheric correction in real time.

When the MRCS was being developed, the experience MIT/LL personnel had with the GRIMS proved invaluable. The core of the MRCS ionospheric correction model came directly from the tried and tested GRIMS. The GRIMS also contributed algorithms for communicating with a GPS receiver that did not require user intervention. When adapted to the MRCS, these routines enabled a largely stand-alone system (Coster, et al., 1994).

Work on the MRCS began in early 1992. Several GPS receivers were researched, and the Allen Osborne Associates (AOA) Turbo Rogue SNR-8100 was finally chosen. The SNR-8100 was capable of tracking up to eight GPS satellites at one time, and was also able to operate under Selective Availability (SA) and Anti-Spoofing (AS). SA and AS are methods used by the Department of Defense to degrade the precision of GPS positioning measurements and to encrypt the signals for non-military users, respectively. The TI4100 would not have been able to track any satellites implementing AS.

The other central piece of hardware for the MRCS was the workstation platform on which it would reside. A new system, at the time, was chosen: the Digital Equipment Corporation (DEC) Alpha 3000/400. The Alpha architecture had only recently been introduced, and promised a relatively fast processing speed for a reasonable amount of money. All peripherals would be commercial, off-the-shelf (COTS) products.

The operating system selected was UNIX. Other than two commercially purchased programs, Visual Numerics PV-Wave, and Empress Software's Empress Relational Database, the MRCS software was adapted from already existing code or written from scratch in the languages C and FORTRAN by Lincoln personnel.

Due to a software rehost in progress during the MRCS development, all changes were frozen out of the tracking system at the FPS-85. This placed the constraint on the MRCS that it had to use the pre-existing IRCS format for communicating with the FPS-85 tracking computer. This meant that the MRCS had to adopt the IRCS TEC map format. The TEC map is a rectangular, latitude/longitude grid representing the ionospheric TEC over the site.

In addition, the only media available for data transfer between the FPS-85 tracking system and the MRCS were 9-track tapes. Given a choice, Lincoln personnel would have selected to use another tape medium, such as 8mm, or, preferably, a direct serial connection to the tracking system.

With these constraints, the MIT Radar Calibration System was built from the foundation of the GRIMS. The system was installed in March 1994, and has been in successful operation since that

time. All elements of the IRCS were duplicated in a format that was transparent to the tracking system.

3.2 Elements of the MRCS

The MRCS implements the three major functional elements described earlier in the metric calibration section. The first component is the calculation of the atmospheric refraction corrections. As discussed above, the MRCS utilizes an AOA Turbo Rogue SNR-8100 GPS receiver to provide the data necessary to calculate ionospheric refraction. By differencing the dual frequency precise positioning signals from up to eight satellites in view, the MRCS is able to compute a real-time model of the ionosphere above and around the FPS-85. This model is translated into the IRCS TEC map format. At twenty minute intervals during tracking, the FPS-85 tracking system will request a TEC map from the MRCS.

Should the GPS receiver become inoperative for any reason, the MRCS provides a backup ionospheric model in software. This model, the Bent model, (Bent, 1976), was also incorporated into the FPS-85 tracking system by Lincoln personnel. Should the MRCS workstation go off-line for any reason, the Bent model is available as a degraded mode solution for ionospheric correction.

The second component of metric data calibration that MRCS provides is a metric quick-look capability. Predicted metric observations are computed at Millstone by Lincoln personnel, and sent on a weekly basis via electronic mail to the MRCS operator at the FPS-85. These predictions, calculated for certain spheres, are transferred to 9-track tape for input into the MRCS. Immediately after a track is performed on one of these targets, the tracking system observations are conveyed to tape and onto the calibration system. The program CALIB, on the MRCS, then compares the tracked observations to the predicted observations. The MRCS operator is thus able to ascertain, minutes after a track, the state of the FPS-85 metric calibration. This capability is especially useful to determine the state of the tracking system after a hardware or software change. A print-out of the track residuals, as well as a graphical plot, is available for reference and archival.

The final component of the metric data calibration that the MRCS provides is the ability to re-compute the sensor model coefficients using data input to the system. Millstone personnel provide weekly, along with the predicted observations, post-fit residuals on tracks performed in the previous week at the FPS-85. These residuals are read into the MRCS also using the 9-track. After a number of weeks, at the MRCS operator's discretion, the post-fit residuals are used by the sensor model program to generate a set of corrections for the sensor model bias coefficients. Again using 9-track, these corrections are transferred to the tracking system to update the master bias file.

The unique feature of the MRCS is that it is the first, and currently only, system to combine all these functions in one package using GPS for the real-time ionospheric refraction correction. What sets the MRCS further apart is that it has an easy-to-learn graphical user interface (GUI). With only a few mouse clicks, the MRCS operator has access to all of the above utilities. The main MRCS screen also displays important information about the status of the GPS receiver, and about the connection to the tracking system. Maintenance tasks, such as backups and database cleanup, are accessible from buttons on the GUI. The user interface is also password locked so that only authorized personnel can operate the system. The MRCS was designed from the ground up to be an integrated, turn-key system which handled all of the FPS-85 calibration tasks.

3.3 Utility of MRCS

There have been several instances where having a calibration system of the quality of the MRCS has enabled large-scale problems in the FPS-85 metric data to be easily diagnosed and fixed. For example, a 700 millisecond time bias was introduced to the FPS-85 timing when a leap second was applied on 31 December, 1995. Careful monitoring of the metric data calibration enabled this problem to be caught relatively quickly, as is evidenced in the Figure 1. The extremely large residuals in the middle of the plot are a direct consequence of the time bias that was introduced.
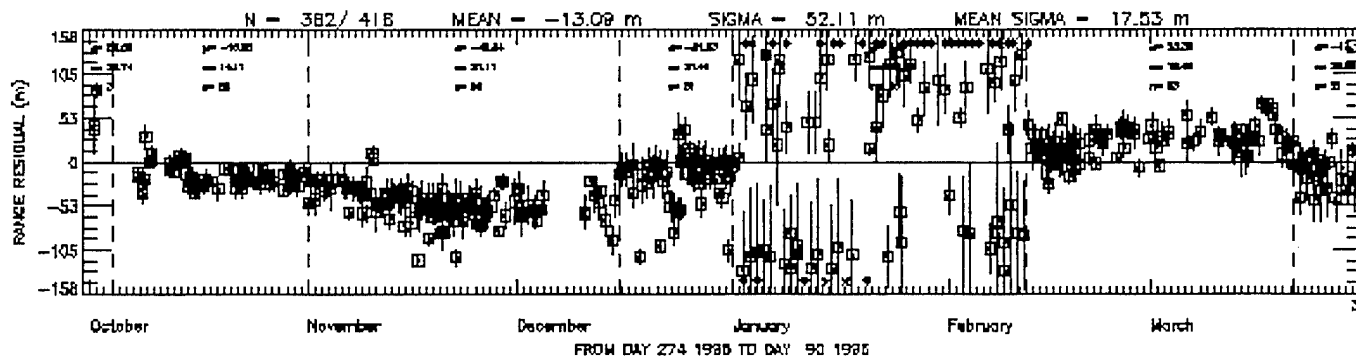

Figure 1. FPS-85 16908 Range residuals vs. Time

The FPS-85 is theoretically capable of range tracking at the zero mean, 15 meter standard deviation level. With the operation of the MRCS over the last three years, the FPS-85 is approaching a zero mean, 20 meter standard deviation level (Thornton, et al, 1997). With continued enhancement to the MRCS capabilities, and refinements to the manner in which they are used, Lincoln personnel believe that the theoretical calibration limit is within reach.

4.0 MRCS UPGRADES

4.1   Current Upgrades

MIT Lincoln Laboratory was recently funded to carry out upgrades to the FPS-85 MRCS that will take the system beyond the turn of the century. The upgrade process will focus on issues of increasing the maintainability of the MRCS, ensuring the prompt resumption of service in case of hardware failure, and bringing the MRCS code base up to compliance for handling the year 2000. In the completion of these main goals, several enhancements will be made to the MRCS software, including an improved Kalman filter ionospheric model, and augmentations to the graphical output capabilities of the system.

Maintainability is an area that concerns mainly the hardware of the MRCS. Spare peripherals were not funded in the original MRCS design. As a result, extended downtime has occurred on two occasions of disk drive failure. Additionally, the 9-track tape drive required repair in several different instances. To address these issues, each peripheral of the MRCS, two disk drives, an 8 mm tape drive, a printer, and a serial port extender, will be duplicated. Furthermore, the 9-track tape, which has been problematic, will be replaced using a 4 mm DAT drive. Data transfer to the tracking system will be accomplished through a personal computer attached to the tracking mainframe. Tracking data will be transferred to the PC over a direct connection. A 4 mm drive

connected to the PC will be used to create a file in the same format as the previous 9-track files, which can then be moved to the MRCS.

Year 2000 (Y2K) compliance is a serious matter as the final years of the current millennium approach. Software that is not able to handle dates in a proper manner is susceptible to errors on the changeover to January 1st, 2000. During the upgrades, the MRCS software will be checked for areas where date handling is not being properly performed. The UNIX operating system on the DEC Alpha workstation will be brought up to a version certified year 2000 compliant.

The year 2000 issue also affects GPS in the following ways. The first concern actually arrives in 1999. GPS system time is kept by counting the weeks from January 5, 1980. The system rolls over at 1024 weeks, which occurs on August 22, 1999. This is a well documented function of the GPS system, so manufacturers are expected to handle this rollover seamlessly. GPS receivers, as well as the main control center and the satellites' on-board software, must also handle the more well-publicized changeover to the year 2000.

The Air Force GPS Joint Program Office has established itself as the point of contact for GPS Y2K topics (Johnson, 1997). They have taken it upon themselves to test GPS receivers from various manufacturers to certify whether the hardware and firmware of these receivers can handle both of the above problems. As of yet, the Allen Osborne Turbo Rogue has not been tested. Before delivery of the MRCS upgrade to the FPS-85, this issue will be addressed.

Another future concern that needs to be addressed in the upgrade is a change in the format of predicted observations and post-fit residuals. Currently, Lincoln Laboratory personnel provide this data, which is used as input to the quick-look feature, and necessary for re-calibrating the sensor bias model coefficients. The requirement for generation of this data is being transferred to Cheyenne Mountain personnel. Kaman Sciences Corporation, with input from Lincoln, is developing new formats for this data. The MRCS must be able to correctly process these new formats in a fashion seamless to the operator. The MRCS will be equipped with the ability to process both the current data structures, and the upcoming structures.

The MRCS operator has reported several minor problems with the system in the three years since its installation. Requests have also been made for modifications that will add specific features. The upgraded MRCS software will incorporate these changes. In addition, in response to operator requests, the data analysis and output capabilities of MRCS will be expanded. The plotting capacity will be extended so that both quick-look residuals and post-fit residuals are available for analysis. The operator will be given control of the date span of the plotted residuals so that the state of the metric calibration in any time period, over any number of passes, can be better assessed.

The MRCS Kalman filter software has been steadily improved over the past three years (Gaposchkin, 1997). The code has been rewritten in the C++ language, where it was previously coded in FORTRAN. Different attributes of the filter have been modified to improve filter performance following loss of lock, in the presence of Anti-spoofing, and in response to other operational issues. In addition, the code to calculate the receiver specific satellite biases will be transferred to the FPS-85. It has been shown that these satellite biases should be calculated for each receiver on a monthly basis (Gaposchkin, 1997).

4.2 Future Upgrades

There are several additional upgrades that would be beneficial to incorporate into the MRCS, but that have not yet been funded. These proposed upgrades include the following:

- Procurement of an Ashtech Z12 for the GPS receiver (12 channel)
- Removal of the tape requirement, replaced by a direct connection to ES/9000
- Rehost of the MRCS software on an up-to-date workstation
- Addition of a weather station for tropospheric modeling
- Internet connection between MHR and MRCS for remote service
- Use of the MIT/LL circus tent model on ES/9000 instead of the IRCS TEC map.

The benefits of these different items are several. For example, Figure 2 shows the ionospheric delay – a value proportional to the TEC – calculated in the presence of Anti-spoofing by the Allen Osborne Turbo Rogue and the Ashtech Z12. As a result of a more sophisticated algorithm used to reconstruct the GPS signal in the presence of AS, the Ashtech Z12 receiver produces an ionospheric TEC correction subject to much less noise than the Turbo Rogue. From Figure 2, it is clear that the Ashtech Z12 pseudo-range data has considerably less noise than that of the AOA Turbo Rogue. In addition, the Ashtech Z12 GPS receiver can track 12 GPS satellites versus the 8 tracked by the older AOA Turbo Rogue receiver currently on site. The newer AOA Turbo Rogue receivers can also track 12 GPS satellites, but the algorithm they use for tracking in the presence of Anti-spoofing is the same. Furthermore, the purchase of an Ashtech Z12 receiver would allow the MRCS at the FPS-85 to remain compatible with the MRCS at Millstone. This would aide greatly in the swift diagnosis of system problems

Grp Delay: Ashtech Z12 vs. AOA Turbo Rogue Sat. 20361
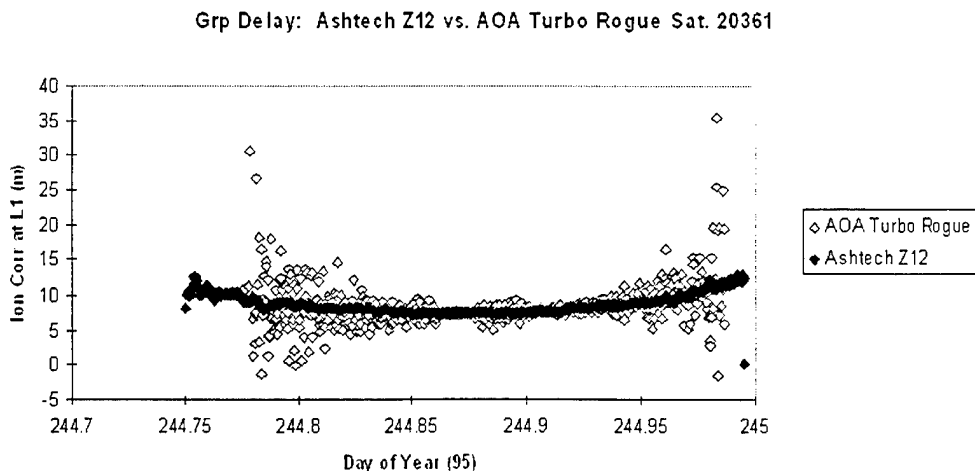
Figure 2. Comparison of the Ionospheric Correction at L1 determined by the Pseudo-Range data of the two different receivers: AOA Turbo Rogue and Ashtech Z12.

To ease the MRCS operator's load, a direct connection between the ES/9000 tracking computer and the MRCS would eliminate several steps in the frequent process of data transfer between the machines. Rehosting the MRCS software on an up-to-date computer system would facilitate future maintainability and would increase performance. The addition of a weather station for tropospheric modeling would allow for significantly better refraction estimates at low elevations

158

(less than 5 degrees). An Internet connection between the Millstone Hill Radar site and the MRCS at the FPS-85 would allow for seamless remote servicing and system trouble-shooting. Finally, the replacement of the IRCS TEC map on the ES/9000 with the circus tent model, the model native to the MRCS, would allow the site access to the full precision of the MRCS ionospheric representation.

5.0 SUMMARY

In summary, through a detailed study (Thornton, et al, 1997), and from operator comments, the MRCS has been shown to have performed very well at the FPS-85, providing reliable and improved calibration. MRCS was the first radar calibration system to utilize an operational real-time ionospheric monitoring system based on GPS. The current upgrades will focus on improving maintainability, ensuring Year 2000 compliance, and adding additional functionality. With these upgrades, and even more so with the implementation of the suggested enhancements, the MRCS will remain at the forefront of radar calibration systems.

6.0 REFERENCES

Bent, R. B., S. K. Llewellyn, G. Neterczuk, and P. E. Schmid, "The Development of a highly successful worldwide empirical ionospheric model and its use in certain aspects of space communications and world-wide total electron content investigations," in Effect of the Ionosphere on Space Systems and Communications, ed. By J. Goodman, NTIS, Springfield, VA, pp. 13-28, 1976.

Coster, A. J., E. M. Gaposchkin, and L. E. Thornton, " Real-Time Ionospheric Monitoring System Using GPS", (1992). Navigation: Journal of the Institute of Navigation, Vol. 39, No.2, Summer 1992.

Coster, A. J., , private communication, 1994.

Johnson, A., "GPS Rollover: Compliance Efforts Under Way," GPS World, p. 62-64, September 1997.

Gaposchkin, E. M. , private communication, 1997.

Thornton, L. E., private communication, 1997.

Near real-time speckle imaging for satellite object identification

Kathy Schulze [a], David Tyler [a], Bruce Stribling [b]

[a] Schafer Corporation, 2000 Randolph Street, Albuquerque, NM 87106
[b] Air Force Research Laboratory, 535 Lipoa Pkwy, Suite 200, Kihei, Maui, HI 96753

ABSTRACT

The main mission of the Maui Space Surveillance Complex (MSSC) is space surveillance, with a prime objective to identify foreign satellites and determine their mission and status. Images of earth-orbiting satellites acquired by ground-based telescopes are blurred by atmospheric turbulence. These blurring effects can be partially overcome by post-mission processing such as speckle imaging (SI). We have developed a parallel implementation of SI to dramatically reduce the time required to reduce satellite imaging data, allowing processed imagery to be transmitted to users within minutes of collection. We are also implementing a near real-time (NRT) SI image feedback capability using this parallel scheme. With NRT feedback, telescope operators can select observing parameters to optimize data quality *while the data is being taken*. NRT processing also allows easy selection of the best data from a long satellite pass for more intensive, post-mission processing (PMP). NRT image processing will yield higher quality data products and better utilization of observatory resources.

1. INTRODUCTION

Speckle imaging[1] techniques have long been used to remove atmospheric turbulence effects without adaptive optics. Observations at the MSSC earlier this decade proved the viability of this technique for high resolution satellite imaging.[2,3] Advances in computer hardware, parallel processing, and high-speed data transmission are allowing radical changes in the way these satellite observing missions occur. High speed transmission of raw data from the camera to a parallel processing system, very fast calibration and image recovery, and high-speed transmission of processed satellite imagery to a video display will allow MSSC operators to view recovered images in near real-time during the pass, within seconds of collection.

Using these images as a "quick-look" tool to adjust parameters such as camera exposure time and optical filter settings, operators can assess and optimize the quality of collected data *while the data is being taken*. Satellite orientation and brightness change rapidly during an observation and between passes of a ground station. If military objectives require, for example, rapid assessment of a new launch, continuous and correct updating of observing parameters can mean the difference between acquisition of high-resolution imagery during the first pass of a ground station and waiting for a subsequent pass. Further, with NRT feedback available during the observations, it's obvious to the operator which data has the best combination of seeing and object brightness conditions. This data can be tagged, easily extracted from even a very large ensemble of data, and reduced using more sophisticated and time-consuming methods than SI[4]. The availability of NRT processing thus means that potentially *all* data collected during a pass is taken using optimal observing parameters, and only the best of the data is used in computation and time-intensive processing.

In Section 2, we discuss current satellite imaging operations at the MSSC. In Section 3, we compare the time required for data reduction using serial and parallel implementations of an SI algorithm. In Section 4, we describe the GEMINI advanced instrumentation package and discuss in detail how rapid data reduction can be used to optimize observatory operations. In Section 5, we briefly describe the parallel SI implementation, and in Section 6, we describe how "supercomputer" power can be obtained for any telescope site, without a link to a supercomputing center. Conclusions are presented in Section 7.

2. CURRENT TELESCOPE OPERATIONS

Current satellite observing missions using SI require collection of camera calibration data, reference star data and object data. After collection, all data is copied from the acquisition system to the processing system for reduction. Until processing, there is no quantitative way to check data (calibration, reference star, or object) quality. Operators rely on video display of unprocessed raw data for subjective quality control and to ensure tracking. Camera exposure times and other parameters are selected based mostly on the operators' experience. If any of the calibration or reference star files are corrupt, or if collection parameters during observations were set in error, the collected data may be unusable or simply yield poor quality images upon processing. There is currently no way to know whether errors are present in calibration data until the data is archived and processing begins, typically after the observing session.

Since large amounts of data can be collected even for a single satellite pass, and conventional image processing methods can be quite slow when executed serially, only portions of the collected data are actually processed. While frame selection schemes[5] can be employed to pick manageable subsets of a larger file for processing according to some quality metric, the selection is usually done by randomly choosing small ensembles out of the large file. The probability of choosing ensembles where seeing and object brightness combine to produce atypically high-quality data is very small.

3. ACCELERATED PROCESSING WITH PARALLEL COMPUTING

We have implemented SI image recovery using the recursive bispectrum technique[6] and parallel processing on the Maui High Performance Computing Center (MHPCC) IBM SP2. The parallel implementation substantially reduces processing time and allows us to reduce all data from an observation session without using any frame selection. Table 1 shows processing times for 10 reference-star/object data pairs using both the serial and the optimized parallel implementations. The parallel implementation is executed on 15 SP2 processors. Ten was chosen as a typical number of satellite observations for a pair of terminator observing periods or one daylight period. Each of the 10 star data files contains 160 images of a calibration (reference) star for use with the SI algorithm. Each of the 10 object files represents a 3-minute satellite pass with 32 ms exposures, yielding 5632 128-squared pixel CCD frames per file. For each of the 10 objects, 352 images are reconstructed using 16 frame ensembles. The time required for both SI implementations to reduce each of the 160-frame reference star ensembles is shown in the first column. The time required to recover a single image, after all camera and star calibrations, is shown in column 2. The time required to reduce each of the 10 5632-frame ensembles to 352 images, once the star calibrations are done, is shown in column 3. The sum of the times in columns 1 and 3 is the time required to create 352 images from the satellite, calibration star, and camera calibration data. This time is shown in column 4. In the fifth column is shown the time required to reduce all 10 data sets to 3520 images (the column 4 time multiplied by 10).

Algorithm	1 star reduction	2 seconds per recovery	3 data reduction time per object	4 total time per pair	5 total data reduction time per session
Bispectrum serial unoptimized	11 minutes 39 seconds	35	3 hours 25 minutes 20 seconds	3 hours 36 minutes 59 seconds	36 hours 8 minutes 20 seconds
Bispectrum parallel optimized	15 seconds	0.75	4 minutes 4 seconds	4 minutes 19 seconds	43 minutes 10 seconds

Table 1

Two things are clear from the results shown: First, if a nominal night's work takes over 36 hours to reduce, most of the data collected must be discarded barring a dedicated staff to reduce it. Second, the dramatic reduction in processing time afforded

162

by parallel SI can have a significant impact on operations tempo and the ability of the MSSC to meet urgent user needs. As discussed below, fast data reduction will impact observatory operations in three ways.

4. THE FUTURE OF SATELLITE OBSERVING - GEMINI

The GEMINI advanced instrumentation package for the MSSC 1.6m telescope consists of detectors and optics to make use of leading-edge image recovery algorithms[7] as well as sophisticated software to acquire, transfer, and reduce data and provide a graphical user environment for operators. GEMINI includes instrumentation to acquire data for computationally-intensive Bayesian estimation algorithms[8,9] capable of producing imagery with resolution significantly greater than that available with SI or other conventional algorithms. Even with access to supercomputing capability, however, these algorithms are relatively time-consuming. As a consequence, only the most promising data should be used. The most unambiguous way to assess data quality for the estimation algorithms is to reconstruct images from the data using a simpler algorithm, such as SI. This approach can be realized with the use of a parallel SI implementation. Reconstruction of all data in a very large ensemble allows easy identification of high-quality data. If high-performance computing resources are then available, the use of time-consuming, sophisticated algorithms becomes practical. Note that later in this summary, we discuss the fact that availability of high-performance parallel computing does not require a link to an outside resource.

In addition to allowing for rapid and complete data quality assessment, the parallel implementation of SI allows near real-time image feedback to the GEMINI operator. All calibration calculations are accomplished prior to the satellite pass. During the pass, satellite data is passed from the data acquisition system via a high-speed data link to the MHPCC. Using 15 SP2 nodes, the data is reduced, and the recovered imagery is passed back to the GEMINI console. The time delay from initial acquisition to console display is approximately 4-5 *seconds*. This delay is short enough that video feedback can effectively be used to vary observing parameters to optimize image quality during the satellite pass. Since all calibration data is reduced prior to the pass, calibration errors can be reported to the console and corrected before satellite observing begins. A flow diagram for GEMINI satellite observing operations is shown in Fig. 1.

Figure 1

5. SYSTEM ENGINEERING OF THE PARALLEL SI CODE

The algorithm used as the starting point for the parallel SI implementation is well-understood, robust, and has been in routine use at the MSSC since 1991. This serial legacy code was first optimized and brought up to Fortran 90 standard. Then, as an initial attempt at parallelization, we developed a code using the "embarrassingly parallel" paradigm; that is, we took advantage of the natural parallelism inherent in this type of image reconstruction problem. The data used to reconstruct one image is totally independent of the data used to generate another. With 16 SP2 nodes available for GEMINI data reduction, this means 15 nodes can be used rather easily to reconstruct one image each. A master process running on the 16th node receives the incoming data stream, divides the data into ensembles large enough to generate one image, distributes the ensembles to the 15 "worker" nodes, then collects the results and returns them to the console. We found that with this implementation, the 15 images were simultaneously available in a little over 10 seconds, for a total time between acquisition and display of nearly 13 seconds. A delay this long makes it quite difficult for the GEMINI operator to use image feedback for optimization of data collection. This led us to seek a more sophisticated implementation with the hope of reducing the feedback time.

The Parallel Bispectrum Flowchart in Figure 2 shows that we divided our 15 SP2 nodes into three groups of 5. Each "team" of 5 has a master and 4 workers. The number of processors in each set was chosen so that, under nominal conditions, the master finishes passing data to the last worker in the set at the same time the first worker to receive data finishes processing. In other words, processing is optimized by equalizing the time required to distribute the data and the time required for one processor to finish its work. In this way, the master processor in each set is never idle, and each worker receives new data as soon as it is ready. With a significant reduction in feedback time, the GEMINI operator can much more easily assess the affect of parameter changes during a satellite pass.
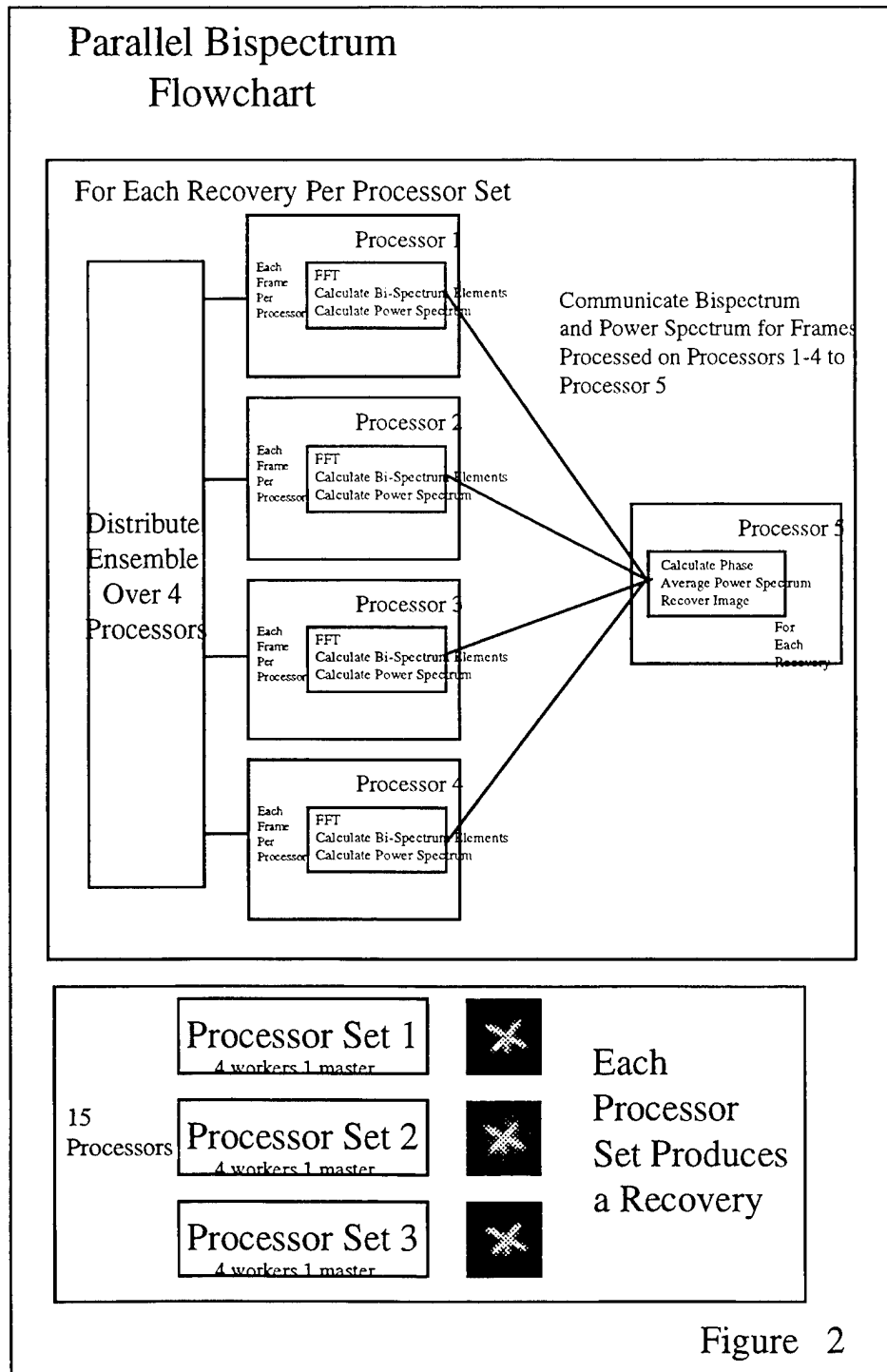

Figure 2

6. ON-SITE "SUPERCOMPUTING"

We have made extensive use of ready access to the Maui High Performance Computing Center for our NRT processing research and development. However, linkage to such a site is not commonly available or even desirable in some cases. We have begun exploration of cost-efficient means to bring supercomputing power to a telescope site using PCs or low-cost workstations. PCs are available now running up to 300 MHz, and 128Mb memory is readily obtainable. These PC systems can run Linux, a version of the Unix operating system, and can host MPICH., the free Message Passing Interface standard for parallel computation. This software would duplicate the operating system and parallel environment of the SP2. Another significant technology development is the "fast ethernet," which can duplicate the high-speed interprocess communication required for efficient parallel computing. The price of each PC would be even lower if the PCs, memory, and ethernet were available on cards, which could then be plugged into a VME chassis. We recommend the use of a Silicon Graphics Onyx workstation, with its rapid-access striped disk , for data acquisition.

7. SUMMARY

We have described the development of near real-time speckle imaging for satellite observations. NRT image processing optimizes satellite observing operations in three ways: First, since all calibrations can be performed quickly and prior to a satellite pass, errors are made manifest *before* data collection, when they can be corrected, rather than during post-mission data reduction. Second, NRT video feedback of reconstructed imagery can be used to optimize observing parameters such as camera exposure time. Finally, even very large amounts of data can be reduced, allowing the best-quality data to be selected for subsequent processing with more sophisticated recovery algorithms, increasing yet again the quality of the observatory product.

8. ACKNOWLEDGEMENTS

9. REFERENCES

1. G.R. Ayers, M.J. Northcott, and J.C. Dainty, "Knox-Thompson and triple correlation imaging through atmospheric turbulence," J. Opt. Soc. Am. A **5**, pp. 963-985 (1988)

2. T.W. Lawrence, D.M. Goodman, and J.P. Fitch, "Speckle imaging of satellites at the U.S. Air Force Maui Optical Station," Appl. Opt. **31**, pp. 6307-6321 (1992)

3. M.C. Roggemann, E.L. Caudill, D.W. Tyler, M.J. Fox, M.A. VonBokern, and C.L. Matson, "Compensated speckle imaging: Theory and experimental results," Appl. Opt. **33**, pp. 3099-3110 (1994)

4. T.J. Schulz, B.E. Stribling, and J.J. Miller, "Multiframe blind deconvolution with real data: Imagery of the Hubble Space Telescope," Opt. Expr. **1**, pp. 355-362 (1997)

5. M.C. Roggemann, C.A. Stoudt, and B.M. Welsh, "Image spectrum signal-to-noise improvements by statistical frame selection for adaptive optics image through atmospheric turbulence," Opt. Eng. **33**, pp. 3254-3264 (1994)

6. C.L. Matson, ``Weighted least-square phase reconstruction from the bispectrum," J. Opt. Soc. Am. A **8**, pp. 1905-1913 (1991)

7. D.W. Tyler, S.D. Ford, B.R. Hunt, R.G. Paxman, M.C. Roggemann, J.C. Rountree, T.J. Schulz, K.J. Schulze, J.H. Seldin, D.G. Sheppard, B.E. Stribling, W.C. Van Kampen, and B.M. Welsh, "Comparison of satellite imaging algorithms using adaptive optics instrumentation," these proceedings.

8. J.H. Seldin, M.F. Reily, R.G. Paxman, B.E. Stribling, and B.L. Ellerbroek, "Space object identification using phase-diverse speckle," in *Image Restoration and Reconstruction II*, T.J. Schulz, ed., Proc. SPIE **3170**, pp. 2-15, San Diego (1997)

9. D.G. Sheppard, B.R. Hunt, and M.W. Marcellin, "Iterative multiframe superresolution algorithms for atmospheric turbulence-degraded imagery," *accepted* for publication in J. Opt. Soc. Am.

Electro-Optical (EO) contribution to the warfighter (orbit class analysis)

G.E. Tromba (18 SPSS); J.P. Field, J.R. Finley, J.S. Juracka, G.J. McGoven (Litton/PRC); M.E. Stringer (1 CACS)

Background

As the space surveillance community is aware, emphasis is being placed on the Space Surveillance Network's (SSN) contribution to the warfighter. The reasons are many, and include:

- Importance of space information as demonstrated during the Gulf War
- Increasing need for military relevant information from space-based assets to ensure the success of Theater CINC missions and deployments
- Ensuring USCINCSPACE receives space related information to provide protection and exploitation of space-based assets under the USCINCSPACE Area Of Responsibility (AOR)
- Increasing need for information collection and processing efficiency during decreasing budgets

Therefore, from the military perspective, to produce more and/or higher quality data which do not relate to the warfighter's mission, as reflected in USCINCSPACE and Theater CINC mission statements, lack military significance and under value the SSN's data contribution. Consequently, space (near and deep) should be viewed as a potentially hostile environment where space assets may be exploited and critical information denied to friendly as well as non-friendly forces. It can also be viewed as a single vast minefield with each mine in constant motion and having a kinetic energy kill potential. Hence, this paper addresses the relative contribution of deep-space ground-based optical and radar sensor systems to the warfighter with a focus on non-friendly deep-space assets.

Defining Support to the Warfighter

During peacetime and wartime, space surveillance sensors provide critical tactical and strategic information to both USCINCSPACE and affected Theater CINCs, unlike other weapon systems which operate solely for one Theater CINC. With that in mind, we need to articulate and maintain situation awareness on what, specifically, we are doing for each CINC.

Within the context of USCINCSPACE, the SSN is a global system of systems operating 24 hours a day, 365 days a year providing him the following products and capabilities:

SOI	**Metric**
-Object Identification--Class & Type	-Location
-Status--is it operational?	-Maneuver Detection
-Characterization	-Collision Avoidance
--Primary/2nd Missions	-Launch/Reentry/Supersynch
--Change Detection	-Numbers/Space Order of Battle (SOB)

As illustrated in figure-1, various sensors offer differing degrees of utility to USCINCSPACE in providing these products.

figure-1

	Position		Stability	Orientation	Configuration
	Range	Angles			
Near Earth	NB	NB optics	NB photo	WB imagery	*imagery*
Deep Space	nb	nb OPTICS	nb PHOTO	*photo*	

Legend: NB = Narrowband   CAPS BOLD = greater capability
WB = Wideband   small letters = lesser capability
italics = demonstrated / development

Two key differences surface when articulating space system value added to a Theater CINC vs. USCINCSPACE. First and foremost, the combatant CINC incurs both personnel and weapon system casualties whereas the space AOR is currently limited to weapon systems. Secondly, the time and space variables each CINC must operate in represent themselves differently for each AOR.

Thus, demonstrating space control utility to the warfighter demands specific answers on:
1. What is up there that can adversely impact my ability to conduct operations, where is it, and what are you going to do to deny or limit the enemy's ability to use it?
2. What is up there that can enhance my ability to conduct operations, where is it, and what are you going to do to prevent its disruption or loss?

The Ever-changing Minefield

To answer the above questions one must accurately characterize the ever-changing space environment. The current number of orbiting objects is approaching 10,000 and continues to grow as more countries develop launch capabilities or have payloads launched for them by other countries. At a minimum, each of these objects has kinetic kill potential whether intended for that purpose or not. A large percentage of these objects are debris, rocket-bodies, or inactive payloads. Therefore, the space environment is an ever-changing minefield of objects both active and inactive that could deny us use of our space assets.

Assuming the space AOR presents itself as an ever-changing minefield, which, if unmapped, may deny our ability to use needed space assets, delineates the impact to USCINCSPACE resources. However, the potential impacts of an inadequately mapped minefield to a Theater CINC go one step further in that ultimately *characterization loss = loss of lives*. Figure-2 illustrates how the ability/inability to accurately characterize this ever-changing minefield positively/negatively impacts a Theater CINC.

figure-2
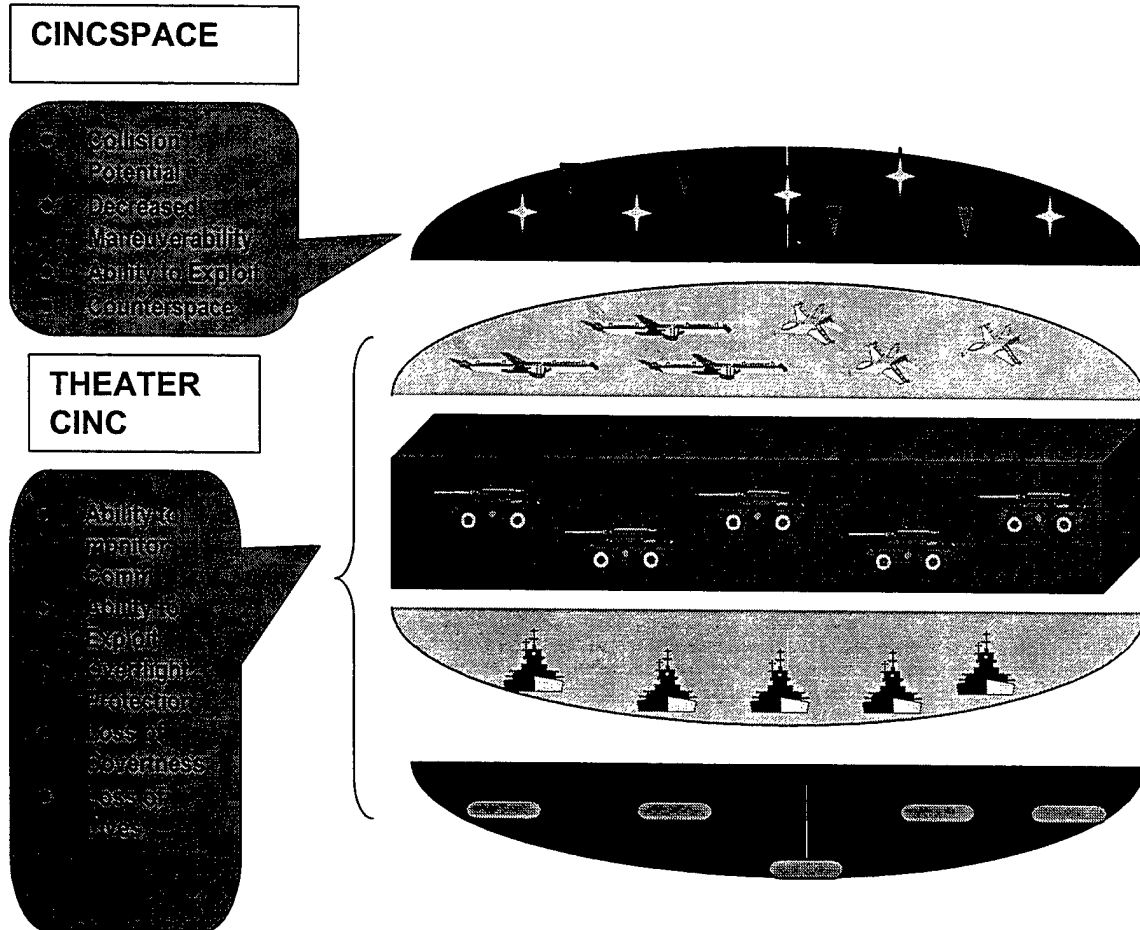
While not a tool in answering the previously identified Theater CINC questions of "what are you going to do to deny or limit the enemy's ability to use it?" or "what are you going to do to prevent its disruption or loss?" metric observations answer an important "where" question. "Where" is key to USCINCSPACE' ability to either do something about an aggressor's ability to use one of their space assets or to prevent disruption or loss of a desired space asset by predicting possible collisions with other space objects. Due to the large number of space objects, and realizing that *all* (debris, rocket-bodies, active/inactive payloads) have the potential to adversely impact a Theater CINC this paper will focus only on one satellite subset--potentially non-friendly payloads.

Methodology

Several assumptions and study boundaries were established. These are:

- Commonwealth of Independent States (CIS), People's Republic of China (PRC), and other (potentially non-friendly) payloads were considered due to their tasking priority. Other objects (rocket bodies and debris) were not considered, although to a lesser extent they potentially contribute to a hostile space environment, as well.
- Deep space was chosen since the focus of the study is directed towards the electro-optical contribution.
- Only deep space cataloged objects were selected since cataloged orbits are well known.
- All SSN sensors were considered. No sensors were excluded from the study. Absence of data assumes no data contribution to the network.
- Four months of data (Mar, Jul, Oct, Dec 97) were collected to ensure a representative sample for the study.
- All data used were real and collected as a result of actual SSN sensor operations. Weather variability and sensor operability were not considered.
- Space object identification (SOI) data contributions were not considered. Only metric data at the observation level were used.

The data reduction process used 1 CACS products and 18 SPSS Det-1 produced derivatives. The study selected 459 deep space payloads from the CIS, PRC, and "other" (potentially non-friendly) from the 1 CACS Satellite Catalog dated December 1997. 1 CACS provided tasked and acquired information from their mission support system CAVENET, with the assistance of Mr. Gil Miller (Mitre) and the SSPAT Oracle Tasking database, on SSN sensors for the complete population of payloads selected. This information was sorted by orbit class (also known as bins), country/organization, and satellite type (i.e., common name). Orbit classes are used to group objects into categories of similar orbits by apogee and perigee. Spreadsheets were created distributing all sensor metric contribution by observation for each bin and satellite number for all payloads selected.

Data Analysis

To narrow the scope and highlight the contribution of optical systems, the contribution percentage of opticals, within this subset of the catalog, was calculated for each orbit class. These data were then graphed to determine which orbit classes would be analyzed in greater detail. Two criterion were used to determine which orbit classes would be analyzed in greater detail. These are: (1) Equal to or greater than 35% of observations collected; and (2) Equal to or greater than 10 cataloged objects per orbit class. Passing these two criterion represent a "significant contribution." Figure 3 illustrates the percentage of observations contributed to each orbit class with the shaded areas depicting the orbit classes where optics contribute greater than 35 percent of the data. However, Orbit classes 52 and 53 were excluded from detailed analysis because they had a sample size of less then 10 objects.

170

figure-3
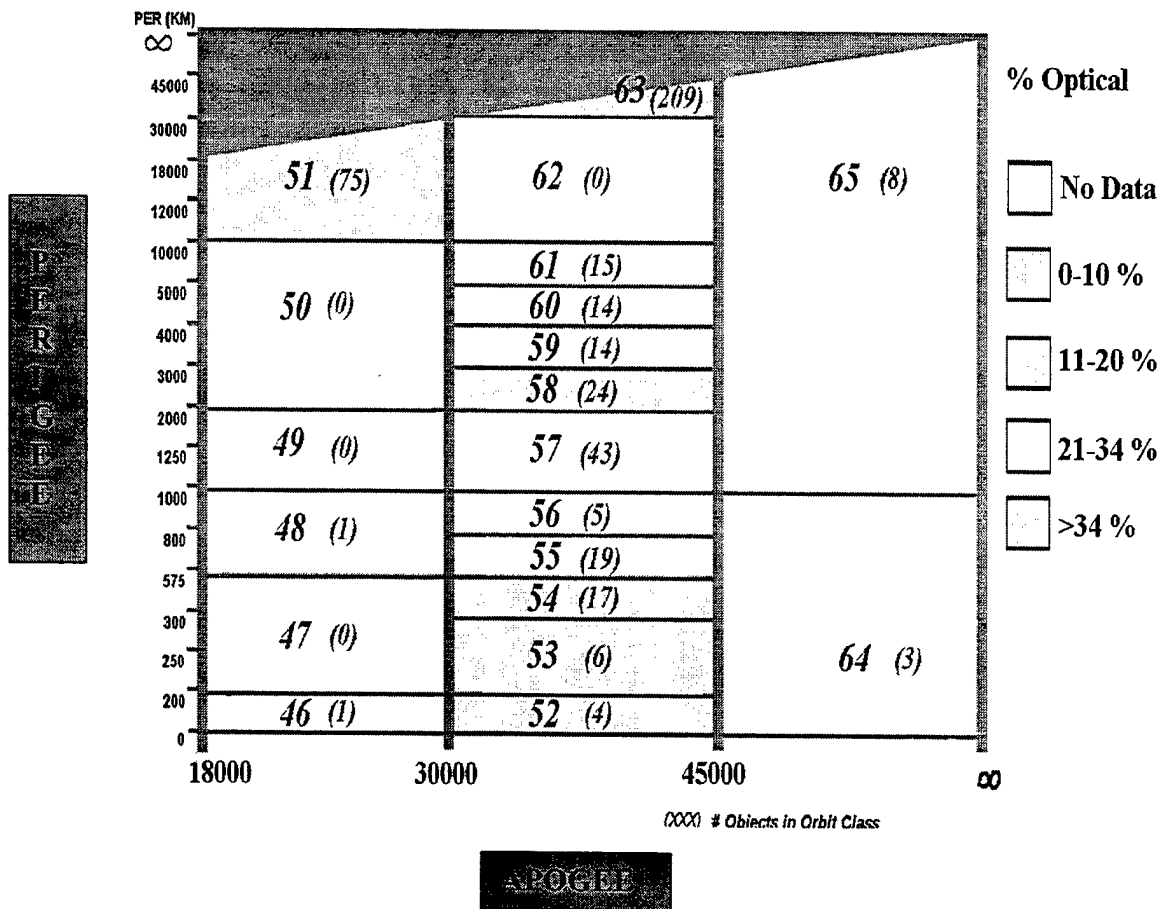
To characterize the specific makeup of each selected orbit class the number of objects belonging to PRC, CIS, and other (potentially non-friendly entities) was calculated and graphed followed by a further breakdown of numbers of specific types of payloads per country/organization. Figures 4-1, 4-2, and 4-3 illustrate these findings.
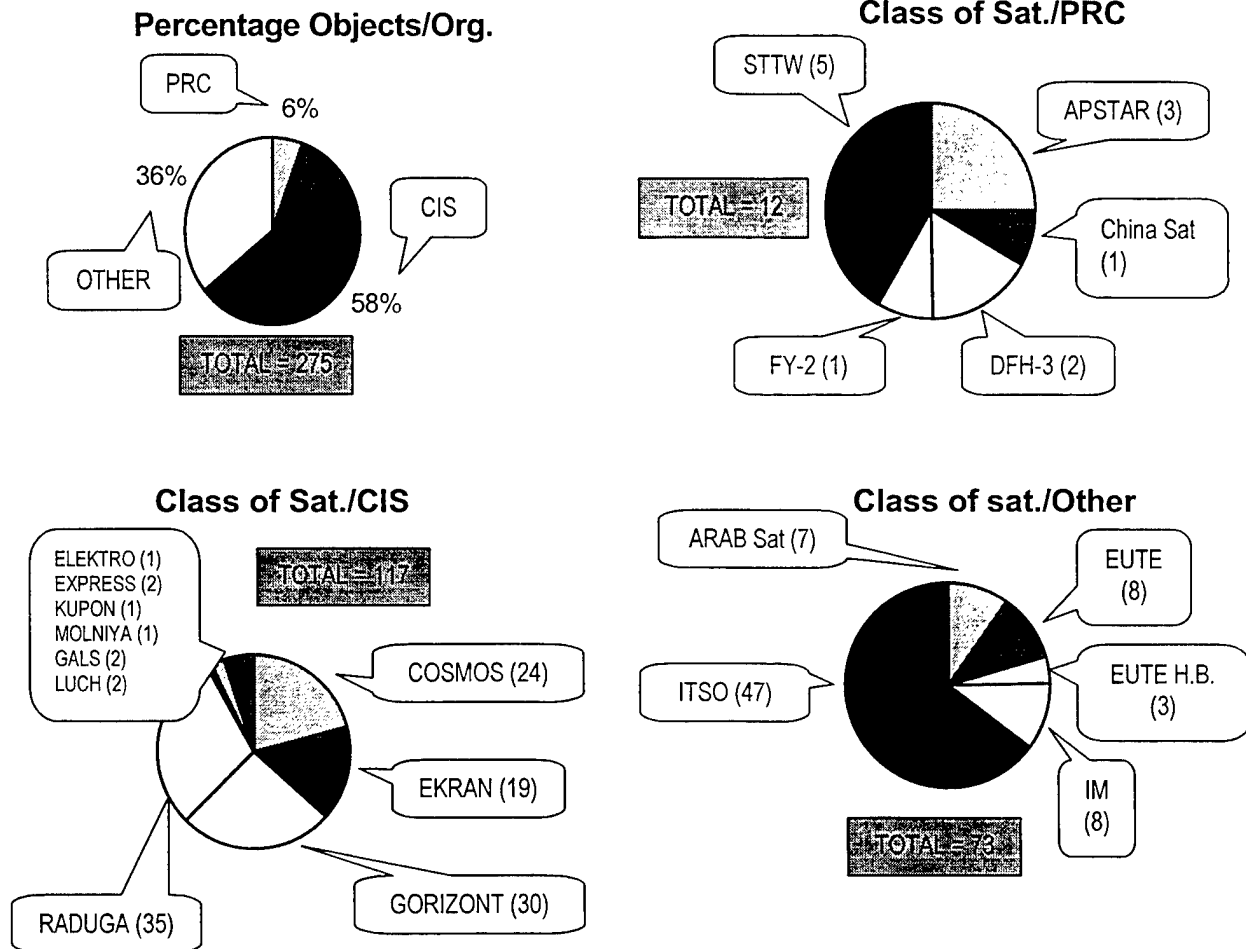
figure 4-1

Orbit Class 63

Percentage Objects/Org.

PRC
6%

36%

OTHER

CIS

58%

TOTAL = 275

Class of Sat./PRC

STTW (5)

APSTAR (3)

TOTAL = 12

China Sat (1)

FY-2 (1)

DFH-3 (2)

Class of Sat./CIS

ELEKTRO (1)
EXPRESS (2)
KUPON (1)
MOLNIYA (1)
GALS (2)
LUCH (2)

TOTAL = 117

COSMOS (24)

EKRAN (19)

RADUGA (35)

GORIZONT (30)

Class of sat./Other

ARAB Sat (7)

EUTE (8)

ITSO (47)

EUTE H.B. (3)

IM (8)

TOTAL = 73

172

figure 4-2

Orbit Class 54

Number Objects/Org. & Class of Sat./CIS

RADUGA — 1   1 — COSMOS

MOLNIYA — 15

TOTAL = 17
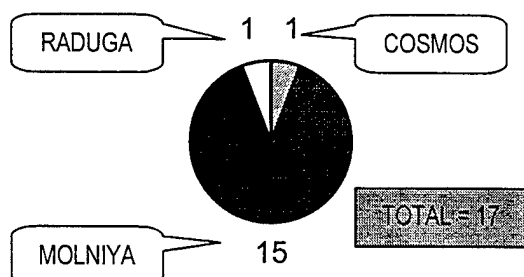
figure 4-3

Orbit Class 51

Number Objects/Org. & Class of Sat./CIS

ETALON (2)

TOTAL = 75

GLONASS (73)
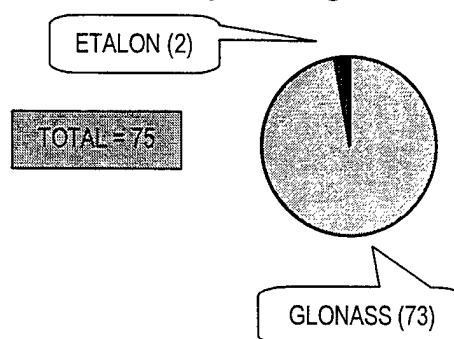
Note: There are no "other" or PRC cataloged payloads in Orbit Class 51

To characterize specific sensor site contribution to the warfighter the predetermined makeup of countries/organizations for each orbit class was analyzed in conjunction with individual sensor site observations for each orbit class (*sensor #s 200, 235, 245, & 951 = optical sensors*). Figures 5-1, 5-2, 5-3 illustrate this sensor site performance within each orbit class against the different payload owner countries/organizations.

Figure 5

Note: This figure identifies the specific sensors and corresponding sensor numbers which had observations against PRC, CIS, and "other" payloads within the identified orbit classes.
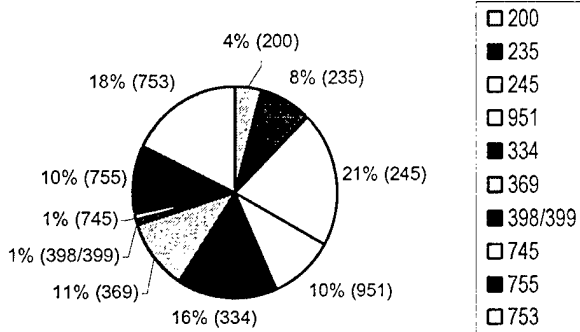
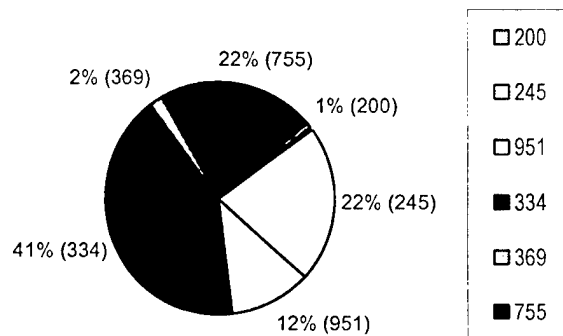| SENSOR NUMBER	SENSOR NAME	SENSOR NUMBER	SENSOR NAME
200	Socorro	388	Beale
235	Maui-GEODSS	394	Thule
245	Diego Garcia	396	Cavalier
951	Maui-MSSS	398/399	Eglin
334	Altair	745	NAVSPASUR
344	Flyingdales	753	Feltwell
369	MILSTONE	755	Misawa
386	Cape Cod		

figure 5-1

Orbit Class 63
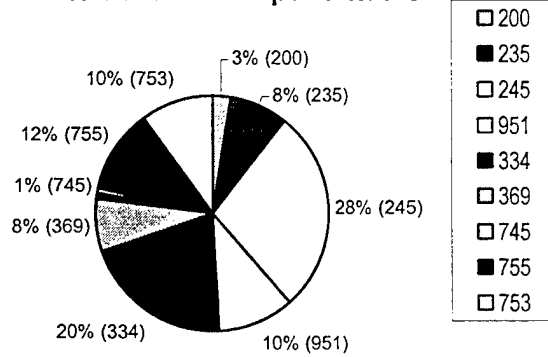

Opticals = 48%

% Contribution/Site

% Contribution per Site/PRC

% Contribution per Site/CIS
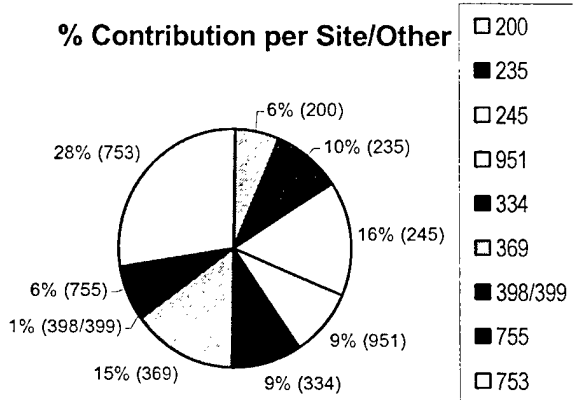
% Contribution per Site/Other
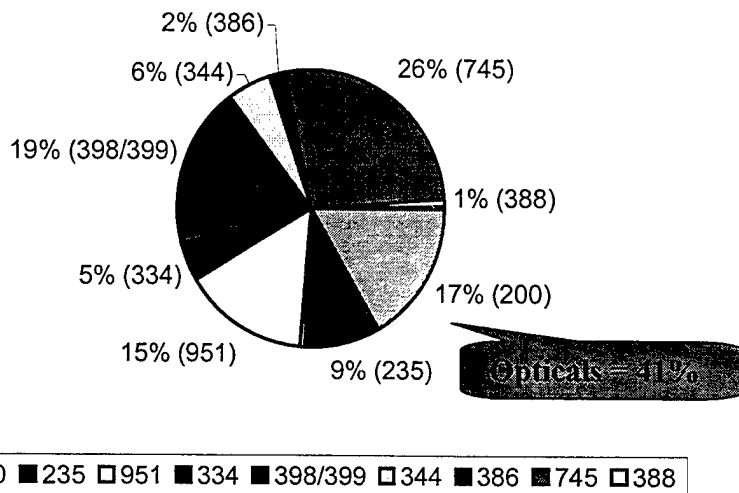
figure 5-2

Orbit Class 54

% Contribution/Site/CIS


```
2% (386)
6% (344)                    26% (745)
19% (398/399)
                            1% (388)
5% (334)
                            17% (200)
15% (951)      9% (235)    Opticals = 41%
```
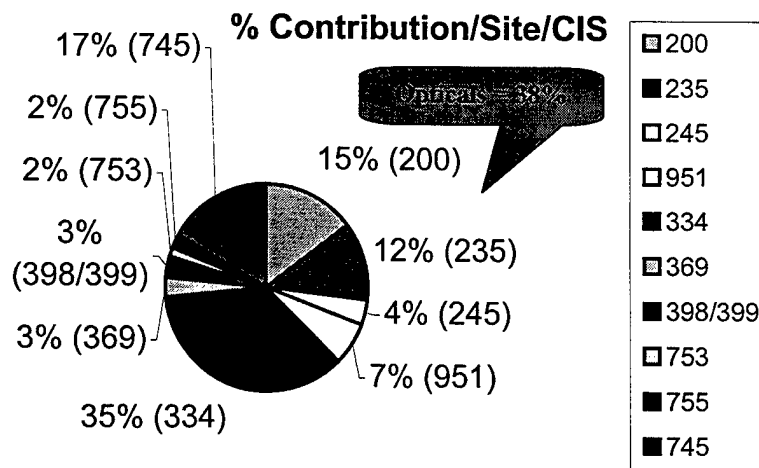
☐200 ■235 ☐951 ■334 ■398/399 ☐344 ■386 ▨745 ☐388

Note: % Contribution per site for PRC & "Other" = 0% since there are no PRC & "Other" payloads in Class 54.

figure 5-3
Orbit Class 51

% Contribution/Site/CIS


```
17% (745)
2% (755)                Opticals = 38%
2% (753)       15% (200)
3%
(398/399)              12% (235)
                       4% (245)
3% (369)
                       7% (951)
35% (334)
```

☐200
■235
☐245
☐951
■334
▨369
■398/399
☐753
■755
■745

Note: % Contribution per site for PRC & "Other" = 0% since there are no PRC & "Other" payloads in Class 51.

Figure 3 illustrates that of the study's subset (i.e. payloads) orbit classes 63 (geo-synchronous), 54 (highly-elliptical/Molniya), and 51 (semi-synchronous) combine to makeup the greatest portion of AFSPC's optical network taskings and observations for metrics. In isolating specific owners and their payloads for these three classes (figures 4-1, 4-2, & 4-3) it is clear the geo-synchronous belt contains the greatest number *and* variety of payloads and payload owners. While the semi-synchronous and Molniya classes are populated by fewer payloads from fewer owners; however, this may change as the number of spacefaring nations and organizations increases.

In determining sensor specific contribution in mapping different orbit classes within the "ever-changing minefield" for the warfighter, figures 5-1, 5-2, and 5-3 clearly illustrate that when focus on either orbit class or payload owner changes so too does a sensor's relative contribution. For geo-synchronous (class 63) payloads opticals constitute a 43% contribution of observations. More specifically, they provide 35%, 49%, and 41% of observations relatively against PRC, CIS, and "other" payloads. With regards to Molniya (class 54) orbit payloads, opticals input a total of 41% of all observations. Since the CIS is identified as the only owner organization in this class, this also delineates optical's specific owner contribution. Lastly, observations against semi-synchronous (class 51) orbiting payloads are accomplished 38% of the time by opticals. As in class 54, the CIS is the only identified payload owner so this also represents the percentage contribution with regards to a specific owner.

The overall optical contribution in accurately mapping the "ever-changing minefield" of space, thereby answering a warfighter's questions of concern, range from 34% to 49%, depending on the orbit class and owner.

The Way Ahead

In order to address the full spectrum of Electro-Optical contribution to the warfighter, three items still need analyzing. First, other satellite subsets (e.g., debris, rocket-bodies) need to be evaluated for sensor contribution because of their kinetic kill potential. Secondly, data collection and analysis of EO's contribution in the area of SOI for both imagery and photometric data still needs to be accomplished. Finally, two key additions to the optical network, destined to positively impact space' contribution to the warfighter, which were not addressed since they are not yet in Initial Operational Capability (IOC) need analysis. These are the addition of Det-4 in Moron, Spain to the 18th SPSS optical network, and the impending installation and operation of the Optical Command Control and Communications Facility (OC3F) at Edwards Air Force Base, CA. After Det-4 achieves IOC there will be optical network coverage in the currently optically uncovered 300° to 10° portion of the geosynchronous belt. Consequently, we expect increased tasking and data collection that will further support the warfighter. Also, the ability to dynamically schedule and re-schedule optical sensors through the OC3F as weather and system capabilities dictate will invariably increase optical sensor tasking efficiency and satisfaction. This will position the OC3F as a possible pathfinder as to the benefits of inter-networking the entire SSN within a dynamic scheduling architecture. As these upgrades are completed and optical SOI performance data collected and analyzed we anticipate covering these topics in full at future forums.

Ultimately, as the number of spacefaring nations and organizations increases the need to satisfy CINCSPACE and Theater CINC requirements of the SSN will only increase. The challenge for the SSN community is, and will be, to continue providing a militarily significant product and understand fully the impacts to each CINC changes in operability and capability make. The measure of relative importance must be the value added to the warfighter's mission to fight and win. If the space surveillance and control community use these criteria for benchmarking contribution the understanding of the SSN's warfighter utility will flow naturally.